Guide to Instruments and Methods of Observation

Volume IV – Space-based Observations

2021 edition

WEATHER CLIMATE WATER

WORLD METEOROLOGICAL ORGANIZATION

WMO-No. 8

Guide to Instruments and Methods of Observation

Volume IV – Space-based Observations

2021 edition

WORLD
METEOROLOGICAL
ORGANIZATION

WMO-No. 8

EDITORIAL NOTE

METEOTERM, the WMO terminology database, may be consulted at https://public.wmo.int/en/meteoterm.

Readers who copy hyperlinks by selecting them in the text should be aware that additional spaces may appear immediately following http://, https://, ftp://, mailto:, and after slashes (/), dashes (-), periods (.) and unbroken sequences of characters (letters and numbers). These spaces should be removed from the pasted URL. The correct URL is displayed when hovering over the link or when clicking on the link and then copying it from the browser.

WMO-No. 8

Chair, Publications Board
World Meteorological Organization (WMO)
7 bis, avenue de la Paix
P.O. Box 2300
CH-1211 Geneva 2, Switzerland

Tel.: +41 (0) 22 730 84 03
Fax: +41 (0) 22 730 81 17
Email: publications@wmo.int

ISBN 978-92-63-10008-5

PUBLICATION REVISION TRACK RECORD

Date	*Part/ chapter/ section*	*Purpose of amendment*	*Proposed by*	*Approved by*

CONTENTS

Page

Page

Page

Page

CHAPTER 1. INTRODUCTION

1.1 HISTORICAL PERSPECTIVE

The era of satellite meteorology started with the launch of the Sputnik satellite series, starting in the late 1950s, which provided the first space measurement of the Earth-atmosphere system (Menzel, 2001). The United States of America started its meteorological space programme with the launch of the Television and Infrared Observation Satellite – 1 (TIROS-1) on 1 April 1960. Before TIROS-1, an experiment on the Explorer VII satellite measured net radiation balance, that is the balance between radiation input from the Sun and radiation exiting the atmosphere as a result of reflection of solar radiation and thermal emission (Smith, 1985).

The first geostationary meteorological satellite, the Applications Technology Satellite – 1 (ATS-1), was launched on 6 December 1966 and featured only daytime viewing capabilities. Weather systems, which had only been depicted until then by synoptic maps and aircraft observations, were able to be visualized at a glance. Their rapidly evolving nature became especially evident with geostationary imagery. The term "nowcasting" emerged, becoming the first application of meteorological satellites. Initially, satellite data were nearly exclusively used for nowcasting, primarily in the form of imagery. Another important application was the derivation of atmospheric motions (Fujita, 1968). Thanks to their ability to provide continuous measurements, geostationary satellites also became essential for monitoring tropical storms and mid-latitude low-pressure systems (Purdom and Menzel, 1996).

A user community also emerged gradually in the field of numerical weather prediction (NWP). The radiances measured by the TIROS operational vertical sounder (TOVS) series on National Oceanic and Atmospheric Administration (NOAA) satellites were used to provide temperature and humidity information for soundings (vertical profiles). For many years, attempts were made to use these temperature and humidity soundings in NWP analogously to the way information from radiosondes was used. NWP reliance on radiosondes suggested satellite data needed to be formatted into radiosonde-like characterization, although satellite radiance measurements represent contributions from broad overlapping layers in the atmosphere and are not single level measurements. Finally, sustained benefits from satellite radiance observations were realized through a paradigm shift in which the measured radiances began to be used directly in an NWP variational assimilation system instead of the derived soundings (Eyre, 1997).

In summary, meteorological satellites provided a completely new look at weather and the Earth-atmosphere system and today furnish a wealth of data which are a sine qua non for state-of-the-art weather prediction at all scales. The prime example is found in NWP: the introduction of space-based measurements has substantially improved NWP forecasts, and nowadays meteorological satellite measurements are a cornerstone for NWP (WMO, 2012). The fact that remote sensing measurements are a vital component in the observing system for global monitoring and prediction is reflected in the growing number of international partnerships being formed to implement integrated and coordinated satellite programmes, as described in a subsequent chapter of the present Guide.

Driven by the high economic value of earth resource exploration and vegetation cycle monitoring, satellite programmes have emerged with a focus on land surface observation. Those satellites have a high spatial resolution yet an infrequent revisit cycle for any given area on Earth. Landsat-1, launched on 23 July 1972, was the first in a series of high-resolution land observation satellites, and coverage from the Satellite pour l'Observation de la Terre (SPOT) series, beginning on 22 February 1986 with SPOT-1, provided imagery at a spatial resolution of 10 to 20 metres.

Exploration of the ocean began with the launch of SeaSat on 27 June 1978, which marked the start of all-weather microwave sensing, both active and passive. Around the same time, on 24 October 1978, came the launch of Nimbus-7, which used passive microwave sensing with the addition of ocean colour monitoring. After the SeaSat altimetry, scatterometry and synthetic aperture radar imagery missions, no active sensing mission was operated until the launch of the

European Remote Sensing Satellite – 1 (ERS-1) on 17 July 1991. The monitoring of sea levels has also become an operational activity, for example with the Jason satellite series. A concise history has been compiled by Wilson et al. (2006).

The socioeconomic benefits of satellite data have been demonstrated and detailed assessments even provide cost–benefit analyses proving the tremendous economic value of meteorological satellite observations for societies and humankind. The report of the European Organization for the Exploitation of Meteorological Satellites (EUMETSAT) on the cost–benefit analysis of the next generation of European polar meteorological satellites (Metop series) provides an example (EUMETSAT, 2014).

1.2 COMPLEMENTARY NATURE OF SPACE-BASED AND SURFACE-BASED MEASUREMENTS

The concept of the Global Observing System was totally revised with the advent of satellites, taking advantage of the complementary nature of surface-based and space-based observations. Space-based systems can observe the Earth-atmosphere system in its entirety. Polar orbiting meteorological satellites (at altitudes of around 800 km) provide global observations, however each area is usually observed only twice per day. Lower orbit altitudes give better spatial resolution and enable active instruments (radar, lidar). More frequent observations require a constellation of polar satellites. The geostationary space-based component (at altitudes of 36 000 km) offers the unique opportunity for uninterrupted coverage and frequent observing cycles.

A striking advantage of satellites is their ability to perform spatially dense observations over the oceans, removing a great limitation of observations for global NWP. Similar arguments hold over continental areas, where observing networks are biased towards populated areas whereas vast areas of land surface are relatively undersampled.

One important difference between space-based remote sensing measurements and surface-based in-situ measurements is due to different integrations in space and time. Space-based measurements integrate the incoming signal over an instantaneous field of view. Surface-based in-situ measurements are usually point-related, although, depending on the observed variable, the measurement may be representative of an area. In the time dimension, the situation is reversed. Space-based measurements are nearly instantaneous, while surface-based in-situ measurements may represent a certain time (for instance measurements from an automatic weather station) or may integrate over a certain time interval, for instance, a radiosonde travels for an extended period through the atmosphere and provides a single profile. These differences need to be considered when comparing satellite and surface measurements.

It should be acknowledged that satellites are not able to perform all required observations with the necessary measurement quality. For certain geophysical variables, no remote sensing principle exists. For others, the required measurement quality is only achievable with ancillary information from accurate surface-based observing systems. In addition, since space-based measurements are of an indirect nature (the primary observed quantity being radiation), surface-based measurements often play a key role for the validation of satellite-derived products. A summary of current capabilities and roles of ground-based and space-based systems is provided by Saunders et al. (2015).

There are still areas where exclusively surface-based systems can provide measurements of acceptable quality. However, even in those cases, satellites can be useful in spatially extending local and sparse ground measurements. In particular, the practice of assimilation makes it possible to transfer information across geophysical variables measured using different

techniques: this means satellite observations contribute to the knowledge of geophysical variables even when the geophysical variable is not directly observed by satellite; a prerequisite is that there must be a physical relationship between the geophysical variable and the radiance observed by satellite. Synergistic use of surface-based and space-based observations is fundamental to the WMO Integrated Global Observing System. In NWP this has been achieved through the process of data assimilation.

REFERENCES AND FURTHER READING

EUMETSAT. *The case for EPS/METOP Second-Generation: Cost Benefit Analysis*; 2014. https://www-cdn.eumetsat.int/files/2020-04/pdf_report_eps-sg_cost-benefit.pdf.

Eyre, J. R. Variational Assimilation of Remotely-Sensed Observations of the Atmosphere. *Journal of the Meteorological Society of Japan* **1997**, *75* (1B), 331–338. https://doi.org/10.2151/jmsj1965.75.1B_331.

Fujita, T. T. Present Status of Cloud Velocity Computations from the ATS I and ATS III Satellites. In *Proceedings of Space Research IX: 11th COSPAR Plenary Meeting*, Tokyo, Japan, 9–21 May 1968; North-Holland Publishing Company: Amsterdam, 1969, pp 557–570.

Menzel, W. P. *Applications with Meteorological Satellites* (SAT-No. 28; WMO/TD-No. 1078). World Meteorological Organization: Geneva, 2001.

Menzel, W. P.; Phillips, J. M. Satellite Meteorology: How It All Started, 50 Years Ago. *Bulletin of the American Meteorological Society* **2009**, *90* (10),1435–1436. https://doi.org/10.1175/2009BAMS2963.1.

Purdom, J. F. W.; Menzel, W. P. Evolution of Satellite Observations in the United States and Their Use in Meteorology. In *Historical Essays on Meteorology 1919–1995: The Diamond Anniversary History Volume of the American Meteorological Society*: Fleming, J. R., Ed.; American Meteorological Society: Boston, 1996; 99–155. https://doi.org/10.1007/978-1-940033-84-6_5.

Smith, W. L. Satellites. In *Handbook of Applied Meteorology*; Houghton, D. D., Ed.; John Wiley and Sons: New York, 1985.

Saunders, R.; Crewell, S.; Gelaro, R. et al. Observations for Global to Convective Scale Models. In *Seamless Prediction of the Earth System: From Minutes to Months* (WMO-No. 1156); WMO: Geneva, 2015.

Wilson, W.S.; Fellous, J.-L.; Kawamura, H. et al. A History of Oceanography from Space. In *Remote Sensing of the Marine Environment*; Gower, J. F. R, Ed.; American Society for Photogrammetry and Remote Sensing: Bethesda, 2006.

World Meteorological Organization (WMO). *Final Report of the Fifth WMO Workshop on the Impact of Various Observing Systems on Numerical Weather Prediction* (WIGOS Techical Report 2012-1). Geneva, 2012.

Note: Detailed descriptions of satellite programmes and instruments are available in the WMO online database of space-based observation capabilities: https://www.wmo-sat.info/oscar/spacecapabilities.

CHAPTER 2. PRINCIPLES OF EARTH OBSERVATION FROM SPACE

This chapter provides an overview of Earth observation from space, including its potential benefits and limitations. It describes basic concepts of orbits and the characteristics of Earth viewing from space. It also introduces the principles of remote-sensing.

2.1 ORBITS AND EARTH VIEWING FROM SPACE

The Earth can be observed from space from different orbits under various viewing conditions. The following issues are considered in this section:

(a) Satellite instrument field of view;

(b) Orbital period, geostationary orbit, observing cycle and repeat cycle;

(c) Orbital precession, Sun-synchronous orbits and drifting orbits;

(d) Elliptical orbits;

(e) Launchers and injection into orbit.

2.1.1 Satellite instrument field of view

The greatest advantage of observing from a satellite platform, rather than from the ground or a balloon, is the wide potential field of view (FOV). Satellite observing platforms usually orbit at a minimum height of 400 km. Often, they orbit much higher, some as far as the geostationary orbit (35 786 km). The FOV depends on the orbital height, the instrument configuration and the intended application. Those may limit the useful range of zenith angles (ζ) under which the Earth can be viewed. If the satellite FOV is characterized as the maximum ground distance potentially viewed from satellite height under a given zenith angle, the relationship set out in Figure 2.1 can be expressed as:

$$\text{FOV} = 2\ R\ \delta\ \pi/180 \qquad \sin(\zeta - \delta) = \frac{R}{H + R}\sin\zeta \qquad (2.1)$$

where R = 6 371 km (Earth's radius), H = orbital height in km, and δ = geocentric angle in degrees.

Table 2.1 presents values of the satellite FOV (in km) as a function of orbital height for typical values of zenith angle ζ. The corresponding geocentric angle δ is also shown.

The potential satellite FOV may not be entirely covered by a single instrument. Either the sensing principle or the technological features of an instrument may set an upper limit to its FOV. For instance, radar altimeters can only operate in a nadir geometry (pointing directly below). They

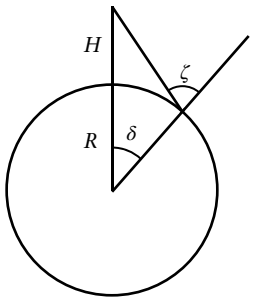

Figure 2.1. Field of view versus zenith angle ζ

Table 2.1. Potential satellite field of view and corresponding geocentric angle, as functions of satellite height and zenith angle, under which the Earth's spot is viewed

Zenith angle for various applications	*H = 400 km*		*H = 600 km*		*H = 800 km*		*H = 35 786 km*	
	FOV	δ	*FOV*	δ	*FOV*	δ	*FOV*	δ
$\zeta = 90°$ (horizon-to-horizon)	4 401 km	19.79°	5 326 km	23.95°	6 076 km	27.32°	18 082 km	81.31°
$\zeta = 85°$ (telecommunications)	3 423 km	15.39°	4 322 km	19.43°	5 057 km	22.74°	16 978 km	76.34°
$\zeta = 70°$ (qualitative use)	1 746 km	7.85°	2 405 km	10.82°	2 980 km	13.40°	13 752 km	61.84°
$\zeta = 60°$ (quantitative use)	1 207 km	5.43°	1 707 km	7.68°	2 157 km	9.70°	11 671 km	52.48°

therefore have no proper FOV, except for the broadening of the beam due to diffraction. Very high-resolution imagers usually have an FOV within a range of several tens of kilometres, as do some synthetic aperture radar (SAR) beam modes.

The satellite motion enables the instrument to cover successive FOVs along the orbit. With an instrument scanning across the satellite track, these constitute a strip of the Earth's surface called a swath. The swath may be centred along the sub-satellite track or be parallel to it for side-looking instruments (for example, SARs). For several purposes (steerable pointing for emergencies, stereoscopy in association with successive orbits, and the like), certain instruments with limited swath may tilt the swath to the side of the track within what is called a field of regard. The swath width is a cross-track component of the actual FOV of the instrument. The concept of swath is not applicable to instruments in geostationary orbit.

2.1.2 Orbital period, geostationary orbit, observing cycle and repeat cycle

The orbital height H determines the orbital period T. The relationship is:

$$T = a\,(1 + \frac{H}{R})^{\frac{3}{2}} \tag{2.2}$$

where a = 84.47 min (T resulting in minutes).

The height, which corresponds to one sidereal day (23 h 56 min 04 s) is 35 786 km. A satellite orbiting at this height is called geosynchronous. The orbit is called geostationary if the orbit lies in the equatorial plane and is run eastward: the satellite appears steady compared to the Earth's surface on the nadir of the equatorial sub-satellite point.

For an inclined orbit with respect to the equatorial plane, the satellite will cross the Equator at a certain longitude. After T minutes, there will be another equatorial crossing at a longitude displaced westward by the number of degrees that corresponds to the Earth's rotation during the orbital period. The difference of longitude (or space distance) between two successive equatorial crossings in the same phase (descending or ascending) is called decalage. Together with the instrument swath, decalage determines the time needed for a full Earth surface observation (observing coverage) (Figure 2.2).

If the instrument swath is at least as large as the decalage, the coverage provided by the two contiguous orbits is continuous. Therefore, the time needed for global coverage (observing cycle) depends on the ratio between instrument swath and decalage.

Table 2.2 shows the period and corresponding decalage for the orbital height examples in Table 2.1. In addition, observing cycles corresponding to several instrument swaths are presented. Those swaths are associated with qualitative and quantitative use; that is with 70°

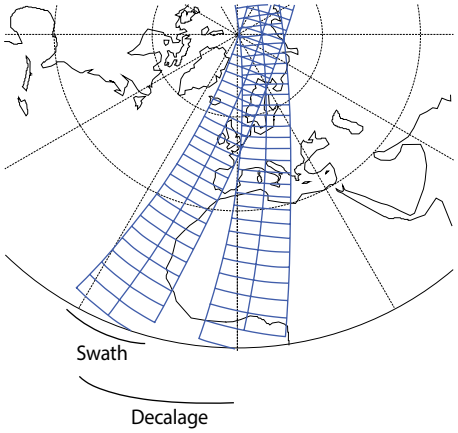

Figure 2.2. Decalage between two successive orbits, and instrument swath

Table 2.2. Period, decalage (shift) and observing cycle for the orbits indicated in Table 2.1

Orbital parameter	$H = 400$ km	$H = 600$ km	$H = 800$ km	$H = 35\,786$ km
Period T	92.6 min	96.7 min	100.9 min	23 h 56 min 4 s
Decalage (shift)	2 570 km	2 690 km	2 800 km	0 km
Observing cycle for $\zeta = 70°$ (day only)	35 h	27 h	23 h	From instrument
Observing cycle for $\zeta = 60°$ (day only)	51 h	38 h	31 h	From instrument
Observing cycle for $\zeta = 70°$ (day and night)	18 h	13 h	11 h	From instrument
Observing cycle for $\zeta = 60°$ (day and night)	26 h	19 h	16 h	From instrument

and 60° zenith angles, respectively. Observing time is halved for instruments capable of observation during the day and night. The decalage and observing cycle are not quoted for $H = 35\,786$ km (geostationary altitude).

For a geostationary satellite, which continuously views the same area of the Earth's surface, the observing cycle is only determined by instrument characteristics and may take a few minutes or less to complete, depending on the area scanned. Within the satellite's area of coverage, geostationary observation is perfectly suited for continuous monitoring. For example, such monitoring is needed to detect instantaneous events like lightning strokes, or for high-frequency temporal sampling of rapidly evolving situations, such as active convection. However, the coverage excludes very high latitudes or any locations too far from the sub-satellite point. Table 2.1 shows that $\delta = 81.31°$ is the maximum geocentric angle.

For a non-geostationary satellite, the orbit is said to have a repeat cycle if it overpasses the same track exactly after a given number of revolutions. During the timespan of a repeat cycle, the satellite track may shift from day to day, following a determined pattern that may exhibit certain periodicities called sub-cycles. Some sub-cycles may be of interest because distinct areas, relatively close to each other, are visited within short time intervals; other sub-cycles may be of interest because the areas covered are spatially adjacent.

If the orbit is Sun-synchronous (see section 2.1.3), the existence of a repeat cycle means that a whole number of revolutions can be completed in exactly a whole number of days. The orbital period determines N, the number of orbits that the satellite runs in 24 h. This is normally not an integer. In order to obtain a repeat cycle of m days, the orbital period is adjusted

to ensure that N multiplied by m is an integer. N can then be expressed in the following form, where n and ℓ are, respectively, the quotient and remainder of the integer division of "$N \cdot m$" by m:

$$N = n + \ell/m \tag{2.3}$$

where n, ℓ and m are integers ($\ell < m$).

Equation 2.3 also applies to non-Sun-synchronous orbits. However, in such cases, the repeat cycle m is no longer expressed in solar days of 24 h but must account for a slight correction due to the drift of the orbit. Table 2.3 provides examples of repeat cycles and main sub-cycles for a number of orbits.

An orbit with a repeat cycle is a necessary feature if a certain location needs to be viewed at fixed intervals under identical conditions. This is true of altimetric measurements for geodetic application, or of high-resolution land observation imagers, used to detect local variations.

Repeat cycles may be useful when the instrument swath is substantially narrower than the shift (decalage) between two successive orbits and global coverage cannot be achieved in a single day. In that case, the sequence of coverage over successive days can be arranged to follow a certain logic if requested. That logic might be to provide regular progression, or to avoid biases due to unsuitable sampling.

Figure 2.3 shows the pattern evolution of orbital passes for an orbit with a one-day sub-cycle (such as for early Landsat). As Figure 2.3 shows, the one-day sub-cycle ensures that each day, the covered strip is adjacent to the one that was observed on the previous day. The width of the covered strip can be tuned to the instrument swath so as to avoid any gaps. The drawback is that, after the first few daily visits over or close to the target area, the next sequence of visits occurs only after the completion of the repeat cycle.

With the current Landsat, the temporal evolution of the orbit tracks during the repeat cycle (16 days) results in two main sub-cycles, as shown in Figure 2.4. The two-day sub-cycle ensures a shorter temporal gap, but the seven-day sub-cycle provides a closer geographical match.

Although the concept of repeat cycles and sub-cycles stems from the requirements placed on the use of narrow-swath instruments, including those with nadir-only viewing, orbits with sub-cycles may also be useful for relatively wide-swath instruments. For example, sounding instruments may have a swath as wide as several thousand kilometres. (For example, the Advanced Microwave Sounding Unit (AMSU) or the Infrared Atmospheric Sounding Interferometer (IASI) have swaths of over 2 200 km). However, the quality of the products retrieved is higher when

Table 2.3. Repeat cycles and main sub-cycles for a number of orbits

	Sun-synchronous orbits					*Non-Sun-synchronous orbit*
Orbital height	*909 km (e.g. Landsat 1–3)*	*705 km (e.g. Landsat 4–8)*	*832 km (e.g. SPOT)*	*791 km (e.g. Envisat)*	*820 km (e.g. Metop)*	*1 336 km (e.g. JASON)*[a]
Period	103.2 min	98.9 min	101.5 min	100.6 min	101.3 min	112.4 min
No. of orbits/day	13 + 17/18	14 + 9/16	14 + 5/26	14 + 11/35	14 + 6/29	12 + 7/10[a]
Cycle	18 days	16 days	26 days	35 days	29 days	10 days[a]
Revolutions/cycle	251	233	369	501	413	127
Main sub-cycle(s)	1 day	7 days, 2 days	5 days	16 days, 3 days	5 days	3 days[a]

Note:
[a] In the case of the Joint Altimetry Satellite Oceanography Network (JASON), which is not Sun-synchronous, the figures refer to a day of 23 h 48 min in duration, that is, 0.99156 of the duration of a solar day.

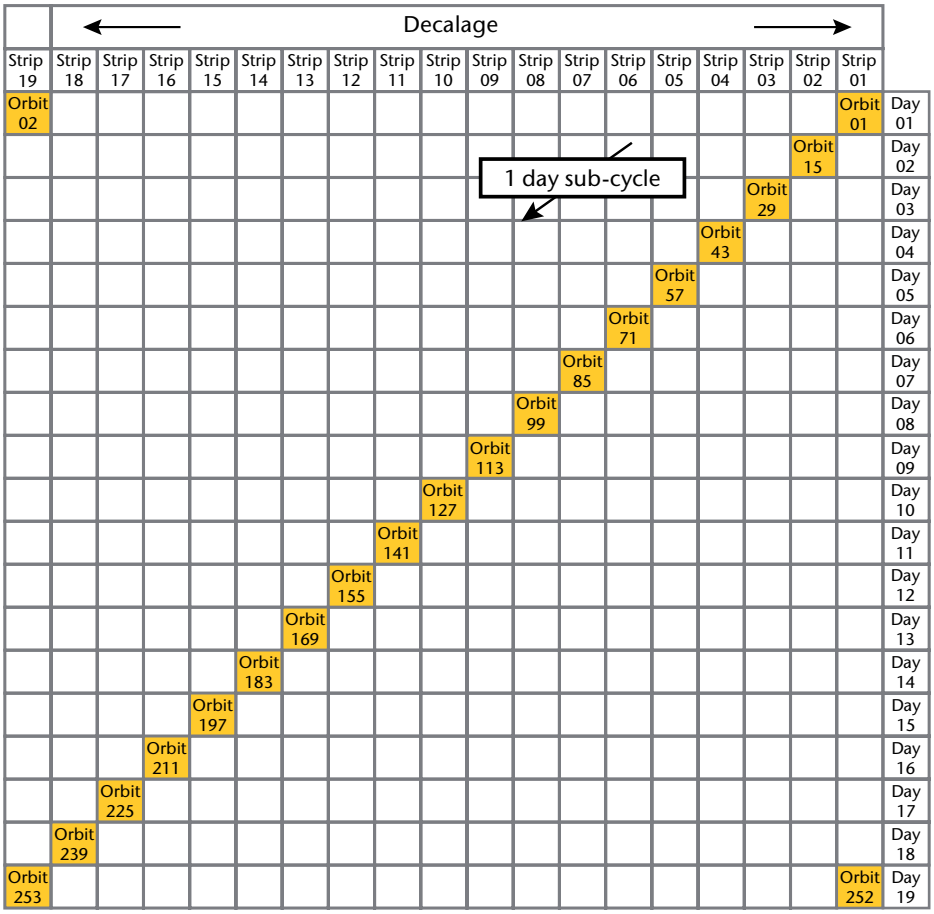

Figure 2.3. Schematic evolution of the orbital track of early Landsat over a repeat cycle (N = 13 + 17/18, repeat cycle: 18 days, 251 revolutions/cycle)

closer to the nadir sub-track. Therefore, there is an interest in ensuring that the coverage provides a fair blend of higher and lower quality data. Orbits for the NOAA satellites and Meteorological Operational (Metop) satellites have a five-day sub-cycle, as shown in Figure 2.5 for Metop.

Repeat cycles and sub-cycles are convenient for several reasons, but a few drawbacks should also be noted:

(a) If the instrument swath is too narrow with respect to the decalage (shift) and the number of orbital passes during the repeat cycle, some areas will never be observed. An extreme case is a nadir-only viewing instrument such as an altimeter.

(b) The day-to-day sequence of observations from a repeat-cycle orbit may introduce sampling biases in the observations (a spurious wavelength corresponding to a repeat cycle or sub-cycles).

(c) Maintenance of the repeat cycle/sub-cycles requires costly satellite orbit control systems.

Therefore, if all instruments on board have a sufficiently wide swath, a repeat cycle or sub-cycle is generally not carried out.

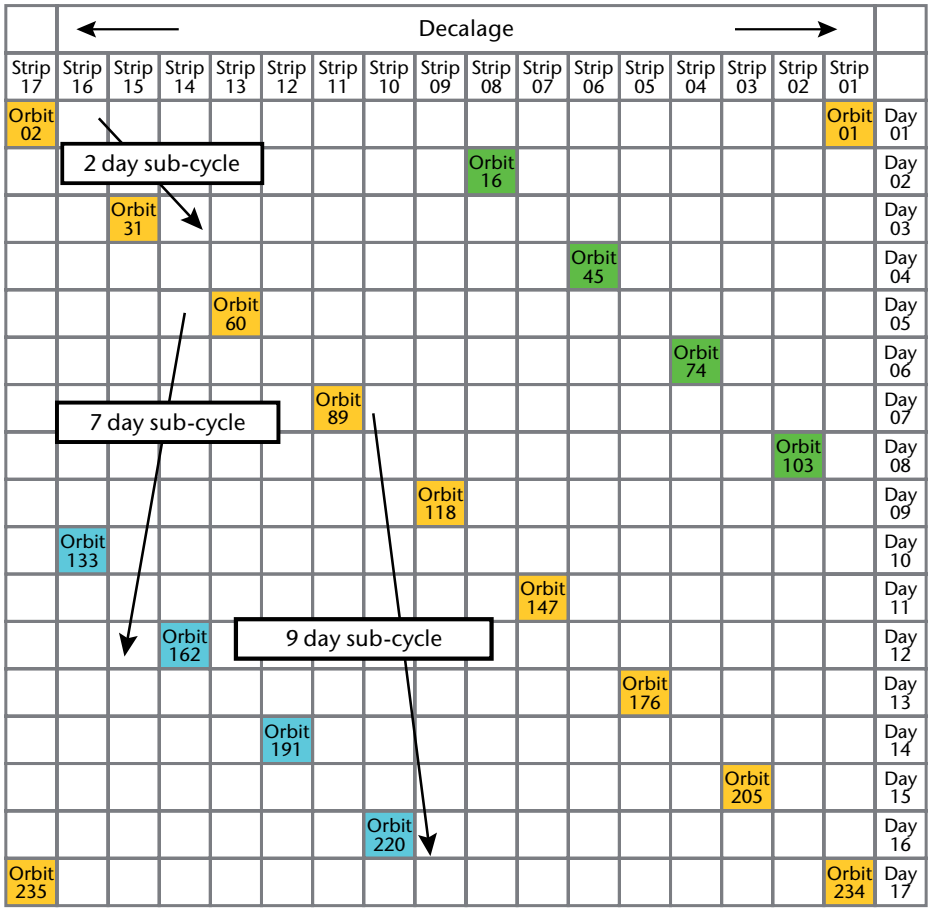

Figure 2.4. Schematic evolution of the orbital track of current Landsat over a repeat cycle ($N = 14 + 9/16$, repeat cycle: 16 days, 233 revolutions/cycle). Three sub-cycles are shown: seven days (westbound), the main one, providing the closest observations in space; two days (eastbound), for closer observations in time; and nine days (eastbound), of marginal interest, the sum of the first two sub-cycles.

2.1.3 Orbital precession, Sun-synchronous orbits and drifting orbits

The orbital plane can lie in the Earth's equatorial plane or be inclined by ε degrees (see Figure 2.6).

For $\varepsilon = 90°$, the satellite follows a meridian line and the orbit is polar. This is very convenient for observing the Earth's surface pole-to-pole.

The gravity field acting on the satellite is perpendicular to the geopotential surface at satellite altitude, which is slightly ellipsoid like the geoid. Where $\varepsilon \neq 90°$, the effect of these forces is a precession of the orbital plane around the polar axis. The precession rate α is computed as:

$$\alpha = -10.02 \cos \varepsilon \left(1 + \frac{H}{R}\right)^{-\frac{7}{2}} \quad \left(\text{degree/day}\right) \tag{2.4}$$

For a purely polar orbit ($\varepsilon = 90°$), the precession rate is thus zero. The orbital plane has an invariant orientation with respect to the fixed stars. However, as the Earth rotates around the Sun over one year, the illumination conditions of the surface, as viewed by the satellite, change every day by 360/365 degrees; that is 59 min. An area viewed in daylight at noon on day t_0 will be viewed in dawn conditions on day $t = t_0 + 3$ months (Figure 2.7, left panel). For measurements in daylight, this would mean different observing conditions day after day, with seasonally-dependent observation times. In particular, when the Earth–Sun direction becomes perpendicular to the orbital plane, the illumination in dawn–dusk conditions makes many measurements impossible.

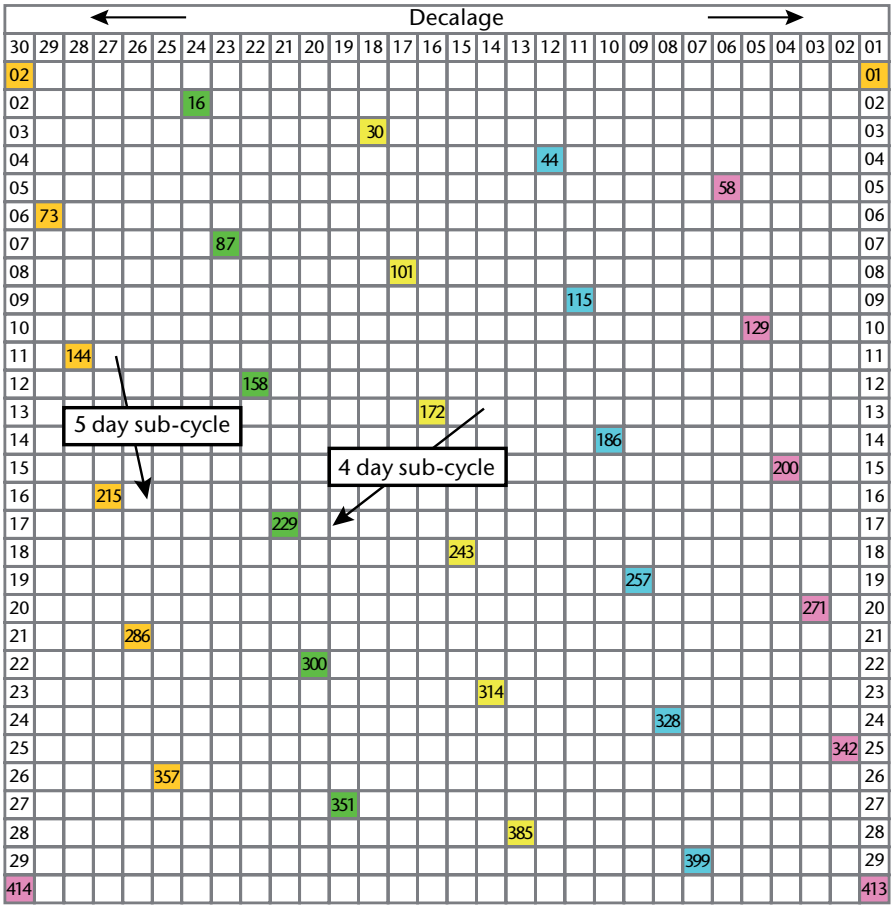

Figure 2.5. Schematic evolution of the orbital track of Metop ($N = 14 + 6/29$, repeat cycle: 29 days, 412 revolutions/cycle). Two sub-cycles are shown: five days (eastbound), the main one, providing the closest observations in space; and four days (westbound), for marginally closer observations in time.

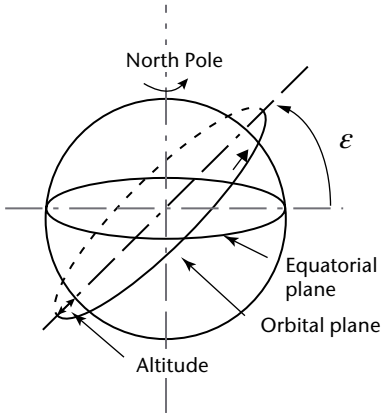

Figure 2.6. Definition of inclined orbit

The orbital inclination ε can be set in such a way that the precession rate exactly matches the yearly revolution of the Earth around the Sun. By imposing the value α = 360/365 (degree/day) in equation 2.4, it is found that the inclination ε_0 must satisfy:

$$\cos \varepsilon_0 = -0.0988 \, (1 + \frac{H}{R})^{\frac{7}{2}} \qquad (2.5)$$

An orbit that satisfies that condition is called Sun-synchronous. The negative value of ε_0 indicates that the orbit is retrograde with respect to the Earth's rotation. The local solar time of the areas overflown by the satellite at a given latitude is constant across the whole year (see Figure 2.7, right panel). Table 2.4 presents the ε_0 values of a number of Sun-synchronous orbits as a function of orbital height.

Table 2.4. Inclination values of Sun-synchronous orbits as a function of orbital height

400 km	*600 km*	*800 km*	*1 000 km*	*1 200 km*	*1 400 km*
97.02°	97.78°	98.60°	99.47°	100.41°	101.42°

Note that the deviation from the polar axis increases with orbital height. This is a drawback for high Sun-synchronous orbits: the poles might not be observed unless the instrument swath is wide enough. However, for relatively low orbital heights, the orbital plane is near-polar.

The most important feature of a Sun-synchronous orbit – the fixed local solar time – may be a disadvantage for certain types of measurements. Diurnally-varying phenomena (for example, convective clouds, precipitation, radiation budget, sea level affected by astronomical tides) display biased sampling if observed from a Sun-synchronous satellite (that is, at a fixed local solar time).

In general, satellites for operational meteorology, land observation and oceanography, with the exception of geodetic-quality altimetry, use a Sun-synchronous orbit. Scientific missions focused on processes affected by diurnal variation, which require unbiased sampling, may favour non-Sun-synchronous (drifting) orbits.

2.1.4 Elliptical orbits

The previous sections are applicable to circular orbits, which are by far the most widely used in Earth observation, particularly for Sun-synchronous and geostationary orbits. However, both near-polar low Earth orbits (LEO) and geostationary Earth orbits (GEO) have several limitations.

A near-polar LEO satellite provides global but infrequent coverage. Even if the instrument swath is as large as the decalage, thus providing contiguous coverage by consecutive orbits, one satellite can cover the whole of the Earth's surface twice a day at most (or even once a day if sensing can be performed either in daylight only or only in night-time conditions). If more frequent global coverage is needed, additional satellites in complementary orbital planes are necessary (see Table 2.5).

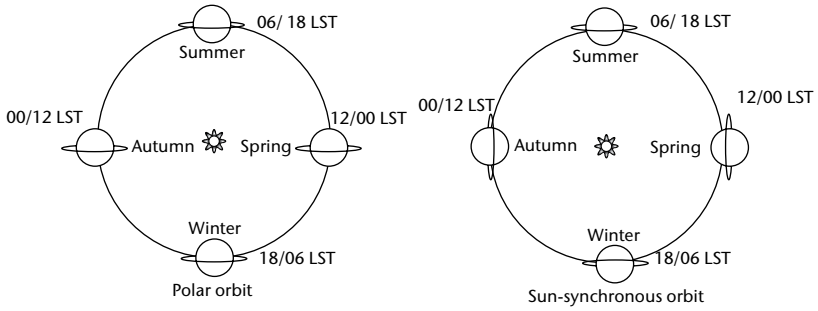

Figure 2.7. Left: Pure polar orbit with changing local solar time (LST) throughout the year; right: Sun-synchronous orbit with fixed LST throughout the year

It is clear from Table 2.5 that any observing cycle shorter than, for instance, three hours, would be extremely demanding, as it would require a constellation of LEO satellites in coordinated orbits.

The coverage improves substantially for high latitudes (see Figure 2.2). For example, coverage is twice as frequent at 60° latitude than at the Equator. In polar regions, the frequency of coverage becomes close to the orbital period T (~100 min) or sub-hourly with more satellites.

A shorter observing cycle may be obtained by leaving aside the Sun-synchronous feature and adopting a lower inclination, but the coverage is then no longer global. Low-inclination orbits are used for monitoring the intertropical zones.

The GEO orbit provides observations at a rate that is limited only by the instrument. However, a constellation of about six satellites around the Equator is needed to cover all longitude sectors up to a latitude of at least 55°; the highest latitudes cannot be covered.

Some of these limitations can be mitigated by adopting an elliptical orbit. On an elliptical orbit, the satellite speed changes along the orbit; it is minimal around the apogee allowing more time for acquiring measurements from the overflown area. Elliptical orbits are usually optimized for specific purposes, particularly for space science, such as to collect in situ measurements up to very high altitudes by physically passing through the ionosphere and plasmasphere.

One problem of elliptical orbits is that, since the argument of the perigee is affected by the secular perturbation, the apogee occurs at latitudes that change with time. The secular perturbation can be compensated for if the orbital inclination is $\varepsilon = \sin^{-1}(4/5)^{1/2} \approx 63.4°$. In this case, the apogee region where the satellite dwells for most of the time is stable. In that position, measurements can be taken very frequently, in a quasi-geostationary fashion.

The highly elliptical orbit (HEO), an elliptic orbit with high eccentricity, has been used for telecommunication satellites and is being considered for Earth observation: Molniya (Figure 2.8), which has a 12 h period and an apogee at 39 800 km; and Tundra, which has a 24 h period and an apogee at 48 300 km. In the Molniya orbit, the satellite is nearly geostationary for about 8 h of the 12 h period. In the Tundra orbit, it is nearly geostationary for about 16 h of the 24 h period.

The Molniya and Tundra orbits only serve one hemisphere in quasi-geostationary fashion. In addition, the 8 h or 12 h quasi-geostationary observing area is centred on a specific local solar time. If all latitudes above 60° have to be covered 24 h a day, three Molniya satellites or two Tundra satellites are required. An interesting variant is the three-apogee orbit with a 16 h period and an apogee at 43 500 km. Table 2.6 presents the main features of Molniya and Tundra orbits. In the apogee position, which is useful for frequent sampling, the height of the satellite exceeds GEO height.

Table 2.5. Number of LEO satellites needed to achieve a required observing cycle (assumed height: H = 800 km)

Instrument swath	*Observing capability*	*Required observing cycle*						
		24 h	*12 h*	*8 h*	*6 h*	*3 h*	*2 h*	*1 h*
2 800 km	Only in daylight	1 sat	2 sat	3 sat	4 sat	8 sat	12 sat	24 sat
	Night and day	0.5 sat	1 sat	1.5 sat	2 sat	4 sat	6 sat	12 sat
1 400 km	Only in daylight	2 sat	4 sat	6 sat	8 sat	16 sat	24 sat	48 sat
	Night and day	1 sat	2 sat	3 sat	4 sat	8 sat	12 sat	24 sat

Table 2.6. Main features of Molniya and Tundra orbits (apogee and perigee heights can be slightly adapted to need)

Orbit type	*Inclination*	*Period*	*Apogee*	*Perigee*	*Coverage (from one satellite)*	*Sats for hemispheric coverage*
Molniya	63.4°	12 h	~39 800 km	~1 000 km	Visible over 2 positions for ~8 h	3
Tundra	63.4°	24 h	~48 300 km	~24 000 km	Visible over 1 position for ~16 h	2

Figure 2.8. The Molniya orbit

2.1.5 Launchers and injection into orbit

Satellites are injected into orbit by a launcher, which has to perform the following functions:

(a) To host the satellite in the fairing, where vital functions for the satellite are ensured. When in the fairing, the satellite is stowed in a compact configuration to minimize volume occupancy and to be protected against the effects of acceleration.

(b) To bring the satellite to orbit. In order to minimize the total mass brought to high altitudes, the launcher is generally structured by stages. The first stage, which is the heaviest since it has to provide the maximum thrust for lift-off, is separated early. The fairing is released at an appropriate altitude. A further one or two stages are fired and separated in sequence.

(c) To release the satellite. For satellites in LEO circular orbits, the launcher releases the satellite directly on the final orbit. For elliptical orbits, the launcher releases the satellite at the perigee and provides it with a last acceleration to acquire the energy corresponding to the intended orbit.

When in orbit, the satellite deploys its solar panels and starts autonomous operations. One of the operations is to reach final orbit by activating its propulsion system. In the case of a geostationary orbit, the satellite is released at a perigee in an elliptical orbit whose apogee is 35 786 km, and is equipped with an apogee boost motor. The motor, which uses solid, hybrid or more often, liquid propellant (a liquid apogee motor), is fired at the apogee to provide the acceleration necessary to circularize the orbit (see Figure 2.9).

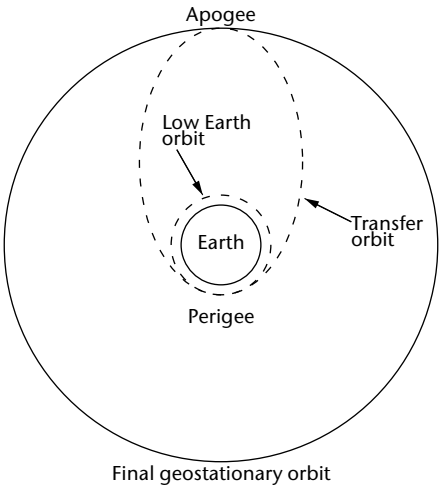

Figure 2.9. Achievement of GEO

Launching a satellite is a complicated and costly exercise. In order to optimize cost-effectiveness, a launch is often shared by several satellites. In this case, the task of the last stage is extended to release the various satellites at different times to separate the orbits. The respective platform propulsion systems will thereafter achieve the transfer to the final orbits.

The launch of small satellites and cubesats forming constellation structures is a good example of the usefulness of multiple launches. One effective launching strategy is known as the Walker Delta Pattern. The orbital inclination ε of all satellites must be the same. Either the launcher releases the satellites at different altitudes, or the satellite propulsion systems spread them into different altitudes. Therefore, each orbit will have a different precession rate, according to equation 2.4, and the orbital phases will differentiate as time elapses. When the orbits of all the satellites are appropriately spaced, the platform propulsion systems will bring each of the satellites to the desired altitude H. Equation 2.4 shows that, in practice, the strategy works well for relatively low inclinations and relatively low altitudes, otherwise the time needed to deploy the constellation becomes too long. For example, the Constellation Observing System for Meteorology, Ionosphere and Climate (COSMIC) (six satellites, $H = 800$ km, $\varepsilon = 71°$) took one year to deploy.

2.2 PRINCIPLES OF REMOTE-SENSING

Earth observation from space is mainly performed by exploiting electromagnetic radiation. The few exceptions are in situ measurements at platform level (of gravity field, magnetic field, electric field and charged particle density in the solar wind). This section deals with remote-sensing of the Earth and focuses on:

(a) The electromagnetic spectrum and the ranges used for remote-sensing;

(b) The basic laws of interaction between electromagnetic radiation and matter;

(c) Observations in the atmospheric windows;

(d) Observations in absorption bands;

(e) Limb sounding and radio occultation;

(f) Active sensing.

2.2.1 The electromagnetic spectrum and the ranges used for remote-sensing

The spectrum of electromagnetic radiation as observed from space (with nadir viewing) is shown in Figure 2.10. The displayed range (0.2 μm to 3 cm (or 10 GHz)) includes all that is used for remote-sensing from space. The variation in wavelength is due to the interposed atmosphere, with transmissivity ranging from 1 (atmospheric window) to 0 (full opacity due to total atmospheric absorption).

Table 2.7 presents definitions of the subdivisions of the spectrum that are generally accepted, though not standardized. In addition to the commonly used wavelength λ and frequency ν, the wave number ν^*, mostly used in spectroscopy, is also quoted.

Table 2.7. Bands of the electromagnetic spectrum exploited for remote-sensing

	Spectrum subdivision	*Wavelength λ*	*Wave number $\nu^* = 1/\lambda$*	*Frequency $\nu = c/\lambda$*
UV	Ultraviolet	0.01–0.38 μm	26 320–1 000 000 cm^{-1}	
B	Blue	0.436 μm	22 935 cm^{-1}	
G	Green	0.546 μm	18 315 cm^{-1}	
R	Red	0.700 μm	14 285 cm^{-1}	
VIS	Visible	0.38–0.78 μm	12 820–26 320 cm^{-1}	
NIR	Near infrared	0.78–1.30 μm	7 690–12 820 cm^{-1}	
VNIR	Visible and near infrared (VIS + NIR)	0.38–1.3 μm	7 690–26 320 cm^{-1}	
SWIR	Short-wave infrared	1.3–3.0 μm	3 330–7 690 cm^{-1}	
SW	Short wave	0.2–4.0 μm	2 500–50 000 cm^{-1}	
LW	Long wave	4–100 μm	100–2 500 cm^{-1}	
MWIR	Medium-wave infrared	3.0–6.0 μm	1 665–3 330 cm^{-1}	
TIR	Thermal infrared	6.0–15.0 μm	665–1 665 cm^{-1}	
IR	Infrared (MWIR + TIR)	3–15 μm	665–3 330 cm^{-1}	
FIR	Far infrared	15 μm–1 mm	10–665 cm^{-1}	300–20 000 GHz
Sub-mm	Submillimetre wave (part of FIR)	0.1–1 mm	10–100 cm^{-1}	300–3 000 GHz
Mm	Millimetre wave (part of MW)	1–10 mm	1–10 cm^{-1}	30–300 GHz
MW	Microwave	0.1–30 cm	0.033–10 cm^{-1}	1–300 GHz

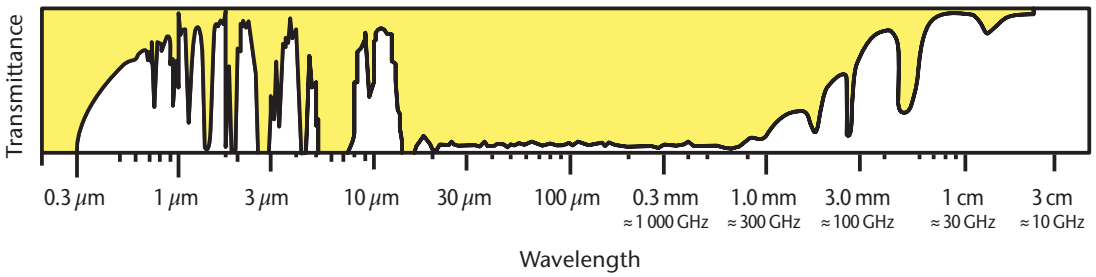

Figure 2.10. Spectrum (transmissivity) of electromagnetic radiation as observed from space with nadir viewing; range: 0.2 μm to 3 cm

A finer subdivision of the MW range and nearby FIR, used for radar but also by extension, for passive radiometry, is provided in Table 2.8.

The overall spectrum shown in Figure 2.10 comprises five distinct regions, each with rather different features.

In the UV region, atmospheric absorption is strong, mainly due to the major air constituents (nitrogen (N_2) and oxygen (O_2)) and trace gases (the most important being ozone (O_3)). The Earth's surface cannot be observed in that spectral region. The radiation source for remote-sensing consists of reflected solar radiation.

The VIS, NIR and SWIR regions, from 0.4 to 3 μm and, in some cases, up to 4 μm, can be sensed by means of reflected solar radiation. This range includes several transparent regions (windows) and many absorption bands (see Figure 2.11).

Table 2.8. Bands used in radar technology (according to the American Society for Photogrammetry and Remote-sensing)

Band	*Frequency range*	*Wavelength range*
P	220–390 MHz	77–136 cm
UHF	300–1 000 MHz	30–100 cm
L	1–2 GHz	15–30 cm
S	2–4 GHz	7.5–15 cm
C	4–8 GHz	3.75–7.5 cm
X	8–12.5 GHz	2.4–3.75 cm
K_u	12.5–18 GHz	1.67–2.4 cm
K	18–26.5 GHz	1.1–1.67 cm
K_a	26.5–40 GHz	0.75–1.18 cm
V	40–75 GHz	4.0–7.5 mm
W	75–110 GHz	2.75–4.0 mm

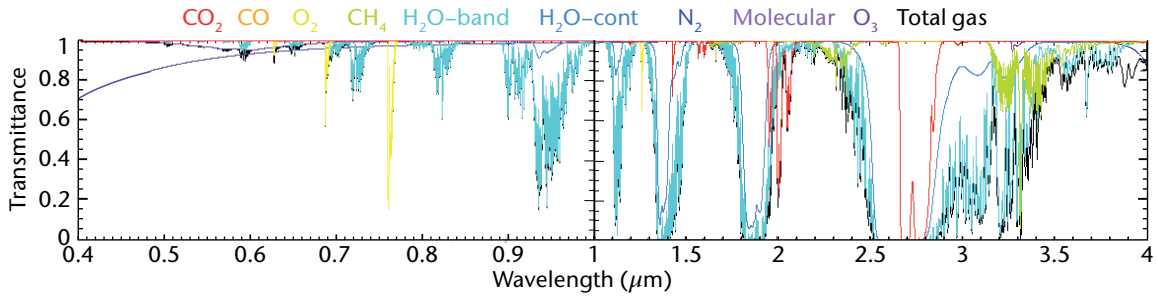

Figure 2.11. Atmospheric spectrum in the range 0.4 to 4.0 μm. It includes several windows and absorption bands from carbon monoxide (CO, about 2.3 μm), carbon dioxide (CO_2, about 1.6, 2.1 and 2.8 μm), methane (CH_4, about 2.3 and 3.4 μm), several oxygen bands (O_2, mainly about 0.77 μm), some nitrogen (N_2) and ozone (O_3) bands, and many important bands of water vapour (H_2O, mainly 0.94, 1.13, 1.37, 1.8 and 2.7 μm). Also shown is the molecular continuum, which prevents using UV for Earth surface and low atmosphere sensing from space.

In the MWIR and TIR regions, from 4 to 15 μm, the radiation source consists of the thermal emission from the Earth's surface and the atmosphere, which is mainly driven by water vapour and carbon dioxide absorption/emission. These are important contributors to the greenhouse effect. This thermal emission combined with the main atmospheric window enables the planet's thermal equilibrium to be maintained at agreeable values (see Figure 2.12).

The next spectral region, the Far IR, ranges from 15 μm to 1 mm (or 300 GHz). It is fully opaque because of the water vapour continuum. In that region, which is difficult to explore because of the lack of efficient detection techniques, there are absorption lines of several important species, such as hydroxil radical (OH), known as a "cleaner" of the atmosphere, and hydrogen chloride (HCl), a reservoir species that releases ozone-aggressive chlorine. Hydroxil radical and hydrogen chloride are only observable in the FIR (for example, about 120 μm ≈ 2 500 GHz and 480 μm ≈ 625 GHz, respectively).

In the MW range, from 1 to 300 GHz, the radiation source consists of the thermal emission from the Earth's surface and the atmosphere. The atmospheric spectrum, starting from 2 GHz and extending to submillimetre frequencies up to 1 000 GHz, is shown in Figure 2.13.

In the portion of the MW range where the atmosphere is more transparent, (that is, at frequencies below about 100 GHz), the wavelengths exceed 3 mm and so are much larger than cloud drop size, except for precipitating clouds. Therefore, the MW range is used for observing the Earth's surface or atmospheric properties in nearly all weather conditions.

Active sensing is conditioned by technology and, in the case of MW, by radio-frequency spectrum regulations. Radar makes use of MW, while lidar makes use of optical wavelengths where suitable sources (crystals) are available. Table 2.9 presents a few commonly used radar frequencies and lidar wavelengths. As a comparison, the table also lists frequencies used by the global navigation satellite system (GNSS) and associated radio-occultation sensing of the atmosphere (see the present volume, Chapter 3, 3.2.7).

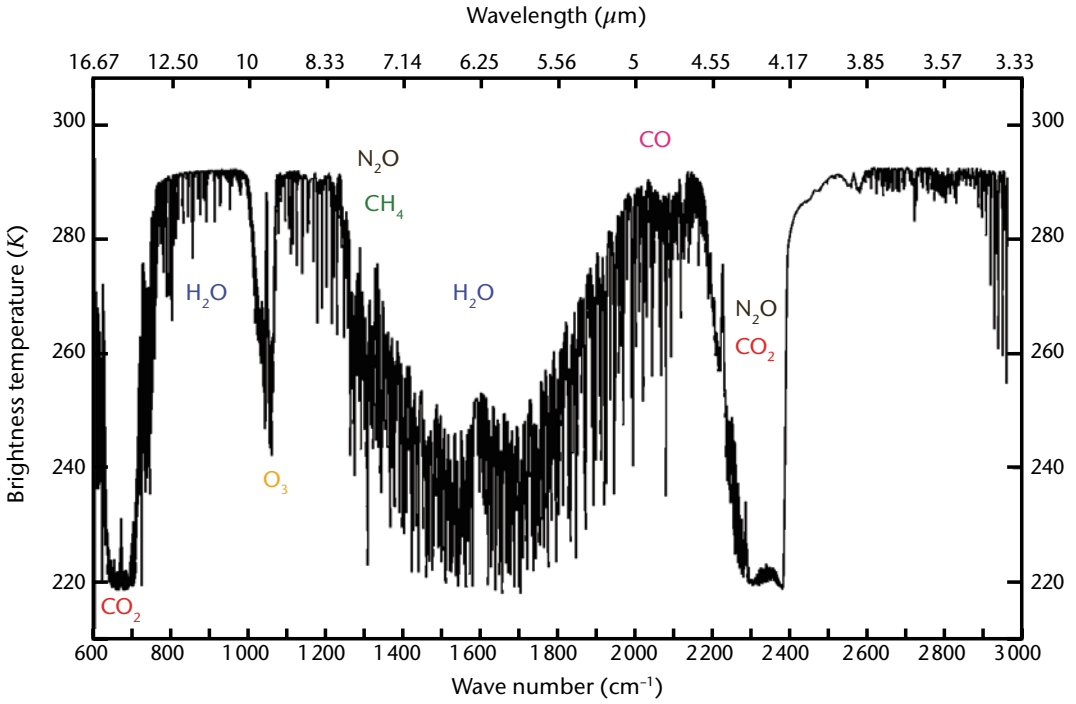

Figure 2.12. Atmospheric spectrum in the range 3.33 to 16.67 μm. The main atmospheric windows are in the ranges 3.7 to 4.0 μm and 10 to 12 μm. There are large absorption bands from water vapour (H_2O) and carbon dioxide (CO_2). Other species are: ozone (O_3, about 9.7 μm), methane (CH_4, about 7.7 μm), carbon monoxide (CO, about 4.6 μm) and nitrous oxide (N_2O, about 4.5 and 7.7 μm).

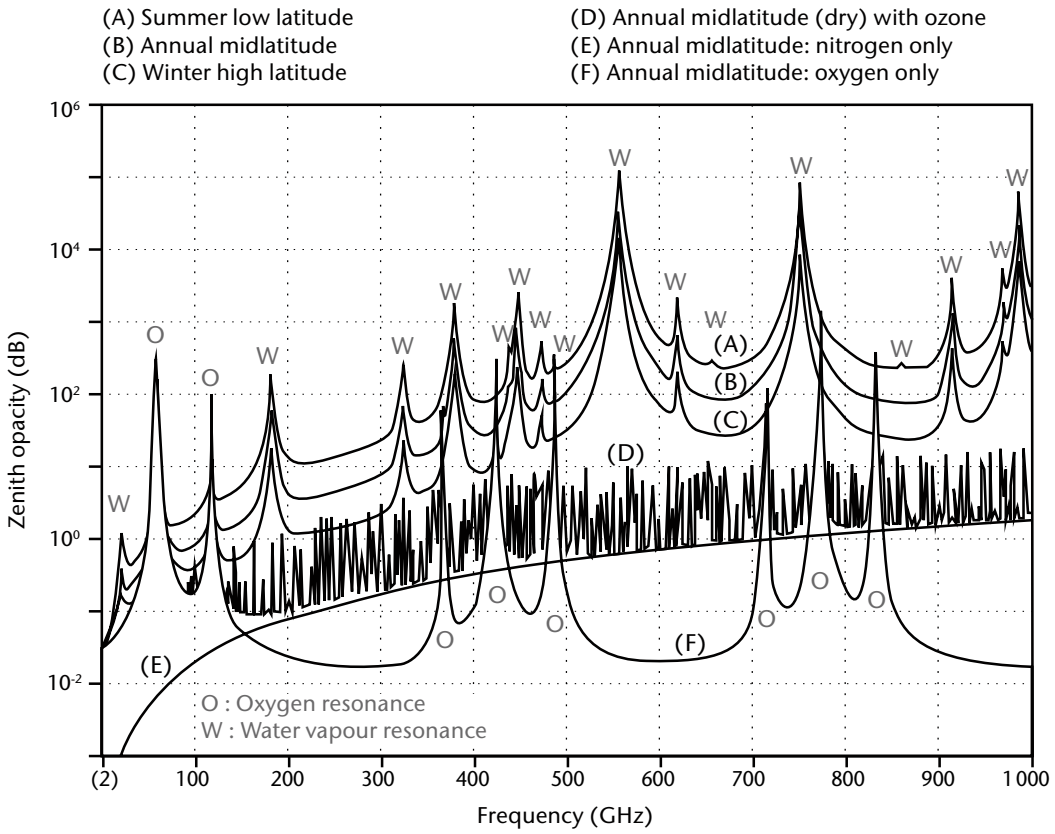

Figure 2.13. Atmospheric spectrum in the range 2 to 1 000 GHz. The dominant feature is the water vapour continuum that grows in opacity as frequency increases into the FIR range. This prevents viewing the Earth's surface at high frequencies from space. Invasive lines of ozone also dominate the spectrum. The most useful features are the oxygen bands (about 57, 118, 388, 424, 487 GHz and above), used to infer atmospheric temperature, and the water vapour bands (about 22, 183, 325, 380, 448 GHz and above).

Source: Klein and Gasiewski (2000).

2.2.2 Basic laws of interaction between electromagnetic radiation and matter

The macroscopic properties of a condensed body at thermodynamic equilibrium that is not affected by chemical or nuclear reactions are summarized in terms of electromagnetic radiation by three coefficients linked by the following equation:

$$\rho(\lambda, T, \zeta, \varphi) + \tau(\lambda, T, \zeta, \varphi) + \varepsilon(\lambda, T, \zeta, \varphi) = 1 \qquad (2.6)$$

In this equation, $\rho(\lambda,T,\zeta,\varphi)$ denotes reflectivity that is the ratio of the backscattered radiation $I(\lambda,T,\zeta,\varphi)$ to the incident radiation $I(\lambda)$; $\tau(\lambda,T,\zeta,\varphi)$ denotes transmissivity, or the fraction of $I(\lambda)$ that crosses the body; and $\varepsilon(\lambda,T,\zeta,\varphi)$ is the fraction of $I(\lambda)$ that is absorbed by the body – it is called emissivity for reasons explained below. The three coefficients depend on the radiation wavelength λ, the body temperature T, and the observing geometry ζ, φ (zenith and azimuth angles, respectively).

Table 2.9. Spectrum utilization from active instruments (radar and lidar) and radio occultation

	Observation	*Instrument*	*Frequency or wavelength*
Radar	Sea-surface wind	Scatterometer, SAR	C band (~5.3 GHz) or K_u band (~13.4 GHz)
	Ocean topography	Altimeter	C band (~5.3 GHz) + K_u band (~13.6 GHz)
	Cloud and precipitation	Rain radar, cloud radar	K_u band (~13.6 GHz) and/or K_a band (~35.5 GHz) or W band (~94 GHz)
	Imagery	Synthetic aperture radar	L band (~1.3 GHz) or C band (~5.4 GHz) or X band (~9.6 GHz)
Lidar	Clear-air wind	Doppler lidar	UV-lidar (355 nm)
	Aerosol, cloud top	Backscatter lidar	UV-lidar (355 nm), VNIR-lidar (532 + 1 064 nm)
	Ice-sheet topography	Altimeter	VNIR-lidar (532 + 1 064 nm)
Radio occultation	Atmospheric refraction	GNSS + Receiver in LEO	L band: ~1 580 + ~1 250 + ~1 180 GHz (Global Positioning System (GPS), Globalnaïa Navigatsionnaïa Spoutnikovaïa Sistéma (GLONASS) and Galileo)

A body that is not reflecting and is totally opaque to radiation on any wavelength (where $\rho = \tau = 0$, and thus $\varepsilon = 1$) is called a black body. It radiates at any temperature, T and over the full λ or ν spectrum, according to Planck's law:

$$B(\lambda, T) = \frac{2\pi hc^2}{\lambda^5} \frac{1}{e^{\frac{hc}{\lambda kT}} - 1} \quad \text{or} \quad B(\nu, T) = \frac{2\pi \nu^3}{c^2} \frac{h}{e^{\frac{h\nu}{kT}} - 1} \tag{2.7}$$

where:

$h = 6.6256 \cdot 10^{-34}$ J s (which is the Planck constant);
$c = 2.99793 \cdot 10^{8}$ m s^{-1} (which is the speed of light in a vacuum); and
$k = 1.38044 \cdot 10^{-23}$ J K^{-1} (which is the Boltzmann constant).

$B(\lambda,T)$ (or $B(\nu,T)$) is the radiative power per unit surface over the hemisphere per unit of wavelength (or frequency). The power radiated per unit of solid angle is B/π. The Planck function for temperatures of 6 000 K and 273.16 K, which are representative of the Sun and the Earth's surfaces respectively, is shown in Figure 2.14.

The power radiated over the full spectrum is:

$$W(T) = \int_0^\infty B(\lambda, T) \cdot d\lambda = \sigma \cdot T^4 \qquad \text{Stefan-Boltzmann law} \tag{2.8}$$

where $\sigma = 5.6681 \cdot 10^{-8}$ W m^{-2} K^{-4}.

The two curves in Figure 2.14 illustrate that the Sun's and Earth's surfaces have very different radiative powers. However, after scaling down the Sun curve by the square of the distance between the Sun and Earth, the two integrated areas become comparable, which reflects the Earth's radiative balance. If the upper curve in the figure is scaled, it is easy to see that the energy (radiative flux density) of solar radiation on Earth is very small for $\lambda > 4\ \mu$m.

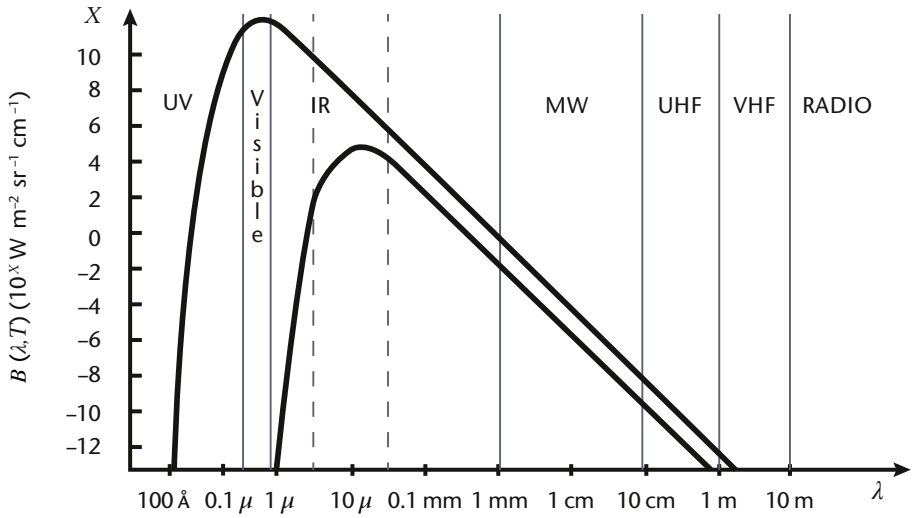

Figure 2.14. The Planck function for T = 6 000 K (the Sun) and T = 273.16 K (the Earth), shown in the higher curve and lower curve, respectively. X values in ordinate are to the power of 10.

A major difference between the two curves in Figure 2.14, after scaling, is the wavelength λ_{max} where the maximum emission occurs. This is given by:

$$\lambda_{max} = \frac{b}{T} \quad \text{with } b = 0.0028981 \text{ m K} \quad \text{Wien law} \tag{2.9}$$

Because of the double-logarithmic scale in Figure 2.14, it is difficult to appreciate how sharp the Planck function is around λ_{max}. In the case of solar radiation (T = 6 000 K) the peak emission occurs around λ_{max} = 0.5 μm and most of that power lies in the 0.2–3.0 μm range. In the case of terrestrial radiation (T = 273.16 K, that is, T = 0 °C) the peak is around λ_{max} = 10 μm and most of the power lies in the 3–50 μm range.

Another interesting feature of the Planck function is that, when moving from λ_{max} to shorter wavelengths, radiative power dramatically decreases, whereas when moving to longer wavelengths, the decrease is more gradual (approximately two thirds of power occurs at wavelengths longer than λ_{max}). For very long wavelengths, or low frequencies, such as those in the MW range, where the argument of the exponential in the Planck function is $h\nu/kT << 1$, the term $e^{h\nu/kT}$ becomes $\approx 1 + h\nu/kT$ and the Planck function thus reduces to:

$$B(\nu, T) = \frac{2\pi k \nu^2}{c^2} T \quad \text{Rayleigh-Jeans law} \tag{2.10}$$

Because of this relationship, radiation measurements in the MW range can be considered as temperature measurements and can be expressed as a brightness temperature (*TB*) in temperature units. While the total radiative power changes with temperature in proportion to T^4 according to the Stefan-Boltzmann law (equation 2.8), that power changes in a linear way in the MW portion of the spectrum. Conversely, when moving towards shorter wavelengths, the Planck function is increasingly dependent on temperature. Terrestrial radiation varies approximately with T^5 in the main TIR window around 11 μm and with T^{12} in the window around 3.7 μm. This is an interesting feature for remote-sensing, since it means that sensitivity to high temperatures is higher at 3.7 μm. Conversely, these shorter wavelengths are less sensitive to low temperatures.

For example:

(a) For a body at 220 K (such as a cloud top in the upper troposphere), the radiation at 11 μm is ~1 200 times greater than at 3.7 μm; but at 300 K (surface), it is only ~130 times;

(b) The sensitivity to temperature changes, (that is, $(\partial B/\partial T)/B$) is three times higher at 3.7 μm than at 11 μm.

As a consequence, 3.7 μm is well suited for surface observations, is optimal for fire detection, and is less useful for high clouds.

The relationship represented by equations 2.7–2.10 is only valid for a black body ($\varepsilon = 1$). For a common body, the relationship can be established through the following conceptual experiment. If a number of bodies in an isolated system only exchange radiation among themselves, it could be assumed that, after a transient time, each of them would reach thermodynamic equilibrium, where the radiation each absorbs according to its absorption coefficient $\varepsilon(\lambda,T)$ is equal to the power it radiates $P(\lambda,T)$. That is, $P(\lambda,T)/\varepsilon(\lambda,T)$ = constant. Assuming that one of the bodies is a perfect black body, this yields:

$$P(\lambda, T) = \varepsilon(\lambda, T) \cdot B(\lambda, T) \qquad \text{Kirchhoff principle} \tag{2.11}$$

This shows that the absorption coefficient introduced in equation 2.6 also controls the body's emission properties, hence the name emissivity. Equation 2.11 indicates two important consequences:

(a) At any wavelength and temperature, a body cannot radiate more than a black body at the same wavelength and temperature;

(b) A body can radiate only at wavelengths at which it can also absorb.

Emissivity ε is a function of wavelength and, to a lesser extent, temperature. For certain bodies, ε may be constant over large portions of the spectrum. If it is constant over the whole spectrum, the body is called grey. The shape of the radiated power $P(\lambda,T)$ is then exactly like $B(\lambda,T)$, although it is damped by a factor ε. The Wien law (equation 2.9) applies unchanged. The Stefan-Boltzmann law becomes $W(T) = \varepsilon \cdot \sigma \cdot T^4$.

The Kirchhoff principle also applies to gaseous materials. Therefore, spectral lines of atmospheric gases are generally (but not always) relevant to both absorption and emission.

2.2.3 Observations in the atmospheric windows

2.2.3.1 *Emerging radiation*

Atmospheric windows are spectral regions where the atmosphere is nearly transparent. There is no region where the atmosphere is fully transparent. All regions have some residual disturbance from species that have a continuum, the most common of which is water vapour in the IR, MW and, to some extent, the SW ranges. Another factor, particularly in SW, is scattering from dry air molecules (mostly N_2 and O_2) and aerosols. Ultimately, the most transparent windows are:

(a) In the SW (Figure 2.11): 0.5–0.9 μm, 1.6–1.7 μm and 2.0–2.3 μm;

(b) In the IR (Figure 2.12): 3.5–4.0 μm and 10–12 μm;

(c) In the MW (Figure 2.13): 80–100 GHz, 25–50 GHz and below 20 GHz.

Equation 2.6 indicates that the coefficients ρ (reflectivity), τ (transmissivity) and ε (emissivity) not only depend on radiation wavelength λ and body temperature T, but also on the geometric condition (zenith angle ζ and azimuth angle φ) of the satellite platform with respect to the body.

In order to simplify the discussion, the following conditions are assumed: vertical viewing from the satellite (Figure 2.15), flat surfaces and radiation towards the zenith (irradiance).

One component, $\tau(\lambda,T) \cdot l\tau(\lambda)$, is transmitted radiation through the body. It can be found where the body is not totally opaque and where a radiation source below it is in the opposite hemisphere compared to the satellite.

The component $\varepsilon(\lambda,T) \cdot B(\lambda,T)$ is emitted radiation, expressed through the Kirchhoff principle (equation 2.11). It is always present unless the body is at absolute thermal zero. It is not present in spectral regions, where the body does not absorb.

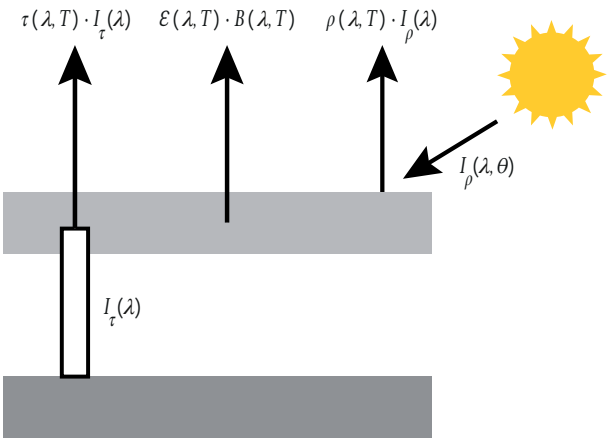

Figure 2.15. The three components of irradiance in space

The component $\rho(\lambda,T) \cdot I\rho(\lambda,\theta)$ is reflected radiation. It is found when a radiation source is in the same hemisphere as the satellite. Figure 2.15 indicates the Sun. However, in the MW range, where solar radiation is virtually zero, the full hemispheric sky radiates as a black body, at temperature $T = 2.725$ K, where the maximum power occurs at $\lambda_{max} = 1.9$ mm (160 GHz). The notation $I\rho(\lambda,\theta)$ indicates that the power of the incoming radiation depends on the angle of incidence θ. Normally for the Sun, $I\rho(\lambda,\theta) = S(\lambda) \cdot \cos\zeta$, where $S(\lambda)$ denotes incoming power with the Sun at its zenith.

Taking account of all components, the radiation reaching the instrument on the satellite can be expressed as:

$$I(\lambda,T) = \tau(\lambda,T)\cdot I_\tau(\lambda) + \varepsilon(\lambda,T)\cdot B(\lambda,T) + \rho(\lambda,T)\cdot I_\rho(\lambda,\theta) \qquad (2.12)$$

There is considerable variation along the spectrum, so that the significance of the measurement is reasonably stable only within narrow bandwidths around a specific wavelength (channels). However, some general information is also contained in a wider range of wavelengths (VIS + NIR + SWIR; MWIR + TIR; MW).

2.2.3.2 *Measurements in the visible, near-infrared and short-wave infrared range*

In this range, there is no thermal emission from the Earth ($B = 0$). Focusing first on the Earth's surface (land and ocean), the transmitted radiation is zero, since there is no source below the Earth's surface. Also when considering that reflectivity is nearly independent of body temperature, equation 2.12 reduces to:

$$I_{sw}(\lambda) = \rho(\lambda)\cdot S(\lambda)\cdot\cos\zeta \qquad (2.13)$$

Since the solar spectrum and observing geometry are known, the information carried by a measurement in a SW channel is uniquely associated to surface reflectivity. Many geophysical variables (vegetation parameters, ocean colour, texture of land) may be estimated by measuring reflectivity at several wavelengths. However, clouds are the objects that are most in evidence in SW. Equation 2.13 is not strictly correct for a cloud surface, since radiation from the underlying surface can transmit through them. However, this effect has a limited impact given:

(a) The total transmissivity through (downward and upward) the atmosphere;

(b) That the cloud is low;

(c) The originating radiation source (the Sun) is stronger than any surface below the cloud;

(d) The reflectivity of the underlying surface is low (except for sand desert, snow and ice);

(e) The reflectivity of clouds ρ is generally higher than any other terrestrial surface.

Therefore, equation 2.13 is a good approximation applicable to most clouds. There are some exceptions such as optically thin clouds (notably, thin cirrus).

Using SW-reflected radiation for quantitative purposes is not an easy exercise, since reflectivity is generally anisotropic. The simplest case occurs when the body, whatever the direction of the incoming radiation, and for any azimuth, homogeneously redistributes the reflected radiation from the zenith according to a cosine-law. This is called Lambertian reflection. In many cases, however, the body exhibits isotropic reflectance properties that should be measured a priori by observations under different viewing directions and for different directions of the incoming radiation. The final computation of the irradiance towards space requires hemispheric integration.

Using SW for Earth observation in atmospheric windows requires spectral sampling at several wavelengths (channels) since at any one wavelength, several bodies may have signatures, and one body may have a signature at several wavelengths. A multichannel capability is therefore necessary to distinguish and simultaneously retrieve the different properties of different bodies. For instance, clouds and snow have identical reflectance in VIS at 0.65 μm, but very different reflectance at 1.6 μm. In addition, channel bandwidths must be appropriate to their purpose. The most stringent are for ocean colour ($\Delta\lambda \approx 10$ nm), and then vegetation ($\Delta\lambda \approx 20$ nm), whereas for other surface features and for clouds, bandwidths of several tens of nanometres can be sufficient. The retrieval of trace gases at solar wavelengths requires a much better spectral resolution. Another feature that affects the quantitative use of VIS + NIR + SWIR is polarization: specular reflection tends to be privileged, with damping of the vertical component of the electric field. The Stokes vector, which in the SW range consists of three components (polarization in three directions with phase differences of 120°), fully describes the electric field, and so provides important information about the body's properties. Multipolarization is important for the observation of those bodies that do not have strong multispectral signatures. Typical examples would be aerosols and cirrus clouds (elongated ice crystals).

2.2.3.3 *Measurements in the medium-wave infrared and thermal infrared range*

In the 4–15 μm range, solar radiation is virtually zero. On the Earth's surface (land and ocean), transmitted radiation is also zero. Furthermore, considering that emissivity is nearly independent from body temperature, equation 2.12 reduces to:

$$I_{\mathrm{IR}}(\lambda, T) = \varepsilon(\lambda) \cdot B(\lambda, T) \tag{2.14}$$

Equation 2.14 is also approximately valid for clouds, since the transmissivity of clouds in IR is rather low (with the exception of thin cirrus).

The emissivity of most land surfaces, and certainly the ocean, is close to 1, with small variance. Therefore the information acquired by a measurement in an IR channel is closely associated with the Planck function (equation 2.7) or for a given wavelength, with the body's temperature.

At a specified wavelength λ or for a narrow channel $\Delta\lambda$ around λ, the Planck function (equation 2.7) may be easily inverted to retrieve the temperature, T:

$$T(\lambda) = \frac{hc}{\lambda k \ \ln\left[1 + \dfrac{2\pi hc^2}{\lambda^5 B(\lambda)}\right]} \tag{2.15}$$

However, T will not be the body's true temperature unless $\varepsilon = 1$. If the body's emissivity is known, and the channel bandwidth $\Delta\lambda$ is sufficiently narrow to enable ε to be considered as constant, an emissivity correction can be applied to the measured quantity (by inverting

$B(\lambda,T) = I_{IR}(\lambda,T)/\varepsilon(\lambda)$), and the body's temperature can be measured. Otherwise, by inverting the measured quantity $B(\lambda,T) = I_{IR}(\lambda,T)$, a temperature *TBB* (equivalent black-body temperature) is obtained that is lower than the body's true temperature.

For a large variety of bodies where ε is close to 1, radiance observation in a TIR atmospheric window enables rather accurate temperature measurement. It is particularly accurate in the case of the sea, whose emissivity is close to 0.98. However, emissivity is not the only effect that needs to be corrected. As previously mentioned, the atmospheric windows are not perfectly transparent. For instance, the main window in TIR, 10–12 μm, is contaminated by the water vapour continuum, particularly on the long-wave side. One way to reduce this disturbance is to split the window into two channels, generally 10.3–11.3 μm and 11.5–12.5 μm. Differential absorption is then used to estimate a correction (total column water vapour can also be estimated as a by-product).

As a result of those effects, equation 2.15 indicates a dependence of the retrieved temperature on the wavelength (although as there is only one body temperature, that dependence should not exist). The spread of values with wavelength implies how certain information might be explained. For instance, by comparing *TBB* measured at 3.7 μm and 11 μm it is possible to explain the difference in terms of different emissivity, or in terms of different contamination of the measurement from clouds.

It is important to note that the 3.7 μm window behaves very differently in daylight and at night. In daylight, it is strongly contaminated by reflected solar radiation, which needs to be subtracted before using the channel for quantitative thermal emission estimates. As previously noted, the 3.7 μm window is much more sensitive to high temperatures than the 11 μm window. However, the 3.7 μm window is of little use for low temperatures, such as those found in cloud tops in the upper troposphere. The differential response to the temperatures of the 3.7 and 11 μm windows can also be used for detecting fog at night.

As regards clouds, equation 2.14 is still approximately valid. However, with the exception of optically thick clouds (typically cumulus or nimbus-stratus), emissivity is lower than unity. Equivalent black-body temperature substantially underestimates true temperature, and a correction must be applied to account for low emissivity. The usual method is to couple the window channel with a channel that is strongly sensitive to water vapour. The difference between the two *TBB* values indicates the cloud emissivity: the larger the difference, the lower the emissivity.

The penetration of infrared radiation in clouds is very low. Measured temperature refers to the top surface, and information about the interior of clouds is poor, especially for dense clouds. However, the temperature of cloud tops that is in equilibrium with air temperature at the same level is very important, because it indicates the altitude of the cloud in the troposphere, and therefore the cloud type.

Information derived from black-body temperature about the cloud-top level is often inaccurate. With thin clouds, such as thin cirrus, the background surface is much warmer than the air at cloud level. As a result, surface radiation transmitted through the cloud adds to the cloud emission, the cloud appears warmer, and the assigned level is underestimated. Conversely, thick cirrus with high emissivity are observed as very cold, and may be confused with cumulonimbus.

In order to resolve such ambiguities, it is useful to plot VIS brightness and IR temperatures as bi-dimensional histograms (Figure 2.16). By using only one band (the projection of the 2D pattern on one axis), several clusters would be unresolved. By contrast, this example shows that 10 different objects can be identified through multi-band analysis. This is a simple example using an old instrument (a very high resolution radiometer (VHRR)) and only two channels in VIS and IR. Current multi-band analysis techniques can operate with many more channels.

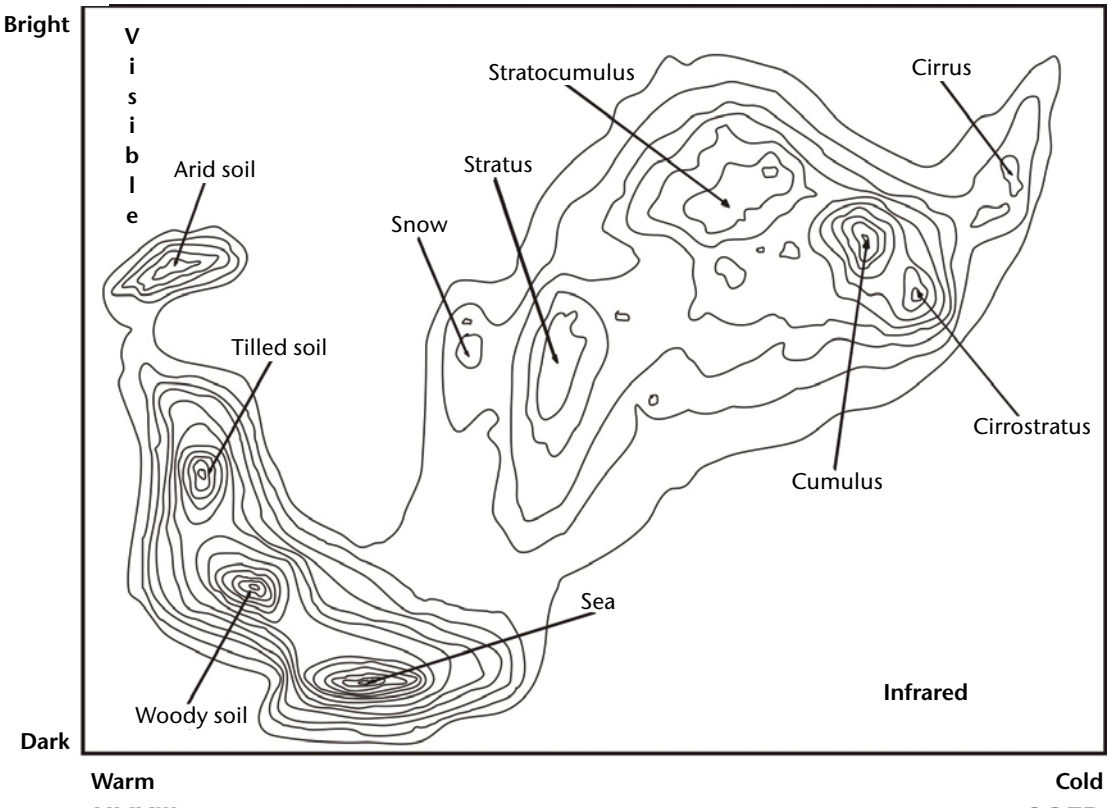

Figure 2.16. Scatterplot of VIS (0.65 μm) versus IR (11.5 μm), enabling the classification of 10 bodies. If projected onto one of either two axes, several clusters would be unresolved.

Source: Bizzarri and Tomassini (1976).

2.2.3.4 ***Measurements in the microwave range***

In the MW range, solar radiation is virtually zero, but there is a diffuse source of incoming radiation: the sky. Transmitted radiance is zero with regard to the Earth's surface, including land and sea. There are only two contributions: thermal emission and reflected radiation. Those are controlled by emissivity and reflectivity coefficients which, since $\tau = 0$, are linked by the condition $\varepsilon + \rho = 1$ (that is, $\rho = 1 - \varepsilon$). By expressing radiative power in units of temperature according to the Rayleigh-Jeans equation (2.10), observed brightness temperature, *TB*, can be rendered:

$$T_B(\nu) = \varepsilon(\nu) \cdot T + \left[1 - \varepsilon(\nu)\right] \cdot T_{\text{sky}}(\nu) \tag{2.16}$$

$T_{\text{sky}}(\nu)$, sky brightness temperature, is composed of background cosmic radiation and the contribution of precipitating clouds; it changes with frequency. In the main window and under non-precipitating conditions, where $\nu \sim 40$ GHz, $T_{\text{sky}}(\nu)$ may be ~140 K. Under heavy precipitation conditions, T_{sky} may reach values as large as ~250 K.

The impact of $T_{\text{sky}}(\nu)$ strongly depends on the value of the emissivity, ε. Sea and land have substantially different ε values.

The emissivity of the sea in the MW range is very low: $\varepsilon \approx 0.5$. As a result, the two components in equation 2.16 have equal weight. In the absence of precipitating clouds, T_{sky} is low and known: the measurement can therefore be associated with sea-surface temperature. The optimal frequency for sea-surface temperature is about 5 GHz (see Figure 2.17) where T_{sky} is much smaller than that at 40 GHz. The measurement is rather accurate and is also applicable in all weather, since the wavelength ($\lambda = 6$ cm) is much longer than any rain droplet. The 5 GHz sea-surface signal intensity is representative of the temperature of a few millimetres of the deep-water layer (sub-skin); that should be compared to a few tens of micrometres in the case of IR (skin

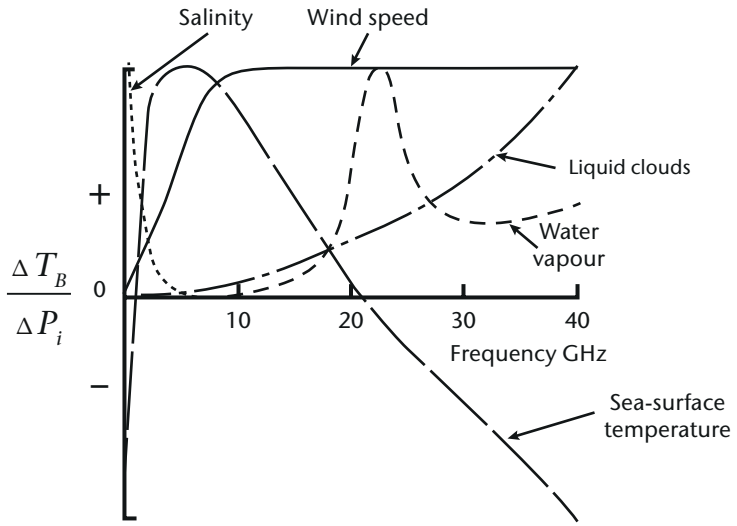

Figure 2.17. Sensitivity (defined as Δ*TB*/Δ*Pi*) of MW frequencies to several geophysical variables (*P*)

temperature). At higher frequencies, T_{sky} strongly increases, especially in the presence of heavy precipitation. The high reflectivity value (1 – ε) is such that the observation is mainly an indicator of precipitation.

Over land, emissivity is close to unity. The second component in equation 2.16 is therefore ineffective, and precipitation is poorly detected. At higher frequencies (~90 GHz (λ = 3 mm)), radiation welling up from the surface is scattered by large droplets, and even more so by ice crystals in clouds. As a result, radiation reaching the satellite is decreased.

Polarization can also be used for measuring precipitation. Radiation reflected from the sea is strongly polarized: when crossing a precipitating cloud, it undergoes depolarization that can be measured to infer precipitation. The differential polarization can also be exploited over land, since the emerging radiation scattered from droplets and ice crystals is polarized.

Observation under several polarizations may also be useful, regardless of the objective of precipitation measurement. Differential polarization is sensitive to surface roughness – an effect which must be taken into account when measuring sea-surface temperature. This can also be used to infer wind speed over the sea, as indicated in Figure 2.17.

Figure 2.17 also indicates that MW radiation is sensitive to ocean salinity, but only at very low frequencies, typically about 1.4 GHz (L band). The figure also shows that in order to measure ocean salinity, it is necessary to account for sea-surface temperature and wind speed (or roughness). Similarly to salinity, there is a water vapour absorption band that contaminates the observation of temperature, wind and liquid cloud (precipitation). That band can also be used to infer total column water vapour (precipitable water) over the sea. In summary, different variables may have different signatures on various channels in the MW as well as the optical fields: multi-channel analysis is therefore needed.

Due to the totally different emissivity values of sea and land surfaces, the most obvious feature in a MW image is the land/sea boundary. Since the emissivity of ice is close to unity, sea ice is also an obvious observable in all weather conditions. MW images are particularly useful for geographical regions that are often overcast. In cases where emissivity is close to unity over land, a decrease in emissivity indicates the presence of water on the surface. This is because the emissivity of a body is controlled by its dielectric constant: water on land is a salt solution, which increases conductivity and thus decreases emissivity. This effect can be exploited to measure surface soil moisture and snow properties.

Soil moisture measurements can be rather accurate on bare soil, but can decrease in accuracy as vegetation increases. In order to penetrate vegetation, and to measure soil moisture at root level, very low frequencies must be used, either in L or P band. At higher frequencies (above 10 GHz), sensitivity to soil moisture is only significant if disturbance by vegetation is accounted for.

Two properties of snow are detectable in the MW range: surface melting conditions and, in the case of shallow snowpack, water equivalent. In the latter case, relatively high frequencies are preferred, as snow tends to be transparent at low frequencies. However, saturation can occur at very high frequency signals in the upper layers of the snowpack. Several frequencies with different penetration depths are therefore needed.

2.2.4 Observations in absorption bands

2.2.4.1 *The radiative transfer equation*

In an atmospheric absorption band, each layer of thickness dz absorbs radiation coming from below and re-emits it. Assuming zero reflectivity of the atmosphere in IR, the atmospheric transmittance from a height z to a satellite altitude H is given by:

$$\tau(\lambda, z) = e^{-\int_z^H \varepsilon(\lambda,z)\cdot N(z)\cdot dz} \tag{2.17}$$

where $N(z)$ is the concentration of the absorbing gas.

The radiative contribution of an atmospheric layer of thickness dz, at height z and associated with a transmittance change of $d\tau$ (I,z), is: $dI(\lambda,z) = B[\lambda,T(z)] \cdot d\tau(\lambda,z)$.

The radiation from the total atmospheric column to the satellite is:

$$I(\lambda) = \int_{\tau(\lambda,z_s)}^{1} B[\lambda, T(z)] \cdot d\tau(\lambda, z) \tag{2.18}$$

where *zs* is the height of the Earth's surface.

A terrestrial contribution should be added, attenuated by the total atmospheric transmittance. In addition, the weighting function can be defined as:

$$K(\lambda, z) = \frac{d\tau(\lambda, z)}{dz} \tag{2.19}$$

The combined radiation reaching the satellite is given by the radiative transfer equation:

$$I(\lambda) = B(\lambda, T_s) \cdot \tau(\lambda, z_s) + \int_{z_s}^{H} B[\lambda, T(z)] \cdot K(\lambda, z) \cdot dz \tag{2.20}$$

Figure 2.18 shows that the transmittance (equation 2.17) tends to 1 as height z increases (that is, as the thickness of the atmospheric layer between height z and satellite altitude H decreases). This is accompanied by a decrease in emissivity ε and a decrease in concentration N of the absorbing gas. The weighting functions have peak values that correspond to the inflection point of the transmittance function. A simple way to read equation 2.20 is that each atmospheric layer of thickness dz contributes to the radiation reaching the satellite according both to its temperature (through the Planck function), and also to its effectiveness to contribute, as quantified by the weighting function. The weighting function depends on the concentration of the absorbing gas and the strength of absorption/emission (ε). The shape is such that low atmospheric layers are penalized because of absorption by the upper layers, and high layers are penalized because of their low concentration of the absorbing gas. The atmospheric layer that exhibits the greatest change in transmittance is usually the layer that contributes the most.

2.2.4.2 *Profile retrieval*

The inversion of equation 2.20 is not a trivial matter. It is a Fredholm equation of the second kind, for which the existence or the uniqueness of the solution are not mathematically guaranteed.

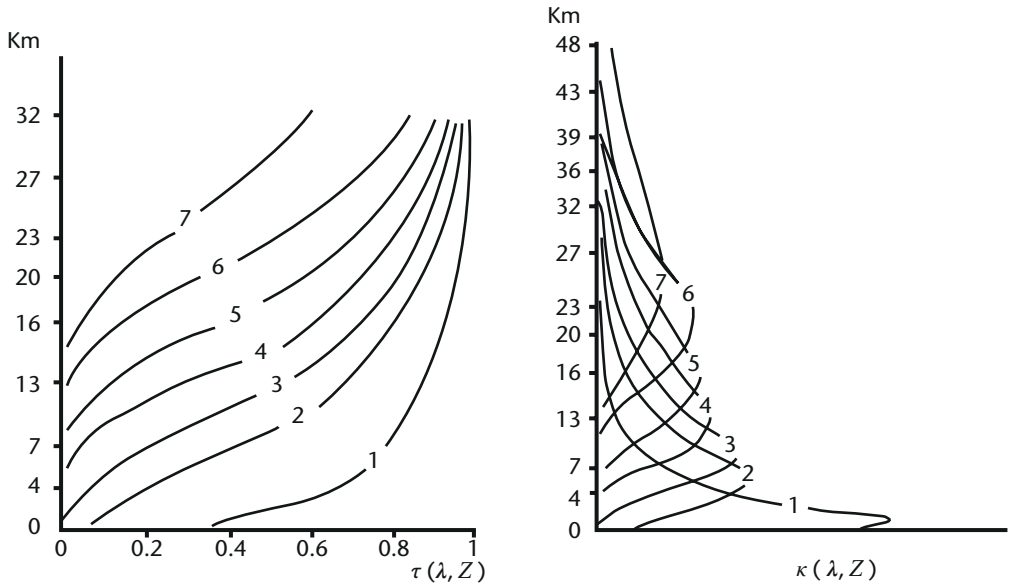

Figure 2.18. Transmissivity (left) and corresponding weighting functions (right) for seven channels in the CO_2 14 μm band

In the present case, the existence is granted by nature. To ensure uniqueness of the solution it is necessary to add constraints to it, since the problem is ill-conditioned. Many methods have been developed since profile sounding from space began. Some are statistical and linear, others are physical and non-linear, while others are a combination of both.

The primary objective is to invert equation 2.20 in order to retrieve an atmospheric temperature profile. This is only possible if the transmittance function is known in advance, which implies working in the absorption bands of a gas that has a known and stable concentration profile. In the IR range, CO_2 has such a profile in the bands around 4.3 and 15 μm (see Figure 2.12). As previously noted, the 4.3 μm band is more sensitive to high temperature, and is thus representative of the lower troposphere. However, that band may be contaminated by radiation from other species, and in daytime, the tail of the solar black-body curve (> 4 μm) cannot be disregarded. The 15 μm band is spectrally more pure, but is somewhat contaminated by the water vapour continuum. The transmittances therefore need to be corrected, either a priori by using external information, or a posteriori, by iterating after the water vapour profile has been retrieved.

The next step is to retrieve the water vapour profile. Once CO_2 absorption band channels have been used to retrieve the temperature profile, H_2O absorption band channels are used. The main band is centred around 6.3 μm, and responds well to high temperature (in the low- to mid- troposphere). For climate monitoring, it is important to measure water vapour in the upper troposphere. But that requires using an 18 μm band, which is technologically difficult to construct due to a lack of efficient detectors in the FIR range.

It is not easy to retrieve a water vapour profile or, more generally, to retrieve the concentration profile of an absorbing gas. The weighting functions of the absorbing gas peak at varying altitudes in the atmosphere, depending on concentration and remote-sensing frequency. In addition, retrieval is intrinsically inaccurate because the transmittance function to be inverted (equation 2.17) defines the content of a thin layer at altitude z as the difference between the respective content of two very thick layers: H to z and H to $(z - \Delta z)$. In other words, a small number is derived by calculating the difference between two large numbers.

Further difficulties arise where clouds are present. If the instantaneous field of view (IFOV) is entirely filled by a cloud with uniform features, a profile may still be retrieved by the same method, although it will only cover the atmosphere above the cloud. If only a fraction η of the IFOV is filled by a cloud of emissivity $\varepsilon_{\text{cloud}}$, the transfer equation becomes:

$$I(\lambda) = (1 - \varepsilon_{\text{cloud}} \cdot \eta)\, I_{\text{clear}}(\lambda) + \varepsilon_{\text{cloud}} \cdot \eta \cdot I_{\text{cloud}}(\lambda) \quad (2.21)$$

where $\varepsilon_{\text{cloud}} \cdot \eta$ is the effective cover.

Several methods (August et al. 2012, Susskind et al. 2014) deal with the effects of clouds. One starts the retrieval process by using the channels with weighting functions that peak above the cloud-top level to achieve a first-guess profile. The first guess is then iterated by changing effective cover values, until the measurements in all other channels fit best. Another method compares a number of nearby IFOVs on the assumption that the signals differ only because of the different fractional covers η, and then extrapolates to zero η.

In any event, it is acknowledged that, when cloud cover in the IFOV exceeds approximately 20%, no attempt should be made to retrieve profiles in IR. The IFOV of sounding instruments used to be several tens of kilometres. Fortunately, that has now been reduced to the order of 10 km, so that the probability of finding a substantial number of cloud-free IFOVs in a given area is much higher.

The problem of clouds is greatly alleviated in the MW range, where sounding is possible for all weather conditions except heavy rain. The species of well-known and constant concentration used for temperature profile retrieval is O_2, with absorption bands in the 50–70 GHz range and at about 118 GHz (not yet used from a satellite). For water vapour, the 183 GHz band can be used effectively. The 22 GHz band provides a weak signal that can provide total column-integrated amount over the sea. There are other absorption bands for temperature and water vapour at higher frequencies, but the radiative effect of the water vapour continuum makes it impossible to observe the troposphere using those spectral bands.

The transfer equation in the MW range is essentially a simpler version of the IR equation (2.20): instead of the Planck function (equation 2.7), it is possible to use the Rayleigh-Jeans approximation with linear temperature dependence (equation 2.10).

The question may arise as to why the MW band is not exclusively used for temperature and humidity sounding, as it performs in nearly all weather conditions. This is because vertical resolution requires a high sensitivity to temperature variations (with height). Vertical resolution is best in the 4.3 μm band, where the Planck function varies roughly in relation to T^{12}. In the 15 μm band, there is less sensitivity because the Planck function varies in relation to T^5. In the MW range, since B is a linear function of T (see equation 2.10), sensitivity $(\partial B/\partial T)/B$ varies in relation to T^{-1} (it decreases as temperature increases). One interesting feature of the various bands is that, whereas the 4.3 μm band is well suited to the lower troposphere, and the 15 μm band is well suited to the middle and high troposphere, the MW band at 57 GHz is better suited to the stratosphere.

Vertical resolution is crucial to temperature and humidity sounding. Figure 2.18 shows an example in which the weighting functions are rather broad. That implies that the degrees of freedom (the number of independent pieces of information) are limited. Weighting functions become narrower when the spectral resolution of the instrument improves. Figure 2.18 relates to a radiometer with only seven channels and a low resolving power ($\lambda/\Delta\lambda \approx 100$); its vertical resolution is ~1.5–2 km in the mid-troposphere. Current sounding instruments (spectrometers) have thousands of channels and a higher resolving power ($\lambda/\Delta\lambda \approx 1\,000$); their vertical resolution is less than 1 km in the mid-troposphere. Further increasing the resolving power to $\lambda/\Delta\lambda \approx 10\,000$ would not improve the vertical resolution of temperature and humidity profiles, but would enable single lines of trace gases to be observed for atmospheric chemistry purposes.

Current instruments for the MW range have already reached maximum vertical resolution performance: it cannot improve beyond ~1.5 km in the mid-troposphere, and will be worse in the lower troposphere because of strong contamination from the ground.

In the short-wave (SW) range (UV, VIS, NIR, SWIR) absorption band measurements are mostly used for atmospheric chemistry through spectroscopic methods. The radiative transfer equation is more complicated than equation 2.20. Instead of thermal radiation as described by Planck's law, the more complex process of scattering is used. Retrieving geophysical variables relies on modelling rather than explicit equations. As well as being used in atmospheric chemistry, the analysis of absorption bands is used for other purposes (see the spectrum in Figure 2.11), such as deriving:

(a) Atmospheric pressure at the Earth's surface: this is derived from estimates of the total column of oxygen in the band around 0.77 μm compared with nearby windows. It is one of the very few approaches available to measure surface pressure from space. Accuracy is limited by the scattering effect of aerosols, implying that the measurement also provides information on aerosols.

(b) Cloud-top height: this is derived from a deficit that arises when the total column of oxygen is measured; the deficit itself is the result of cloud masking the lower part of the column. In principle, this is more accurate than calculating the cloud-top height from the equivalent black-body temperature in IR, correcting for cloud emissivity, and transforming temperature into height using a temperature profile.

(c) Total column water vapour: the signal in one or more of the water vapour bands (about 0.94 or 1.37 μm) is compared with a signal from nearby windows. This can be more accurate than using IR or MW profiling.

2.2.4.3 ***Limb sounding***

Figure 2.18 shows how weighting functions become broader as height increases. This indicates that the vertical resolution of temperature and humidity profiles using passive IR or MW radiometry degrades with increasing altitude. The resolution obtained from using spectrometers is currently considered adequate (~1 km) in the mid-troposphere; but it becomes marginal (~2 km) at tropopause level, where much better resolution is required. In the stratosphere, the vertical resolution degrades further and rapidly becomes unusable. Two techniques offer help: limb sounding (including through occultation of the Sun, moon or stars) and radio occultation.

In cross-nadir sensing mode, vertical resolution is determined by the sharpness of the weighting functions, which is in turn controlled by spectral resolution. In limb mode, vertical resolution is determined by mechanical scanning, that is, by the instrument IFOV across the atmosphere when viewed transversally in the Earth's limb region (Figure 2.19). Vertical resolution depends on the step change rate, which is tuned to the instrument viewing aperture and to the intensity of available radiation. It is generally set to between one and three kilometres. Horizontal resolution is relatively inaccurate, since the measurement is integrated over a large optical path, as shown in Figure 2.19. The total optical path may be thousands of kilometres long, but the effective path, once weighted by atmospheric density, extends to some 300–500 km around the tangent point.

The sources of radiation are solar radiation reflected from the atmosphere, or atmospheric thermal radiation in the IR or MW ranges. In general, limb observations address not only temperature and humidity profiles, but also trace gases for atmospheric chemistry purposes.

In the SW range (UV, VIS, NIR, SWIR), the atmosphere can be scanned by directly pointing to the Sun while the Sun is setting or rising (occultation). Observation is conducted by measuring the damping of spectral lines in the solar spectrum. Sun occultation has the great advantage of avoiding any mechanical movement of the instrument telescope, and any calibration. That is because the spectra measured during occultation are compared to the solar spectrum measured shortly before (or after) occultation under the same conditions. One disadvantage is that, at least for polar-orbiting satellites, coverage is limited to high latitudes, where a satellite can observe sunrise or sunset as it enters or leaves the night arc of its orbit. More extended coverage is possible by using moon occultation, while all latitudes can be covered through occultation of the stars. However, less radiation is available in those cases.

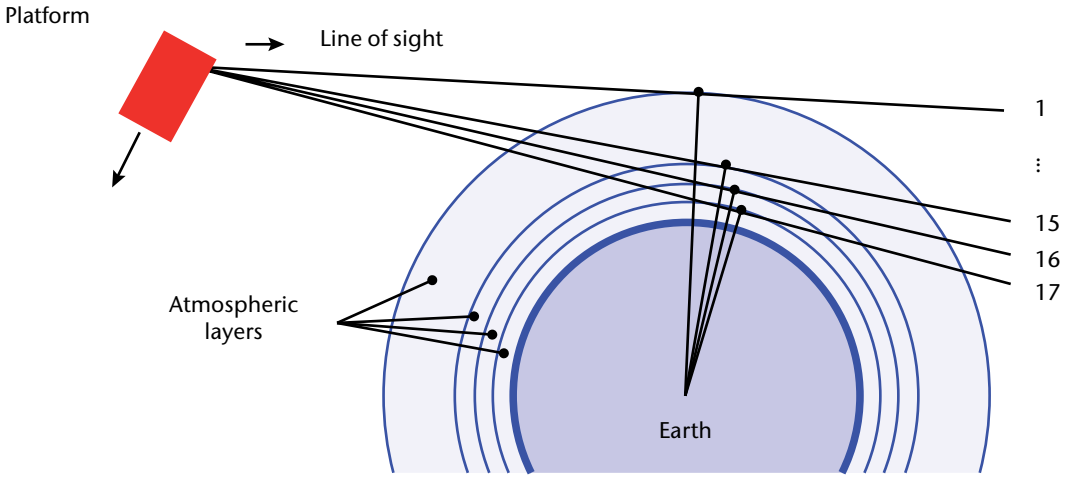

Figure 2.19. Geometry of limb scanning

2.2.4.4 *Lightning*

Lightning: a very narrow (~1 nm wide) near-infrared wavelength band is used to observe the neutral atomic oxygen emission line triplet near 0.774 μm. This part of the lightning spectrum represents about 10% of the total lightning optical energy. Strong absorption from oxygen obscures the Earth's surface and enables flashes to be detected at cloud top even in daylight. The intensity (total optical energy), areal extent, and number of flashes in a given period and trend over a given area are representative diagnostic attributes of convection, including cloud electrical energy, microphysics, kinematics and precipitation. In developing storms lightning extent is compact, and as convective storms grow upscale or merge the lightning may extend over several hundreds of kilometres. In addition, lightning is a response to the build-up of thundercloud charge and is a natural source of NO_x in the atmosphere.

2.2.5 Active sensing

The sensing methods described above assume that the sources for remote-sensing are reflected solar radiation and the Earth's emitted thermal radiation (plus other minor sources, such as background sky radiation in MW and the moon or stars in occultation). These natural sources enable passive sensing, for which observation wavelengths are largely determined by natural targets. In active sensing, the source is artificial and the sensing wavelength is not entirely driven by the physical properties of the target. Instead, the wavelength can be chosen, while also taking account of signal generation and propagation constraints. The following active sensing principles are considered:

(a) Radio occultation (for high vertical resolution profiles of temperature and humidity);

(b) Radar (for altimetry, scatterometry, cloud and precipitation, and imagery);

(c) Lidar (for clouds and aerosols, air motion, altimetry, and atmospheric chemistry).

2.2.5.1 *Radio occultation*

Radio occultation is one of a number of limb-sounding techniques. It has a totally different approach compared to passive radiometric techniques. An artificial source (in this case, the signal from a navigation satellite: GPS, GLONASS, Galileo or Compass) is tracked by a receiver on a satellite in LEO (Figure 2.20).

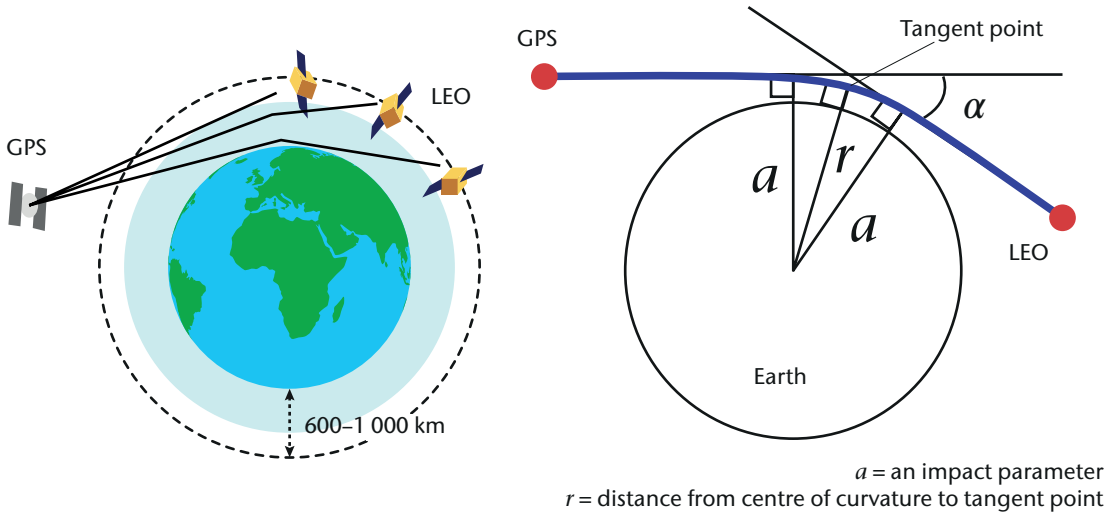

Figure 2.20. Principle of radio-occultation sounding. During the setting or rising of the GPS satellite over the horizon of the LEO satellite, the refraction induced by the crossed atmosphere changes the direction of propagation by a bending angle α.

The change of propagation direction due to refraction by the crossed atmosphere (bending angle α) is converted into a phase shift. The shift is accurately measured and then converted into a refractivity profile during the occultation process, which lasts approximately 90 s. The magnitude of the refraction depends on the temperature and water vapour concentration in the atmosphere.

The refractivity is linked to the atmospheric variables as follows:

$$N = (n-1)\cdot 10^6 = 77.6\cdot p/T + 3.75\cdot 10^5 \cdot p_w/T^2 \qquad (2.22)$$

where N is refractivity, n is refractive index, p is dry-air pressure, pw is water vapour partial pressure, and T is temperature. The coefficients for p and pw are given in hPa, and in kelvin for T.

The phase shift is ultimately a time measurement, one of the most accurate measurements in physics. The other key parameter is the distance between satellites. Since time and distance are fundamental metric quantities, radio occultation provides absolute measurements (not requiring calibration): this is a very attractive feature in terms of climate monitoring, when the magnitude of the refraction depends only on the temperature and water vapour concentration in the atmosphere. In fact, long-term observations of radio occultation are considered a benchmark among methods of detecting climate change.

Radio occultation data are difficult to process for two reasons: first, the position of the tangent point (see Figure 2.20, right hand panel) moves during the profile measurements; and second, pressure, temperature and humidity are not measured independently. Therefore, 4D assimilation into a numerical weather prediction model is needed. It is less complex to retrieve temperatures from the upper troposphere and stratosphere, since water vapour content is very low. Temperature retrieval is similarly straightforward in the lower troposphere, where water vapour is responsible for most variance.

The vertical resolution of radio occultation profiles in the upper troposphere and stratosphere, (approximately 0.5–1.0 km) cannot be matched by cross-nadir viewing IR or MW measurements (1.5–2 km). In addition, the frequencies used (L band: see Table 2.9) are insensitive to clouds, even if precipitating. As a result, although essentially performed in limb mode, the measurement can be extended down to the Earth's surface, in order to observe, for example, atmospheric discontinuities such as the top of the planetary boundary layer. Furthermore, radio occultation is one of the few methods that can infer surface pressure: this is done by correlating the height of the tropopause and the air pressure at ground level.

In order to account for the signal rotation induced by the ionosphere, transmissions from navigation satellites exploit at least two nearby frequencies. As by-products of the correction process, information relevant to space weather is obtained, such as total electron content and electron density profile.

2.2.5.2 ***Radar***

Radars (radio detection and ranging) transmit pulsed signals to the object to be observed, and collect the backscattered signal. In essence, radars measure distance (or range) and the backscattered power resulting from the radar reflectivity or radar cross-section of the body.

The radar equation may be written in different forms. The easiest to understand is:

$$P_s = \frac{P_t \cdot G}{4\pi \cdot r^2} \cdot \sigma \cdot \frac{1}{4\pi \cdot r^2} \cdot A_{\text{eff}} \tag{2.23}$$

where *Ps* is the power backscattered to the antenna, *Pt* is the power transmitted by the antenna, G is the antenna gain, A_{eff} is the effective area of the radar receiving antenna, *r* is the distance, and σ is the radar cross-section. Therefore:

$PtG/4\pi r^2$ is the power hitting the target at distance *r*;
$PtG/4\pi r^2 \cdot \sigma$ is the power reflected by the target;
$PtG/4\pi r^2 \cdot \sigma/4\pi r^2$ is the fraction of (isotropically) reflected power reaching back the antenna.

The antenna gain may be expressed as $G = 4\pi \cdot A_{\text{eff}}/\lambda^2$ (a relation that derives directly from the diffraction law). Expressing the effective area of the radar's receiving antenna A_{eff} from this alternative expression and inserting it into equation 2.23 yields:

$$P_s = \frac{P_t \cdot G^2 \cdot \lambda^2}{64\pi^3 \cdot r^4} \cdot \sigma \tag{2.24}$$

Different types of radar favour the measurement of either range accuracy (altimeters) or reflectivity/cross-section accuracy (scatterometers). Radar for clouds and precipitation focus on both range (for vertical profiling) and reflectivity. One feature that can be emphasized is image resolution by synthetic aperture radar.

Radar altimetry

The main purpose of altimetry is to measure the sea level and to map it so as to determine ocean dynamic topography. The radar characteristics are optimized to enhance range measurement as much as possible. Sea level is measured in terms of the time taken for a radar pulse to reach the sea surface and return to the satellite. Because sea level is computed as distance from the satellite, the satellite needs to be located with extreme accuracy. One or more of the following systems is used to ensure precise orbits:

(a) Laser tracking of the satellite by ground stations and laser-reflecting mirrors on the satellite;

(b) Radio positioning based on networks of ground transmitting-receiving stations and a transponder on the satellite;

(c) A GPS receiver aboard the satellite.

One drawback of radar altimetry is that viewing must be limited to nadir-only; otherwise echoes from surrounding areas interfere with time analysis. As a result, the observing cycle is very long. Corrections to the signal are requested to account for: ionospheric rotation (the two frequencies used are: ~13.6 GHz (main) and ~5.3 GHz (support)); and water vapour (a co-aligned MW radiometer is used at ~23 GHz (main) and ~35 GHz and/or ~19 GHz (support)).

In addition to measuring the range, an altimeter also records and analyses fluctuations and measures the intensity of the echo. The observations provided are:

(a) Significant wave height: derived from analysis of the spread in time of the collected echoes;

(b) Sea level: derived from filtering wave-related fluctuations and considering the instantaneous satellite altitude with respect to the geoid;

(c) Wind speed: derived from analysis of the fluctuation of the intensity of the echoes;

(d) Improved knowledge of the geoid: derived from long-term statistics of observed sea levels;

(e) Total electron content: derived as a by-product of the correction for ionospheric rotation.

Radar scatterometry

The primary application of spaceborne scatterometry has been measurements of near-surface winds over the ocean. Unlike radar altimetry, where the focus is on range measurement, radar scatterometry optimizes the accuracy of the measured radar cross-section σ (see equation 2.24), which is often normalized and called σ^0 (sigma-naught). While the ranging subsystem may be absent from the instrument, calibration must be extremely accurate.

The radar cross-section is a function of the target's dielectric property, the viewing geometry and the incident radiation (wavelength, polarization). Scatterometers are mainly used to derive sea-surface wind. The target is capillary waves, which are closely associated with wind stress. Sigma-naught changes with wind speed, relative wind direction and sight line. By measuring σ^0 under several azimuth angles, both speed and direction can be determined.

The relationship between σ^0 and wind is complicated: the practical solution is empirical or semi-empirical. Furthermore, it is not a unique relationship in terms of direction: with two viewing angles, several ambiguities remain (fewer ambiguities remain with three angles). When σ^0 values are directly assimilated into a numerical weather prediction model that accounts for wave–atmosphere interaction, ambiguities are solved by the model.

The differences between wind measurements taken with scatterometers and those taken with passive MW radiometers can be summarized as follows: (i) passive MW generally provides information on wind speed only; information on direction can only be acquired if several radiometric channels are equipped with full polarization capability; (ii) information from scatterometry is generally better quality, especially for low wind speeds; for high speeds (more than ~20 m/s), passive MW has good potential.

Primarily designed for sea-surface wind, scatterometers provide several kinds of observation:

(a) Sea-surface wind in all weather conditions (C band) or nearly all weather conditions (K_u band);

(b) Air pressure over the sea surface (achieved by applying geostrophic relations to wind maps);

(c) Soil moisture in scarcely vegetated areas (using C band, and occasionally K_u band);

(d) Leaf area index or total biomass in dense vegetation (forest);

(e) Ice type (age, roughness) at the polar caps;

(f) Snow water equivalent (for which K_u band is preferred).

Cloud and precipitation radar

While the radar altimeter focuses on ranging and the radar scatterometer focuses on the radar cross-section, cloud and precipitation radar emphasizes both. Ranging is necessary to measure the vertical profile of cloud particles, while σ is required to infer the concentration and size of reflecting particles. However, the accuracy required for ranging in order to obtain a precipitation profile is of the order of 100 m, instead of 1 cm for altimetry.

For rain droplets, provided that their diameter D is less than $\lambda/10$ (that is, in Rayleigh-scattering conditions), the radar cross-section is:

$$\sigma = \frac{\pi^5}{\lambda^4} \cdot K^2 \cdot D^6 \qquad \text{where } K \text{ is the dielectric constant} \tag{2.25}$$

The total backscattered radiation received by the radar is the sum of all reflectors of all diameters in the IFOV. Assuming a Marshall-Palmer distribution ($N_0 \cdot e^{-\Lambda D}$) for the particle diameters, total reflectivity can be expressed as:

$$Z = \frac{\pi^5}{\lambda^4} \cdot \int_0^{D_{\max}} K^2 \cdot N_0 \cdot e^{-\Lambda D} \cdot D^6 \cdot dD \qquad (\text{valid for } D \ll \lambda) \tag{2.26}$$

Equations 2.25 and 2.26 are generally applicable to ground-based meteorological radar that use S band (~10 cm) or C band (~5 cm). They are to be compared with D ~ 0.5 cm, which is typical of precipitating clouds. Those frequencies are not used from space, as the corresponding IFOV on the ground that has a reasonably-sized antenna is too coarse. Due to frequency regulations, the frequencies that can be exploited by a spaceborne radar are ~14 GHz (~2 cm), ~35 GHz (~0.9 cm) and ~94 GHz (~0.3 cm). Therefore, equations 2.25 and 2.26 are not fully applicable, but must be corrected in a complex way to account for Mie scattering conditions.

Once the reflectivity Z is measured, there are several ways to convert Z into precipitation rate R. First, it is necessary to infer the precipitation rate at the surface. That cannot be directly measured from space, but must instead be derived from measured properties in the vertical column associated with the precipitation profile.

Cloud and precipitation radar is the only technique that can provide measurements of the cloud base, an important variable for aeronautical meteorology and for climate. The accuracy and reliability of the measurement depends on the radar frequency; the radar must also penetrate the full cloud thickness. From an operational viewpoint, cloud and precipitation radars have several disadvantages, particularly their limited swath, which prevents frequent observing cycles. And so, although passive MW imagery continues to be used as the basis for frequent precipitation observation, the accuracy of precipitation data from passive MW radiometry still needs to be improved. The continuing availability of at least one radar in space is necessary for "calibrating" the system of passive MW radiometers, along the lines of the concept for the Global Precipitation Measurement mission.

Synthetic aperture radar

In the MW range, spatial resolution is limited by diffraction. For a side-looking radar that views $\theta°$ off nadir, at orbital height H, with an antenna diameter L, and assuming a flat surface, the IFOV is:

$$\text{IFOV} = 1.24 \cdot \frac{H \cdot c}{\cos\theta \cdot L \cdot \nu} \tag{2.27}$$

Table 2.10 shows the IFOV and L relationship for radar in several bands, assuming that $\theta = 23°$ and $H = 700$ km (parameters of the SAR on SeaSat, Figure 2.21). It illustrates that the requirements for IFOV = 1 km would be very difficult to meet, and requirements for IFOV = 100 m or below would be impossible with a real-aperture antenna concept.

In the SAR concept (Figure 2.21) the antenna is elongated along the satellite motion. Its narrow dimensions determine the swath and are parallel to the sub-satellite track. The longer side determines the area where signals are to be analysed. The radar footprint corresponds to that

Table 2.10. Examples of corresponding resolutions and antenna sizes for typical frequencies used in SAR

	L band (~1.3 GHz)	*C band (~5.4 GHz)*	*X band (~9.6 GHz)*
IFOV for L = 1 m	220 km	60 km	30 km
Required L for IFOV = 1 km	220 m	52 m	30 m
Required L for IFOV = 100 m	2 200 m	520 m	300 m
Required L for IFOV = 10 m	22 000 m	5 200 m	3 000 m

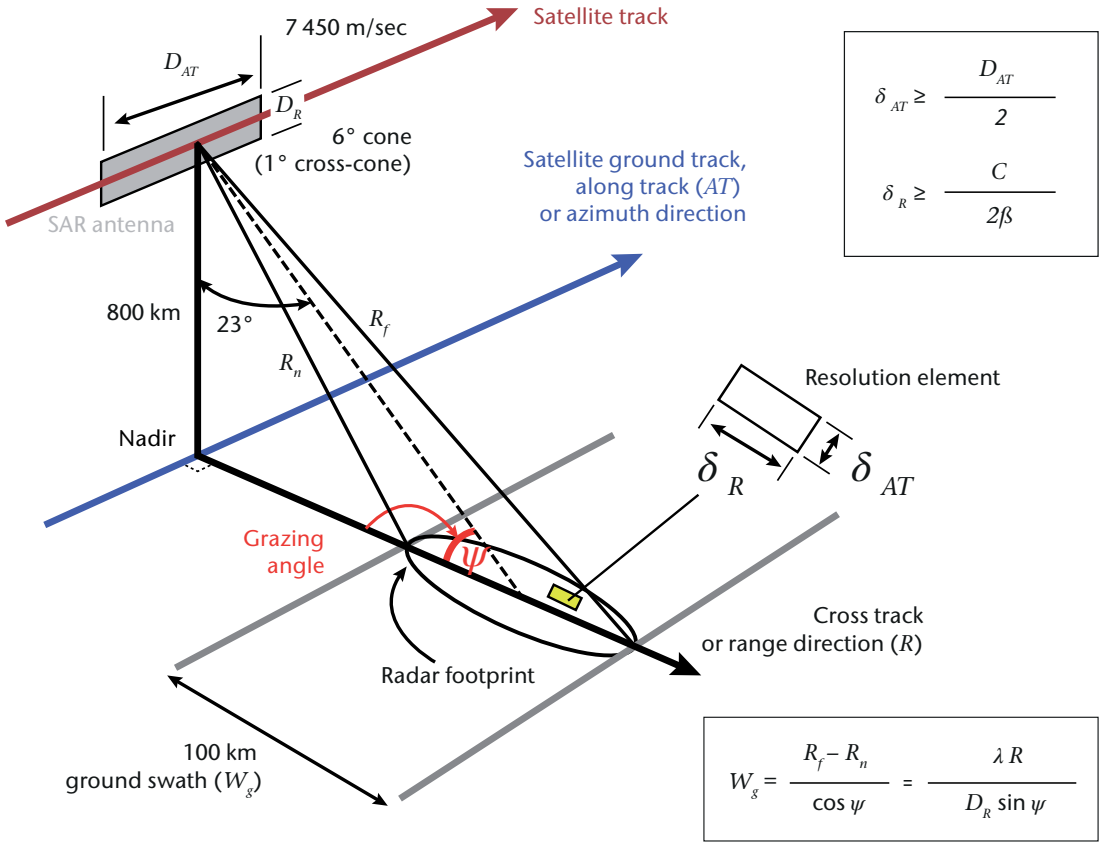

Figure 2.21. Principle of SAR

of a real-aperture antenna, while the situation is varied for the resolution elements in the field (pixels). The pixels across the swath are at different distances from the satellite. The satellite can locate them due to its ability to distinguish small-range changes. The echoes from the pixels ahead of the sub-satellite cross-track line are affected by a positive Doppler shift (where a frequency is higher than the one transmitted); the echoes from the pixels behind that line undergo a negative Doppler shift. By capturing the moment of shift inversion, the pixels can be assigned to a location along the satellite track.

SAR may be used in different operating modes, depending on the trade-off between resolution and swath, and on the combination of transmitted and received polarizations. One operating mode is designed for wave spectra. A small part of the image (a vignette) is sampled at intervals. With Envisat, for example, the vignette is 5 km x 5 km at the best spatial resolution of 30 m, and

sampled at 100 km intervals along the track. The echoes in the vignette are analysed to plot the power spectra, from which it is possible to determine the dominant wave direction, the dominant wave length/period and power associated with significant wave height.

The list of SAR applications is long, although not all bands are suitable for all applications:

(a) Ocean circulation features (eddies) and waves (preferably L band);

(b) Ocean pollution and oil spills (preferably C band);

(c) Sea-ice cover and type (age) (any band);

(d) Land-ice cover (glaciers) (any band);

(e) Snow melting conditions and snow water equivalent (preferably X band);

(f) Surface soil moisture (preferably L band, especially for the areas around plant roots);

(g) Vegetation type (preferably C band) and total biomass (preferably P band);

(h) Land use and urbanization (preferably C band);

(i) Geological structure detection (preferably X band);

(j) Disaster monitoring and damage inventories (preferably X band);

(k) Ship traffic surveillance and military surveillance (preferably X band).

Other important applications are possible through interferometry because the phase control of the SAR signal is extremely accurate. Signals from different orbits of the same satellite or different satellites can be accurately co-registered in order to implement interferometry. This enables, for instance, land surface topography to be obtained for an improved digital elevation model, and iceberg heights to be measured.

By using interferometry between passes of the same satellite in an orbit with a repeat cycle, it is possible to measure changes such as iceberg drift, variations of glacier cover and lake extent, volcanic surface topography changes and bradyseisms, coastal erosion and urbanization.

2.2.5.3 ***Lidar***

Lidar (light detection and ranging) gives us precise, accurate measurements at fine resolution of a range of phenomena. With advances in lasers, optics and geodetics, lidar technology has been advancing rapidly. There have been recent launches for atmospheric, ecosystem, and cryospheric sciences from the European Space Agency (ESA) and the National Aeronautics and Space Administration (NASA). Although in principle, lidar could be used to scan an area for imaging purposes, lidar systems in space have so far only been nadir-pointing or monodirectional. While the principle of lidar is similar to that of radar, the electromagnetic range is different: MW is used for radar, while SW is used for lidar. Most lidars make use of wavelengths in the UV (for example, 355 nm), VIS (for example, 532 nm), NIR (for example, 1 064 nm) or SWIR (for example, 1 550 nm) ranges; longer wavelengths (for example, 10.6 μm) may also be used. The source is a laser (light amplification by stimulated emission of radiation). It is extremely directional, but the large distance between the satellite and the Earth means that significant electric power would be an issue, and a larger telescope would be needed to collect the

backscattered signal. There are technical issues such as the deterioration of the optical system due to the laser illumination. In summary, the use of lidar in space requires considerably more resources compared to passive systems. The following existing missions are lidar-based:

(a) Backscatter lidar for profiling aerosol and clouds;

(b) Doppler lidar for wind profile in clear air;

(c) Lidar altimeter specifically for sea ice, land ice, and for vegetation height;

(d) Differential absorption lidar (DIAL) for atmospheric chemistry;

(e) Wind Doppler lidar.

Cloud and aerosol lidar

Backscatter lidar primarily deals with the observation of aerosols and clouds. This implies the use of wavelengths that are similar in size to very small aerosols (~1 μm). In order to capture more aerosol/cloud properties (size, phase, extinction/scattering ratio, and ultimately, type), more concepts have been developed. Elastic backscatter lidar has the simplest design. It measures the profile of attenuated backscatter, which, at any altitude, is the product of backscatter (both Rayleigh and Mie) multiplied by the attenuation of the overlying atmosphere (for example, due to scattering and absorption of overlying cloud/aerosol layers). A separate constraint/assumption must be applied to retrieve aerosol/cloud backscatter and, importantly, aerosol/cloud extinction, which is often the geophysical parameter of interest. Some elastic backscatter lidars employ two wavelengths (532 and 1064 nm) to enable the ability to discrimination aerosols from clouds. Also, instruments can be designed with polarization sensitivity to discriminate between spherical and non-spherical scatterers, allowing identification of cloud phase (ice vs. water) and providing information on aerosol type (for example, discrimination of dust from spherical aerosol types). As noted in the section on altimetry below, altimeters can also provide aerosol and cloud profile information similar in nature to an elastic backscatter lidar.

A more capable variant of the backscatter lidar is the high-spectral-resolution lidar (HSRL), which employs a single-frequency laser transmitter and wavelength discrimination in the receiver to separate Mie and Rayleigh scattering components. The HSRL technique enables unambiguous and independent measurement of aerosol backscatter and extinction without external constraints or assumptions that can lead to inaccuracies in standard backscatter lidar retrievals. HSRLs also provide more information (particle extinction-to-backscatter ratio) to constrain inference of aerosol type. Appropriately configured Doppler wind lidars based on the incoherent detection technique can also provide HSRL measurements in addition to wind measurements.

Backscatter lidars tend to be medium- to large-size instruments (for example, with telescope diameters between 0.6 and 1 m). The single-laser-shot footprints are a few tens of metres in diameter, and vertical sampling resolutions have varied from 30 m to a few hundred metres. For some applications (for example, studies of strongly scattering clouds), single-shot, full-resolution data are employed. For weaker features or retrievals demanding higher signal-to-noise ratio, averaging data in the vertical and over multiple laser shots (that is, in the horizontal) are employed.

Designed primarily for aerosols (the most demanding mission), the backscatter lidar enables different kinds of observations to be made, including:

(a) Vertical profile of aerosol backscatter, extinction and depolarization, from which can be determined aerosol layer heights (including PBL height as determined from gradients in aerosol backscatter), aerosol optical depths, and, depending upon system capability, aerosol type and extinction-to-backscatter ratio (HSRL only);

(b) Cloud-top height (much more accurately than with passive NIR and IR techniques);

(c) Optical thickness of thin clouds (cirrus) and cloud base of semi-transparent clouds;

(d) Cloud phase (if polarization sensitive) and, for opaque water clouds, constraints on cloud droplet effective radius and number concentration;

(e) Similar properties of polar stratospheric clouds.

Backscatter lidar data have also been used to estimate ocean properties, including sea-surface roughness, sea-surface wind speed and near-surface particulate backscatter, as well as particulate organic carbon and phytoplankton biomass.

Doppler lidar

Doppler lidar deals primarily with the observation of wind profiles, a key variable for weather forecasting. A Doppler lidar instrument is deployed on the Atmospheric Dynamics Mission – Aeolus (ADM-Aeolus).

The current operational technique available for observing wind profile consists of tracking the movement of clouds or water vapour patches in successive images, either from geostationary satellites, or from polar orbiting satellites in polar areas with frequent satellite overpasses. This limits the opportunity to take measurements only at altitudes where tracers are present (generally one layer, sometimes two). With hyperspectral IR sounding in GEO, frequent water vapour profiles are available, and water vapour patterns can be tracked at several heights. However, vertical resolution and accuracy are expected to be limited.

Atmospheric feature tracking (for example, clouds and water vapour) is a proven technique for the estimation of winds. Doppler lidar enables measurement of winds in clear air, whereby tracers are aerosols and molecules. Obviously, Doppler lidar provides a more direct estimation of the wind field.

Wind lidar was implemented on the ESA ADM-Aeolus mission (Källén 2008). For wind lidar, coverage is a major limitation. Since currently one instrument only covers a line parallel to the sub-satellite track, a constellation of satellites would be required to provide better spatial and temporal coverage.

Another difficulty with wind lidar is that measurement can only be along-sight (1D). That means that in order to retrieve the required 2D horizontal component, assimilation into a numerical weather prediction model is necessary.

The Doppler lidar is primarily designed for wind, which is the most demanding mission. It provides several kinds of observations, including wind profile in clear air or in the presence of thin cirrus, aerosol profile (from echo intensity) and cloud-top height.

Lidar altimeter

Radar altimeters can provide measurements as accurate as a few centimetres. However, at above 20 km, their horizontal resolution is quite coarse. By implementing SAR processing of the along-track signal, the resolution can be brought to ~300 m, which is still insufficient for accurately detecting boundaries. Another limitation of radar altimeters is their unsuitability for observing surfaces with high emissivity (and thus low reflectivity) in the MW range, such as land and ice.

Lidar does not have those limitations. The horizontal resolution can be a few tens of metres and the vertical resolution less than 10 cm. That fine resolution makes it possible to capture the border between sea water and polar ice and (after successive passes) to profile the height along-track in order to map ice thickness.

In order to operate over the sea, even though reflectance in the VNIR range is very low, a lidar altimeter must have a large telescope (aperture ~1 m). For improved cost-effectiveness, a sensor using a second wavelength is usually added to observe the atmosphere (for example, 1 064 nm is used for surface and 532 nm is used for atmosphere). In this case, a lidar altimeter operates as an ordinary backscatter lidar.

As with any other altimeter, the lidar altimeter requires extremely accurate orbit determination, since the basic ranging measurement provides the distance of the object from the satellite in orbit. Precise orbit determination is achieved by a GPS receiver, and laser ranging from a network of ground stations with an array of retroreflectors on the satellite.

Lidar altimeter applications include:

(a) Sea-ice thickness and polar cap topography;

(b) Sea level and ocean-dynamic topography;

(c) Contribution to improved knowledge of the geoid;

(d) Land-surface topography, including glaciers and lakes;

(e) Surface properties;

(f) Aerosol profile and aerosol properties;

(g) Cloud-top height, optical thickness of thin clouds and cloud base of semi-transparent clouds;

(h) Polar stratospheric clouds;

(i) Atmospheric discontinuities such as cloud topped planetary boundary layer;

(j) Ecosystem – forest height and structure.

Differential absorption lidar

The DIAL technique utilizes atmospheric Rayleigh and Mie backscattered return signals from a tunable single frequency, pulsed laser to directly measure range resolved profiles of atmospheric trace gas concentrations. Two or more spectrally close laser pulses are transmitted to the atmosphere nearly simultaneously (0.2–1 ms separation) with one pulse tuned to the centre or wing of a gas absorption line, and the other tuned to a less absorbing spectral location. The separation between the two or more transmitted wavelengths is typically <1 nm to minimize biases resulting from differences in atmospheric backscatter coefficients. The retrieval of gas concentration profiles is achieved using the DIAL technique which exploits the differential attenuation of the backscattered signals between the absorbing and non-absorbing wavelengths along with a priori knowledge of the differential absorption cross-section over a range bin ΔR. Given that the laser on–off pulse pair(s) temporal and spectral separation are small (≤1 ms and <1 nm, respectively), it can be assumed that the instrument constants and atmospheric volume scattering coefficients are constant between the online and offline atmospheric return signals. As a result, airborne and space-based DIAL has the potential to enable high-accuracy measurements of trace gases throughout the troposphere, as they are self-calibrating and not prone to bias resulting from aerosol and cloud contamination. The DIAL technique is mature and has been exploited for airborne measurements of water vapour and ozone profiles for decades. These airborne prototypes have demonstrated that the DIAL technique is the only viable remote sensing approach to real high spatial resolution profiles of trace gases from the upper troposphere down to the planetary boundary layer. Although it is readily deployed from aircraft, implementation of space-based DIAL has not been realized to-date due to limitations in scalability and efficiency of pulsed lasers, and availability of

efficient and single photon sensitive detectors. Several NASA and ESA programmes are currently advancing technologies required to carry out water vapour DIAL measurements from space within the next decade.

Exploiting the DIAL technique for atmospheric trace gas profiling from space requires sufficient atmospheric scattering and detection sensitivity. For gas concentration measurements where appropriate absorption line strengths lie beyond the near-infrared portion of the optical spectrum and atmospheric scattering and detector efficiency is limited, a variant of the DIAL technique, the Integrated Path DIAL (IPDA) technique, can be used to measure the weighted column gas concentration using strong surface echos. The IPDA approach has recently been demonstrated from aircraft for high-accuracy and precision measurements of CH_4 and CO_2. MERLIN, a pathfinder mission led by the German Aerospace Centre (DLR) and France's National Centre for Space Studies (CNES) is currently under development to demonstrate the feasibility of CH_4 IPDA measurements from space. Other programmes in Asia are also advancing technologies required to enable CO_2 IPDA measurements from space.

Examples of possible applications for DIAL and IPDA are:

(a) H_2O DIAL by exploiting absorption bands in the 820 nm and 935 nm spectral regions;

(b) O_3 DIAL by exploiting the absorption continuum in the 290–320 nm spectral region;

(c) Column CO_2 IPDA by exploiting lines at 1.57 μm in the 1.6–1.7 μm window or in the 2.0–2.3 μm window;

(d) Column CH_4 IPDA by exploiting lines in the 1.65 μm spectral region.

2.3 SPACE AND GROUND SEGMENTS

Earth observation from space implies a complex system composed of (i) a space segment to perform observations, and (ii) a ground segment to manage the space segment, process and disseminate observation data.

2.3.1 Space segment

The space segment of a satellite system includes:

(a) The platform (also referred to as the bus);

(b) The instruments installed on board;

(c) The communication tools to receive commands and convey the instrument output to the ground.

The size and/or mass of satellites for Earth observation can range over two orders of magnitude:

(a) Nanosat: 1-10 kg (actually unlikely to be used for operational Earth observation);

(b) Cubesat: a class of nanosats made up of multiples of 10 cm × 10 cm × 10 cm cubic units each having a mass of no more than 1.33 kg;

(c) Microsat: 10–100 kg;

(d) Minisat: 100–500 kg;

(e) Smallsat: 500–1 000 kg;

(f) Mediumsat: 1–2 tons;

(g) Large facility: > 2 tons.

2.3.1.1 *Platform services*

The satellite platform hosts the instruments and provides several services:

(a) Power supply for instruments, telecommunications, and all other satellite subsystems;

(b) Navigation facilities for geographical referencing of observations;

(c) Attitude control for correct pointing of instruments and stabilization;

(d) Thermal control to keep the instruments within specified operating conditions;

(e) Housekeeping devices to monitor and control the status of all satellite subsystems;

(f) Propulsion for orbit keeping and, if needed, orbit change;

(g) Processing capability to administrate the various platform subsystems;

(h) Processing capability to handle instrument data and format data streams to be transmitted;

(i) Storage device for on-board global data recording;

(j) Communication facilities to receive commands from the ground;

(k) Communication facilities to transmit observational and housekeeping data to the ground;

(l) Other communication services, where the platform has a data relay function only.

2.3.1.2 *Navigation and positioning systems*

Navigation and positioning systems are necessary for geolocation of observed data, both during viewing, and afterwards for ground processing. The following systems are used:

(a) Laser retroreflectors;

(b) GNSS receivers;

(c) Radio-positioning systems;

(d) Star trackers.

Laser retroreflectors

These are mirrors which tend to be corner cubes. They reflect laser beams sent to the satellite by laser-equipped ground sites during positioning sessions. Laser retroreflectors are used on many satellites for a posteriori precise orbit determination. This is achieved by post-processing a number of measurements in night-time and clear sky only. The analysis involves a full network of coordinated ground stations. The results are sparse and only available after a certain delay. However, they are so accurate that they can be used for space geodesy applications.

Radio-positioning systems

These systems are specifically designed to support altimetry missions. They comprise radio links between the satellite on the one hand, and ground transmitting and/or receiving stations on the other. Positioning is performed in near real time and, with improved accuracy, after post-processing. Two examples of such systems are:

(a) Doppler Orbitography and Radiopositioning Integrated by Satellite (DORIS), which measures the Doppler shift of signals from ground stations;

(b) Precise Range and Range-rate Equipment (PRARE), which measures differential signals from a network of ground stations.

GNSS receivers

These systems make use of the phase difference of signals from several satellites in the GNSS. The GNSS includes the navigation satellite constellations of the United States of America (GPS), the Russian Federation (GLONASS), the European Union (Galileo), and China (Compass, known as Beidou in Chinese). A large number of satellites currently use GNSS receivers to support their navigation. Positioning is performed in real time.

Star trackers

These are charge-coupled device imagers that track bright stars, recognize their pattern, and send information to a satellite's attitude control system. Star trackers provide continuous monitoring of satellite attitude much more accurately than systems based on horizon-sensing. This is necessary for instruments that require accurate pointing information (such as limb sounders), both for active attitude control during flight and for subsequent instrument data processing. An increasing number of satellites are now being equipped with star trackers.

2.3.1.3 *Orientation and stabilization*

The orientation and stabilization systems are primary platform features that determine instrument pointing capability.

The side of the platform on which the sensors are placed should ideally be kept facing the Earth's surface, unless the satellite mission has a different purpose (such as monitoring the Sun). Since the platform tends to keep a steady orientation in relation to the stars during its orbital motion, a stabilization mechanism is required.

The stabilization mechanism known as spinning is most straightforward, as it is passive and inertial. The spin axis tends to have a constant orientation in relation to the stars, and therefore does not fulfil the Earth orientation requirement. For GEO satellites, if the spin axis is set parallel to the Earth's rotational axis, the Earth's surface is scanned for a small amount of time (about 5% of the satellite's orbiting time) during each satellite rotation. For low orbiters, the orientation of the spin axis may be set specifically to enable instruments to be pointed towards the Earth's surface for a fraction of time. In any event, spin stabilization is only suitable when an instrument's radiometric budget is sufficient to carry out the measurements for which the instrument was designed, in spite of the small fraction of useful observing time. In addition, spin stabilization can only be implemented for one instrument, or very few instruments, on one platform.

Three-axis stabilization is much more suitable for maintaining a constant orientation towards the Earth and also supports more instruments on one platform. This allows for active control of the satellite attitude with respect to rotations around: the axis perpendicular to the orbital plane (pitch), the axis tangent to instantaneous motion in orbit (roll), and the nadir direction (yaw).

Active control is critical, because it implies accurate attitude determination (by, for example, horizon detection, star trackers or GNSS receivers) and efficient actuators (such as micropropulsion devices, gyros, very fine-angle change detectors and efficient control electronics). A loss of active control is among the primary causes of mission failure. Active control may affect data quality because of limited accuracy, particularly in the case of high-resolution instruments and high orbits (GEO), and mechanical perturbation of instrument pointing associated with turning on the actuators.

In addition to the main orientation and stabilization systems (spinning and three-axis control), smart attitude control systems are also in use, especially with small satellites. For instance, the gravity-gradient system uses a long boom that tends to the nadir direction, and thus keeps one side of the platform pointing towards the Earth's surface.

2.3.1.4 ***Housekeeping system***

A basic trade-off for satellite design lies between the capabilities that are implemented on board and those that can be achieved on the ground if sufficient information regarding on-board features is available. Hardware implementation on board may be expensive, prone to irrecoverable failure, and provide limited performance. Therefore, it is advisable to reserve hardware implementation to cases where it is absolutely indispensable and reasonably safe. Moreover, the housekeeping system provides all the ancillary information necessary to accurately process data on the ground.

The housekeeping system manages both the platform (deformations, temperature of radiant surfaces, attitude, status of power generators and all other subsystems) and the instruments (status and temperatures of the various parts, control signals for electronics, and the like). In general, instrument housekeeping is at least partially implemented inside the instrument itself.

The amount and completeness of housekeeping constitutes a discriminating factor for the class of a satellite. Operational satellites are equipped with plenty of housekeeping devices for subsystem monitoring and the possible activation of recovery manoeuvres, such as by switching to redundant units. Housekeeping information is also a basic element of accurate instrument calibration and data georeferencing.

Notwithstanding the importance of a good housekeeping system, there are limitations to the accuracy of what can be achieved by such software processing. The residual errors of software corrections or reconstructions may exceed what is allowed by the application. Therefore, certain corrections need to rely on on-board hardware.

2.3.1.5 ***Data transmission***

The platform must transmit to the ground the observation results from the various instruments. Whatever the satellite height over the Earth's surface, radio transmission to the Earth will have to cross the ionosphere and plasmasphere, which block the propagation of electromagnetic waves with frequencies lower than the critical plasma frequency (~25 MHz). Direct visibility is needed between the transmitters and the receivers both on the satellite and the ground station.

The simplest method of collecting observed data from a satellite is by direct broadcast in real-time. For a LEO satellite, a ground station will acquire all the data that a satellite transmits when passing within the acquisition range. The size of the acquisition range is the same as a satellite's FOV for zenith angle $\zeta = 90°$ (in principle), or $\zeta = 85°$ (with a reduced risk of interferences from ground sources or occlusion from orography). Table 2.1 shows that, for a satellite height of 800 km for instance, the acquisition range is a circle with a diameter of 5 000 km (for $\zeta = 85°$ or elevation = 5°).

Where the satellite velocity is in the region of 400 km/min and the satellite pass is centred over the acquisition station, the acquisition session lasts 15 min at most, and is reduced to a few minutes for peripheral passes.

This type of acquisition is the most convenient because it provides the observed data to the user in real time for immediate processing. However, only data observed and transmitted during the satellite pass inside the acquisition range can be acquired by the local receiving station. For GEO, direct broadcast can be continuously received by a station located within the FOV.

An alternative way for a LEO satellite to receive data is to store the observed data on board and transmit the data on command, when the satellite overflies a central acquisition station. The central station, also used to send commands to the satellite, has the same acquisition range as any local station. If it is placed at a high latitude, then the central station can collect data from many orbits. Table 2.4 shows that most Sun-synchronous orbits pass less than 10° from the pole, so that a central station placed at a latitude of, for instance, 80° will intercept all orbits and provide global data acquisition. The store-and-dump acquisition method has the advantage of enabling data recovery for the whole globe, but also has several drawbacks:

(a) Access to data is slower, since the delay includes the time needed to: run the whole orbit (up to 100 min), receive at the central station (about 10 min), relay to the central processing facility (about 10 min) and redistribute to the users (about 10 min). The total delay in the availability of data is therefore 2–3 h.

(b) The satellite has to transmit the data accumulated in one orbit (about 100 min) during the time it spends within the acquisition range of the central station (about 10 min). Therefore data rate and bandwidth need to be one order of magnitude higher than for direct read-out, which heavily impacts on the cost, size and complexity of the station. This acquisition mode is suitable for a satellite operator but generally not suitable for an individual user.

(c) There are instruments with data rates so high that they cannot be fully stored on board: selection of data to be stored may be needed, either by reducing the resolution or by prior selection of frames (for example, the local area coverage (LAC) mode of NOAA Polar-orbiting Operational Environmental Satellites (POES)).

If not acquired locally in real time, the data gathered in a central processing facility need to be retransmitted to the users, generally after preprocessing. In the case of GEO satellites, a transponder on the same satellite can be used for data retransmission to local user stations.

For LEO satellites, between the two extreme cases (direct read-out providing data over a limited area in real time, or store-and-dump of global data with 2–3 hours' delay), there are alternative or complementary data recovery schemes, which can use:

(a) Several downlink stations spread over the globe, including one near each polar region; this reduces the length of time that data need to be stored on board the spacecraft;

(b) A network of direct read-out stations spread over the globe; each one acquires data on limited areas and retransmits them to data centres; this reduces the delay in the availability of data to a few tens of minutes, but does not necessarily achieve global coverage; or

(c) A data relay satellite that receives data in real time from observing platforms and relays them to a central processing facility; this reduces the delay in the availability of data to a few minutes.

Data recovery timeliness is a critical issue for operational satellites; that is particularly the case for meteorology, because of the coexisting requirements for timeliness and global coverage. For research and development applications, the timeliness requirement is less stringent, and the store-and-dump method tends to be used in conjunction with an effective archiving and retrieving facility, which provides advanced data stewardship.

2.3.1.6 *Data collection services*

In addition to providing Earth observation data from a platform in orbit, satellites can support other services, and so act as a telecommunications relay. The most common forms of such relays are:

(a) Data collection from in-situ platforms located on the ground, on aircraft, on balloons, on buoys, on ships and even on migrating animals. The data collection platform (DCP) may transmit all the time, at fixed intervals, or upon interrogation from the satellite. Mobile platforms may be located from the satellite if in LEO. GEO satellites serve either DCPs within their line of sight (regional) or DCPs carried on mobile platforms (ships, aircraft, and the like) that migrate among the views of different GEO satellites (international).

(b) Search and rescue distress signals are detected from transmitting equipment carried by those in distress. The request for help is then relayed to one of the centres of a worldwide search and rescue network. Search and rescue payloads are on several operational meteorological satellites in LEO and GEO. The service from LEO is called the Search and Rescue Satellite-aided Tracking System (SARSAT), while the GEO-based service is known as Geostationary Search and Rescue (GEOSAR).

(c) Relay of meteorological information from meteorological centres to end users as a broadcast, or to selected centres within view of a GEO satellite. The central facility of the system may perform the uplink or delegate it to auxiliary stations close to the information production centre that are equipped to uplink the satellite.

2.3.2 Ground segment

The ground segment of a satellite system includes:

(a) The central station for satellite command and global data acquisition;

(b) Peripheral stations for data acquisition;

(c) Mission and operation control centres;

(d) Data processing and archiving centres;

(e) Data and product distribution systems.

2.3.2.1 *Central station for satellite command and global data acquisition*

This element of the ground segment may be generically termed the command and data acquisition station (CDA). Typical tasks of a CDA are:

(a) To collect command sequences from the mission and operation control centre and uplink commands to the satellite (for payload configuration, satellite configuration, orbit control, and the like);

(b) To acquire satellite telemetry data (for attitude and orbit determination, satellite and payload status, and the like) and immediately deliver it to the mission and operation control centre(s);

(c) To acquire geophysical and ancillary data (housekeeping, calibration, and the like) and deliver it to the data processing and archiving centres;

(d) To index the acquired data streams with accurate time and orbital elements.

It is possible to have only one primary CDA for geostationary satellites. For near-polar satellite systems, it is possible to avoid blind orbits by placing the CDA at a very high latitude (such as Svalbard at 78° N). The two polar CDA stations are the baseline for the NOAA, EUMETSAT and CMA missions. For low-inclination orbits, a network of CDAs is necessary, with one acting as the main CDA.

CDAs use S-band frequencies (about 2 100 MHz) to command the satellite. S band is nearly insensitive to weather and less critical to pointing accuracy. For geophysical data acquisition, the L band is used (about 1 700 MHz) if the data rate is below 10 Mbps; otherwise either the X band is used (about 8 GHz) for data rates of up to some 100 Mbps; or the K_a band (about 26 GHz) is used for data rates of several hundreds of Mbps.

2.3.2.2 *Mission and operation control centres*

These elements may be generically termed the operation control centre (OCC). Their tasks are:

(a) To collect information on satellite, payload, and orbit status from the CDA and (in the case of the orbit only) from other ranging stations;

(b) To collect requirements for elements including payload configuration and measurement sequence planning from data processing and archiving centres, and from other users entitled to input requirements into the mission plan;

(c) To analyse the information on satellite, payload, and orbit status, and on payload or mission configuration requirements; to generate instrument performance monitoring reports; to elaborate the operations plan and deliver commands to the CDA for uplinking the satellite;

(d) To provide data processing and archiving centres with ancillary information, which is relevant for data processing and results from activities relating to operations, payload or mission control (including accurate orbit determination, satellite attitude behaviour and payload status).

Mission control centres are closely connected with users, application centres and scientific teams. OCCs are closely connected with CDAs and the units responsible for satellite development. OCCs also have full knowledge of satellite design features. The two centres are often co-located, although this is not compulsory, and should preferably be secured by a back-up centre.

2.3.2.3 *Data processing and archiving centres*

These elements are responsible for:

(a) Acquiring geophysical, calibration and selected auxiliary data from CDAs;

(b) Acquiring auxiliary data on orbit, satellite and payload from OCCs;

(c) Monitoring instrument calibration and performing inter-calibration as appropriate;

(d) Generating and controlling the quality of various products;

(e) Archiving all products;

(f) Distributing a selection of products;

(g) Analysing mission status, payload status and requirements for mission planning;

(h) Delivering requirements for payload and mission control to OCCs.

Core products are normally generated by the satellite operator at a central facility. External specialized centres may supplement those by processing other specific products.

Satellite data archiving requires the maintenance of high levels of hardware availability for data ingest and storage, as well as discovery and retrieval services, with provision for long-term data preservation over decades. Data must be associated with metadata that contain all the information necessary to use and evaluate the data. Comprehensive, standardized metadata, and standardized globally interoperable catalogue systems enable data discovery to be extended to a worldwide scale within the WMO Information System.

2.3.2.4 ***Data and products distribution***

Depending on data volumes and timeliness requirements, several methods of accessing data and products are available:

(a) Direct read-out from the satellite (when available; particularly prevalent among LEO satellites). This provides the best timeliness but presupposes the capability to receive raw data on an appropriate receiving station and to pre-process that data with an adequate software package.

(b) Near-real-time satellite retransmission of data after on-ground preprocessing or full processing. For GEO satellites, retransmission may be performed through the same satellite. Currently, retransmission is best achieved through commercial telecommunications satellite channels, such as the GEONETCast system, which consists of three coordinated services: EUMETCast (of the European Organization for the Exploitation of Meteorological Satellites), CMACast (of the China Meteorological Administration), and GEONETCast-Americas (of NOAA). JMA maintains the Himawari-Cast. Using this approach, dissemination services can be optimized within the ground segment, while taking into account the various missions and product sources available independently of the design constraints of any particular satellite.

(c) Near-real-time retransmission of data via specialized networks such as the WMO Global Telecommunication System.

(d) Push and pull distribution of data by authorized operational users in near real time from data processing centres.

(e) Data processing centres in the era of ‘big data’ can also distribute real-time data to cloud computing services for additional processing, archiving and retrieval of products by the user community. Cloud service providers allow direct computer processing of the data without requiring further distribution, while making the data more easily accessible.

(f) Active FTP retrieval from data centres for non-real-time data, specifically from archives.

Data and product distribution may be subject to conditions, depending on the status and data policy of the space agency running the programme (operational, research and development, commercial) and what the programme will be used for. Access to data retransmission services is generally controlled by encryption and subject to registration, even if no charges are levied.

2.3.2.5 ***User receiving stations***

User stations are installed to make use of real-time or near-real-time data transmission from the satellite. Depending on the satellite access modality and the user requirement, there may be:

(a) High-data-rate acquisition stations for full reception of the data available either by open access or by agreement with the satellite owner;

(b) Low-data-rate acquisition stations for a data selection of either reduced volume or quality;

(c) Receiving terminals of commercial telecommunication satellites used for data dissemination after preprocessing or processing in the data-processing and archiving centre.

Frequencies used by the high-data-rate acquisition stations are in the X band (about 8 GHz), which is used for data rates of up to approximately 100 Mbps. The low-data-rate acquisition stations make use of relatively low frequencies (L band: about 1 800 MHz for GEO). Commercial telecommunication satellite terminals use Ku band (about 11 GHz) or C band (about 3.8 GHz).

2.3.2.6 ***Product processing levels***

Satellite observations are retrieved from the raw data acquired from the instruments though a processing chain. Different processing levels are usually referred to, the detailed definitions of which depend on the instrument in question. Table 2.11 provides a generic description of these processing levels.

Level 0 data are processed from the raw data stream by removing communication artefacts (such as synchronization frames and communication headers) and appending all necessary auxiliary data, including housekeeping and station-added information on timing and tracking. Level 0 data should be archived permanently to enable reprocessing with an updated instrument model (such as improved calibration or georeferencing).

Level 1a or 1.0 data consist of instrument files (counts) in the original instrument projection, with an appended (but not applied) deformation matrix or algorithm for georeferencing and calibration coefficients. The process from Level 0 to Level 1a/1.0 is fully reversible. Level 1a/1.0 data are normally permanently archived, although in principle they could be reproduced if Level 0 data have been archived.

Level 1b or 1.5 data consist of calibrated, co-registered and geolocated data in physical units (generally radiances), still in the original instrument projection. The process from Level 1a/1.0

Table 2.11. Generic description of processing levels (to be adapted to each instrument)

Level	*Description*	
0	Instrument and auxiliary data reconstructed from satellite raw data after removing communications artefacts.	
1	Instrument data extracted, at full original resolution, with geolocation and calibration information.	1a (for LEO) or 1.0 (for GEO): calibration and geolocation attached but not applied. 1b (for LEO) or 1.5 (for GEO): calibration and geolocation applied. 1c, 1d, etc: optional for specific instruments.
2	Geophysical product retrieved from a single instrument in the original projection.	
3	Geophysical product retrieved from a single instrument, mapped on uniform space and time grid scales, possibly on a multi-orbital (for LEO) or multi-temporal (for GEO) basis. Irreversible process due to resampling.	
4	Composite multi-sensor and/or multi-satellite products; or result of model analysis.	

to Level 1b/1.5 is not reversible because of truncation, discretization and resampling operations. Although Level 1b/1.5 may in any case be reprocessed from Level 1a/1.0 or Level 0, the processing effort is such that, in general, Level 1b/1.5 data are permanently archived.

Level 1c data are processed from the Level 1b data of certain instruments to enable end users to make use of that data. The process may be fully reversible (for example, spectra from interferograms by Fourier transform) but equally may not be (such as with apodized spectra). In general, these data are permanently archived. For certain instruments, further Level 1 steps (1d, 1e, and the like) may be defined (the addition of a cloud flag, for instance).

Level 0 and Level 1 processing is performed by the satellite operator. Where there is a direct readout, the satellite operator generally ensures the availability of Level 0 and Level 1 preprocessing software to local data users.

Level 2 products are generated from Level 1 data by applying algorithms that make limited use of external information. Data quality information is appended. These products are generated in the original instrument projection and tend to be permanently archived.

Level 3 products are generated by compositing a sequence of Level 2 products from successive orbits (with LEO) or at successive times (with GEO). Possible gaps in the sequence may be filled by interpolation. Due to the resampling operations implied by mapping on uniform space and time grids, Level 3 is an irreversible process. Products are generated offline by the satellite operators or by end users; they tend to be permanently archived.

Level 4 products are generated by blending data from different instruments on the same or different satellites, either with other data sources, or by assimilation in a model. In Level 4 products, the contribution of a specific satellite instrument may be hardly recognizable.

REFERENCES AND FURTHER READING

August, T.; Klaes, D.; Schlüssel, P. et al. IASI on Metop-A: Operational Level 2 Retrievals after Five Years in Orbit. *Journal of Quantitative Spectroscopy and Radiative Transfer* **2012**, *113* (11), 1340–1371. https://doi.org/10.1016/j.jqsrt.2012.02.028.

Källén, E. Special Issue with Manuscripts Related to ESA's Atmospheric Dynamics Mission/Aeolus. *Tellus A: Dynamic Meteorology and Oceanography* **2008**, *60* (2), 189–190, https://doi.org/10.1111/j.1600-0870.2007.00296.x.

Susskind, J.; Blaisdell, J. M.; Iredell, L. Improved Methodology for Surface and Atmospheric Soundings, Error Estimates, and Quality Control Procedures: The Atmospheric Infrared Sounder Science Team Version-6 Retrieval Algorithm. *Journal of Applied Remote Sensing* **2014**, *8* (1), 1–34. https://doi.org/10.1117/1.JRS.8.084994.

CHAPTER 3. REMOTE-SENSING INSTRUMENTS

This chapter provides an overview of basic instrument concepts. It introduces the high-level technical features of representative types of Earth observation instruments.

3.1 INSTRUMENT BASIC CHARACTERISTICS

A large variety of instruments and sensing principles are used in Earth observation. The key instrument features introduced here are:

(a) Scanning, step-stare, swath and observing cycle;

(b) Spectral range and resolution;

(c) Spatial resolution (IFOV, pixel, ground sample distance (GSD), angular sample distance (ASD), modulation transfer function (MTF));

(d) Radiometric resolution.

3.1.1 Scanning, step-stare, swath and observing cycle

The most characteristic feature of an instrument is the way in which it scans the scene to acquire the necessary observations. That depends on the type of orbit (geostationary Earth orbit or non-geostationary orbit), on the platform attitude control (spinning or three-axis stabilized), on the design of the instrument, and sometimes on the specific type of measurement being taken. Only the most common scanning techniques will be described in this chapter.

Scanning refers to the motion of the instrument line of sight (LOS) over the scene of interest while collecting data. The data collected during a scan are referred to as a swath. Motion from one part of the scene to another part without collecting data is referred to as slewing. A stare is a special subset of scanning where the LOS motion relative to the scene is zero. The slew from one stare to the next is often referred to as a step.

A driving requirement for scanning is whether the scene should be observed with continuity (imagery) or can be sampled (sounding). A similar scanning mode may be used in both cases. However, imagery requires continuous scene coverage, while sounding can accommodate sampling with gaps.

Non-geostationary orbits include all orbits where the Earth's surface is moving relative to the spacecraft. These include LEO, moderately elliptical orbit (MEO) and HEO. The most common is LEO.

In non-geostationary orbits, a 2D Earth scene scanning can use satellite motion for an along-track dimension. A cross-track scan can then be provided by a rotating scan mirror (Figure 3.1). For imaging, rotation speed is synchronized with satellite motion so that the cross-track image lines come out contiguously. In other words, the angular motion of the spacecraft between scan mirror rotations equals the along-track dimension of the swath.

In the case of GEO, there is no satellite motion with respect to the Earth's surface. The two scanning dimensions must therefore be generated either by the instrument or by satellite rotation. In Figure 3.2, it is assumed that the satellite is spin-stabilized: the west–east scan is provided by the satellite rotation, while the north–south scan is obtained by a step motor. For a three-axis stabilized platform, the instrument must generate both west–east and north–south LOS motion.

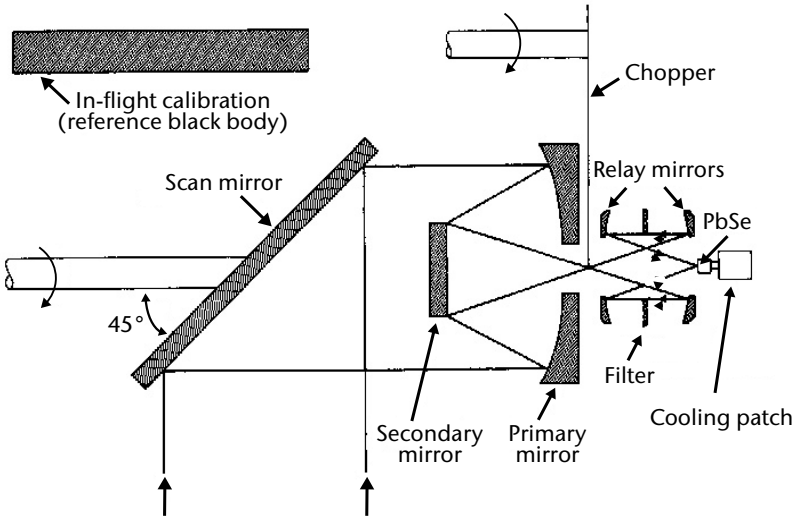

Figure 3.1. Typical scheme of a scanning radiometer in LEO

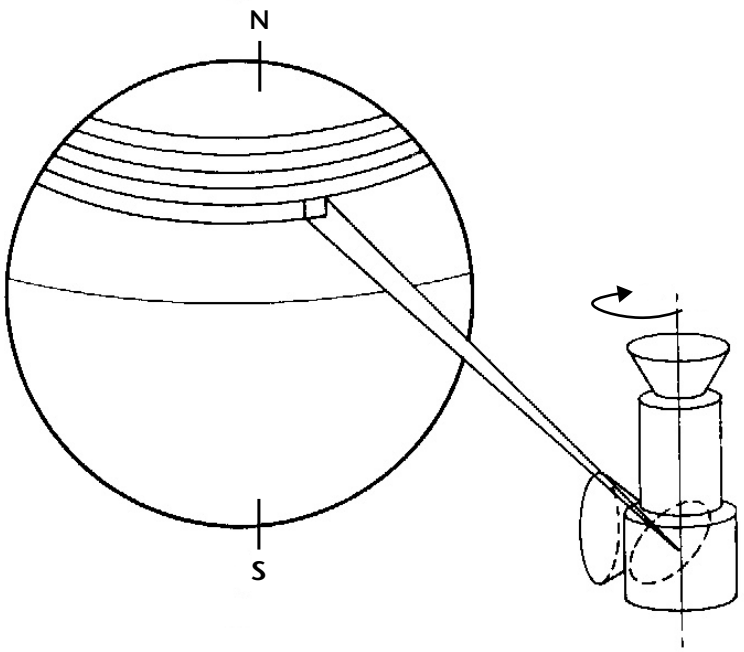

Figure 3.2. Schematic scanning from a spin-stabilized GEO

The advent of array detectors has led to additional scanning possibilities (Figure 3.3). With LEO, a linear array can be placed orthogonally to the satellite track, and can scan the scene without any mechanical movement (pushbroom scanning). Under another scheme, the linear array can be placed parallel to the track; cross-track mechanical scanning will then scan several lines in parallel (whiskbroom scanning). With GEO, whiskbroom scanning is now the rule. For instance, the 16-band Advanced Baseline Imager (ABI) on GOES-R scans from 322 lines in the infrared (IR) channels to 1 460 lines in the highest-resolution visible spectrum (VIS) channel. For sounding or for imaging with a two-dimensional detector array, a step-stare scheme can be used in any orbit.

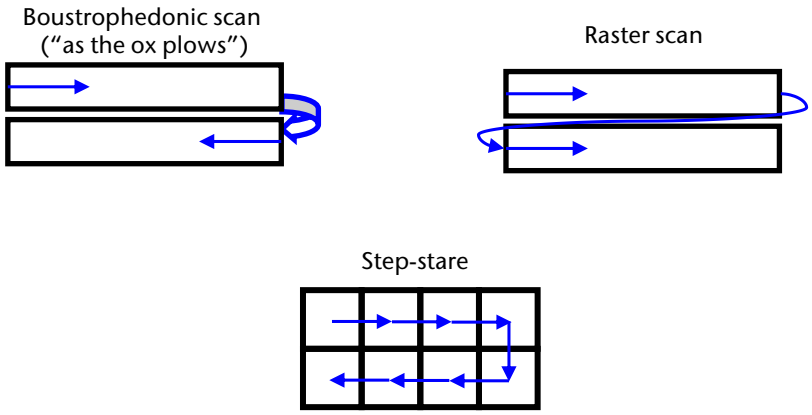

Figure 3.3. Boustrophedonic, raster and step-stare scan patterns

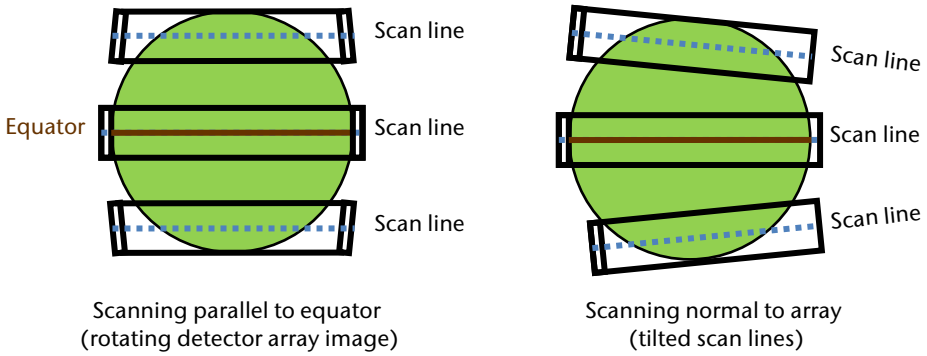

Figure 3.4. Single-mirror barrel-roll scanner: parallel scans to equator result in detector array image rotation; angled scans can be normal to detector array

When using a large detector array in an optical instrument, one must consider the effect that scanning has upon the rotation of the FOV of the detector array, which can complicate image processing. There are many types of scan mirror configurations. This discussion will address the two most common types: single-mirror barrel-roll scanner and two-mirror orthogonal scanner.

With a single-mirror barrel-roll scanner (as illustrated in Figure 3.4), the FOV of the detector is rotated by an angle equivalent to the angle of rotation (relative to the FOV at nadir). When there is only one detector element (for example, Advanced Very High Resolution Radiometer (AVHRR)), this rotation does not significantly impact the image because the centre of the pixel is still the centre. However, for a linear or two-dimensional array, this FOV rotation can be important because the relative location of the pixels is constantly changing with scan angle. For GEO instruments, the scan angle only varies over ±4.4 degrees, so the rotation does not matter for short arrays (for example, GOES-15 Imager) but can be significant for long arrays (for example, GOES-16 ABI). For LEO instruments, however, the scan angle varies over ±54 degrees, which results in a significant rotation of even very short detector arrays, which is why some LEO instruments do not use a single-mirror barrel-roll scanner.

A two-mirror orthogonal scanner (Figure 3.5) allows more rapid and adaptive scanning along the swath. When arranged so the mirror closest to the Earth adjusts the north–south LOS pointing and the mirror closest to the telescope adjusts the west–east LOS pointing, then west-to-east swaths parallel to the equator can be collected at any north–south location by setting the north–south mirror and then changing the position of the west–east mirror.

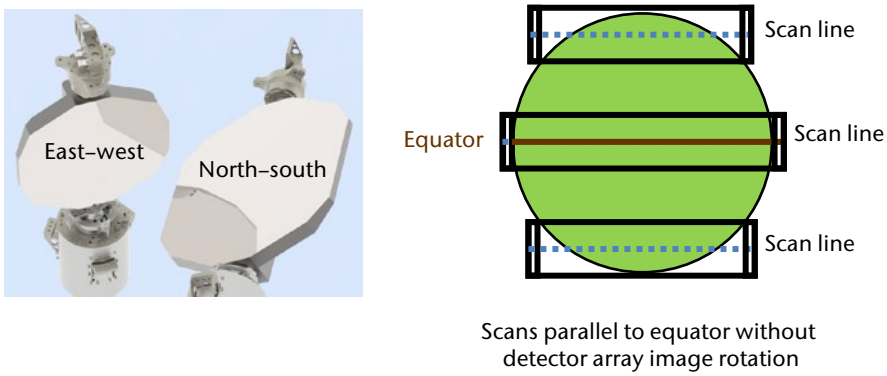

Figure 3.5. Two-mirror orthogonal scanner: scans parallel to equator without detector array image rotation

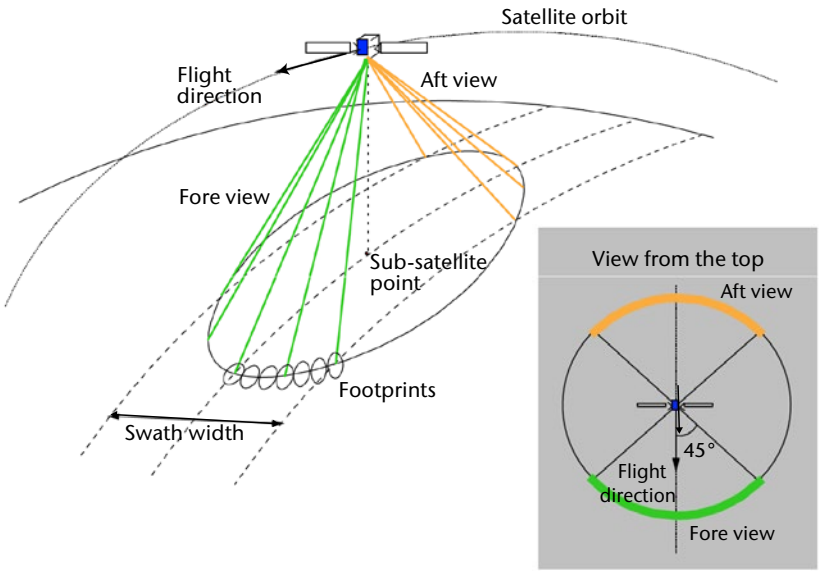

Figure 3.6. Geometry of conical scanning

A very convenient scanning mechanism for polarization-sensitive measurements is conical scanning (Figure 3.6). In this geometry, the incidence angle is constant. Therefore, the effect of polarization does not change along the scan line (an arc). By contrast, the incidence angle for cross-track scanning changes along the scan line, when moving from the nadir to the image edge. This invariance of the polarization effect across the image is very important for microwave (MW) measurement in window channels, where radiation reflected from elements such as the sea surface is strongly polarized. The measurement of the differential polarization constitutes important information that would be very difficult to use if the incidence angle changed across the scene. Another interesting feature of conical scanning is that the resolution remains constant across the whole image.

A disadvantage of conical scanning is that, with the selected incidence angle, the FOV does not normally reach the horizon. For example, the swath from an 800 km orbital height is ~1 600 km for a typical zenith angle of 53°, which is optimal for enhancing differential polarization information in MW. By contrast, the swath for a cross-track scanning instrument is close to 3 000 km, assuming a ± 70° zenith angle range, as shown in the present volume, Chapter 2, Table 2.1.

The swath is an important feature of an instrument in LEO since it determines the observing cycle. Chapter 2, Table 2.2 of the present volume outlines that, for a Sun-synchronous orbit at 800 km, one instrument with a swath of at least 2 800 km provides one global coverage per day for measurements operated in daytime only (for example, visible and short-wave (SW) sensors), or two global coverages per day for measurements operated day and night (for example, IR or MW sensors). MW conical scanning instruments generally provide one global coverage per day.

Estimating the observing cycle for typical LEO instruments

The order of magnitude of the observing cycle (Δt, in days) for a given swath can be estimated by a simple calculation. Considering the Equator's length (~40 000 km), the number of orbits per day (~14.2) and assuming that there is no significant overlap between adjacent swaths at the Equator, the calculation is as follows:

(a) For day and night sensors (IR or MW) operating on both ascending and descending passes: Δt = 1 400/swath (for example, for a MW conical scanner with 1 400 km swath: Δt = 1 day);

(b) For daytime only sensors (SW) operating on only one pass per orbital period: Δt = 2 800/swath (for example, for VIS land observation with 180 km swath: Δt = 16 days).

The concept of swath is not applicable for instruments with no cross-track scanning, such as altimeters or cloud radars. Where that is the case, the cross-track sampling interval Δx at the Equator replaces "swath" in the relationship above. It is also useful to estimate the global average of this sampling interval. The interval is given by a slightly different relationship because of shorter orbit spacing at higher latitudes:

(a) At an average cross-track sampling interval Δx, the typical time needed for global coverage is:

  (i) $\Delta t = 900/\Delta x$ for day and night sensors (for example, the Environmental Satellite (Envisat) Radar Altimeter – 2 (RA-2): Δx = 26 km, Δt = 35 days);

  (ii) $\Delta t = 1\,800/\Delta x$ for daytime only (for example, the National Oceanic and Atmospheric Administration (NOAA) Solar Backscatter Ultraviolet (SBUV) instrument: Δx = 170 km, Δt = 11 days).

(b) Reciprocally, in a time interval Δt (for example, the orbit repeat cycle or a main sub-cycle) the average cross-track sampling interval obtained is:

  (i) $\Delta x = 900/\Delta t$ for day and night sensors (for example, the Joint Altimetry Satellite Oceanography Network (JASON) altimeter: Δt = 10 days, Δx = 90 km);

  (ii) $\Delta x = 1\,800/\Delta t$ for daytime only (for example, NOAA SBUV: Δt = 5 days, Δx = 360 km).

Limb sounders are generally considered as non-scanning instruments in the cross-track direction. Assuming a cross-track sampling interval Δx = 300 km which is equal to the horizontal resolution of the measurements, the relationships above yield the following observing cycles:

(a) Δt 3 days for day and night sensors (for example, MIPAS on Envisat: 3 days = 1 orbit sub-cycle);

(b) Δt 6 days for daytime sensors (for example, SCIAMACHY-limb on Envisat: 6 days = 2 orbit sub-cycles).

For instruments providing sparse but well-distributed observations, the coverage cycle or the average sampling can be estimated by comparing the number of events and their resolution with

the Earth's surface to be covered. In the example of radio occultation using GPS and GLONASS, each satellite is able to provide about 1 000 observations per day, with a typical measurement resolution of 300 km for a total Earth's surface of 510 million km^2. Therefore:

(a) Time required with one satellite providing 1 000 observations/day:
Δt = 510 000 000/300/300/1 000 = 5.7 days;

(b) Number of satellites required for an observing cycle Δt: N = 5.7/Δt (for example, for Δt = 0.5 days, the number of satellites is close to 12).

Sun-, moon- or star-occultation instruments are an extreme case. Sun or moon occultation provides very few measurements per day, and only at the high altitudes of the day/night terminator in the case of the Sun, or at somewhat lower latitudes for the moon. Star occultation may provide several tens of measurements per day (for example, 40 for the Envisat Global Ozone Monitoring by Occultation of Stars (GOMOS)), evenly distributed by latitude.

3.1.2 Spectral range: radiometers and spectrometers

Another major characteristic feature of an instrument is the spectral range over which it operates. As discussed in the present volume, Chapter 2, 2.2, the spectral range determines which of the body's properties can be observed including reflectance, temperature and dielectric properties. Within the spectral range, there may be window regions and absorption bands, which mainly address condensed or gaseous bodies, respectively.

A spectral range may be more or less narrow, depending on the effects to be enhanced, or on the disrupting factors that need to be eliminated. The sub-divisions of a band or a window covered by an instrument are called channels. The number of channels depends on the number of pieces of independent information which have to be extracted from one band. If a limited number of well-separated channels are sufficient for the purpose, the instrument may only include those channels, and it is called a radiometer. If the information content rapidly changes with the frequency along the spectral range to the extent that channels must be contiguous, the instrument is called a spectrometer.

The technique adopted for channel separation, or for spectrometer subrange separation, is a major characteristic of the instrument. There are essentially two possible ways to physically separate two channels towards individual detectors (or detector arrays) and associated filter systems. First, the beam could be focused on a field stop and split into two bands by a dichroic mirror. The advantage is that co-registration is ensured, as the two channels look at the same FOV (which could comprise an array of IFOVs). However, if the two wavelengths are too close to each other (for example, a split window), a dichroic mirror cannot separate them sharply enough. The second solution is to let the full beam produce the image in the focal plane and set detectors (or detector arrays) with different filters (thus identifying different channels) in different parts of the focal plane (in-field separation). It is a much simpler solution, but as each channel looks at a different IFOV, co-registration can be more challenging. Combined solutions are possible: Figure 3.7 illustrates the solution implemented in the GOES-R ABI to separate the 16 channels using two beam splitters and 16 separate linear detector arrays. Current detector arrays are much larger than they have been in the past, which makes in-field separation more convenient.

Spectrometers provide continuous spectral sampling within the spectral range or in a number of spectral subranges. (These subranges are sometimes called channels and should not be confused with the channels of a radiometer). There are several types of spectrometer, the simplest of which is the prism. Others include grating spectrometers and interferometers; the most common interferometers are the Michelson and the Fabry-Pérot. Figure 3.8 shows the scheme of a Michelson interferometer.

With an interferometer, at any instance in time all detector elements are observing the same spectral channel but each spectral channel is observed at a slightly different time. For a dispersive spectrometer (for example, a grating spectrometer), all spectral channels are collected

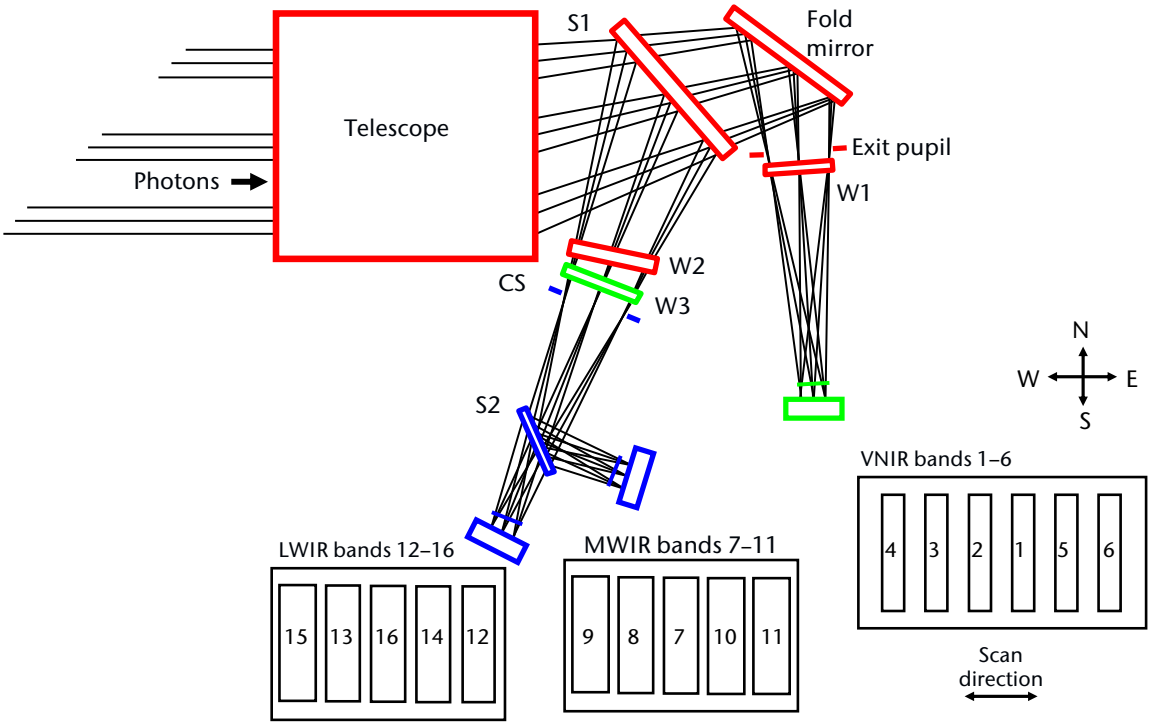

Figure 3.7. Channel separation scheme in ABI on GOES-R

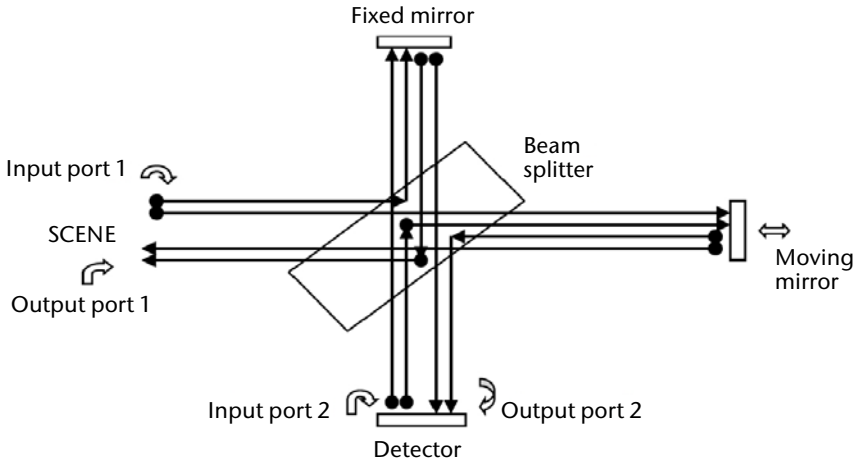

Figure 3.8. Scheme of a Michelson interferometer emphasizing the two input and output ports

simultaneously but each detector element is observing a different spectral band. Each approach has advantages and disadvantages. The optimum design for a spectrometer depends upon the mission.

The spectral resolution of a spectrometer is an important feature. The resolution of a Michelson interferometer is determined by the maximum length of the optical path difference (OPD) between the rays reflected by the fixed and moving mirrors. Referring to the unapodized resolution, the formula is:

$$\Delta\nu = 1/\mathrm{OPD}_{\max} \tag{3.1}$$

For example, in IASI, an instrument mounted on the Meteorological Operational (Metop) satellite, the excursion of the moving mirror is ± 2 cm. Therefore, OPD_{max} = 4 cm and $\Delta\nu$ = 0.25 cm^{-1}. If fine analysis of the spectrum is needed (for instance, to detect trace gas lines), apodization that implies a factor ~2 is required. The apodized resolution is therefore $\Delta\nu$ = 0.5 cm^{-1}.

For a grating spectrometer, the resolution is determined by the number of grooves, N, and the chosen order of diffraction, m. The resolving power $\lambda/\Delta\lambda$ is given by:

$$\lambda/\Delta\lambda = m \cdot N \tag{3.2}$$

For a Michelson interferometer, the spectral resolution is constant with a variable wavelength. For a grating spectrometer, however, it is the resolving power that is constant, and the spectral resolution that changes with wavelength. If a grating spectrometer is to cover a wide spectral range, that range should be subdivided into subranges that use different orders of diffraction, m. Resolving power may thus change based on subrange.

For a radiometer, the number of channels and their bandwidths play an equivalent role to spectral resolution for a spectrometer.

3.1.3 Spatial resolution (instantaneous field of view, pixel, ground sample distance, angular sample distance, and the modulation transfer function)

Colloquially, spatial resolution is a measure of the ability to distinguish different features within an image. In optical systems, the optics collect the light and form the image, the detector elements record it, and both limit the resolution.

The IFOV is probably the closest to what is commonly meant by resolution. In optical instruments (that is, SW, and IR instruments), it is determined by the beamwidth of the optics and the size of the detector. In MW it is determined by the size of the antenna.

In optical systems, the size of the IFOV is designed primarily on the basis of energy considerations (see 3.1.4). The IFOV may be determined by the shape of the detector; and although that may be square, the contour of an IFOV is not unduly sharp. In fact, the image of a point is a diffraction figure called point spread function (Figure 3.9). The IFOV is the convolution of the point spread function and the spatial response of the detector.

The energy entering the detector is also determined by the integration time between successive signal readings. During image scanning, the position of the LOS in the along-scan direction will change by an amount called sampling distance. Sampling distance is the product of the LOS velocity and the time interval between detector samples. When plotted in a rasterized 2D pattern, a pixel (picture element) appears as a series of rectangular elements. In the x-direction (along-scan direction), the pixel spacing corresponds to the sampling distance. In the y-direction (cross-scan), the pixel spacing corresponds to the LOS spacing of the detector array elements (within a swath) and the satellite motion during the time distance from one swath to the next (or the step motion in the north–south direction from GEO).

Angular sample distance (ASD) is the change in the LOS angle between detector samples. Many instruments have a constant ASD.

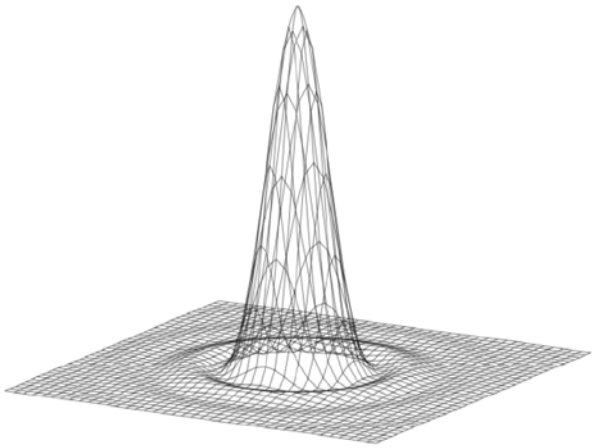

Figure 3.9. Shape of the point spread function

Ground sample distance (GSD) is the distance on the surface of the Earth between detector samples. Due to the curvature of the Earth, instruments with a constant ASD have a continuously varying GSD. Some instruments use variable aggregation and/or resampling (either on board or ground processing) to calculate pixels with a more uniform GSD from detector samples with a constant ASD.

Note: The fact that a sampling distance for an instrument is specified in linear units does not necessarily mean it has a constant GSD. ASDs are frequently expressed in units of linear dimension rather than angle in order to more easily be intuitively understood by the users of the data (for example, 1 km rather than 28 microradians). When this is done, the linear dimension used is equal to the GSD at nadir.

Resampling is simply using an appropriately weighted average of detector samples to calculate a pixel value. For instruments that utilize resampling, it is important to distinguish between the samples (what is read out from the detector elements) and pixels (the output of the resampler).

The pixel size is often confused with the resolution. That is because users can directly perceive the size of the picture element, whereas the IFOV is an engineering parameter that the user cannot see. In the along-scan direction, the IFOV of each pixel typically overlaps with its adjacent pixels. Nevertheless, it is wrong to think that resolution can be improved simply by reducing the integration time, since the integration time must be long enough to collect sufficient photons to ensure an appropriate radiometric accuracy (see 3.1.4).

There is a balance between the size of the IFOV and the size of the pixel. When the sampling distance is equal to the IFOV size, an imager is often described as “perfect”, although “maximum efficiency” might be a better term. For such an instrument the IFOVs are continuous and contiguous across the image. Such a system collects the minimum number of pixels needed to avoid gaps in the image. If the size of the pixel is less than the IFOV, that is, there is overlap between successive IFOVs, then the instrument is often described as “oversampled”. If the size of the pixel is greater than the IFOV, that is, there are gaps between successive IFOVs, then the instrument is usually described as “undersampled”.

However, the ideal ratio of IFOV to pixel size depends upon how the imagery is to be used. Oversampling is useful to reduce aliasing effects (undue enhancement of high spatial frequencies). When the IFOV is equal to 4.88 times the pixel size, the system meets the Nyquist criteria – meaning it can faithfully capture all spatial frequencies up to the IFOV size. Typically, however, reduced fidelity for the higher spatial frequencies and some minor aliasing is worth the significant reduction in data rate and improved radiometric accuracy achieved by using a

pixel size much closer to the IFOV size. Undersampling may be necessary when more energy must be collected in order to ensure the required radiometric accuracy. Examples of relationships between IFOV and pixel are:

(a) AVHRR: IFOV = 1.1 km; pixel = 1.1 km along-track, 0.80 km along-scan (oversampled) (AVHRR is a constant ASD instrument);

(b) SEVIRI: IFOV = 4.8 km; pixel = 3.0 km across-scan and along-scan (oversampled);

(c) ABI 0.64 μm (red) channel west–east: IFOV = 12.4 μrad; sample ASD = 11 μrad; pixel ASD = 14 μrad (0.5 km). Note that ABI's IFOV and sample ASD were optimized in conjunction with its resampling algorithm to deliver a desired MTF for the resulting pixel image.

The MTF is a quantitative way to assess spatial resolution. It is closely linked to the concept of IFOV and pixel. It is even more directly linked to the aperture diameter, "L", of an instrument's primary optics. The MTF represents the capability of the instrument to correctly manage the response to amplitude variation at the scene. It is the ratio between the observed amplitude, and the true signal amplitude from the scene, figured as sinusoidal. The observed amplitude is damped due to factors such as the diffraction from the optical aperture, the "window" introduced by the detector and smearing from integrating electronics. The effect of integrating the radiation over an ideal (squared) detector introduces a contribution to the MTF:

$$\mathrm{MTF}_{\mathrm{window}}(f) = \mathrm{sinc}(\pi \cdot \mathrm{IFOV} \cdot f), \text{ with } f = 1/(2\,\Delta x)\left(\mathrm{km}^{-1}\right) \text{ and } \mathrm{sinc}\, y = \frac{\sin y}{y} \qquad (3.3)$$

This shows that, for Δx = IFOV, MTF = sinc (π/2) = 2/π. Therefore, even for a "perfect" imager, MTF is lower than unity. The value $2/\pi \approx 0.64$ corresponds to the area of a half sinusoid inscribed in a square. The concept of MTF must be seen as closely associated with radiometric accuracy: it specifies at which spatial wavelength two features are actually resolved if their radiation differs by just the detectable minimum. Two features whose radiation differs by substantially more than the detectable minimum can be resolved, even if they are substantially smaller. However, if they are as small as IFOV/2, then MTF = 0, and they can in no way be resolved (f = 1/IFOV is called the cut-off frequency).

It is interesting to note how $\mathrm{MTF}_{\mathrm{window}}$ changes at different spatial wavelengths measured in terms of IFOV (where spatial wavelength is $2\,\Delta x$). Table 3.1 can be derived from equation 3.3:

Table 3.1. Variation of the $\mathrm{MTF}_{\mathrm{window}}$ function of the ratio Δx/IFOV

Δx/IFOV	1/2	2/3	1	2	3	4	5	6
$\mathrm{MTF}_{\mathrm{window}}$	0	0.30	0.64	0.90	0.95	0.97	0.98	0.99

This shows that features as small as two thirds of the IFOV can be resolved, but only if their radiances differ by more than three times the detectable minimum. It also shows that features twice as large as the IFOV can be resolved if their radiance difference exceeds the minimum by 10%.

The other major contribution to the MTF is diffraction. The relation is:

$$\mathrm{MTF}_{\mathrm{diffraction}} = \frac{2}{\pi}\left[\cos^{-1}\left(\frac{f}{f_d}\right) - \frac{f}{f_d}\sqrt{1-\left(\frac{f}{f_d}\right)^2}\right] \qquad (3.4)$$

where $f = 1/(2\,\vartheta\,H)$ (with H = satellite height above the Earth's surface); ϑ = angular resolution (that is, IFOV/H); $f_d = L/(\lambda\,H)$; L = aperture of the primary optics; and thus $f/f_d = \lambda/(2\,\vartheta\,L)$.

Diffraction is dominant when the wavelength λ is relatively large (as with microwaves), when the optics aperture is relatively small, or when the satellite altitude is relatively large (as with GEO). The value $MTF_{diffraction} = 0.5$ occurs for $f/f_d = 0.41$, that is:

$$\vartheta = 1.22\frac{\lambda}{L} \tag{3.5}$$

which is the classical law of diffraction.

In summary, what is commonly meant by the term "resolution" involves at least three parameters. Although they should be considered in context, each one is more closely associated with a different perception:

(a) IFOV: not visible to the user; controls the radiometric budget of the image;

(b) Pixel: provides direct perception of the degree of detail in the image;

(c) MTF: by monitoring the amplitude restitution, provides the perception of contrast.

3.1.4 **Radiometric resolution**

Although scarcely visible to the user, radiometric resolution is a defining element of instrument design. Scanning mechanisms, spectral resolution, spatial resolution, integration time and optics apertures are all designed to fulfil radiometric resolution requirements. Radiometric resolution is the minimum radiance difference necessary to distinguish two objects in two adjacent IFOVs. The observed difference is a combination of the true radiance difference between two bodies (signal) and the difference observed even when the contents of the IFOVs are identical (noise). The signal-to-noise ratio (SNR) is one way of expressing radiometric resolution.

Noise is a function of several factors, as set out in the radiometric performance formula:

$$\mathrm{NESR} = \frac{2F}{D^* \cdot \Delta\nu \cdot \tau \cdot \sqrt{\pi \cdot t \cdot \Delta\Omega}} \tag{3.6}$$

where:

NESR = noise equivalent spectral radiance (unit: W m^{-2} sr^{-1} $(cm^{-1})^{-1}$, that is, per unit of wave number);

$F = f/L$, F-number (f = system focal length, L = telescope aperture);

D^* = detectivity (strongly depending on ν);

$\Delta\nu$ = spectral resolution (expressed in terms of wave number $\nu = 1/\lambda$);

τ = instrument transmissivity;

t = integration time;

$\Delta\Omega$ = system throughput, given by the product of $(\pi \cdot L^2/4)$ by (IFOV^2/H^2); where:

$\pi \cdot L^2/4$ = areal aperture of the telescope;

H = satellite altitude;

IFOV^2/H^2 = solid angle subtended by the IFOV.

In general, when defining $I(\nu)$ = spectral radiance at instrument input (unit: W m^{-2} sr^{-1} $(cm^{-1})^{-1}$), this leads to:

$$\mathrm{SNR} = I(\nu)/\mathrm{NESR} \tag{3.7}$$

For SW, the input radiance is the solar spectral radiance corrected for the incidence angle and reflected according to body reflectivity (or albedo, if the body can be approximated as a Lambertian diffuser). Equations 3.6 and 3.7 lead to:

$$\frac{\text{SNR}}{\text{IFOV}\sqrt{\Delta\nu \cdot t}} \propto L \quad \text{(at a specific input radiance } I(\nu) \text{ or albedo } \rho) \tag{3.8}$$

That relationship explicitly links user-oriented parameters such as SNR, spectral resolution $\Delta\nu$, IFOV and integration time t to the size of the primary optics L.

In the case of narrowband IR channels, radiometric resolution is usually quoted as:

$$\text{NE}\Delta\text{T} = \frac{\text{NESR}}{dB / dT} \tag{3.9}$$

where B = Planck function, and $\text{NE}\Delta\text{T}$ = noise equivalent differential temperature at a specific temperature T.

With $\text{NE}\Delta\text{T}$, the performance formula 3.6 can be rewritten as follows:

$$\text{NE}\Delta\text{T} \cdot \Delta\nu \cdot \text{IFOV} \cdot \sqrt{t} = \frac{4H}{\pi \cdot dB / dT} \cdot \frac{F}{L \cdot D^* \cdot \tau} \tag{3.10}$$

The left-hand side of formula 3.10 shows user-oriented parameters (radiometric, spectral, horizontal and time resolutions), while the right-hand side shows instrument sizing parameters (F-number, optics aperture, detectivity and transmissivity). This formula is not valid in all circumstances, but is instructive for a rough analysis in many instances. Cases where the formula is not valid mainly occur when the detector itself constitutes the dominant noise source, or when the detector response time is not short enough in comparison with the available integration time. This is normally the case in the far infrared (FIR) range. But it may also be the case with shorter wavelengths if, for instance, microbolometers or thermal detectors are used in order to operate at room temperature. In other words, D^*, which obviously depends on ν, may be heavily dependent on the available integration time.

In the case of broadband channels, the concept of NESR, as expressed in equation 3.6, must be redefined in terms of integrated noise over the full spectral range of each channel. In that case, it is also possible to obtain a relationship similar to formula 3.10:

$$\text{NE}\Delta\text{R} \cdot \text{IFOV} \cdot \sqrt{t} \propto \frac{1}{L} \tag{3.11}$$

where $\text{NE}\Delta\text{R}$ = noise equivalent differential radiance (unit: W m^{-2} sr^{-1}).

The situation is different in the microwave range for two reasons. First, the need to limit the antenna size means that diffraction law establishes a link between the IFOV and the optics aperture L:

$$\text{IFOV} = \frac{1.24 \cdot H \cdot c}{L \cdot \nu^*} \tag{3.12}$$

where ν^* = frequency = c/λ; and c = speed of light.

Thus, there is less latitude for trade-off parameters. Second, the detection mechanism is based on comparing the scene temperature with the "system temperature", which increases with the bandwidth. The final outcome is that the equivalent of equations 3.8, 3.10 and 3.11 in the MW range is:

$$\text{NE}\Delta\text{T} \cdot \sqrt{\Delta\nu^* \cdot t} = T_{\text{sys}} \tag{3.13}$$

where T_{sys} = system temperature.

The system temperature depends on many technological factors, and increases sharply as frequency increases. On the one hand, equation 3.13 shows that, in the case of MW, radiometric resolution can only marginally be improved by increasing bandwidth and integration time, since the benefit only grows with the square root. On the other hand, because of the

diffraction-limited regime, the usual way to increase SNR by increasing optics aperture is not applicable. That is because, if the antenna diameter is increased, the IFOV is reduced commensurately (see equation 3.12).

This short review highlights the direct impact of user and mission requirements on instrument sizing. In addition, it shows how important it is to formulate requirements in a way that leaves room for optimization, without necessarily compromising the overall required performance. For instance with reference to equation 3.10, it is possible to draw a number of conclusions.

(a) For a given set of instrument parameters (L, F, τ and D^*), some user-driven parameters (NEΔT, $\Delta\nu$, IFOV and t) can be enhanced at the expense of others. In certain cases, this can be done at the software level during data processing on the ground. However, if all user requirements become more demanding and no compromises are made, a larger instrument will be necessary.

(b) The effect of NEΔT, $\Delta\nu$ and IFOV on instrument size is linear in relation to the optics diameter L. The effect of t (the integration time, driven by the requirement to cover a given area in a given time) is damped by the square root. Therefore, requirements for increased coverage and/or more frequent observation have a lesser impact than requirements for improved spatial, spectral and radiometric resolution.

(c) Increasing the optics aperture L has a significant impact on instrument size. Since it is very difficult to implement optical systems with F-number = $f/L < 1$, an increase in L implies an increased focal length, and therefore a volumetric growth of overall instrument optics. For example, a reduction in the IFOV from three to two kilometres would double the instrument mass.

3.2 INSTRUMENT CLASSIFICATION

In this section, Earth observation instruments are classified according to their main technical features. The following instrument types are considered:

(a) Moderate-resolution optical imager;

(b) High-resolution optical imager;

(c) Cross-nadir scanning short-wave sounder;

(d) Cross-nadir scanning infrared sounder;

(e) Microwave-imaging radiometer or microwave-sounding radiometer;

(f) Limb sounder;

(g) Global navigation satellite system radio-occultation sounder;

(h) Broadband radiometer;

(i) Solar irradiance monitor;

(j) Lightning imager;

(k) Cloud radar and precipitation radar;

(l) Radar scatterometer;

(m) Radar altimeter;

(n) Imaging radar (synthetic aperture radar);

(o) Space lidar;

(p) Gravity sensor;

(q) Solar activity, solar wind or deep space monitor;

(r) Space environment monitor;

(s) Magnetosphere or ionosphere sounder.

Most instrument types are subdivided into more detailed categories. Examples are provided to illustrate how instrumental features can be suited to particular applications. A comprehensive list of satellite Earth observation instruments, with their detailed descriptions, is available through the WMO online database of space-based capabilities, available from the WMO Space Programme website.

3.2.1 Moderate-resolution optical imager

This instrument has the following main characteristics:

(a) Operates in the VIS, NIR, SWIR, MWIR and TIR bands (that is, from 0.4 to 15 μm);

(b) Discrete channels, from a few to several tens, separated by dichroics, filters or spectrometers, with bandwidths from ~10 nm to ~1 μm;

(c) Imaging capability: continuous and contiguous sampling, with spatial resolution in the order of one kilometre, covering a swath of several hundred to a few thousand kilometres;

(d) Scanning: generally cross-track, but sometimes multiangle, and sometimes under several polarizations;

(e) Applicable in both LEO and GEO.

Depending on the spectral bands, number and bandwidth of channels, and radiometric resolution, the application fields may include:

(a) Multi-purpose VIS/IR imagery for cloud analysis, aerosol load, sea-surface temperature, sea-ice cover, land-surface radiative parameters, vegetation indexes, fires, and snow cover. The extent of the spectral range is a critical instrument feature;

(b) Ocean-colour imagery, aerosol observation and vegetation classification. The number of channels with narrow bandwidth in VIS and NIR is a critical instrument feature;

(c) Imagery with special viewing geometry, for the best observation of aerosol and cirrus, accurate sea-surface temperature, land-surface radiative parameters including bidirectional reflectance distribution function. The critical instrument features are the number of viewing angles and, when available, polarizations.

Tables 3.2–3.6 describe three examples of multi-purpose VIS/IR imagers (AVHRR/3 in LEO, MODIS in LEO and SEVIRI in GEO), one example of an ocean-colour imager (MERIS) and one example of an imager with special viewing geometry (POLDER). MODIS is an experimental sensor and plays a particular role as a wide scope multi-purpose VIS/IR imager. It is largely used to help define the specifications of follow-on operational instruments. The main uses of its various groups of channels are highlighted in Table 3.3.

Table 3.2. Example of multi-purpose VIS/IR imager operating in LEO: AVHRR/3 on NOAA and Metop

AVHRR/2/3	*Advanced Very High Resolution Radiometer*
Satellites	NOAA-15, NOAA-16, NOAA-17, NOAA-18, NOAA-19, Metop-A, Metop-B, Metop-C
Mission	Multi-purpose VIS/IR imagery for cloud analysis, aerosol load, sea-surface temperature, sea-ice cover, land-surface radiative parameters, normalized difference vegetation index, fires, snow cover, etc.
Main features	6 channels (channel 1.6 and 3.7 are alternative), balanced VIS, NIR, SWIR, MWIR and TIR
More information	https://www.wmo-sat.info/oscar/instruments/view/60 https://www.wmo-sat.info/oscar/instruments/view/61 https://www.wmo-sat.info/oscar/instruments/view/62

Table 3.3. Example of multi-purpose VIS/IR imager operating in LEO: MODIS on EOS-Terra and EOS-Aqua

MODIS	*Moderate-resolution Imaging Spectroradiometer*
Satellites	EOS-Terra and EOS-Aqua
Mission	Multi-purpose VIS/IR imagery for cloud analysis, aerosol properties, sea- and land-surface temperature, sea-ice cover, ocean colour, land-surface radiative parameters, vegetation indexes, fires, snow cover, total ozone, cloud motion winds in polar regions, etc.
Main features	36-channel VIS/IR spectro-radiometer
More information	https://www.wmo-sat.info/oscar/instruments/view/296

Table 3.4. Example of multi-purpose VIS/IR imager operating in GEO: SEVIRI on Meteosat Second Generation

SEVIRI	*Spinning Enhanced Visible Infrared Imager*
Satellites	Meteosat-8, Meteosat-9, Meteosat-10, Meteosat-11
Mission	Multi-purpose VIS/IR imagery for cloud analysis, aerosol load, sea-surface temperature, land-surface radiative parameters, normalized difference vegetation index, fires, snow cover, wind from cloud motion tracking, etc.
Main features	12 channels, balanced VIS, NIR, SWIR, MWIR and TIR
More information	https://www.wmo-sat.info/oscar/instruments/view/503

Table 3.5. Example of ocean-colour imager operating in LEO: MERIS on Envisat

MERIS	*Medium Resolution Imaging Spectrometer*
Satellite	Envisat
Mission	Ocean-colour imagery, aerosol properties, vegetation indexes, etc.
Main features	15 very narrow-bandwidth VIS and NIR channels
More information	https://www.wmo-sat.info/oscar/instruments/view/277

Table 3.6. Example of imager with special viewing geometry: POLDER on PARASOL

POLDER	*Polarization and Directionality of the Earth's Reflectances*
Satellite	PARASOL
Mission	Imagery with special viewing geometry, for best observation of aerosol and cirrus, land–surface radiative parameters including bidirectional reflectance distribution function, etc.
Main features	Bidirectional viewing, multipolarization, 9 narrow-bandwidth VIS and NIR channels
More information	https://www.wmo-sat.info/oscar/instruments/view/405

3.2.2 High-resolution optical imager

This instrument has the following main characteristics:

(a) Wavelengths in the VIS, NIR and SWIR bands (0.4 to 3 μm) with possible extension to MWIR and TIR;

(b) Variable number of channels and bandwidths:

  (i) Single channel (panchromatic) with around 400 nm bandwidth (for example, 500–900 nm);

  (ii) 3–10 multispectral channels with around 100 nm bandwidth;

  (iii) Continuous spectral range (hyperspectral); typically has 100 channels with around 10 nm bandwidth;

(c) Spatial resolution in the range of less than one metre to several tens of metres;

(d) Imaging capability: continuous and contiguous sampling, covering a swath ranging from a few tens of kilometres to approximately 100 km, often addressable within a field of regard of several hundreds of kilometres;

(e) Applicable in LEO. GEO is not excluded but not yet in use.

High-resolution optical imagers may perform a number of missions, depending on the spectral bands, the number and bandwidth of channels, and steerable pointing capability. Those missions include:

(a) Panchromatic imagers: surveillance, recognition, stereoscopy for digital elevation model, and the like. Critical instrument features are the resolution and the steerable pointing capability;

(b) Multispectral imagers: land observation for land use, land cover, ground water, vegetation classification, disaster monitoring, and the like. Critical instrument features are the number of channels and the spectral coverage;

(c) Hyperspectral imagers: land observation, especially for vegetation process study, carbon cycle, and the like. Critical instrument features are the spectral resolution and the spectral coverage.

Tables 3.7–3.9 describe an example of a panchromatic imager (WV60), a multispectral imager (ETM+) and a hyperspectral imager (Hyperion).

Table 3.7. Example of panchromatic high-resolution imager: WV60 on WorldView-1

WV60	*World View 60 camera*
Satellite	WorldView – 1
Mission	Surveillance, recognition, stereoscopy for digital elevation model, etc.
Main features	Panchromatic, resolution: 0.5 m, steering capability, 60 cm telescope aperture
More information	https://www.wmo-sat.info/oscar/instruments/view/697

Table 3.8. Example of multispectral high-resolution imager: ETM+ on Landsat-7

ETM+	*Enhanced Thematic Mapper +*
Satellite	Landsat-7
Mission	Land observation for land use, land cover, ground water, vegetation classification, disaster monitoring, etc.
Main features	8 channels: 1 panchromatic, 6 VIS, NIR and SWIR, 1 TIR Resolution: 15 m, 30 m and 60 m
More information	https://www.wmo-sat.info/oscar/instruments/view/136

Table 3.9. Example of hyperspectral high-resolution imager: Hyperion on NMP EO-1

Hyperion	
Satellite	New Millennium Program Earth Observing – 1 (NMP EO-1)
Mission	Land observation, especially for vegetation process study, carbon cycle, etc.
Main features	VIS/NIR/SWIR grating spectrometer with 220 channels (hyperspectral) in two groups, covering the ranges 0.4–1.0 μm and 0.9–2.5 μm respectively Channel bandwidth: 10 nm Resolution: 30 m
More information	https://www.wmo-sat.info/oscar/instruments/view/204

3.2.3 Cross-nadir scanning short-wave sounder

This spectrometer has the following main characteristics:

(a) Operates in the ultraviolet (UV), VIS, NIR and SWIR bands (0.2 to 3 μm);

(b) Spectral resolution ranging from a fraction of a nanometre to a few nanometres;

(c) Spatial resolution in the order of 10 km;

(d) Horizontal sampling not necessarily continuous and contiguous;

(e) Scanning capability can be from nadir-only pointing to a swath of a few thousand kilometres;

(f) Applicable both in LEO and GEO.

Depending on spectral bands and resolution, cross-nadir scanning SW sounders may be used in atmospheric chemistry for monitoring a number of species, mostly determined by the spectral bands used:

(a) UV only: ozone profile;

(b) UV and VIS: ozone profile and total column or gross profile of a small number of other species, such as BrO, NO_2, OClO, SO_2 and aerosol;

(c) UV, VIS and NIR: ozone profile and total column or gross profile of several other species, such as BrO, ClO, H_2O, HCHO, NO, NO_2, NO_3, O_2, O_4, OClO, SO_2 and aerosol;

(d) UV, VIS, NIR and SWIR: ozone profile and total column or gross profile of many other species, such as BrO, CH_4, ClO, CO, CO_2, H_2O, HCHO, N_2O, NO, NO_2, NO_3, O_2, O_4, OClO, SO_2 and aerosol;

(e) NIR and SWIR, possibly complemented by MWIR and TIR: total column or gross profile of selected species, such as CH_4, CO, CO_2, H_2O and O_2.

Tables 3.10 and 3.11 describe one example with full spectral coverage (SCIAMACHY-nadir in LEO) and another with reduced spectral coverage (UVN in GEO).

Table 3.10. Example of cross-nadir scanning SW sounder in LEO: SCIAMACHY-nadir on Envisat

SCIAMACHY-nadir	*Scanning Imaging Absorption Spectrometer for Atmospheric Cartography – nadir scanning unit*
Satellite	Envisat
Mission	Atmospheric chemistry, tracked species: BrO, CH_4, ClO, CO, CO_2, H_2O, HCHO, N_2O, NO, NO_2, NO_3, O_2, O_3, O_4, OClO, SO_2 and aerosol
Main features	Spectral range: UV/VIS/NIR/SWIR Imaging capability: grating spectrometer covering eight bands, 8 192 channels, with 7 polarization channels
More information	https://www.wmo-sat.info/oscar/instruments/view/478

Table 3.11. Example of cross-nadir scanning SW sounder in GEO: UVN on Meteosat Third Generation (MTG)

UVN	*Ultraviolet, Visible and Near-infrared sounder (Also known as Sentinel 4)*
Satellites	MTG-S1, MTG-S2
Mission	Atmospheric chemistry, tracked species: BrO, ClO, H_2O, HCHO, NO, NO_2, NO_3, O_2, O_3, O_4, OClO, SO_2 and aerosol
Main features	Spectral range: UV/VIS/NIR Imaging capability: grating spectrometer covering 3 bands, 1 470 channels
More information	https://www.wmo-sat.info/oscar/instruments/view/584

3.2.4 Cross-nadir scanning infrared sounder

These radiometers or spectrometers have the following main characteristics:

(a) Wavelengths in the MWIR and TIR bands (3–15 μm) with a possible extension to FIR (up to 50 μm) and auxiliary channels in the VIS/NIR bands;

(b) Spectral resolution in the order of 0.1 cm^{-1} (very high resolution), 0.5 cm^{-1} (hyperspectral) or 10 cm^{-1} (radiometer);

(c) Spatial resolution in the order of 10 km;

(d) Horizontal sampling not necessarily continuous or contiguous;

(e) Scanning capability can be from nadir-only pointing to a swath of a few thousand kilometres;

(f) Applicable both in LEO and GEO.

Depending on their spectral bands and resolution, cross-nadir scanning IR sounders may be used for atmospheric temperature and humidity profiling, and/or in atmospheric chemistry for a number of species:

(a) Radiometers provide coarse-vertical-resolution temperature and humidity profiles;

(b) Spectrometers provide high-vertical-resolution temperature and humidity profiles, coarse ozone profiles, total column and gross profile of a small number of other species, such as CH_4, CO, CO_2, HNO_3, NO_2, SO_2 and aerosol;

(c) Very high-resolution spectrometers that are specifically for atmospheric chemistry provide profiles or total columns of C_2H_2, C_2H_6, CFC-11, CFC-12, CH_4, $ClONO_2$, CO, CO_2, COS, H_2O, HNO_3, N_2O, N_2O_5, NO, NO_2, O_3, PAN, SF_6, SO_2 and aerosol.

Tables 3.12–3.14 set out three examples: a radiometer in GEO (Sounder on Geostationary Operational Environmental Satellite (GOES)); a hyperspectral sounder in LEO (IASI on Metop) and a very high-resolution spectrometer in LEO (TES-nadir on EOS-Aura).

Table 3.12. Example of radiometric cross-nadir scanning infrared sounder in GEO: Sounder on GOES

GOES Sounder	
Satellites	GOES-8, GOES-9, GOES-10, GOES-11, GOES-12, GOES-13, GOES-14, GOES-15
Mission	Coarse-vertical-resolution temperature and humidity profiles
Main features	Radiometer: 18 narrow-bandwidth channels in MWIR/TIR + 1 VIS
More information	https://www.wmo-sat.info/oscar/instruments/view/526

Table 3.13. Example of hyperspectral cross-nadir scanning infrared sounder in LEO: IASI on Metop

IASI	*Infrared Atmospheric Sounding Interferometer*
Satellites	Metop-A, Metop-B, Metop-C
Mission	High vertical-resolution temperature and humidity profile Coarse ozone profile Total column or gross profile of a number of other species, such as CH_4, CO, CO_2, HNO_3, NO_2, SO_2 and aerosol
Main features	Spectrometer: spectral resolution 0.25 cm^{-1} (unapodized), MWIR/TIR spectral range, interferometer with 8 461 channels and a one-channel embedded TIR imager
More information	https://www.wmo-sat.info/oscar/instruments/view/207

Table 3.14. Example of very high-resolution cross-nadir scanning infrared sounder in LEO: TES-nadir on EOS-Aura

TES-nadir	*Tropospheric Emission Spectrometer – nadir scanning unit*
Satellite	EOS-Aura
Mission	Atmospheric chemistry: profiles or total columns of C_2H_2, C_2H_6, CFC-11, CFC-12, CH_4, $ClONO_2$, CO, CO_2, COS, H_2O, HNO_3, N_2O, N_2O_5, NO, NO_2O_2, O_3, PAN, SF_6, SO_2 and aerosol
Main features	Spectrometer, spectral resolution: 0.059 cm^{-1} (unapodized), MWIR/TIR spectral range, imaging interferometer: four bands; 40 540 channels
More information	https://www.wmo-sat.info/oscar/instruments/view/563

3.2.5 Microwave radiometers

These radiometers have the following main characteristics:

(a) Frequencies from 1 to 3 000 GHz (wavelengths from 0.1 mm to 30 cm);

(b) Channel bandwidths from a few MHz to several GHz;

(c) Spatial resolution from a few kilometres to approximately 100 kilometres, determined by antenna size and frequency;

(d) Horizontal sampling not necessarily continuous or contiguous;

(e) Scanning: cross-track (swath in the order of 2 000 km), conical (swath in the order of 1 500 km, possibly providing single or dual polarization) or nadir-only;

(f) Applicable in LEO.

Depending on their frequency, spatial resolution, and scanning mode, MW radiometers may perform a number of missions:

(a) Multi-purpose MW imagery for precipitation, cloud liquid water and ice, precipitable water, sea-surface temperature, sea-surface wind speed (and direction if multipolarization is used), sea-ice cover, surface soil moisture, snow status, water equivalent, wetland, ecosystem monitoring, mapping flooding disasters, and the like. Critical instrument

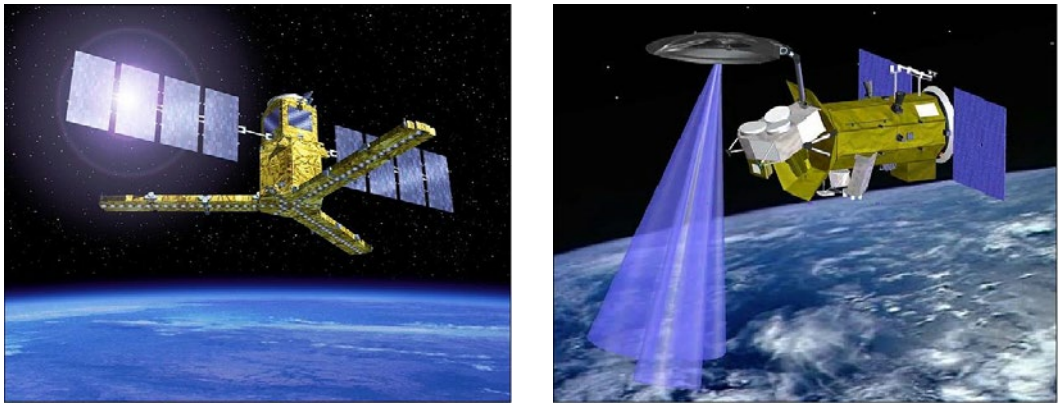

Figure 3.10. Sketch view of SMOS with MIRAS (left) and the satélite de aplicaciones científicas – D (SAC D) with Aquarius (right). The Aquarius real aperture antenna measures 2.5 m in diameter. The MIRAS synthetic aperture antenna is inscribed in a circle that measures 4 m in diameter.

features are: the extension of the spectral range, from 19 GHz as a minimum (possibly 10 GHz, or ideally 6–7 GHz) to at least 90 GHz; and conical scanning to make use of differential polarization under conditions of a constant incidence angle;

(b) Nearly-all-weather temperature and humidity sounding, which is also relevant for precipitation. Critical instrument features are the channels in absorption bands: O_2 for temperature (main frequency: 57 GHz) and H_2O for humidity (main frequency: 183 GHz);

(c) Sea-surface salinity and volumetric soil moisture. One critical instrument feature is the low frequency in the L band (main frequency: 1.4 GHz); this implies the use of very large antennas (see Figure 3.10);

(d) Atmospheric correction in support of altimetry missions. Critical instrument features are the frequency of the water-vapour 23 GHz band and its nearby windows; and the nadir viewing, co-centred with an altimeter.

Tables 3.15–3.18 describe a multi-purpose radiometer (AMSR-2), a temperature and humidity sounder (ATMS), a low-frequency radiometer (MIRAS) and a nadir-viewing radiometer (AMR).

Table 3.15. Example of multi-purpose MW imager: AMSR-2 on Global Change Observation Mission – Water "SHIZUKU" (GCOM-W)

AMSR-2	*Advanced Microwave Scanning Radiometer – 2 (AMSR-2)*
Satellite	GCOM-W
Mission	Multi-purpose MW imagery for precipitation intensity at surface (liquid or solid), sea-surface temperature, sea-ice cover and type, wind speed (near surface), biomass, cloud liquid water, integrated water vapour, land surface temperature, snow cover and water equivalent, surface soil moisture, etc.
Main features	Spectral range: 6.9–89 GHz, 7 frequencies, 16 channels, windows channels only, Conical scanning
More information	https://space.oscar.wmo.int/instruments/view/amsr2

Table 3.16. Example of MW temperature/humidity sounder: ATMS on Suomi National Polar-orbiting Partnership (NPP) and Joint Polar Satellite System (JPSS)

ATMS	*Advanced Technology Microwave Sounder*
Satellites	Suomi-NPP, JPSS-1 (NOAA-20), JPSS-2, JPSS-3 and JPSS-4
Mission	Nearly-all-weather temperature and humidity sounding; also relevant for precipitation
Main features	Spectral range: 23–183 GHz, 22 channels, including the 57 and 183 GHz bands Cross-track scanning
More information	https://www.wmo-sat.info/oscar/instruments/view/53

Table 3.17. Example of L-band MW radiometer: MIRAS on SMOS

MIRAS	*Microwave Imaging Radiometer using Aperture Synthesis*
Satellite	Soil Moisture and Ocean Salinity (SMOS)
Mission	Sea-surface salinity, volumetric soil moisture
Main features	Very large synthetic aperture antenna, single L-band frequency (1.413 GHz) Several polarimetric modes
More information	https://www.wmo-sat.info/oscar/instruments/view/287

Table 3.18. Example of non-scanning MW radiometer designed to support altimetry: AMR on JASON

AMR	*Advanced Microwave Radiometer*
Satellites	JASON-2, JASON-3
Mission	Atmospheric correction in support of the altimeters of JASON-1 and JASON-2
Main features	3 frequencies: 18.7 GHz, 23.8 GHz and 34 GHz
More information	https://www.wmo-sat.info/oscar/instruments/view/26

3.2.6 Limb sounders

This family of instruments has the following main characteristics:

(a) Scanning of the Earth's limb: this determines vertical resolution (in the range 1–3 km), the observed atmospheric layer (in the range 10–80 km), and spatial resolution (about 300 km along-view);

(b) Spectrometers using the UV/VIS/NIR/SWIR (200–3 000 nm) bands, the MWIR/TIR (3–16 μm) bands, or the high-frequency range of MW (100–3 000 GHz);

(c) Spatial resolution, from a few tens of kilometres to a few hundreds of kilometres in the transverse direction;

(d) Horizontal sampling, limited to one or a few azimuth directions;

(e) Applicable only in LEO.

Limb sounders can observe the high troposphere, stratosphere and mesosphere with high vertical resolution, and are mainly used for atmospheric chemistry. Depending on their spectral bands, limb sounders may track different species:

(a) SW spectrometers for a number of species, depending on the part of the spectrum covered; for the full range (UV/VIS/NIR/SWIR), the main species are: BrO, CH_4, ClO, CO, CO_2, H_2O, HCHO, N_2O, NO, NO_2, NO_3, O_2, O_3, O_4, OClO, SO_2 and aerosol;

(b) IR spectrometers for a number of species, depending on the part of the spectrum covered; for the full range (MWIR/TIR), the main species are: C_2H_2, C_2H_6, CFCs (CCl_4, CF_4, F11, F12, F22), CH_4, $ClONO_2$, CO, COF_2, H_2O, HNO_3, HNO_4, HOCl, N_2O, N_2O_5, NO, NO_2, O_3, OCS, SF_6 and aerosol;

(c) MW spectrometers for a number of species, depending on the part of the spectrum covered; for the range 100–3 000 GHz, the main species are: BrO, ClO, CO, H_2O, HCl, HCN, HNO_3, HO_2, HOCl, N_2O, O_3, OH and SO_2;

(d) Occultation sounders, tracking the Sun, the moon or the stars, for a number of species, depending on the part of the spectrum covered; for the full range (UV/VIS/NIR/SWIR) the main species are: H_2O, NO_2, NO_3, O_3, OClO and aerosol.

Tables 3.19–3.22 show limb sounders that use SW (SCIAMACHY-limb), IR (MIPAS), MW (MLS) and occultation in SW (SAGE-III ISS).

Table 3.19. Example of limb sounder using SW: SCIAMACHY-limb on Envisat

SCIAMACHY-limb	*Scanning Imaging Absorption Spectrometer for Atmospheric Cartography – limb scanning unit*
Satellite	Envisat
Mission	Chemistry of the high atmosphere Tracked species: BrO, CH_4, ClO, CO, CO_2, H_2O, HCHO, N_2O, NO, NO_2, NO_3, O_2, O_3, O_4, OClO, SO_2 and aerosol
Main features	UV/VIS/NIR/SWIR grating spectrometer, eight bands, 8 192 channels, with 7 polarization channels
More information	https://www.wmo-sat.info/oscar/instruments/view/477

Table 3.20. Example of limb sounder using IR: MIPAS on Envisat

MIPAS	*Michelson Interferometer for Passive Atmospheric Sounding*
Satellite	Envisat
Mission	Chemistry of the high atmosphere Tracked species: C_2H_2, C_2H_6, CFCs (CCl_4, CF_4, F11, F12, F22), CH_4, $ClONO_2$, CO, COF_2, H_2O, HNO_3, HNO_4, HOCl, N_2O, N_2O_5, NO, NO_2, O_3, OCS, SF_6 and aerosol
Main features	IR spectrometer: Michelson interferometer, range 685–2 410 cm^{-1} (4.15–14.6 μm), spectral resolution 0.035 cm^{-1} (unapodized), 60 000 channels/spectrum NESR: 50 nW cm^{-2} sr^{-1} cm at 685 cm^{-1}, 4.2 nW cm^{-2} sr^{-1} cm at 2 410 cm^{-1}
More information	https://www.wmo-sat.info/oscar/instruments/view/286

Table 3.21. Example of limb sounder using MW: MLS on EOS-Aura

MLS	*Microwave Limb Sounder*
Satellite	EOS-Aura
Mission	Chemistry of the high atmosphere Tracked species: BrO, ClO, CO, H_2O, HCl, HCN, HNO_3, HO_2, HOCl, N_2O, O_3, OH and SO_2
Main features	MW spectrometer: 5-band, 36 sub-bands, 1 000 channels Millimetre-submillimetre heterodyne radiometer at frequencies of 118 GHz (9 bands), 190 GHz (6 bands), 240 GHz (7 bands), 640 GHz (9 bands) and 2 500 GHz (5 bands)
More information	https://www.wmo-sat.info/oscar/instruments/view/293

Table 3.22. Example of limb sounder using SW in occultation: SAGE-III on ISS

SAGE-III ISS	*Stratospheric Aerosol and Gas Experiment – III for the ISS*
Satellite	International Space Station (ISS)
Mission	Atmospheric chemistry in the stratosphere Tracked species: H_2O, NO_2, NO_3, O_3, OClO and aerosol
Main features	UV/VIS/NIR/SWIR (290–1 550 nm), 9-band solar and lunar occultation grating spectrometer
More information	https://www.wmo-sat.info/oscar/instruments/view/693

3.2.7 Global navigation satellite system radio-occultation sounders

These instruments have the following main characteristics:

(a) GNSS receivers using at least two L-band frequencies around 1 180 GHz, 1 250 GHz and 1 580 GHz;

(b) Earth's limb observation, from surface to satellite altitude during the occultation phase of satellites from the GNSS constellations (such as GPS, GLONASS, Galileo and Compass/Beidou);

(c) Directional antennas: aft-looking (for setting GNSS), forward-looking (for rising GNSS), and toroidal (for navigation);

(d) Effective spatial resolution at around 300 km along the direction from the LEO satellite to the occulting GNSS satellite; a few tens of kilometres in the transverse direction;

(e) Horizontal sampling limited by the daily number of occultation events: from 250 to 1 500 events by satellite, depending on the number of GNSS systems received, and on the aft-looking/forward-looking tracking capability;

(f) Supported by a complex system of ground stations (see Figure 3.11);

(g) Applicable in LEO only.

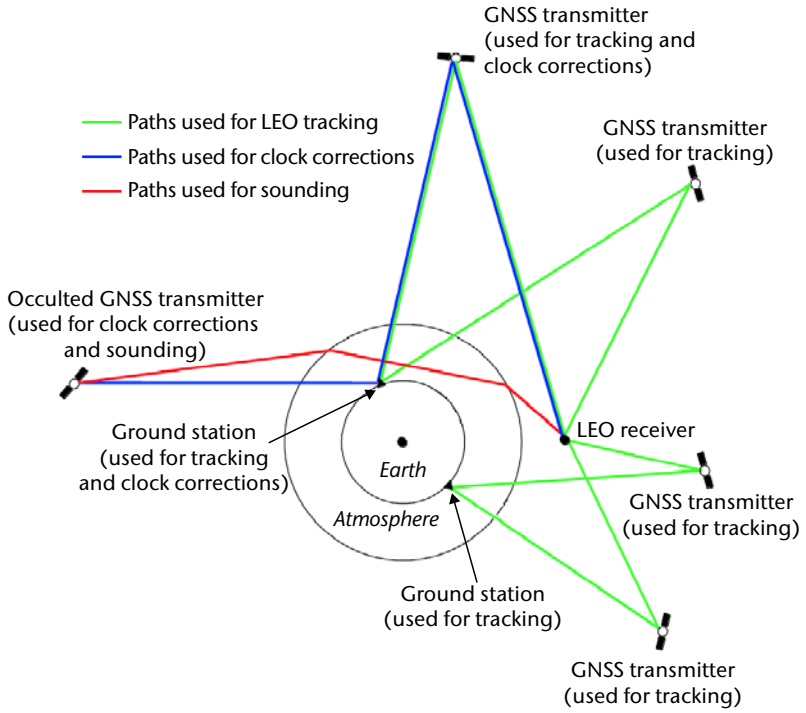

Figure 3.11. The overall system for radio occultation

Depending on their detailed features, GNSS radio-occultation sounders can provide different types of information:

(a) The signal-sampling time interval determines the vertical resolution of temperature, humidity and density profiles;

(b) Measurement sensitivity to the low atmospheric layers is determined by the size of the occultation antennas and the time-sampling technique;

(c) The number of frequencies that are used affects the accuracy of two ionospheric measurements: total electron content and electron density profile;

(d) The number of occultation events per day depends on the number of GNSS constellations used (GPS, GLONASS, Galileo, Beidou), the number of receiving channels for simultaneous tracking of further GNSS satellites, and the antenna accommodation feature: only aft-looking, only forward-looking, or both.

Table 3.23 sets out the main features of an example of a radio-occultation sounder (GRAS).

Table 3.23. Example of radio-occultation sounder: GRAS on Metop

GRAS	*GNSS Receiver for Atmospheric Sounding*
Satellites	Metop-A, Metop-B, Metop-C
Mission	High-vertical-resolution temperature, humidity and density profiles
Main features	Measuring the phase delay due to refraction during occultation between a navigation satellite and the LEO satellite, GNSS constellation: GPS, frequencies: L1 = 1 575.42 MHz and L2 = 1 227.6 MHz, 8 receiving channels: 4 for occultation, 8 for navigation
More information	https://www.wmo-sat.info/oscar/instruments/view/174

3.2.8 Broadband radiometers

These instruments have the following main characteristics:

(a) Wavelengths in the bands of total radiation emerging from the Earth and the atmosphere (0.2–300 μm) as well as from the fraction represented by reflected solar radiation (0.2–4.0 μm);

(b) One broadband channel, integrating over each of the two bands, and optional narrow-bandwidth channels in VIS and/or TIR to collect information on clouds within the IFOV;

(c) Cross-track scanning with continuous and contiguous sampling, to cover a swath of a few thousand kilometres with a spatial resolution of the order of 10 km;

(d) Applicable in LEO and GEO; observation from the L1 Lagrange libration point also is possible.

Broadband radiometers are designed to measure the Earth radiation budget – upward LW and SW irradiance at the top of the atmosphere (TOA). Accuracy depends on their detailed features:

(a) The greatest possible extension of the SW end of the spectrum into the UV range, and of the LW end of the spectrum into the FIR range, with a maximally flat response inside those ranges;

(b) Built-in multiviewing capability to convert radiance into irradiance;

(c) Supportive narrowband channels to collect information on clouds within the IFOV.

Tables 3.24 and 3.25 set out an example of a broadband radiometer in LEO (CERES) and one in GEO (GERB).

Table 3.24. Example of broadband radiometer in LEO: CERES on TRMM, EOS-Terra/Aqua, Suomi-NPP and JPSS

CERES	*Clouds and the Earth's Radiant Energy System*
Satellites	TRMM, EOS-Terra, EOS-Aqua, Suomi-NPP, JPSS-1
Mission	Earth radiation budget: upward LW and SW irradiance at TOA
Main features	Two broadband channels and one narrowband channel Either: two units, one for cross-track scanning, one for biaxial scanning for irradiance computation, or: one unit operating in alternative modes
More information	https://www.wmo-sat.info/oscar/instruments/view/78

Table 3.25. Example of broadband radiometer in GEO: GERB on Meteosat Second Generation

GERB	*Geostationary Earth Radiation Budget*
Satellites	Meteosat-8, Meteosat-9, Meteosat-10, Meteosat-11
Mission	Earth radiation budget: upward LW and SW irradiance at TOA
Main features	Two broadband channels
More information	https://www.wmo-sat.info/oscar/instruments/view/153

3.2.9 Solar irradiance monitors

These instruments have the following main characteristics:

(a) Wavelengths in the solar radiation range 0.15–50 μm;

(b) Integration over the full range (total solar irradiance) and/or spectroscopy in the 0.15–3.00 μm range;

(c) Total solar irradiance is measured by absolute techniques, such as active cavity radiometers pointing at the Sun;

(d) Applicable both in LEO and in GEO.

Solar irradiance monitors complement broadband radiometers in order to measure the Earth radiation budget. They also contribute to solar activity monitoring for the purpose of space weather observation. Detailed features that affect their performance are:

(a) Extending their sensitivity to within the solar radiation range;

(b) Their capability to provide spectral information in context in the UV/VIS/NIR/SWIR ranges.

Table 3.26 sets out the main features of an example of a solar irradiance monitor in LEO (TSIS).

Table 3.26. Example of solar irradiance monitor in LEO: TSIS on JPSS – Free Flyer (FF)

TSIS	*Total and Spectral Solar Irradiance Sensor*
Satellite	International Space Station (ISS)
Mission	Solar irradiance monitoring (total and spectrally resolved)
Main features	Assemblage of: Four active cavity radiometers for total irradiance (total irradiance monitor: range of 0.2–10 μm), prism spectrometer for spectral irradiance (spectral irradiance monitor: range of 0.2–2.0 μm; spectral resolution: 0.25–33 nm)
More information	https://www.wmo-sat.info/oscar/instruments/view/580

3.2.10 Lightning imagers

These instruments have the following main characteristics:

(a) Detector matrix (CCD): continuous Earth observation in a very narrow O_2 band at 777.4 nm;

(b) Measurement of flash occurrence, spatial extent (area) and intensity in the IFOV;

(c) Spatial resolution of 5–10 km;

(d) Continuous and contiguous horizontal sampling; full disk from GEO and swath of several hundred kilometres from LEO;

(e) Applicable in LEO and GEO.

Lightning imagery and flash rate tendency is useful as a proxy for updraft intensification/convective vigor, convective precipitation, continuing current, and NOx generation. Different sampling is applicable from LEO and GEO:

(a) From LEO, the measurement is available for the interval during satellite motion in which one Earth's spot is visible within the FOV of the CCD matrix (about 90 seconds);

(b) From GEO, monitoring is continuous.

Tables 3.27 and 3.28 set out an example of a lightning imager in LEO (LIS) and one in GEO (GLM).

Table 3.27. Example of lightning imager in LEO: LIS on TRMM

LIS	*Lightning Imaging Sensor*
Satellite	Tropical Rainfall Measuring Mission (TRMM)
Mission	Proxy for convective intensification and severe storm development, proxy for convective precipitation, proxy for NOx generation
Main features	CCD camera operating at 777.4 nm (O_2) to count flashes and measure their spatial extent and intensity
More information	https://www.wmo-sat.info/oscar/instruments/view/250

Table 3.28. Example of lightning imager in GEO: GLM on GOES

GLM	*Geostationary Lightning Mapper*
Satellites	GOES-R (GOES-16), GOES-S (GOES-17), GOES-T, GOES-U
Mission	Proxy for convective precipitation and turbulence, proxy for NOx generation, study of the Earth electric field.
Main features	CCD camera operating at 777.4 nm (O_2) to count flashes and measure their intensity
More information	https://www.wmo-sat.info/oscar/instruments/view/157

3.2.11 Cloud radar and precipitation radar

These instruments have the following main characteristics:

(a) Operating frequencies in Ku (~14 GHz), Ka (~35 GHz) or W (~94 GHz) bands;

(b) Pulse repetition rate that results in a vertical resolution of a few hundred metres;

(c) Spatial resolution of 2–5 km;

(d) Continuous and contiguous horizontal sampling; swath from nadir-only to several hundreds of kilometres;

(e) Only applicable in LEO.

The operating frequency determines possible applications:

(a) Ku band is suitable for heavy rain (liquid, with droplets that may exceed 1 cm). Non-precipitating clouds (droplets of less than 0.1 mm) are totally transparent, and light precipitation can hardly be detected. At these relatively low frequencies, electronic

switching, which is necessary to avoid mechanical movements of large antennas, is relatively easy. Relatively wide swaths (several hundreds of kilometres) can therefore be implemented.

(b) Ka band is suitable for light rain (from stratiform clouds) and snowfall. Electronic switching is still possible, and swaths of a few hundreds of kilometres can be implemented.

(c) W band is suitable for non-precipitating clouds (droplets of less than 0.1 mm). Several studies have also reported that this can be applied to the observation of precipitating cloud systems, specifically on the edges of precipitation or in cases of no precipitation, including the eye of tropical cyclones.

Tables 3.29 and 3.30 set out an example of a dual-frequency (Ku and Ka) precipitation radar (DPR) and an example of a W-band cloud radar (CPR on CloudSat).

Table 3.29. Example of precipitation radar: DPR on GPM Core Observatory

DPR	*Dual-frequency Precipitation Radar*
Satellite	Global Precipitation Measurement (GPM) Core Observatory
Mission	Vertical profile of heavy rain (liquid), light rain and snowfall
Main features	Dual-frequency imaging radar, frequencies: 13.6 GHz and 35.55 GHz, sensitivity: 0.5 mm/h at 13.6 GHz; 0.2 mm/h at 35.55 GHz
More information	https://www.wmo-sat.info/oscar/instruments/view/125

Table 3.30. Example of cloud radar: CPR on CloudSat

CPR	*Cloud Profiling Radar*
Satellite	CloudSat
Mission	Vertical profile of non-precipitating cloud water (liquid and ice)
Main features	Frequency: 94.05 GHz, sensitivity: –30 dBZ
More information	https://www.wmo-sat.info/oscar/instruments/view/91

3.2.12 Radar scatterometers

These instruments have the following main characteristics:

(a) Operating frequencies in C (~5 GHz) or Ku (~14 GHz) bands;

(b) Very accurate calibration in order to measure backscatter coefficients (σ^0) from sea capillary waves;

(c) Spatial resolution: 10–50 km;

(d) Continuous and contiguous horizontal sampling; swath of approximately 1 000 km;

(e) Only applicable in LEO.

There are two concepts, mainly differing by the scanning principle (see Figure 3.12):

(a) Electronic scanning: side-looking, generally uses C band and provides three azimuth views for differential σ^0. It is more accurate for low-intensity sea-surface wind and for soil moisture.

(b) Conical scanning: generally uses Ku band, with two beams and two polarizations. It provides four azimuth views for differential σ^0.

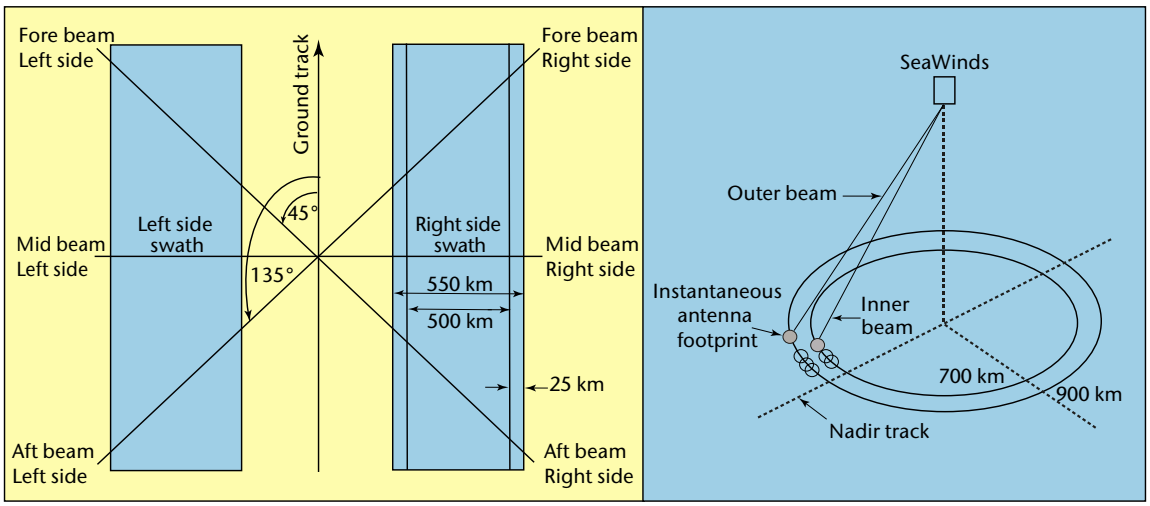

Figure 3.12. Two concepts for multiviewing scatterometers. Left: six antennas for three σ = s under azimuth angles, 45°, 90° and 135° respectively, on both the left and right side of the sub satellite track (ASCAT on Metop). Right: conical scanning of an antenna with two beams and two polarizations, for σ = s under four azimuth angles for areas in the inner circle (SeaWinds on QuikSCAT). The ASCAT concept leaves an uncovered strip of ~700 km around the sub satellite track. In the SeaWinds concept, there appears to be no gap, but accuracy is poor in the inner part of the swath around the sub satellite track.

Tables 3.31 and 3.32 describe radar scatterometers using pushbroom scanning (ASCAT) and conical scanning (SeaWinds).

Table 3.31. Example of pushbroom radar scatterometer: ASCAT on Metop

ASCAT	*Advanced Scatterometer*
Satellites	Metop-A, Metop-B, Metop-C
Mission	Sea-surface wind vector; large-scale soil moisture
Main features	C band (5.255 GHz), left and right side-looking, 3 antennas on each side
More information	https://www.wmo-sat.info/oscar/instruments/view/47

Table 3.32. Example of conical-scanning radar scatterometer: SeaWinds on QuikSCAT

SeaWinds	
Satellite	Quick Scatterometer (QuikSCAT) mission
Mission	Sea-surface wind vector
Main features	Ku band (13.4 GHz), conical scanning, 2 beams, 2 polarizations
More information	https://www.wmo-sat.info/oscar/instruments/view/482

3.2.13 **Radar altimeters**

These instruments have the following main characteristics:

(a) Operating frequencies in Ku band (~14 GHz), with auxiliary C band (~5 GHz), or Ka band (~35 GHz);

(b) Very accurate ranging measurement between the satellite and the Earth's surface;

(c) Spatial resolution in the range of 20 km;

(d) Exclusively nadir-pointing;

(e) Only applicable in LEO.

Radar altimeters generally operate in Ku band, using C band for correction of the signal rotation induced by the ionosphere. They are linked to a nadir-pointing MW radiometer for water vapour correction. Their accurate ranging is used for ocean topography: the echo spread provides information on significant wave height, while the echo intensity provides information on wind speed.

Depending on the detailed features of the instrument and of the satellite orbit, altimeters may be optimized for different applications:

(a) Relatively high, non-Sun-synchronous orbit (for example, 1 336 km), where inclination provides high stability to the orbit (for example, 66°); especially suited to solid Earth (geoid) and ocean circulation;

(b) SAR-like processing of the return echoes to synthesize higher spatial resolution along the sub-satellite track (see Figure 3.13);

(c) Parallel antennas to implement wide-swath altimetry by interferometry; particularly useful for land use including on inland waters, such as lakes;

(d) Dual frequency (C and Ku bands), which provides information on the total electron content between a satellite and the Earth's surface.

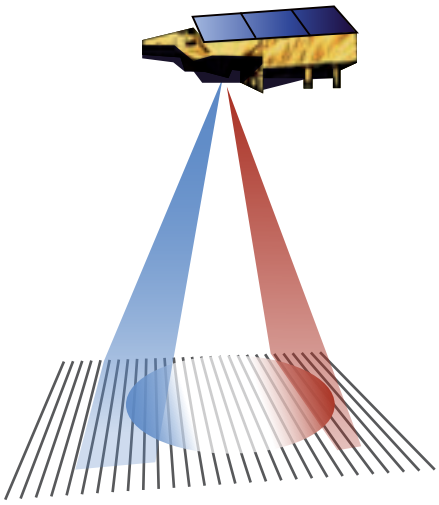

Figure 3.13. Enhancing along-track altimeter resolution by SAR-like signal processing

Table 3.33 sets out the main features of a radar altimeter with data of geodetic quality (Poseidon-3).

Table 3.33. Example of radar altimeter: Poseidon-3 on JASON-2

Poseidon-3	*Solid-state radar altimeter – 3*
Satellite	JASON-2
Mission	Ocean topography, the geoid, significant wave height, wind speed, total electron content
Main features	2 frequencies: 5.3 GHz; 13.58 GHz
More information	https://www.wmo-sat.info/oscar/instruments/view/407

3.2.14 Imaging radar (synthetic aperture radar)

This wide range of instruments has the following main characteristics:

(a) Operating frequencies in P (~0.4 GHz), L (~1.3 GHz), S (~2.7 GHz), C (~5.3 GHz), X (~9.6 GHz), or Ku (~17.2 GHz) bands. The L, C and X bands are most commonly used;

(b) Several combinations of polarizations in transmission and reception: HH, VV, VV/HH, HH/HV and VV/VH;

(c) There is a trade-off between spatial resolution and swath: a 1–30 m resolution is associated with a swath of 30–100 km; but a 100–1 000 m resolution is associated with a swath of 300–500 km;

(d) Side looking, generally on one side, maintaining high resolution within a field of regard of several hundreds of kilometres;

(e) Applicable in LEO only.

Figure 3.14 illustrates the operating modes of ASAR, a C-band synthetic aperture radar (SAR).

The operating frequency is a critical feature, optimized for the purposes for which an SAR is designed:

(a) P band is most suited to biomass monitoring and hydrological mapping;

(b) L band is best suited to wave observation and volumetric soil moisture;

(c) S band is best suited to volumetric soil moisture;

(d) C band covers a wide range of applications: sea ice, wave parameters by spectral analysis of image segments, surface soil moisture, snow parameters, glaciers, ground water, and the like. However, each individual parameter can be optimally observed at other frequencies;

(e) X band provides the best spatial resolution, and is therefore best suited to surveillance;

(f) Ka band is specifically suited to snow, which is transparent at lower frequencies;

(g) Interferometry of the signals from one SAR at different times or two SARs flying in tandem enables the measurement of the digital elevation model and the detection of contour changes (such as coastlines and lakes) and elevation (for example, volcano top surface).

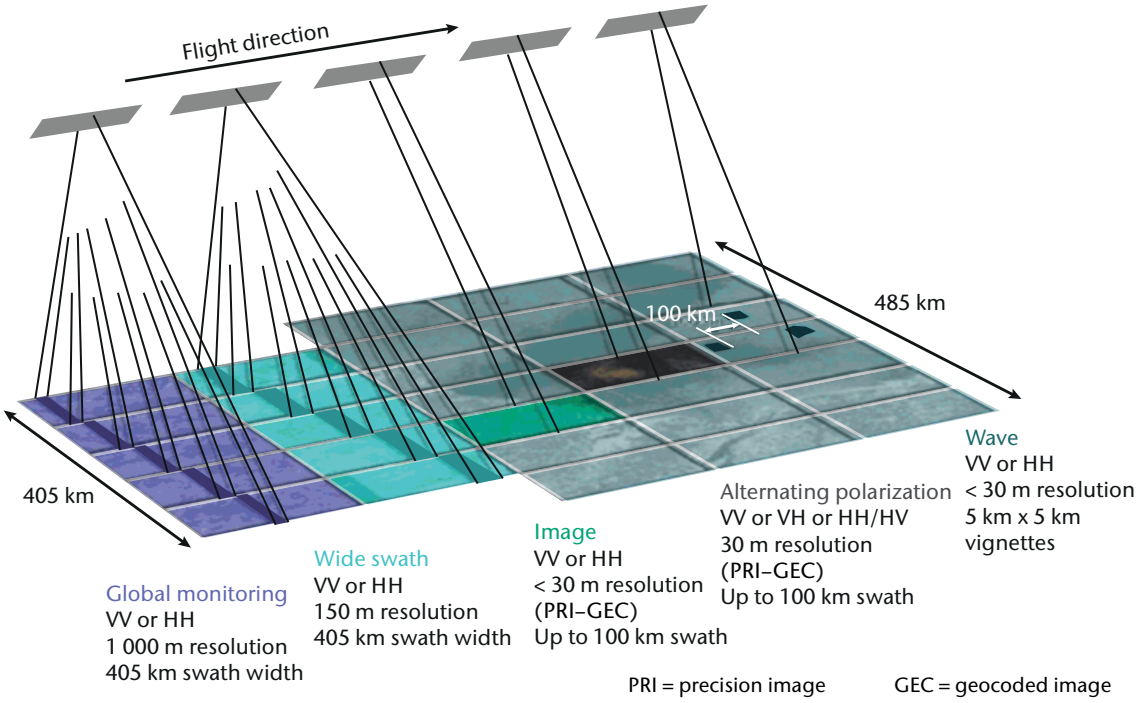

Figure 3.14. Operating modes of ASAR on Envisat. In the global monitoring and wide swath modes, the swath is 405 km and is linked to either a 1 000 m or 150 m resolution. In the image and alternating polarization modes, a 100 km swath with a 30 m resolution can be pointed to one of seven positions within a field of regard of 485 km. In the wave mode, vignettes of 5 km x 5 km with 30 m resolution are sampled at every 100 km along track.

Table 3.34 records the main features of a C-band SAR (ASAR).

Table 3.34. Example of C-band SAR: ASAR on Envisat

ASAR	*Advanced Synthetic Aperture Radar*
Satellite	Envisat
Mission	Sea ice, wave parameters by spectral analysis of image segments, surface soil moisture, snow parameters, glaciers, ground water, etc.
Main features	C-band SAR, frequency: 5.331 GHz, multipolarization and variable pointing/resolution
More information	https://www.wmo-sat.info/oscar/instruments/view/44

3.2.15 Lidar-based instruments

This group of instruments has the following main characteristics:

(a) Operating wavelengths in the UV (for example, 355 nm), VIS (for example, 532 nm), NIR (for example, 1 064 nm), or SWIR (for example, 1 600 nm) bands;

(b) Possible dual wavelength, two receivers (for Mie and Rayleigh scattering); polarimetry;

(c) Horizontal resolution within a 100 m range, often degraded by up to 50 km in order to collect enough de-correlated samples;

(d) Vertical resolution within a 100 m range (approximately 10 cm for lidar altimeters);

(e) Non-scanning: either nadir-viewing or oblique.

A space lidar is a voluminous instrument that needs to be optimized for specific applications:

(a) Doppler lidars generally operate in UV, for both Mie and Rayleigh scattering, in order to track aerosol and air molecules; oblique view is used to measure radial wind in clear air and aerosol;

(b) Backscatter lidars operate at one (on UV) or two (VIS and NIR) wavelengths, often with more polarizations; nadir view is used for obtaining aerosol profiles, cloud-top height and atmospheric discontinuities, such as the height of the top of the planetary boundary layer and of the tropopause;

(c) Lidar altimeters usually operate at two wavelengths (VIS and NIR); nadir view is used, as is very high-vertical resolution (for sea-ice elevation) and horizontal resolution (for ice boundaries);

(d) Differential absorption lidar operate at one wavelength centred on the absorption peak of one trace gas, in UV, VIS, NIR or SWIR, and nearby windows; nadir view is used for high-vertical-resolution observation of, for example, O_3, H_2O and CO_2.

Tables 3.35–3.38 give details of a Doppler lidar (ALADIN), a backscatter lidar (CALIOP), a lidar altimeter (GLAS) and a differential absorption lidar (CO_2 lidar).

Table 3.35. Example of Doppler lidar: ALADIN on ADM-Aeolus

ALADIN	*Atmospheric Laser Doppler Instrument*
Satellite	Atmospheric Dynamics Mission (ADM) – Aeolus
Mission	Wind profile in clear air, aerosol profile, cloud-top height
Main features	Single-wavelength (355 nm), side-looking; 35° off-nadir High spectral resolution laser for distinguishing aerosol types
More information	https://www.wmo-sat.info/oscar/instruments/view/17

Table 3.36. Example of backscatter lidar: CALIOP on CALIPSO

CALIOP	*Cloud–Aerosol Lidar with Orthogonal Polarization*
Satellite	Cloud–Aerosol Lidar and Infrared Pathfinder Satellite Observations (CALIPSO)
Mission	Aerosol profile, cloud-top height and atmospheric discontinuities (height of the top of the planetary boundary layer and of the tropopause)
Main features	Two wavelengths (532 and 1 064 nm), measurements at two orthogonal polarizations
More information	https://www.wmo-sat.info/oscar/instruments/view/73

Table 3.37. Example of lidar altimeter: GLAS on ICESat

GLAS	*Geoscience Laser Altimeter System*
Satellite	Ice, Cloud and Land Elevation Satellite (ICESat)
Mission	Polar ice sheet thickness and topography, cloud-top height, aerosol
Main features	Dual-wavelength lidar (532 and 1 064 nm)
More information	https://www.wmo-sat.info/oscar/instruments/view/155

Table 3.38. Example of differential absorption lidar: CO_2 lidar on ASCENDS

CO_2 lidar	
Satellite	Active Sensing of CO_2 Emissions over Nights, Days, and Seasons (ASCENDS)
Mission	Monitoring CO_2 with unprecedented accuracy by using lidar
Main features	Wavelength: 1.572 μm for CO_2 Option for O_2 at 1 260 or 765 nm also considered
More information	https://www.wmo-sat.info/oscar/instruments/view/86

3.2.16 Gradiometers/accelerometers

Knowledge of the gravity field is crucial for modelling the solid Earth. Several space techniques address this subject.

(a) The long-wave components of the gravity field are measured through radar or lidar altimetry, or through precise orbitography (for example, with laser ranging, radio positioning, GNSS, star tracking).

(b) Short-wave components (anomalies and perturbations of the gravity field) are observed at satellite altitude by accelerometers or gradiometers, in association with satellite-to-satellite ranging systems. An accelerometer measures the variation of the gravity field along the satellite trajectory. A gradiometer comprises a network of accelerometers, which measures the gravity-gradient tensor. Satellite-to-satellite ranging systems are transmitter-receiver systems, usually in K band (24 GHz) and Ka band (32 GHz). They are designed to accurately measure the distance and its variations between satellites flying in coordinated orbits. The same measurements are possible through the simultaneous reception of signals from tens of GNSS satellites: that determines positioning changes highly accurately.

Tables 3.39 and 3.40 describe a gradiometer/accelerometer (EGG) and a satellite-to-satellite ranging system (HAIRS).

Table 3.39. Example of accelerometer/gradiometer: EGG on GOCE

EGG	*Three-axis Electrostatic Gravity Gradiometer*
Satellite	Gravity Field and Steady-state Ocean Circulation Explorer (GOCE)
Mission	Solid Earth Observation of the Earth's gravity field along the orbit
Main features	Three pairs of 3-axis accelerometers, specially assembled to measure the gravity-gradient tensor, accuracy: 10^{-12} m s^{-2}, resolution: 2 10^{-12} m s^{-2} Hz$^{-1/2}$
More information	https://www.wmo-sat.info/oscar/instruments/view/127

Table 3.40. Example of satellite-to-satellite ranging system: HAIRS on Gravity Recovery and Climate Experiment (GRACE)

HAIRS	*High Accuracy Inter-satellite Ranging System*
Satellites	GRACE (2 satellites flying in tandem, 220 km apart)
Mission	Solid Earth Observation of the Earth's gravity field along the orbit
Main features	Dual-frequency ranging, in K band (24 GHz) and Ka band (32 GHz), accuracy: 10 μm
More information	https://www.wmo-sat.info/oscar/instruments/view/176

3.2.17 Solar activity monitors

Solar activity is monitored either by remote-sensing or in situ in the solar wind, from deep space and Earth's orbit. Several measurement approaches are possible:

(a) Electromagnetic radiation: measured by radiometers, spectrometers and polarimeters for γ-rays (less than 0.001 nm), X-ray (0.001–10 nm), extreme UV (10–120 nm), UV (120–380 nm), VIS (380–780 nm) and longer wavelengths including radio waves (more than 1 m);

(b) Energetic particles (electrons, protons, α-particles, ions, cosmic rays, neutrons): the energy range is generally broken down into high-, medium- and low-energy; the boundaries of the ranges depend on the type of charged particle; measurements can be integrated over the full energy range, or over partial ranges; spectroscopy within a range may also be performed;

(c) Magnetic and electric fields, directly measured in the solar wind, and inferred in the photosphere; those fields are inferred from measurements in the solar wind or from spectroscopy of VIS solar images using the Zeeman effect, Doppler analysis or multipolarization;

(d) Measurements can be performed by: integrating over the full solar disk; imaging the solar disk; or imaging the corona only by occulting the disk (a coronagraph);

(e) A specific observation is that of solar irradiance, either total or spectrally resolved (see 3.2.9).

An example of an instrument package for solar activity monitoring from the L1 Lagrange libration point, SOHO, is described in Table 3.41.

Table 3.41. Example of solar activity monitoring package: SOHO instrumentation

SOHO instrumentation	
Satellite	Solar and Heliospheric Observatory (SOHO)
Mission	Sun monitoring from the L1 Lagrange point
Main features	Solar atmosphere remote-sensing instrument package, Solar wind "in situ particle" instrument package, Helio-seismology instrument package (study of the Sun's interior).
More information	https://www.wmo-sat.info/oscar/satellites/view/458

3.2.18 Space environment monitors

Space environment monitoring at platform level provides information used for monitoring and making predictions about overall space weather conditions, as well as for platform safety. The instrumentation generally includes:

(a) Charged particle detectors, designed for specific ranges of energy, either integrated or spectrally resolved;

(b) Magnetometers and electrometers.

An example of an instrument package for in situ space environment monitoring, GGAK-M, is described in Table 3.42.

3.2.19 Magnetometers and electric field sensors

Magnetic and electric fields in the magnetosphere can be measured in situ as the satellite moves along its orbit. If the orbit is highly eccentric, it crosses the magnetosphere at different altitudes, thus providing 3D profiles. Gradients of the fields are better observed when more satellites are flown together in coordinated orbits. Usual instruments are:

(a) Either scalar or vector magnetometers;

(b) Electron fluxometers (used to compute the electric field).

An example of an instrument package, Cluster, for 3D observation of the magnetosphere, which uses four satellites, is described in Table 3.43.

Table 3.42. Example of space environment monitoring package: GGAK-M on Meteor-M

GGAK-M	*Geophysical Monitoring System Complex*
Satellites	Meteor-M N1, Meteor-M N2, Meteor-M N2-1, Meteor-M N2-2
Mission	Space environment monitoring at platform level
Main features	Spectrometer for Geoactive Measurements (MSGI-MKA) package: Electron fluxes in the energy range 0.1–15 keV (high-sensitivity channel) Ion (proton) fluxes in the energy range 0.1–15 keV (high-sensitivity channel) Electron fluxes in the energy range 0.1–15 keV (low-sensitivity channel) Monitoring of integral electron fluxes with a threshold energy of 40 keV Radiation Monitoring System (KGI-4C) package: Total proton flux threshold energy of: 5, 15, 25, 30 and 40 MeV Total electron flux threshold energy of: 0.17, 0.7, 1.7, 2.0 and 3.2 MeV Proton fluxes with threshold energies of: 25 and 90 MeV
More information	https://www.wmo-sat.info/oscar/instruments/view/822

Table 3.43. Example of magnetosphere monitoring package: Cluster instrumentation

CIS	*Cluster Ion Spectrometry*
Satellites	Cluster A, B, C and D (four satellites flying together in coordinated orbits)
Mission	Monitoring of the 3D magnetosphere
Main features	Package of the following instruments: Fluxgate Magnetometer (FGM), Spatio-temporal Analysis of Field Fluctuations (STAFF), Electric Fields and Waves (EFW), Waves of High Frequency and Sounder for Probing of Density by Relaxation (WHISPER), Wide Band Data (WBD), Digital Wave Processor (DWP), Electron Drift Instrument (EDI), Cluster Ion Spectrometry (CIS) experiment, Plasma Electron and Current Analyzer (PEACE), Research with Adaptive Particle Imaging Detectors (RAPID), Active Spacecraft Potential Control (ASPOC)
More information	https://www.wmo-sat.info/oscar/instruments/view/766

CHAPTER 4. SATELLITE PROGRAMMES

The measurements described in the present volume, Chapter 2, are performed within satellite programmes[1] implemented by space agencies with either an operational mandate to serve particular user communities, or a priority mandate for research and development.

International coordination among satellite operators is achieved within the Coordination Group for Meteorological Satellites (CGMS), the primary goal of which is to maintain the operational meteorological and climate monitoring constellations, and the Committee on Earth Observation Satellites (CEOS), which has initiated "virtual constellations" with thematic objectives (ocean surface topography, precipitation, atmospheric composition, land surface imaging, ocean surface vector wind, ocean colour radiometry and sea-surface temperature).

Non-governmental entities, including commercial providers, are also increasingly developing and deploying missions, aiming to provide operational services.

In addition to the core meteorological constellations in geostationary and near-polar Sun-synchronous orbits, these programmes include environmental missions focusing on specific atmospheric parameters, ocean and ice, land observation, solid Earth or space weather. Many of these environmental missions are designed and operated in a research or demonstration context. However, some have been extended over time leading to a degree of operational maturity, and some have paved the way for an operational follow-on. These result in sustained observation of environmental components. Research satellites are used in terrestrial and space weather operational forecast models and products. Further information on measurement principles and uncertainties for geophysical variables can be found in the present volume, Chapter 5.

For each type of application, satellite missions may be seen as constituent parts of constellations of spacecraft that, in many cases, will deliver their full benefit only when implemented in a coordinated fashion, ensuring synergy among the different sensors.

The following mission categories are considered:

(a) Operational meteorological satellites;

(b) Specialized atmospheric missions;

(c) Missions on ocean and sea ice;

(d) Land-observation missions;

(e) Missions on solid Earth;

(f) Missions on space weather.

4.1 OPERATIONAL METEOROLOGICAL SATELLITES

The system of operational meteorological satellites constitutes the backbone of the space-based part of the WMO Integrated Global Observing System (WIGOS). It is split into two components, according to the orbital characteristics:

(a) Constellation in geostationary or highly elliptical orbit;

(b) Constellation in Sun-synchronous orbits.

[1] Details on these programmes are available in the WMO Observing Systems Capability Analysis and Review Tool (OSCAR) online database on space-based capabilities, which is updated on a regular basis, https://www.wmo-sat.info/oscar/spacecapabilities.

The following website provides annually updated information on the status and postion of the operational meteorlogical satellites: https://community.wmo.int/activity-areas/wmo-space-programme-wsp/global-planning.

4.1.1 Satellite constellation in geostationary or highly elliptical orbit

GEO is particularly suited for operational meteorology because it enables very frequent sampling (at sub-hourly or minute rates) as necessary for rapidly evolving phenomena (daily weather) or detecting events such as lightning, volcanic eruptions and forest fires. The spatial resolution typically is of the order of 1 km to 3 km. The primary observations from the geostationary orbit are:

(a) Cloud evolution (detection, cover, top height and temperature, type, water phase at cloud top, particle size, and the change of those parameters in time);

(b) Frequent profile of temperature and humidity to monitor atmospheric stability;

(c) Winds by tracking clouds and water-vapour patterns (winds at different levels can be inferred from the tracking of water vapour at different levels in clear skies);

(d) Convective precipitation (in combination with MW data from LEO satellites, lightning detection and by observing cloud top temperature and its temporal changes);

(e) Rapidly changing surface variables (sea-surface temperature in coastal zones, fires);

(f) Ozone and other trace gases affected by diurnal variation or arising from changing sources.

One drawback of the geostationary orbit is the poor visibility at high latitudes, beyond about 60° for quantitative measurements and 70° for qualitative. This limitation can be overcome by using high-eccentricity inclined orbits (Molniya, Tundra or three-apogee orbits) instead of the geostationary orbit (see the present volume, Chapter 2, 2.1.4). Additionally, the diffraction limit due to the small angles subtended by the large distance poses challenges for very high-resolution optical imagery and MW radiometry. MW observation for all-weather temperature and humidity sounding and quantitative precipitation measurement from GEO should be feasible by using high frequencies, as the technology becomes available.

The requirement for global non-polar frequent observations from the geostationary satellites calls for six regularly-spaced spacecraft (Figure 4.1). In an operational constellation, backup satellites are required to provide redundancy above this minimum.

Table 4.1 lists the operational programmes that agreed to contribute to the constellation of meteorological geostationary satellites and their nominal positions. Other positions may be used on a temporary basis, for instance in contingency situations.

4.1.2 Satellite constellation in Sun-synchronous orbits

The Sun-synchronous orbit provides global coverage necessary for applications such as global numerical weather prediction (NWP), polar meteorology, and climatology. For these applications, very frequent sampling is less critical than global coverage and high accuracy.

The primary contributions from Sun-synchronous orbits are:

(a) Information on vertical profiles of temperature and humidity derived from radiances and radio occultation measurements as primary input to NWP;

(b) Cloud observations at high latitudes complementing GEO;

(c) Precipitation observations by MW radiometry;

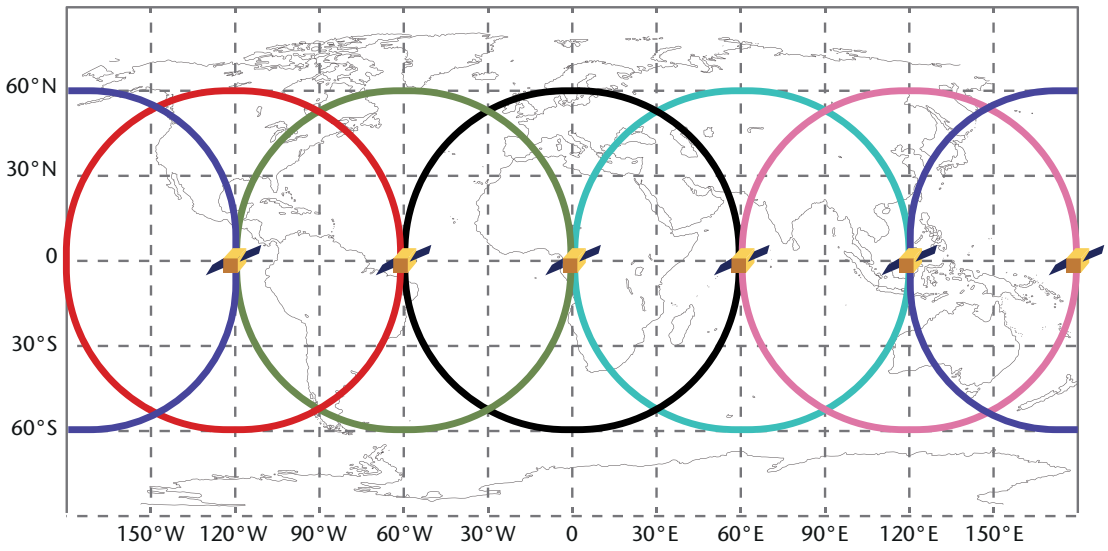

Figure 4.1. Coverage from six regularly-spaced geostationary satellites. The circles subtend a geocentric angle of 60°, considered the practical limit for quantitative observations (for qualitative use, images actually extend beyond). All latitudes between 55°S and 55°N are covered.

Table 4.1. Present and planned satellite programmes of the operational meteorological system in GEO

Acronym	*Full name*	*Responsible*	*Nominal position(s)*
GOES-16 and GOES-17	Geostationary Operational Environmental Satellite	NOAA	75.2°W and 137.2°W
Meteosat	Meteorological Satellite	EUMETSAT	0°
Electro/GOMS	Electro/Geostationary Operational Meteorological Satellite	RosHydroMet	76°E, 14.5°W and 166°E
INSAT and Kalpana	Indian National Satellite and Kalpana	ISRO	74°E and 93.5°E
FY-2 and FY-4	Feng-Yun-2 and follow-on Feng-Yun-4	CMA	79°E, 86.5°E, 112°E and 105°E
COMS and GEO-KOMPSAT	Communication, Oceanography and Meteorology Satellite and follow-on Geostationary Korea Multi-purpose Satellite	KMA	128.2°E or 116.2°E
Himawari/MTSAT	Himawari, including Multifunctional Transport Satellite	JMA	140°E

Note :
NOAA = National Oceanic and Atmospheric Administration of the United States of America
EUMETSAT = European Organization for the Exploitation of Meteorological Satellites
RosHydroMet = Federal Service for Hydrometeorology and Environmental Monitoring of the Russian Federation
ISRO = Indian Space Research Organization
CMA = China Meteorological Administration
KMA = Korea Meteorological Organization
JMA = Japan Meteorological Agency

(d) Surface variables (sea and land surface temperatures, vegetation and soil-moisture indexes);

(e) Ice cover, snow, hydrological variables;

(f) Surface radiative parameters (irradiance, albedo, photosynthetically active radiation, fraction of absorbed photosynthetically active radiation);

(g) Ozone and other trace gases for environment and climate monitoring.

Additional advantages of Sun-synchronous and other low Earth orbits are the capability to perform active sensing in the MW (radar) and optical (lidar) ranges and limb measurements of the higher atmosphere. Global coverage at roughly four-hour intervals can be achieved by three Sun-synchronous satellites in coordinated orbital planes crossing the equator at, for instance, 05:30, 09:30 and 13:30 local solar time, provided that the instrument swath is sufficiently wide and the measurement can be performed by both day and night (see Figure 4.2). Table 4.2 lists the operational programmes contributing now or in the future to the constellation of meteorological Sun-synchronous satellites as of 2012.

4.2 SPECIALIZED ATMOSPHERIC MISSIONS

4.2.1 Precipitation

Precipitation is a basic meteorological variable, but its measurement requires the exploitation of the microwave spectral range at a resolution consistent with the scale of the phenomenon and at relatively low frequencies; this implies large instruments. Moreover, the relation between passive MW sensing and precipitation is not explicit. Only total-column precipitation is measured, and only in a few channels. The retrieval problem is strongly ill-conditioned and requires modelling of the vertical cloud structure, which can only be observed by radar. TRMM (launched in 1997), that carries associated passive and active MW sensors, has enabled algorithms to be developed that allow much better use of passive measurements.

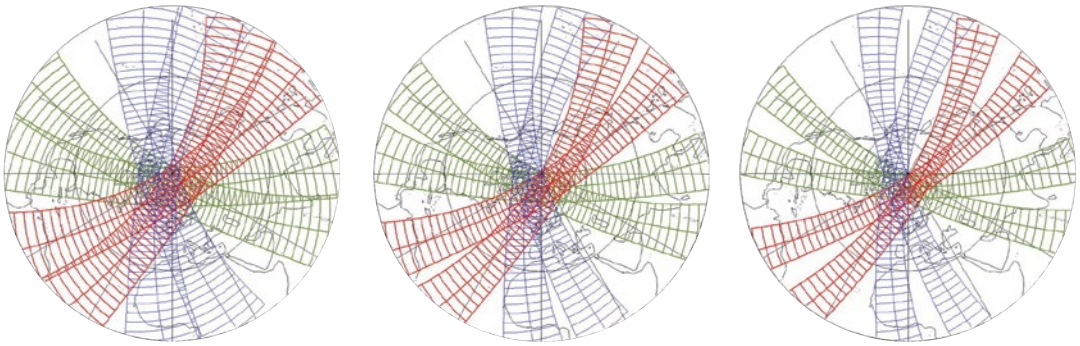

VIS/IR imagery with cross-track scanning – swath 2 900 km

IR/MW sounding with cross-track scanning – swath 2 200 km

Microwave radiometer with conical scanning – swath 1 700 km

Figure 4.2. Coverage from three Sun-synchronous satellites of height 833 km and equatorial crossing time (ECT) regularly spaced at 05:30 d (descending node), 09:30 d and 13:30 a (ascending node). For the purpose of this schematic diagram, all satellites are assumed to cross the equator at 1200 universal coordinated time (UTC). The figure refers to a time window of 3 h and 23 min (to capture two full orbits of each satellite) centred on 1200 UTC. Three typical swaths are considered. Nearly three-hour global coverage is provided for the VIS/IR imagery mission, whereas for the IR/MW sounding mission coverage is nearly complete at latitudes above 30 degrees. For microwave conical scanners, global coverage in three hours would require eight satellites.

Table 4.2. Present and planned satellite programmes of the operational meteorological system in LEO

Acronym	*Full name*	*Responsible*	*Height*	*Nominal ECT*
NOAA	National Oceanic and Atmospheric Administration	NOAA	833 km	13:30 a
Suomi-NPP	Suomi National Polar-orbiting Partnership	NOAA, NASA	833 km	13:30 a
JPSS	Joint Polar Satellite System	NOAA	833 km	13:30 a
DMSP	Defense Meteorological Satellite Program	DoD	833 km	05:30 d
GOSAT	Greenhouse Gas Observing Satellite	JAXA	613 km	13:00 d
Metop	Meteorological Operational Satellite	EUMETSAT	817 km	09:30 d
Metop-SG	Meteorological Operational Satellite – Second Generation	EUMETSAT	817 km	09:30 d
OCO	Orbiting Carbon Observatory (OCO-2/OCO-3 ISS)	NASA	705/400 km	13:30 a/NA
FY-3	Feng-Yun-3	CMA	836 km	10:00 d and 14:00 a
Meteor-M	Meteor, series “M”	RosHydroMet	830 km	09:30 d and 15:30 a
Meteor-MP	Meteor, series “MP”	RosHydroMet	830 km	09:30 d and 15:30 a

Note :
NASA = National Aeronautics and Space Administration (United States)
DoD = Department of Defense (United States)
JAXA = Japan Aerospace Exploration Agency
For other organizations, please refer to the notes of the previous tables in this chapter

TRMM has enabled the concept of the GPM mission (launched in 2014) to be developed that is being implemented in an international context. Its objective is to provide global coverage of precipitation measurements at three-hour intervals. Since the baseline instrument is an MW conical scanning radiometer with limited swath, the three-hour frequency requires eight satellites in regularly distributed near-polar orbits (Figure 4.3). In addition to those “constellation satellites”, a “Core Observatory” in inclined orbit equipped with a dual-frequency precipitation radar enables all other measurements from passive MW radiometers to be “calibrated” when constellation and core-satellite orbits cross one another.

RainCube, a 6U CubeSat with a 35 GHz radar instrument to observe precipitation, is an example of how small satellite platforms can enhance space-based observations. Beyond the missions specifically tailored for precipitation observation, any operational mission equipped with MW radiometers (for example, Defense Meteorological Satellite Program (DMSP)) can contribute to the composite system.

4.2.2 **Radio occultation**

Radio occultation of GNSS satellites is a powerful technique for providing temperature and humidity profiles with a vertical resolution that is unachievable by nadir-viewing instruments. Operational implementation has been achieved, for example, with the EUMETSAT Metop satellites. Studies at NWP centres have demonstrated positive impact of radio-occultation measurements on NWP performance. Highest impact is obtained in the upper troposphere and lower stratosphere.

Figure 4.3. Concept of the Global Precipitation Measurement mission

4.2.3 Atmospheric radiation

A limitation of NWP and general circulation models is the representation of diabatic heating rates due to radiative processes in the atmosphere. Aerosols, cloud interior (particularly ice), radiation fluxes within the 3D atmosphere in addition to the top of the atmosphere and the Earth surface, are their main factors. These are often not sufficiently well known, and some of these variables require observing instruments (lidar, cloud radar, etc.) that are not yet feasible for multi-purpose operational meteorological satellites. Thus, the observation of atmospheric radiative fluxes, either directly or in support of improved calculations, relies on instruments flown either in operational programmes or on dedicated missions.

Measurement of broadband atmospheric radiatiave flux densities in the long-wave spectrum at the top of the atmosphere was the first observation performed from space in October 1959 on Explorer VII. At the time of the first TIROS flights the Earth's planetary albedo and the global radiation budget was poorly known. The radiation budget is an essential climate variable, so the continuous observation of its components (short-wave and long-wave) is crucial.

Observing atmospheric radiation fields (or the quantities which are needed to compute atmospheric radiation fields) requires contributing factors to be observed in parallel, for example temperature and humidity profiles, clouds, aerosol, trace gases. An approach to observe such geophysical parameters nearly simultaneously is the concept of formation flying. This has been implemented as the A-Train (Figure 4.4). In this concept, several satellites are flying on nearly the same Sun-synchronous orbit, at 705 km altitude, ECT ~13:30 ascending node, following each other along the same ground track within a few seconds.

4.2.4 Atmospheric chemistry

Atmospheric chemistry has grown in importance over time. Attention was focused initially on ozone monitoring, especially after the discovery of the ozone hole; then on the greenhouse effect as a driver of global warming; and, finally air quality, for its impact on living conditions in the biosphere. Depending on the objective, the instrumentation may be quite simple (such as for total column of one or few species) or very complicated (such as for vertical profiles of families of species).

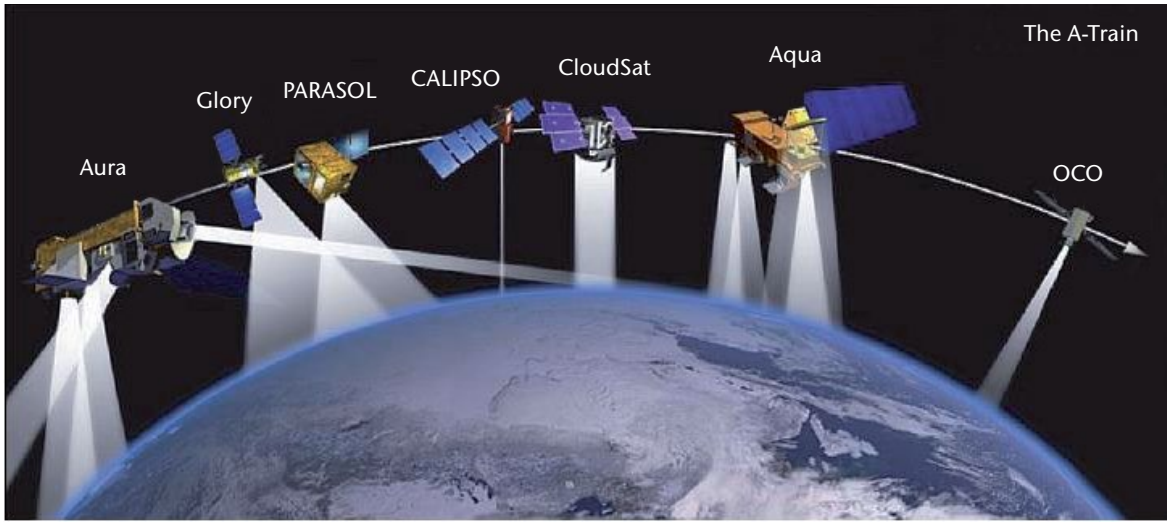

Figure 4.4. The spread of equatorial crossing times across the satellites addressing atmospheric radiation (Glory, PARASOL, CALIPSO, CloudSat and EOS-Aqua) is about two minutes. Note that there may be some changes in the satellites participating in the A-Train; for instance PARASOL was removed after five years, EOS-Aura has been added, Glory failed at launch, the Orbiting Carbon Observatory (OCO), lost at launch, was replaced by OCO-2/OCO-3 ISS, and the Global Change Observation Mission for Water - 1 (GCOM-W1) has been added.

It is noted that:

(a) On meteorological satellites, IR hyperspectral sounders primarily designed for temperature and humidity sounding do contribute to atmospheric chemistry observation, but their performance for chemistry is currently limited to total columns of a few greenhouse species. The UV, VIS and NIR instruments are designed to measure ozone and other species, including CO2;

(b) Some atmospheric-chemistry missions are hosted on multi-purpose satellites (for example, Metop, JPSS) and some on dedicated atmospheric-chemistry satellites.

Nimbus-7 (with stratospheric and mesospheric sounder (SAMS), limb infra-red monitor of the stratosphere (LIMS), total ozone mapping spectrometer (TOMS), SBUV), launched in 1978, was a multi-purpose mission that collected data on ozone, the stratosphere, ocean conditions and global weather. The first comprehensive mission for atmospheric chemistry, the UARS, was exploiting limb sounding. When launched in 1991 it was by far the largest Earth observation satellite ever in orbit (mass at launch: 6 540 kg). Table 4.3 provides a list of satellites either substantially addressing, or fully dedicated to, atmospheric chemistry.

4.2.5 Atmospheric dynamics

The study of atmospheric dynamics involves missions measuring the 3D wind field, a difficult issue since the wind per se does not have a signature in the electromagnetic spectrum. Nevertheless, considerable effort has been devoted and continues to be devoted to the subject, since wind is a primary observation for NWP and general circulation models.

Deriving wind characteristics from the motion of clouds or other atmospheric patterns (water vapour) was an early and widely used application of geostationary satellites. Still today, it is the operational practice providing thousands of wind vectors every day. Tracking clouds or water vapour patterns, however, determines the wind at one level only. For large areas, all tracers tend to be in the same altitude range, thus limiting the vertical resolution in practice to one or two levels. With the future advent of hyperspectral sounders in GEO, frequent water vapour profiles,

Table 4.3. Satellite programmes with strong or exclusive focus on atmospheric chemistry

Acronym	*Full name*	*Responsible*	*Measurements*
EOS-Aura	Earth Observation System – Aura	NASA	UV/VIS nadir, MW limb
GOSAT-1, GOSAT-2	Greenhouse Gas Observing Satellite	JAXA	NIR/SWIR/MWIR/TIR nadir
Odin	Odin	SNSB	UV/VIS/NIR limb, MW limb
OCO-2/ OCO-3 ISS	Orbiting Carbon Observatory	NASA	NIR/SWIR nadir
SCISAT	Scientific Satellite	CSA	UV/VIS/NIR and SWIR/MWIR/ TIR Sun occultation
Sentinel-4	Sentinel-4 on Meteosat Third Generation	ESA, EUMETSAT, EC	UV/VIS/NIR nadir
Sentinel-5P	Sentinel-5 precursor	ESA, EC	UV/VIS/NIR/SWIR nadir
Sentinel-5	Sentinel-5 on Metop Second Generation	ESA, EUMETSAT, EC	SW nadir

Note:
CSA = Canadian Space Agency
EC = European Commission
ESA = European Space Agency
MWIR = medium-wave infrared
NIR = near infrared
SNSB = Swedish National Space Board
SWIR = short-wave infrared
TIR = thermal infrared
For other organizations, please refer to the notes of the previous tables in this chapter

with their patterns, will be available at additional heights, and a broad vertical resolution will be achieved in clear air. Atmospheric motion winds are also derived over polar areas from polar-orbiting satellites, taking advantage of the frequent overpasses.

In a similar vein to GEO, MISR (Terra, Aqua) uses a stereophotogrammetric technique to simultaneously retrieve the height and cross-track (east–west) motion of clouds. This technique relies on MISR's nine cameras, which provide high resolution views of a single scene from different angles over a period of several minutes. An automatic pattern-matching algorithm finds cloud-top features that are common among the MISR camera images and determines the displacement of these features over time, similar to the successive scene displacement approach used to retrieve geostationary satellite derived winds.

With advent of ESA's ADM/Aeolus mission a first Doppler lidar has been deployed that is capable of measuring horizontal line-of-sight (HLOS) winds with high vertical resolution in clear air.

Winds are also of interest in the stratosphere and mesosphere, where clouds and water vapour have no characteristic pattern, and there are no turbulence eddies or dense aerosols either. The technique applicable here is measurement of the Doppler shift of narrow lines in the oxygen band around 760 nm. Demonstrated by UARS, the technique is exploited by the Thermosphere, Ionosphere, Mesosphere Energetics and Dynamics mission (TIMED) with TIMED Doppler Interferometer (TIDI).

4.3 MISSIONS ON OCEAN AND SEA ICE

Certain observations of ocean and sea ice have been provided by meteorological satellites since the very beginning of the space era. VIS imagery, the very first application of meteorological satellites, is capable of sea-ice mapping. IR imagery added the capability to measure sea-surface

temperature. MW and SAR imagery extended the observing capability to measure sea-surface temperature and ice cover to all-weather conditions, and added the capability to sea-surface wind speed. Radar scatterometry started in 1978. These observations of sea-surface temperature, sea-surface wind, and ice cover are still provided by operational meteorological satellites. Further measurements, including altimetry, ocean colour, salinity, and waves, are performed in the framework of non-meteorological programmes, sometimes dedicated to ocean and sea ice.

Table 4.4 lists satellite programmes addressing ocean and sea ice.

Table 4.4. Satellite programmes addressing missions on ocean and sea ice

Acronym	*Full name*	*Responsible*	*Oceanographic missions*
COMS	Communication, Oceanography and Meteorology Satellite	KIOST	Ocean colour from GEO with GOCI
Coriolis	Coriolis	DoD	Surface wind by MW polarimetry
CryoSat-2	Cryosphere Satellite	ESA	Radar altimetry for ice
CYGNSS	Cyclone Global Navigation Satellite System	NASA	Sea-surface wind observation in tropical cyclone
EOS-Aqua	Earth Observation System – Aqua	NASA	Ocean colour
EOS-Terra	Earth Observation System – Terra	NASA	Ocean colour
FY-3	Feng-Yun-3	CMA	Ocean colour Surface wind by C- and K_u-band scatterometer
GCOM-C	Global Change Observation Mission for Climate	JAXA	Ocean colour
GCOM-W	Global Change Observation Mission for Water	JAXA	Multi-purpose MW imagery (large antenna)
GEO-KOMPSAT-2B	Geostationary Korea Multi-purpose Satellite	KIOST	Ocean colour from GEO with GOCI-II
HY-1	Hai Yang-1	NSOAS, CAST	Ocean colour
HY-2	Hai Yang-2	NSOAS, CAST	Radar altimetry Surface wind by K_u-band scatterometer
ICESat-2	Ice, Cloud and Land Elevation Satellite	NASA	Lidar altimetry for ice
Jason series	Jason - 3	NOAA, EUMETSAT, NASA, CNES	Ocean topography, Radar altimetry, geoid
JPSS	Joint Polar Satellite System	NOAA	Ocean colour
Meteor M/MP N3	Meteor-M and Meteor-MP, flight units N3	RosHydroMet	Ocean colour Surface wind by K_u-band scatterometer
Metop and Metop-SG	Meteorological Operational satellite and follow-on Metop Second Generation	EUMETSAT	Surface wind by C-band scatterometer
OceanSat	Satellite for the Ocean	ISRO	Ocean colour Surface wind by K_u-band scatterometer
SARAL	Satellite with Argos and Altika	CNES, ISRO	Radar altimetry

Acronym	*Full name*	*Responsible*	*Oceanographic missions*
Sentinel-3	Sentinel-3	ESA, EC, EUMETSAT	Ocean colour, Ocean topography Radar altimetry
Sentinel-6A/B	Sentinel-6A/B	ESA, EUMETSAT, EC, CNES, NASA, NOAA	Ocean topography
SMAP	Soil Moisture Active Passive	NASA	Sea-surface salinity
SMOS	Soil Moisture and Ocean Salinity	ESA	Ocean salinity (synthetic aperture antenna)
SWOT	Surface Water and Ocean Topography	NASA, CNES, CSA, UKSA	Ocean topography and waves
Suomi-NPP	Suomi National Polar-orbiting Partnership	NOAA, NASA	Ocean colour

Note:
CAST = China Academy of Space Technology
CNES = National Centre for Space Studies (France)
DoD = Department of Defense (United States)
KIOST = Korea Institute of Ocean Science and Technology
NSOAS = National Satellite Ocean Application Service (China)
UKSA = United Kingdom Space Agency
For other organizations, please refer to the notes of the previous tables in this chapter

4.3.1 Ocean topography

Radar altimetry is used to observe sea-surface height (SSH) or ocean topography. The developments started in the mid-1970s, and since then radar altimetry technology has evolved, leading to higher accuracy and better spatial resolution of SSH variations. For instance, 100-km spatial scales with a 10-day revisit cycle are measured with Topex/Poseidon and the Jason satellite series, whereas the upcoming NASA/CNES Surface Water and Ocean Topography (SWOT) mission will measure approximately 10-km spatial scales, yet still with a 10-day revisit cycle. Multiple satellites in different orbits would provide higher spatial resolution of SSH variations. In order to obtain a precise long-term climate data record of sea-level change, the measurement biases of different satellites need to be determined. These can be addressed with overlapping satellite missions (see Table 4.4).

4.3.2 Ocean colour

Ocean colour observation is important for a range of applications and oceanographic research because ocean colour data carry information on substances suspended in ocean water. These substances can be inorganic matter or organic substances such as phytoplankton. Global observations of the vast ocean areas are only possible via remote sensing from satellites. Ocean colour observations from space started in 1978 with NASA's Coastal Zone Color Scanner (CZCS). Since then other instruments have been launched. For instance, ocean colour is observed with multi-purpose sensors like NASA's Moderate-resolution Imaging Spectroradiometer (MODIS) on board the Aqua and Terra satellites, and the ESA's MEdium Resolution Imaging Spectrometer (MERIS) onboard Envisat and Sentinel-3. More recently other ocean colour sensors were launched, including the Indian Ocean Colour Monitor (OCM-2) on board the Indian Oceansat-2 satellite, the Visible Infrared Imaging Radiometer Suite (VIIRS) instrument on the US Suomi-NPP and JPSS satellites and the Ocean and Land Colour Instrument (OLCI) on Sentinel-3. The Korean Geostationary Ocean Color Imager (GOCI) is the first ocean colour instrument in a geostationary orbit, and it will be succeeded by an improved instrument on the Korean GK-2A satellite. Geostationary orbit allows more frequent observations of ocean colour, enabling observation of short-term changes in ocean colour, for example those related to tidal changes (see Table 4.4).

4.3.3 Sea-surface wind

Wind over the sea surface is a basic measurement for oceanography since it drives atmospheric forcing, hence surface currents, and the intensity of air–sea interaction. Of course, it is also an important geophysical variable for weather prediction, enabling derivation of surface pressure that cannot be directly measured from space. Therefore, several wind-observing instruments are part of the operational meteorological mission. Table 4.4 records the missions addressing sea-surface winds that are able to provide both speed and direction (radar scatterometer either in the C band operated in the pushbroom manner, which involves scanning a swath straight down, or in the K_u band with conical scanning; and polarimetric MW passive radiometers). Other passive MW radiometers, that can contribute to wind-speed observation, are mentioned only for multi-purpose MW imagers with large antennas.

4.3.4 Sea-surface salinity

Salinity is a basic measurement for oceanography since, with temperature, it controls water density, hence the vertical motion in the thermo-haline layer. Furthermore, it controls the ocean's ability to remove trace gases from the atmosphere. Measuring salinity from space is possible only by low-frequency MW radiometry (L band around 1.4 GHz), which requires large antennas. Missions addressing sea-surface salinity are based either on a synthetic-aperture antenna, or on a real-aperture antenna (see Table 4.4).

4.3.5 Waves

The observation of waves is important for ocean operations, in the open ocean and even more so in coastal zones. It is also important for coastal-zone climatology. Unfortunately, waves are difficult to observe from space, since the direct measurement from the radar altimeter provides only the significant wave height, and only along the satellite track. The altimeter missions are listed in Table 4.4.

The 2D wave field can be observed by spectral analysis of SAR imagery. In principle, any scene from a SAR image could be processed to provide the dominant wave direction and period, as well as the directional energy frequency spectrum. In practice, the scenes are sampled at intervals during the whole orbit, and stored on board since the associated data rate is rather low. The Envisat ASAR performs this function in wave mode.

4.4 LAND-OBSERVATION MISSIONS

All imagery missions of the operational meteorological satellites provide information on several geophysical variables characterizing land surface. Specifically:

(a) VIS/IR imaging instruments: land surface temperature, soil moisture indexes, several vegetation indexes, several fire parameters, radiative parameters, ice and snow cover;

(b) MW imaging instruments: all-weather land surface temperature, surface-soil moisture, several ice and snow parameters;

(c) Radar scatterometers: surface-soil moisture, total biomass, snow water equivalent.

However, the design of the instruments flown on operational meteorological satellites is driven by the main objective of describing the surface–atmosphere interface processes, as necessary (and sufficient) for weather analysis and prediction and by the need for the observed spatial-temporal scales to be consistent with climate monitoring requirements. This section focuses on satellite programmes addressing land applications as primary objectives, for geophysical variables such as land cover and use, fraction of vegetated land, vegetation type, lake and glacier cover, topography, small-scale soil moisture and snow parameters for hydrology.

These applications require spatial resolutions at the scale of metres or a few tens of metres, which imply using optical bands (especially VIS) or imaging radar (SAR). Another application of very high-resolution optical imagery or SAR is security, including disaster monitoring, control of compliance with internationally agreed protocols for environmental protection, etc.

4.4.1 Main operational or near-operational missions

Land observation has been the second space application, after meteorology, to give rise to operational programmes. The first land-observation satellite, initially named the Earth Resources Technology Satellite, thereafter re-named Landsat-1, was launched by NASA in July 1972. Since then, other space agencies and commercial providers have undertaken land-observation programmes, often in a fairly operational way. Table 4.5 lists the programmes that have a demonstrated heritage of continuity or are designed for long-term continuity.

Table 4.5. Land-observation satellite programmes designed for long-term continuity

Acronym	*Full name*	*Responsible*	*Programme objective/nature*
Amazônia	Amazônia	INPE	Vegetation monitoring
ASNARO	Advanced Satellite with New System Architecture for Observation	NEC, USEF	Commercially-oriented programme
CartoSat	Satellite for Cartography	ISRO	Cartography update
CBERS	China-Brazil Earth Resources Satellite	CAST, INPE	Earth resources search and management
GeoEye	GeoEye	Maxar	Commercial programme
KANOPUS-V	KANOPUS Vulkan	Roscosmos	Vegetation monitoring
Landsat series	Landsat and Landsat Data Continuity Mission	USGS, NASA	Earth natural resources, land cover and land use change
Planet	Constellation of various satellites (Planetscope, RapidEye, Skysat)	Planet.com	Commercial Earth imaging
Resurs DK and P	Resurs-DK and Resurs-P	Roscosmos	LEO, high-inclination
Pléiades	Pléiades	CNES	Land-use and hazard management
ResourceSat series	Satellite for Earth Resources	ISRO	Earth resources search and management
Sentinel-2	Sentinel-2	ESA, EC	Vegetation monitoring
SPOT 4, 5	Satellite Pour l'Observation de la Terre	CNES	Earth resources search and management
SPOT 6, 7	Satellite Pour l'Observation de la Terre	SpotImage	Commercially-oriented programme
WorldView	World View	Maxar	Commercial programme

Note:
INPE = National Institute for Space Research (Brazil)
NEC = Nippon Electric Company
USEF = Institute for Unmanned Space Experiment Free Flyer (Japan)
USGS = US Geological Survey
For other organizations, please refer to the notes of the previous tables in this chapter

4.4.2 The Disaster Monitoring Constellation

The Disaster Monitoring Constellation (DMC) initiative was originally promoted by British National Space Centre (BNSC). The principle of DMC (see Figure 4.5) was to have about five satellites in the same orbit, separated by about 20 min, in such a way that the (narrow) swath of the instruments of one satellite (~600 km) was contiguous with the next, thus ensuring daily global coverage. The first DMC satellite was AlSat-1, launched in November 2002. A cluster of three satellites, UK-DMC-1, NigeriaSat-1 and Bilten Satellite, was placed in orbit by a single launch in September 2003. Over time, more partners joined the constellation, and the instrumentation became more elaborate. Table 4.6 depicts the current situation, which includes satellites not strictly part of the DMC, but close in objective, structure and instrumentation.

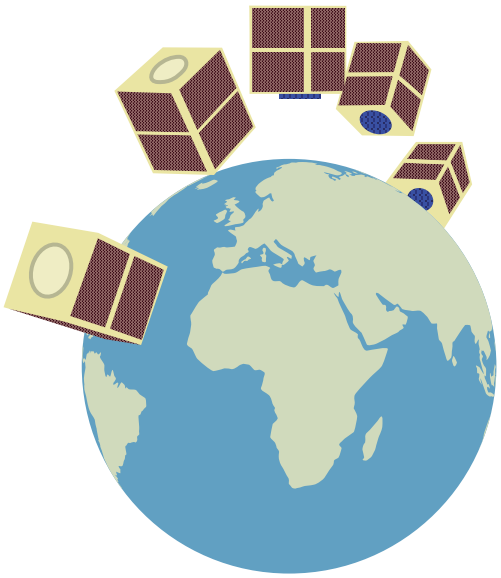

Figure 4.5. Concept of the DMC, based on five satellites dephased by about 20 min

Table 4.6. Satellite programmes of the DMC and similar

Acronym	*Full name*	*Responsible*	*Instrument capability*
AlSat	Algeria Satellite	CNTS, Algeria	Multi-spectral and panchromatic
BJ	Beijing	NRSCC, China	Multi-spectral and panchromatic
Deimos	Deimos	CDTI, Spain	Multi-spectral
DubaiSat	Dubai Satellite	EIAST, United Arab Emirates	Multi-spectral and panchromatic
EnMAP	Environmental Mapping and Analysis Programme	DLR, Germany	Hyperspectral
FORMOSAT-2	Formosa Satellite – 2	NSPO, Taiwan Province of China	Multi-spectral and panchromatic
HJ A, B	Huan Jing A and B	CAST, China	Hyperspectral and multispectral
Ingenio (SEOSat)	Ingenio (Spanish Earth Observation Satellite)	CDTI, Spain	Multi-spectral and panchromatic

Acronym	*Full name*	*Responsible*	*Instrument capability*
KOMPSAT	Korea Multi-purpose Satellite	KARI, Republic of Korea	Multi-spectral and panchromatic
NigeriaSat	Nigeria Satellite	NASRDA, Nigeria	Multi-spectral and panchromatic
PRISMA	Precursore Iperspettrale della Missione Applicativa	ASI, Italy	Hyperspectral and panchromatic
RapidEye (5 sats)	RapidEye (5 satellites)	DLR, Germany	Multi-spectral
Rasat	Earth observation satellite	Tübitak-Uzay, Turkey	Multi-spectral and panchromatic
SSOT	Sistema satelital para observación de la tierra	ACE, Chile	Multi-spectral and panchromatic
SumbandilaSat	Sumbandila Satellite	SANSA, South Africa	Multi-spectral
THEOS	Thailand Earth Observation System	GISTDA, Thailand	Multi-spectral and panchromatic
TopSat	TopSat	BNSC, UK	Multi-spectral and panchromatic
UK-DMC	UK Disaster Monitoring Constellation	BNSC, UK	Multi-spectral
X-Sat	X Satellite	NTU, Singapore	Multi-spectral

Note:
ACE = Chilean Space Agency
ASI = Italian Space Agency
BNSC = British National Space Centre
CDTI = Centre for the Development of Industrial Technology
CNTS = National Centre of Space Technology
DLR = German Aerospace Centre
EIAST = Emirates Institution for Advanced Science and Technology
GISTDA = Geo-informatics and Space Technology Development Agency
KARI = Korea Aerospace Research Institute
NASRDA = National Space Research and Development Agency
NRSCC = National Remote-sensing Centre of China
NSPO = National Space Organization
NTU = Nanyang Technological University
SANSA = South African National Space Agency
For other organizations, please refer to the notes of the previous tables in this chapter

4.4.3 All-weather high-resolution monitoring (by synthetic aperture radar)

All missions listed for land observation have a common limitation: observations are not available in the presence of clouds. In most cases, night-time is also a limitation since most instruments use only the VIS spectral range. In an emergency, when high resolution is needed, it is very important to have an all-weather sensing capability, which can be provided only by SAR. Several SAR missions are available, many of them being managed with a perspective for long-term operational continuity.

The number of SARs in orbit is important, since SAR instruments have a narrow swath, whereas their application to disaster monitoring requires frequent revisit times. In addition, the SAR principle is applicable with a single frequency, whereas various features to be observed have "signatures" at different frequencies. The Shuttle Imaging Radar with Payload C/X-SAR mission

(SIR-C/X-SAR), flown twice on the US Space Shuttle in April and September 1994, demonstrated the benefit of having simultaneous SAR imagery in the L, C and X bands (L and C provided by NASA, X by DLR and ASI).

Table 4.7 lists all current and planned missions equipped with an SAR, grouped by frequency band and responsible agency.

4.5 MISSIONS ON SOLID EARTH

Since the early days of space missions, satellites have been used to reconstruct the shape of the geoid by means of various orbits of different heights, inclinations and eccentricity. The main purpose was internal: to support mission analysis for orbiting satellites. As time passed and technology has improved, the purpose has evolved towards the study of the Earth itself.

Table 4.7. Current and planned SAR programmes

Acronym	*Full name*	*Responsible*	*Frequency band*
ALOS	Advanced Land Observing Satellite	JAXA, Japan	L band
SAR-L (NISAR)	NASA-ISRO Synthetic Aperture Radar	NASA, ISRO	L band
SAOCOM-1	Satélite argentino de observación con microondas – series 1	CONAE, Argentina	L band
SAOCOM-2	Satélite argentino de observación con microondas – series 2	CONAE, Argentina	L band
SMAP	Soil Moisture Active Passive	NASA	L Band
HJ-1C	Huan Jing 1C	CAST, China	S band
SAR-S (NISAR)	NASA-ISRO Synthetic Aperture Radar	NASA, ISRO	S band
RADARSAT-2	RADARSAT	CSA, Canada	C band
RCM	RADARSAT Constellation Mission	CSA, Canada	C band
RISAT-1	Radar Imaging Satellite – 1	ISRO, India	C band
Sentinel-1(A,B,C,D)	Sentinel-1(A,B,C,D)	ESA	C band
CSG	Constellation of Small Satellites for Mediterranean Basin Observation (COSMO) SkyMed Second Generation	ASI, Italy	X band
CSK	COSMO-SkyMed	ASI, Italy	X band
KOMPSAT-5	Korea Multi-purpose Satellite – 5	KARI, Republic of Korea	X band
Meteor M and MP	Meteor-M and Meteor-MP	RosHydroMet	X band
Paz (SEOSAR)	Paz (Spanish Earth Observation SAR)	CDTI, Spain	X band
RISAT-2	Radar Imaging Satellite – 2	ISRO, India	X band
TerraSAR-X	TerraSAR-X	DLR, Germany	X band
TanDEM-X	TanDEM-X	DLR, Germany	X band

Note:
CONAE = National Space Activity Commission (Argentina)
For other organizations, please refer to the notes of the previous tables in this chapter

The satellite objectives for solid Earth are (see Figure 4.6 for definitions):

(a) To provide a very accurate determination of the geoid, which is the basis for several associated applications, particularly conversion of altimeter measurements into sea level and ocean topography. The most common technique uses radar altimetry from orbits of relatively high altitude and high stability;

(b) To infer crustal dynamics by monitoring local site positions from satellites in well-known and stable orbits; common techniques are laser ranging and ground-based GPS receivers;

(c) To infer the dynamics of the outermost layers of the Earth (lithosphere, mantle); common techniques use measurements of the gravity field and its anomalies by very low-orbiting satellites, and satellite-to-satellite tracking;

(d) To collect information on the inner parts of the globe (liquid core, solid core) inferred through observation of the magnetosphere in satellite measurements of the magnetic and electric fields.

This section considers two families of missions:

(a) Those referring to the geoid and crustal positioning and movements (space geodesy);

(b) Those referring to the lithosphere and inner layers (Earth interior).

Table 4.8 lists missions specific to solid Earth, for either geodesy or the interior.

4.5.1 Space geodesy

The primary technique for reconstructing the geoid (the equipotential surface which would coincide exactly with the mean ocean equilibrium surface, if the oceans were at rest and extended through the continents) is radar altimetry. Other information on the geoid stems from the precise positioning systems on any satellite. Several of them are worthy of mention:

(a) Laser retro-reflectors, to accurately measure the distance and rate of change for the satellite from the laser source on the ground;

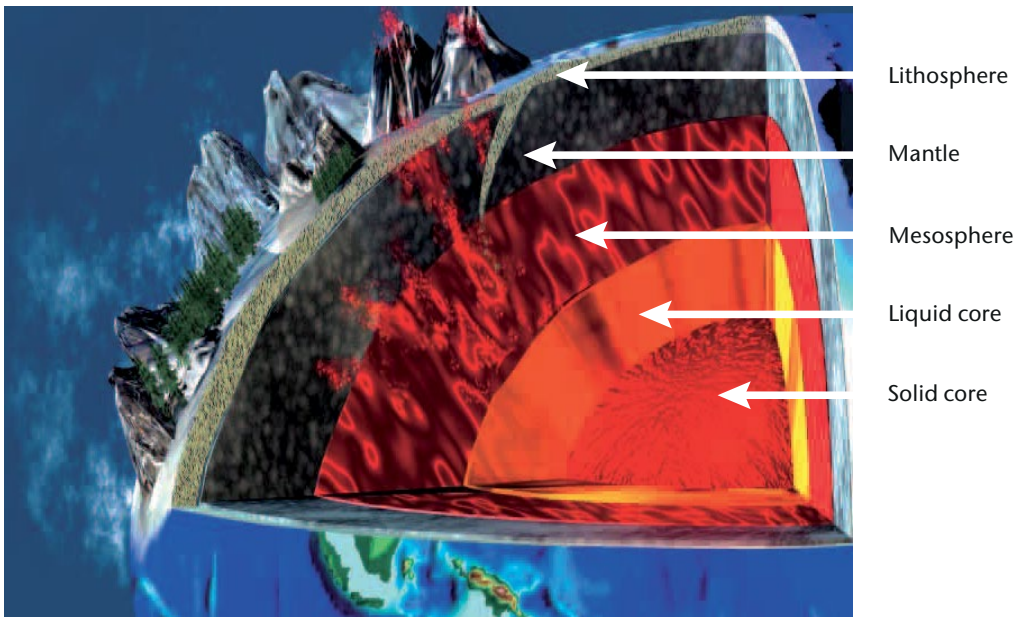

Figure 4.6. Stratification of the solid Earth

(b) On-board transponder of signals from ground transmitting-receiving stations;

(c) Two-way and dual-frequency microwave tracking system for ground receiving stations;

(d) GNSS;

(e) Star trackers, utilized for satellite attitude control but also contributing to precise orbitography.

The primary purpose of these systems is to support precise orbit determination as necessary for certain instruments performing the satellite mission, the most sensitive of which are altimeters and limb sounders. The benefit for the geodetic mission stems from the statistical analysis of the data. In this section the focus is on the application with the opposite objective: to establish the position of a ground station assuming that the orbit is well known. To this effect, an International Terrestrial Reference System for space geodesy has been established to collect and analyse data in a number of coordinated centres. The system includes a few satellites having space geodesy as a unique objective. These are listed in Table 4.8.

4.5.2 Earth's interior

The representation of the geoid is now fairly precise, despite its complexity. With the help of mathematical models using spherical harmonics, the achieved accuracy is now in the range of 1 cm or less. Figure 4.7 shows a current view of the geoid. It may be observed that, in this representation, the Earth's surface is not at all a regular ellipsoid, although the vertical range of the geoid height is contained within 200 m. The regularity of the geoid is affected by undulations of different wavelengths ranging from many thousands of kilometres to a few hundred. One objective is to associate these anomalies with the Earth's interior, first of all to the lithosphere because of its relevance to volcanism and earthquakes.

Specific missions for studying the Earth's interior exploit gravity and gravity-gradient observations, representative of the external layers (lithosphere, mantle and upper mesosphere); and magnetic and electric fields, significant for the internal layers (lower mesosphere, liquid core and solid core) (see Figure 4.6). Table 4.8 lists missions on the Earth's interior.

Table 4.8. Missions specific to solid Earth

Acronym	*Full name*	*Responsible*	*Sensing systems*
STARLETTE and Stella	Satellite de taille adaptée avec réflecteurs laser pour les études de la terre, and Stella	CNES	Laser ranging
LAGEOS 1 and 2	Laser Geodynamics Satellite, 1 and 2	ASI, NASA	Laser ranging
LARES	Laser Relativity Satellite	ASI	Laser ranging
GRACE (2 sats)	Gravity Recovery and Climate Experiment	NASA, DLR, CNES	Accelerometer, laser ranging, satellite-to-satellite ranging
SWARM (3 sats)	The Earth's Magnetic Field and Environment Explorers	ESA, CNES, CSA	Accelerometer, electric field sensor, magnetometers

Note: For organizations, please refer to the notes of the previous tables in this chapter

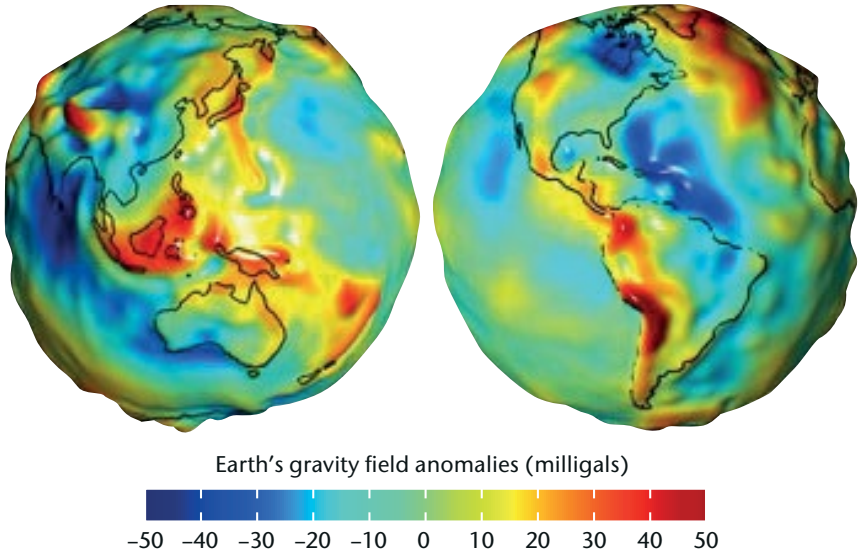

Figure 4.7. Three-dimensional visualization of geoid undulations. (1 Gal = 0.01 m/s² and 1 mGal ≈ 10^{-6} g_0)

4.6 MISSIONS ON SPACE WEATHER

Although the term "space weather" is relatively recent, the relevant activities started with the advent of the space era, if not before, because space weather has a strong impact on the safety of satellites in orbit and of man in space. Awareness and prediction of the space environment has now become a prerequisite for the long-term sustainability of space activities. In addition, there is increasing awareness of the impact of space weather on facilities on the Earth.

Space weather is characterized by electromagnetic bursts from the X to the radio bands, solar energetic particle events, and perturbations in the solar wind density and speed, such as interplanetary coronal mass ejections propagating plasma blobs. In particular, the solar wind modulations compress and shape the magnetosphere, and this effect propagates lower down to the thermosphere and ionosphere. Telecommunications and even power grids, pipelines and other conducting networks on the Earth's surface are affected (by geomagnetically induced currents, for example). Rapid magnetic changes on the ground, that occur during geomagnetic storms and are associated with space weather, can also be important for activities such as geophysical mapping and hydrocarbon production. Correlations have been discovered between travelling ionospheric disturbances and atmospheric gravity waves in the thermosphere.

Monitoring space weather implies two main aspects: monitoring the electromagnetic and particle solar emission as well as the solar wind to characterize the modulation source (solar activity), and monitoring the effects of this activity within the magnetosphere and down to the Earth's surface.

4.6.1 Solar activity monitoring

There have been space missions to understand solar physics since the early days of the space era, either from deep space orbits or from Earth orbits.

Two "sentinels" of solar wind, the joint NASA/ESA SOHO mission and the NASA Advanced Composition Explorer (ACE) mission, were launched in 1995 and 1998, respectively. SOHO and ACE have been placed at the L1 Lagrangian point (at 1% of the Earth–Sun distance upstream of the Earth). From that vantage point the two satellites measure solar wind and the associated magnetic field approximately one hour before they reach the Earth. In 2006, in collaboration with several European scientific institutes, NASA launched the Solar–Terrestrial Relations

Observatory, two satellites moving in the Earth's orbit around the Sun, viewing the Sun from changing positions to obtain a stereoscopic view of the dynamics of coronal mass ejection and, at the same time, to measure the local features, at the satellite position, of the solar wind.

Several missions in Earth orbit are also carrying instruments dedicated to continuous monitoring of solar activity. Table 4.9 lists the satellites monitoring solar activity from positions in deep space or in Earth orbit. In addition, some geostationary meteorological satellites (GOES or FY-4 series) contribute or will contribute to solar monitoring.

4.6.2 Magnetosphere and ionosphere monitoring

Closer to the Earth (see Figure 4.8(a) and (b)), the thermosphere and ionosphere are the layers where space weather is more turbulent. The main driver of the ionization state of the ionosphere is solar electromagnetic radiation (extreme ultraviolet and ultraviolet) which, in turn, is modulated by solar activity. The ionosphere is affected by waves, storms and travelling disturbances. Through interaction with magnetic storms, energetic particles and electrical currents can occur, which affect radio propagation. Mapping electron density in the ionospheric "E-region" enables ionospheric conductivity and currents to be inferred. When associated with magnetic field data, this information enables the internal component of the magnetic field (due to the solid Earth) to be discriminated from external components. Small-scale irregularities and eddies of the ionosphere can cause scattering of radio waves (scintillation), which affects the reliability of radio links crossing the ionosphere.

Table 4.9. Missions specific to solar activity monitoring

Acronym	*Full name*	*Responsible*	*Orbit*
ACE	Advanced Composition Explorer	NASA	L1 Lagrange point
Aditya-1	Aditya-1	ISRO	LEO, Sun-synchronous
DSCOVR	Deep Space Climate Observatory	NOAA, NASA	L1 Lagrange point
Hinode	Hinode (former name: SOLAR-B)	JAXA	LEO, Sun-synchronous
IRIS	Interface Region Imaging Spectrograph	NASA	LEO, Sun-synchronous
Picard	Picard	CNES	LEO, Sun-synchronous
PROBA 1 and 2	Project for On-board Autonomy 1 and 2	ESA	LEO, Sun-synchronous
RHESSI	Reuven Ramaty High Energy Solar Spectroscopic Imager	NASA	LEO, low-inclination
SDO	Solar Dynamics Observatory	NASA	Geosynchronous, low inclination
SOHO	Solar and Heliospheric Observatory	ESA, NASA	L1 Lagrange point
Solar Orbiter	Solar Orbiter	ESA, NASA	Solar orbit
Solar Probe Plus	Solar Probe Plus	NASA	Solar orbit
STEREO (2 sats)	Solar–Terrestrial Relations Observatory	NASA	Ecliptic plane
TIMED	Thermosphere, Ionosphere, Mesosphere Energetics and Dynamics mission	NASA	LEO, high-inclination
WIND	Comprehensive Solar Wind Laboratory for Long-term Solar Wind Measurements	NASA	L1 Lagrange point

Note: For organizations, please refer to the notes of the previous tables in this chapter

4.6.2.1 *Observation of the magnetosphere*

Missions dedicated to the magnetosphere have a long-standing heritage. Two significant current examples are the Time History of Events and Macroscale Interactions during Substorms (THEMIS) and the Magnetospheric Multiscale mission (MMS).

THEMIS is a NASA mission launched in 2007. It consists of a constellation of five small satellites in highly eccentric orbits, crossing the magnetosphere at several altitudes (see Figure 4.9), with periods ranging from 0.8 to 4 days.

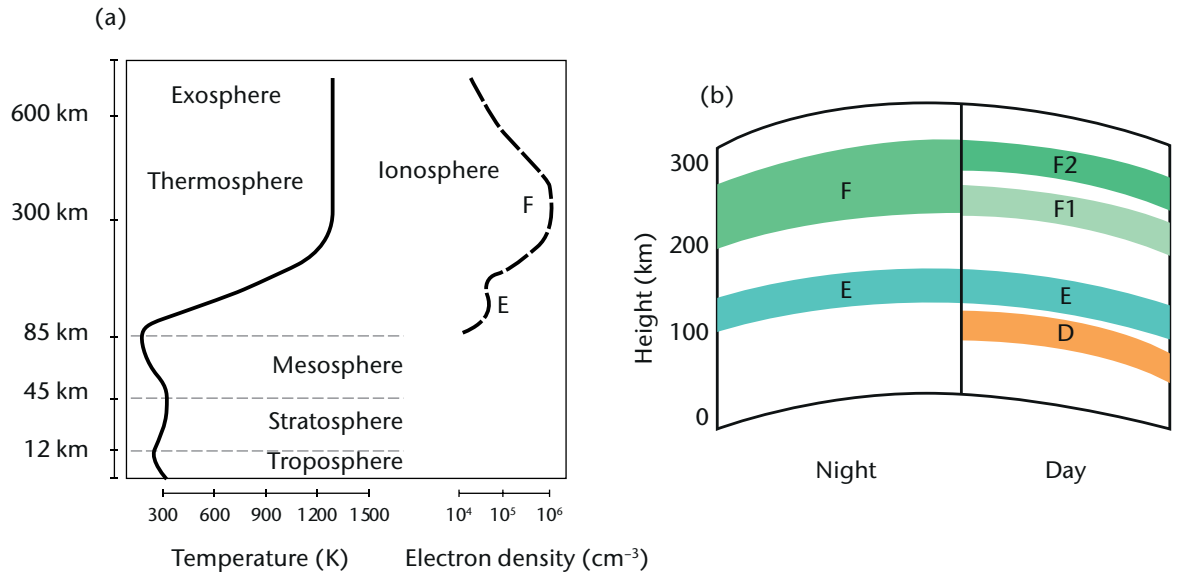

Figure 4.8. (a) Atmospheric stratification below and above the mesopause; (b) Layers of denser electronic content. The densest layer is F2, present day and night.

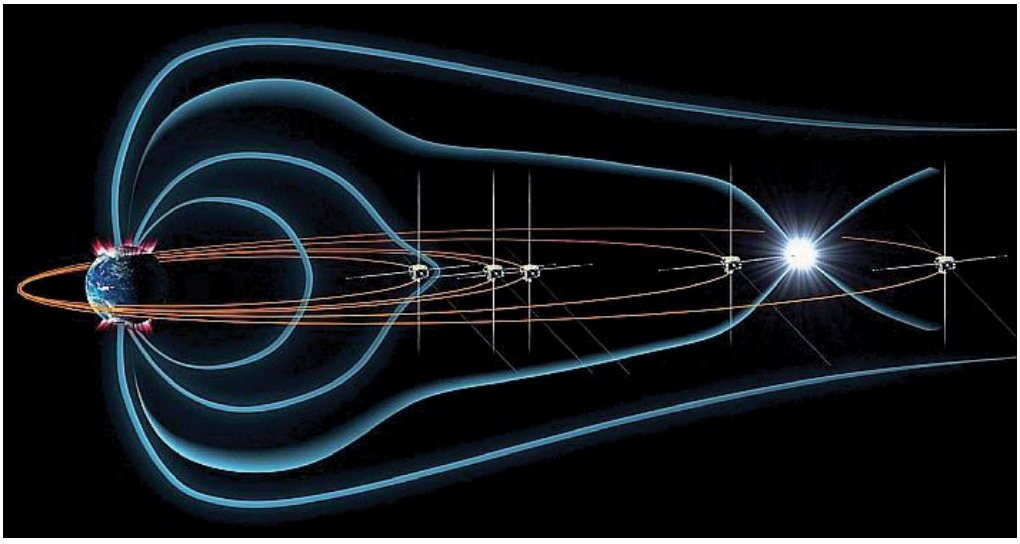

Figure 4.9. The orbits of the five THEMIS satellites in the magnetosphere. The white flash represents the energy released by a magnetospheric substorm.

THEMIS measures the magnetic field, electric fields and charged particles in order to address the physical processes in near-Earth space that initiate the violent eruptions of the aurora occurring during substorms in the Earth's magnetosphere. The system also includes a number of ground stations, to detect auroras and measure the surface magnetic field.

The MMS mission developed by NASA is based on a constellation of four satellites with highly eccentric orbits spread across the magnetosphere, similarly to THEMIS (see Figure 4.10). Plasma analysers, energetic particle detectors, magnetometers, and electric field instruments are used to study the microphysics of magnetic reconnection, the ultimate driver of space weather. Table 4.10 lists a number of missions specifically addressing the magnetosphere.

Section 4.5 describes a number of missions in lower orbit that also carry instruments relevant to the magnetosphere:

(a) Ørsted: Fluxgate Vector Magnetometer and scalar Overhauser Magnetometer;

(b) SAC-C: Magnetic Mapping Payload/Ørsted-2 (MMC/Ørsted-2);

(c) CHAMP: Magnetometer Instrument Assembly System;

(d) SWARM: Absolute Scalar Magnetometer, Vector Field Magnetometer and Electric Field Instrument.

4.6.2.2 ***Observation of the ionosphere***

With the advent of radio occultation sounding, the profile of the electron density across the ionosphere has become the best measurable geophysical variable associated with space weather.

The signal from navigation satellites (GPS, GLONASS, Compass, Galileo) is affected by the rotation of the electric field and the delay induced by the ionosphere. In order to correct for this effect, at least two frequencies are used. Currently, three frequency bands are used: ~1 180 MHz, ~1 580 MHz and ~1 250 MHz. Differentiating the two or more signals yields information on:

(a) The total electron content;

(b) The electron density profile.

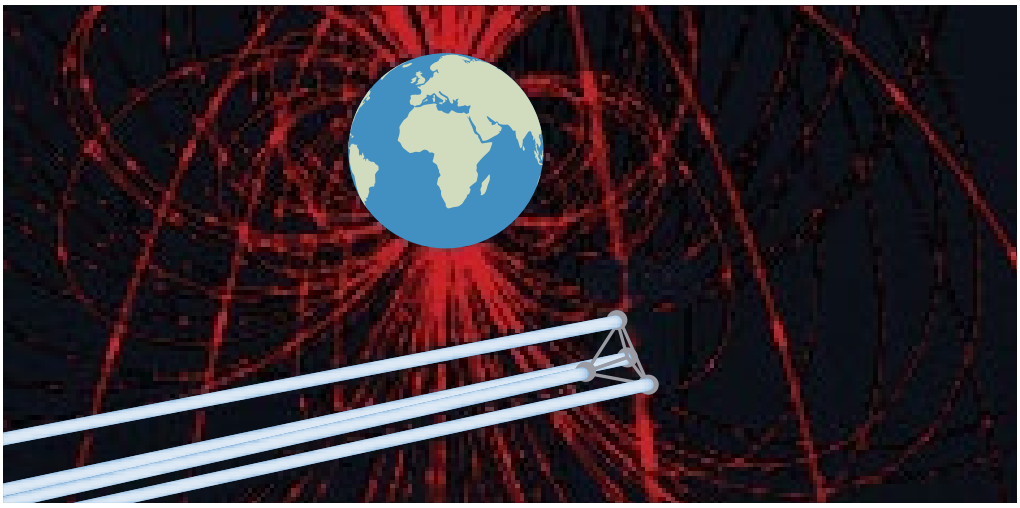

Figure 4.10. The four MMS satellites flying in formation. Tetrahedral pattern is used to capture the 3D structure of the encountered reconnection sites.

Table 4.10. Non-exhaustive list of missions orbiting inside the magnetosphere

Acronym	*Full name*	*Responsible*	*Orbit*
Arctica-M	Arctica-M	RosHydroMet	Molniya orbit
ARTEMIS	Acceleration, Reconnection, Turbulence, and Electrodynamics of the Moon's Interaction with the Sun	NASA	Lunar orbit
C/NOFS	Communication/Navigation Outage Forecasting System	DoD, NASA	LEO, low inclination
CASSIOPE	Cascade SmallSat and Ionospheric Polar Explorer	CSA	Highly elliptic, high inclination, relatively low altitude
Cluster (4 sats)	Cluster	ESA, NASA	Highly elliptic, polar inclination, tetrahedral formation flight
Geotail	Geotail	JAXA, NASA	Extremely elliptic, low inclination, crossing the moon orbit
IBEX	Interstellar Boundary Explorer	NASA	Highly elliptic, low inclination
IMAGE (or Explorer 78)	Imager for Magnetopause-to-Aurora Global Exploration	NASA	High-eccentricity polar orbit
Ionozond (5 sats)	Ionozond	Roscosmos	Four sats in Sun-synchronous orbit, one in drifting orbit
MMS (4 sats)	Magnetospheric Multiscale mission	NASA	Highly elliptic, low inclination, tetrahedral formation flight
SAMPEX (or Explorer 68)	Solar Anomalous and Magnetospheric Particle Explorer	NASA	Polar orbit
THEMIS (5 sats)	Time History of Events and Macroscale Interactions during Substorms	NASA	Highly elliptic, low inclination, apogees at five different altitudes
TWINS (2 sats)	Two Wide-angle Imaging Neutral-atom Spectrometers	NASA, United States Air Force	Molniya orbit
VAP (2 sats)	Van Allen Probe (formerly RBSP, Radiation Belt Storm Probes mission)	NASA	Highly elliptic, low inclination, crossing the radiation belts

Note: For organizations, please refer to the notes of the previous tables in this chapter

The total electron content, although integrated along-view, is measured for changing tangent heights; it is therefore possible to reconstruct the vertical profile by tomography. Several radio occultation payloads are being flown, on both multi-purpose satellites and dedicated facilities (such as COSMIC, COSMIC-2).

Radar altimeters also provide total electron content observations by exploiting two frequencies, generally ~13.5 GHz and ~5.3 GHz. The coverage is only at nadir and tomography is not possible; however, since altimetry missions are often orbited at high altitude (1 336 km for Jason, for example), the measurement includes the lower part of the plasmasphere (the layer above the thermosphere, from ~1 000 to ~40 000 km altitude).

Total electron content can also be measured directly by phase-delay analysis of the two or three frequencies transmitted by a GNSS satellite and received by a LEO satellite. In this case, total electron content is observed along the path from the GNSS satellite (orbit altitude ~20 000 km)

to the LEO satellite (orbit altitude ~800 km), thus in the medium plasmasphere. The number of available GNSS satellites is rather large: ~24 each for GPS and GLONASS systems, ~30 for Galileo, ~35 for Compass, with a total close to 110 and a fair global distribution.

4.6.2.3 *Space environment observation from operational meteorological satellites*

The constellations of operational meteorological satellites substantially contribute to space weather monitoring. In many cases the focus is on the in situ detection of energetic particle events, which are a threat to the on-board electronics and other subsystems sensitive to corpuscular radiation. Magnetic and electric fields are also measured in many cases, as well as solar activity. The orbits of meteorological satellites, however, do not meet all the needs of space environment monitoring: for instance the 90 to 300 km height range cannot be covered and Sun-synchronous orbits cannot capture the diurnal cycle, thus introducing a sampling bias. Nonetheless, the long-term, continuous availability of a high number of meteorological satellites constitutes a valuable contribution to space weather monitoring.

Table 4.11 presents the information available from operational meteorological satellite series related to space weather. Radio occultation payloads (see section 4.2.2) are omitted.

Table 4.11. Operational meteorological missions carrying instruments relevant to space weather

Satellite series	*Payload for in situ space environment monitoring*
GOES 11 to 15	Space Environment Monitor (SEM): suite of instruments for charged particles, solar X-ray and magnetic field Solar X-ray Imager (SXI)
GOES R, S, T, U	Space Environment In Situ Suite (SEISS) for charged particles in solar wind and cosmic rays Extreme Ultraviolet Sensor/X-Ray Sensor Irradiance Sensors (EXIS) Solar Ultraviolet Imager (SUVI) Magnetometer (MAG)
Electro-L Electro-M	GGAK-E: Heliogeophysical Instrument Complex for charged particles of solar wind and cosmic rays
FY-2	SEM for charged particles of solar wind
FY-4	SEM for charged particles of solar wind Solar X-EUV (SXEUV): imaging telescope for incoming X-rays and extreme UV from the Sun
Himawari-8/9	Space Environment Data Acquisition monitor (SEDA) for measuring electron and proton flux
NOAA 15 to 19 Metop A, B	SEM/2 for medium-energy and total-energy proton detection
JPSS	SEM for National Polar-orbiting Operational Environmental Satellite System (SEM-N): including a spectrometer for precipitating electrons and ions, a spectrometer for medium-energy particles, and omni-directional detectors for high-energy particles
DMSP F16 to S20	Special Sensor Ion and Electron Scintillation Monitor (SSIES) Special Sensor Precipitating Electron and Ion Spectrometer (SSJ5) Special Sensor Magnetometer (SSM) Special Sensor Ultraviolet Limb Imager (SSULI) Special Sensor Ultraviolet Spectrographic Imager (SSUSI)
Meteor-M	Geophysical Monitoring System Complex (GGAK-M), including: Spectrometer for Geoactive Measurements (MSGI-MKA) Radiation Monitoring System (KGI-4C)

Satellite series	*Payload for in situ space environment monitoring*
Meteor-MP	Geophysical Monitoring System Complex, improved after GGAK-M (GGAK-MP)
FY-3 A, B	SEM for charged particles of the solar wind
FY-3 C to G	Space Environment Suite (SES), including: SEM, same as on FY-3A and FY-3B Wide-Field Auroral Imager (WAI) Ionospheric Photometer (IPM)

CHAPTER 5. SPACE-BASED OBSERVATION OF GEOPHYSICAL VARIABLES

5.1 INTRODUCTION

This chapter offers an overview of geophysical variables that can be observed from space and of the performance that can be expected for their derivation. The performance is estimated by taking into account the physical principle involved in each measurement technique and the state-of-the-art instrument technology at the time of writing this document and in the foreseeable future.

Assumptions are made to provide a representative estimation technique in each case. The figures do not necessarily represent the actual performance of a particular instrument, but are intended to illustrate the relative performances of the various remote-sensing techniques.

5.1.1 Processing levels

For the purpose of the present Guide, the discussion is limited to geophysical variables that can be retrieved by processing the output from a single instrument or a set of closely associated instruments. Product derivation may involve complex algorithms, physical or statistical models, and supporting information from external sources, either ancillary (necessary for processing) or auxiliary (to help processing). The present chapter focuses on products that can be derived with a limited amount of external information, where this external information only plays a minor role compared with that of the satellite instrument output, and no significant bias can be introduced by a model. For instance, modelling of the physical phenomenon controlling the variable, radiative transfer models, and inversion retrieval models, are within the scope of this chapter. Beyond the scope of this chapter, for example, are assimilations that merge several measurements and background fields, that combine the physics of the phenomenon and the dynamics of the model to the point where the satellite contribution to the output product is barely recognizable.

This chapter will focus on Level 2 products, and some Level 3 and Level 4 products for which there is a well-established and recognized methodology (see the processing levels defined in the present volume, Chapter 2, 2.3.2.6, Table 2.11).

5.1.2 Product quality

For satellite imagery used directly for human interpretation, several quality criteria can be considered; these include spatial resolution, geo-location accuracy, calibration stability across consecutive images, or, in the case of RGB composite imagery, colour constancy in representing a given property within the observed scene. These components of the image product quality are not discussed further here.

In this chapter, the aim is to address the quality of quantitative products with numbers that can be used in automatic procedures and numerical models. This evaluation can then be compared with the requirements for the same products.

Product quality is specified here by:

(a) Atmospheric volume (for vertical profiles);

(b) Horizontal resolution (Δx);

(c) Vertical resolution (Δz) (for vertical profiles);

(d) Observing cycle (Δt);

(e) Accuracy (uncertainty);

(f) Timeliness (δt).

5.1.2.1 *Atmospheric volumes (relevant to 3D observations)*

User requirements may differ according to the layer of the atmosphere being considered. The figure below shows the definitions of the atmospheric volumes used in the WMO observation requirements database.

While users' requirements may change in a stepwise mode when moving along the vertical, the quality of satellite-derived products changes with height in a smooth way, depending mainly on the vertical gradient of the quantity, with better performance being achieved at steeper gradients. A step change occurs when the required vertical resolution cannot be achieved by cross-nadir scanning instruments and limb scanning becomes necessary. For the sake of simplicity, different product performances are often considered for the troposphere, the stratosphere, and the total atmospheric column (where applicable). It is often true that quality will softly degrade with increasing altitude in the troposphere, and the same in the stratosphere. Product quality is only quoted above the height of 1 km; below 1 km the accuracy is too irregular and difficult to estimate.

5.1.2.2 *Horizontal resolution*

The horizontal resolution (Δx) is the convolution of several features (sampling distance, degree of independence of the information relative to nearby samples, the point spread function, etc.). For simplicity, it is generally agreed to refer to the sampling distance between two successive product values carrying independent information.

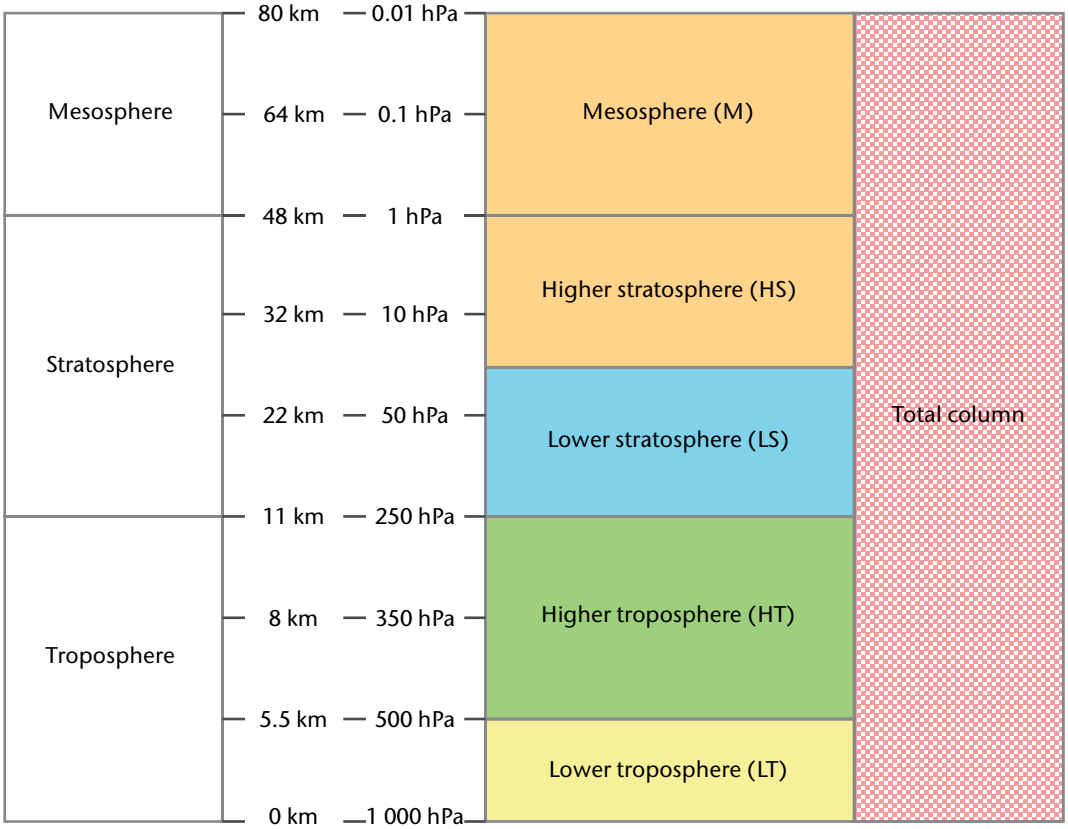

Atmospheric volumes defined by users. The higher stratosphere and mesosphere (HS&M) go together. The heights and pressures are qualitative, and refer to mid-latitudes/yearly average. The planetary boundary layer is part of the lower troposphere.

The horizontal resolution of the geophysical variable being measured is controlled by instrument features (primarily the IFOV), the sampling distance, or pixel, and the modulation transfer function) and by the processing scheme that may be designed to take account of interfering effects (such as clouds in the IFOV). For example, if clouds prevent the measurement being useful, it may be convenient to process pixel arrays searching or extrapolating for the less contaminated measurement in the cell of size Δx. The number of pixels to be co-processed depends on the spectral range used to perform the measurement (down to one for all-weather microwaves, for example) and on the available spectral information (when more spectral channels are available, a smaller cluster of pixels is needed). The extreme case is when a large pixel array (32 x 32, for instance) is needed to characterize the geophysical variable (an example is the inference of atmospheric motion vectors from the displacement of highly correlated cloudy pixel arrays within two images at different times).

For parameters such as cloud cover or snow cover, a sufficient number of samples (pixels) in the $\Delta x \cdot \Delta x$ cell is necessary to achieve the required accuracy. For cloud-disturbed surface measurements of slowly-changing variables (such as snow) it may be necessary to apply a multi-temporal analysis that waits for the clouds to move away (this would be a Level 3 product). It is generally possible, within limits, to trade off horizontal resolution against accuracy during product generation. Often, the product horizontal resolution is larger than a single pixel in order to enhance the SNR to meet the product accuracy requirements.

For cross-nadir scanning instruments, the instrument IFOV or pixel size gets larger from the sub-satellite point towards the swath edge; the product horizontal resolution performance must therefore be averaged across the instrument swath.

For conical scanners, the along-scan resolution is constant, but the cross-scan resolution is degraded by the cosine of the azimuth angle (the IFOV is nearly elliptical). The quadratic average in the along- and across-scan directions must be considered, and account has to be taken of the IFOV elongation in the along-scan direction due to the line-of-scan motion during the measurement integration time. If a single antenna is used for several frequencies, the resolution will change with frequency due to diffraction.

For limb sounding, the horizontal resolution is determined by the viewing geometry. The atmospheric path may physically extend for a few thousand kilometres, but the effective path (which accounts for higher atmospheric density around the tangent height) is around 300 km along-view. Across the viewing direction, although the transversal IFOV may be much narrower (tens of kilometres), the product resolution is determined by the number of azimuth views (in most cases only one, fore or aft). For the sake of simplicity, the typical horizontal resolution of limb measurements is taken as 300 km.

5.1.2.3 ***Vertical resolution***

The vertical resolution (Δz) is also defined by referring to the vertical sampling distance between two successive product values, carrying independent information.

The vertical resolution of the product depends on the sensing principle, the instrument spectral range and the number of channels or spectral resolution. The weighting function may be more or less broadened in the vertical depending on the spectral resolution and range (worse in MW, better in the optical ranges). Moreover, the spectral channels may be narrow enough to observe single lines of the absorbing/emitting gas, or a few lines or line bands. If several lines are included in the channel, the weighting function will be broadened since it will average surface emission between the lines (peaking in the lower atmosphere) and atmospheric emission in the lines (peaking at higher altitudes). In general, resolving power $\lambda/\Delta\lambda \approx 100$ enables broad-resolution retrieval of temperature vertical profiles with roughly 2 km vertical resolution; $\lambda/\Delta\lambda \approx 1\,000$ enables higher vertical resolution retrieval of temperature at about 1 km along with total-column retrieval of trace gases; $\lambda/\Delta\lambda \approx 10\,000$ is needed for trace-gas profiles. The gas density has a bearing on the achievable vertical resolution, so that with increasing altitude the vertical measurement resolution degrades.

It should be noted that the weighting function shifts to higher altitudes as the instrument viewing angle shifts from nadir to swath edge. This is due to the longer path length through the atmosphere with increasing view angle. The transmittance is an exponential function of the number of absorbing molecules in the path of the escaping radiation; a more oblique angle entails a greater likelihood of encountering more molecules in the upper atmosphere and hence the weighting function moves up in altitude.

The vertical resolution depends on the sensitivity of the wavelength to temperature. IR sensitivity to temperature is higher in the MWIR range (about 3–6 μm), thus the weighting functions are narrower in the lower troposphere and very broad in the higher troposphere and stratosphere. Short waves are less sensitive to temperature, so the vertical resolution is relatively homogeneous with altitude. As governed by the spectral Planck function, MW is relatively more sensitive to cold temperature and the vertical resolution is relatively good in the stratosphere.

In the stratosphere and above, the vertical resolution achievable by cross-nadir scanning is poor. Limb scanning offers better vertical resolution; it is performed by mechanical scanning along the vertical (angular IFOV combined with the scan rate) and is in the range of 1 to 3 km (which is not possible with cross-nadir scanning). The vertical resolution achieved by limb sounding degrades with altitude, as the SNR degrades with decreasing gas concentration. Occultation instruments (including radio occultation) have a vertical resolution that is determined by the sampling rate during the occultation phase. During ground processing, an algorithm performs some vertical integration as a trade-off against product accuracy.

5.1.2.4 ***Observing cycle***

The observing cycle (Δt) is defined as the time required to achieve global coverage (for LEO) or full disk coverage (for GEO). It is closely linked to the scanning capability of the instrument and to the orbital features. The relationship between observing cycle and scanning mechanism has been extensively discussed in the present volume, Chapter 3, 3.1.1. However, the instrument observing cycle may not coincide with the product observing cycle since not all observations taken during an instrument observing cycle may be useful for a given product. For example, a clear-sky mapped product may exhibit too many gaps due to cloud-affected observations. Thus the effective product observing cycle is a compromise between the minimum theoretical observing cycle that will have many gaps, and multi-temporal analysis degrading the product observing cycle but producing a more regular product field (generated by a Level 3 process). The compromise takes into account the sensitivity of the spectral band to the disturbing factor and the intrinsic time-variability of the desired geophysical parameter (which might not tolerate delays entailed by multi-temporal analysis). In another example, multi-temporal analysis might be necessary to collect enough signal when the required product accuracy cannot readily be achieved.

For most meteorological variables the required observing cycle prevents multi-temporal analysis. The solution is at system level, by establishing the number of satellites available to measure the geophysical variable. A global observing cycle shorter than 12 h (for measurements in IR and MW) or 24 h (for measurements involving SW) requires more satellites in regularly spaced orbits. For a 3 h cycle, four satellites are needed, provided the instrument swath is as large as the decalage (VIS/IR imagers, for example). For limited-swath instruments (such as MW radiometers of the GPM mission) the 3 h cycle requires eight satellites.

The observing cycle may be shortened at the expense of global coverage by using low-inclination orbits. The extreme limit is $\Delta t <$ one orbital period for a quasi-equatorial orbit run from east to west. Latitudes beyond the reach of the instrument swath will not be covered.

For satellites in GEO orbits, the observing cycle depends on the instrument refresh cycle. It may be minutes if the observation is unaffected by clouds; otherwise multi-temporal analysis may be needed. A constellation of six regularly-spaced GEO satellites provides coverage of all latitudes below 55°, rising to 70° and above for longitudes close to that of the six GEO locations.

Instruments with only nadir-viewing (non-scanning) provide infrequent global coverage. Limb-scanning instruments, including radio occultation, have a similar drawback (see the present volume, Chapter 3, 3.1.1). For these instruments, the observing cycle is difficult to define.

5.1.2.5 *Accuracy (uncertainty)*

Accuracy is defined as the "closeness of the agreement between a measured quantity value and a true quantity value of the measurand" (from the *International Vocabulary of Metrology – Basic and General Concepts and Associated Terms (VIM)*, Joint Committee for Guides in Metrology (JCGM) 200: 2012). In fact, accuracy is a qualitative concept, while the quantitative expression corresponding to the accuracy is the uncertainty (see Chapter 1, 1.6.2 of Volume I). The uncertainty is a combined result of several instrument features: random error, bias, sensitivity, repeatability, and the like. In the present volume (space-based observations), the uncertainty is generally characterized by the root-mean-square (RMS) error range, namely the RMS difference (observed – true values) of the measurement. The uncertainty of a satellite-derived observation of a geophysical variable is driven by the physical principle linking the satellite measurement to the observed variable, and in particular by the sensitivity of the measurement to variations of this variable. Expressing accuracy quantitatively in terms of RMS, but not taking into account the exact statistical distribution of the differences with regard to the true values traceable to the International System of Units (SI), is common to space-based observations. Particular consideration should be given to the methods used to determine any uncertainty value, all involved uncertainty budget components, the chosen confidence interval (usually 68% instead of the required 95%; see Chapter 1, 1.6.2 of Volume I) and the ways of assuring traceability to SI.

There is always a trade-off between spatial, radiometric and spectral resolution. High spatial resolution means low IFOV and low radiometric resolution. To obtain relatively high spatial resolution and high radiometric resolution requires decreasing the spectral resolution. Radiometric resolution is thus a driving factor of the uncertainty because it controls the strength of both the signal and noise of the observation. These determine the noise equivalent differential temperature, or the signal-to-noise ratio, or the noise equivalent spectral radiance, as defined in the present volume, Chapter 3, 3.1.4. However, the product uncertainty is also strongly affected by the retrieval algorithm and by the trade-off with the other quality features (Δx, Δz and Δt). Furthermore, the nature of the target (intensity of the emitted or scattered signal), the sensitivity of the sensing technique to the geophysical variable, and the efficiency in filtering out disturbing factors (such as clouds) have a pronounced impact on the final product uncertainty.

For a new instrument, evaluating the uncertainty requires sensitivity studies based on complicated simulations.

In the present volume, product uncertainty is estimated from the heritage of past and current instruments, and simulation of planned instruments. Some validation of satellite-derived product accuracy (discussed in the present volume, Chapter 6) enters into estimates for past and current instruments; for future instruments a theoretical calculation is performed.

5.1.2.6 *Timeliness*

Timeliness (δ_t) is defined as the time elapsed between the moment the observation is taken and the availability of the product assuming routine operations. Timeliness depends on the satellite transmission facilities, the availability of acquisition stations, the processing time required to generate the product, and the overall data management.

In this Guide, the timeliness δ_t of the various products has not been evaluated because it is a system feature that is not determined solely by the instrument.

5.1.3 Evaluation of satellite product quality

This chapter provides an overview of the satellite products that can potentially be retrieved from current or planned instruments, for geophysical variables of the following eight themes:

(a) Basic atmospheric (3D and 2D) variables;

(b) Cloud and precipitation variables;

(c) Aerosols and radiation;

(d) Ocean and sea ice;

(e) Land surface (including snow);

(f) Solid Earth;

(g) Atmospheric chemistry;

(h) Space weather.

This list of observation products is limited to "elementary" geophysical variables; it does not include products that can be derived from other products.

For each satellite product, the applicable remote sensing principles are indicated, together with any observing conditions or limitations. The annex to the present chapter contains an evaluation of the achievable quality in terms of RMS error,[1] Δx, Δz and Δt, based on the characteristics of state-of-the art instruments that are being developed at the time of writing this Guide, and expected to be operational by 2020.

5.2 BASIC ATMOSPHERIC 3D AND 2D VARIABLES

Table 5.1 lists basic variables for weather prediction, including NWP, that are observable from space.

Other basic variables such as atmospheric pressure, temperature and humidity at surface; and wind vertical component are not included because they cannot be reliably measured from space with current technology.

Table 5.1. Geophysical variables considered under the theme "Basic atmospheric (3D and 2D) variables"

Atmospheric temperature	Wind and wind profile (horizontal components of wind vector)	Height of the top of the planetary boundary layer	Height of the tropopause
Specific humidity	Wind vector over the surface (horizontal)	Temperature of the tropopause	

[1] Note that RMS error used in this volume corresponds approximately to an expanded uncertainty with a coverage factor of $k = 1$, while in the rest of this Guide a coverage factor of $k = 2$ is generally used (see Chapter 1, 1.6.3.3 of Volume I and the *Evaluation of Measurement Data – Guide to the Expression of Uncertainty in Measurement* (JCGM 100:2008)). The use of k = 2 is explained in Volume I, Chapter 1, 1.6.2. It is consistent with international standards approved by the International Committee for Weights and Measures (Comité international des poids et mesures (CIPM), see Manual on the WMO Integrated Global Observing System (WMO-No. 1160), par. 2.3.1.3).

5.2.1 **Atmospheric temperature**

Definition: 3D field of the atmospheric temperature – Required from surface to top of atmosphere (TOA) (layers: LT, HT, LS, HS&M) – Physical unit: kelvin (K) – Uncertainty unit: K.

Method 1: IR spectroscopy – Principle: IR emission from different atmospheric layers, selected by using spectral intervals of different absorption strength in bands of CO_2 (~4.3 and 15 μm). Applicable in both LEO and GEO.

Method 2: MW/sub-mm radiometry – Principle: MW and sub-millimetre wave emission from different atmospheric layers, selected by using spectral intervals of different absorption strength in bands of O_2 (~54, 118 and potentially 425 GHz). Applicable in both LEO and potentially GEO.

Method 3: GNSS (consisting of GPS and the Russian satellite navigation system, GLONASS) radio-occultation – Principle: Atmospheric refraction of L-band signals from the global navigation satellite system received by a LEO satellite during the occultation phase. Applicable only in LEO.

Method 4: Limb sounding – Principle: Emission by lines (in IR or MW) or line broadening (in SW) as observed by high-resolution spectrometers intended for atmospheric chemistry operating in the Earth's limb. Applicable only in LEO.

5.2.2 **Specific humidity**

Definition: 3D field of the specific humidity (that is, the ratio between the mass of water vapour and the mass of moist air) in the atmosphere – Required from surface to TOA (layers: LT, HT, LS, HS&M) + total column – Physical units: g/kg for layers, kg/m^2 for total column – Uncertainty unit: % for layers, kg/m^2 for total column.

Method 1: IR spectroscopy – Principle: IR emission from different atmospheric layers, selected by using spectral intervals of different absorption strength in bands of H_2O (~6 and potentially ~18 μm) with support of CO_2 (~4.3 and 15 μm). Applicable in both LEO and GEO.

Method 2: MW/sub-mm radiometry – Principle: MW and sub-mm wave emission from different atmospheric layers, selected by using spectral intervals of different absorption strength in bands of H_2O (183 and potentially 324, 380 GHz and others at higher frequencies) with necessary support of O_2 (~54, 118 and potentially 425 GHz). Applicable in LEO and potentially in GEO.

Method 3: GNSS radio-occultation – Principle: Atmospheric refraction of L-band signals from the GNSS received by a LEO satellite during the occultation phase. Applicable only in LEO.

Method 4: DIAL – Principle: Backscattered radiation in an NIR water-vapour absorption band (~935 nm for example) and a side window by DIAL. Applicable only in LEO.

Method 5: Limb sounding – Principle: Emission (in IR or MW/sub-mm), absorption (in Sun or star occultation of SW) or scattering (in SW) by lines as observed by high-resolution spectrometers intended for atmospheric chemistry operating in the Earth's limb. Applicable only in LEO.

Method 6: IR split window – Principle: By-product of the retrieval of surface temperatures from IR images (split-windows such as 11 and 12 μm). Suitable only for total column. Applicable in both LEO and GEO.

Method 7: MW imaging (23 GHz) – Principle: MW emission in a weak H_2O band (~23 GHz), associated with a nearby window (19 or 37 GHz). Suitable only for total column over the sea. Applicable in LEO and potentially in GEO.

Method 8: NIR imaging (935 nm) – Principle: Differential reflectance between an NIR water-vapour absorption band (~935 nm for example) and a side window by narrow-bandwidth radiometers. Suitable only for total column. Applicable in both LEO and GEO.

5.2.3 Wind profile (horizontal components of the wind vector – U and V)

Definition: Global wind profiles of the horizontal vector components (2D) of the 3D wind vector – Required from surface to TOA (layers: LT, HT, LS, HS&M) – Physical unit: m/s – Uncertainty unit: m/s.

Method 1: Doppler lidar – Principle: Direct measurements of horizontal wind profiles from laser pulses backscattered by air molecules, and aerosol and cloud particles, tracked by means of the Doppler effect of scattered light along the laser beam line of sight. Applicable only in LEO.

Method 2: VIS/IR image sequences – Principle: Atmospheric motion vectors (AMVs) extracted from IR/VIS satellite imagery by tracking clouds and water vapour features in consecutive image sequences. Applicable in both LEO and GEO.

Method 3: IR sounder – Principle: 3D wind profiles extracted from motion detected in humidity and ozone fields retrieved from IR sounder instruments. Applicable in both LEO and GEO.

Method 4: VIS/IR images in varying geometry – Principle: Parallax is used to determine the height of atmospheric features in multiple images. The small time difference is further used to infer displacement. Features may be due to clouds and aerosol recognized and tracked in VIS/IR image sequences. Applicable in both LEO and GEO.

Method 5: Limb sounding – Principle: Doppler shift and broadening of spectral lines of O_2, O_3, OH – observed by high-resolution VIS spectrometers operating in the Earth's limb in the HS&M. Applicable only in LEO.

5.2.4 Wind vector over the surface (horizontal)

Definition: Horizontal vector components (2D) of the 3D wind vector, conventionally measured at 10 m height – Required over sea and land surface (all methods below apply over sea). Physical unit: m/s – Uncertainty unit: m/s.

Method 1: Radar scatterometry – Principle: Backscattered radiation from capillary waves by medium-frequency radar (about 1 to 15 GHz). More viewing angles are used to determine direction. Applicable only over the sea. Applicable only in LEO.

Method 2: Polarimetric MW radiometry – Principle: Emitted and scattered MW radiation in atmospheric windows at several frequencies (10, 19, 37 GHz for example). Three Stokes parameters to be measured (at least four polarizations, for example), preferably four (requiring six polarizations). Applicable only over the sea. Wind direction only above 8 m/s. Applicable only in LEO.

Method 3: MW imagery – Principle: Emitted and scattered MW radiation in atmospheric windows at several frequencies (such as 1.4, 10, 19, 37 GHz). At least two polarizations needed. Applicable only over the sea. Only speed measured. Applicable only in LEO.

Method 4: Radar altimetry – Principle: Backscattered radiation from sea surface by medium-frequency radar (~13 GHz). Wind speed associated with echoes scattered from capillary waves. Applicable only over the sea. Only speed measured. Only nadir. Applicable only in LEO.

Method 5: GNSS-R – Principle: Reflected signals of opportunity from GNSS satellites, which are forward scattered off the sea surface, express the local wind speed at the specular point. Applicable only over the sea. Only speed measured. Applicable only in LEO.

5.2.5 Height of the top of the planetary boundary layer

Definition: Height of the surface separating the planetary boundary layer from the free atmosphere – Physical unit: km – Uncertainty unit: km.

Method 1: Backscatter lidar – Principle: Backscattered radiation in UV, VIS or NIR by lidar. Applicable only in LEO.

Method 2: From IR sounding – Principle: Derived from IR sounding of temperature and humidity. Applicable in both LEO and GEO.

Method 3: From GNSS sounding – Principle: Derived from GNSS radio-occultation sounding of temperature and humidity. Applicable only in LEO.

5.2.6 Height of the tropopause

Definition: Height of the surface separating the troposphere from the stratosphere – Physical unit: km – Uncertainty unit: km.

Method 1: Backscatter lidar – Principle: Backscattered radiation in UV, VIS or NIR by lidar. Two wavelengths preferred. Applicable only in LEO.

Method 2: From IR sounding – Principle: Derived from IR sounding of temperature. Applicable in both LEO and GEO.

Method 3: From GNSS sounding – Principle: Derived from GNSS radio-occultation sounding of temperature. Applicable only in LEO.

5.2.7 Temperature of the tropopause

Definition: Atmospheric temperature at the height of the surface separating the troposphere from the stratosphere – Physical unit: K – Uncertainty unit: K.

Method 1: From IR sounding – Principle: Derived from IR sounding of temperature. Applicable in both LEO and GEO.

Method 2: From GNSS sounding – Principle: Derived from GNSS radio-occultation sounding of temperature. Applicable only in LEO.

Method 3: From limb sounding – Principle: Derived from limb sounding of temperature. Applicable only in LEO.

5.3 CLOUD AND PRECIPITATION VARIABLES

This theme includes the basic variables observable from space for actual weather analysis, and for short-term prediction and nowcasting, as well as for hydrology. Table 5.2 lists these variables.

Table 5.2. Geophysical variables considered under the theme "Cloud and precipitation variables"

Cloud-top temperature	Cloud-base height	Cloud ice	Precipitation (liquid or solid)
Cloud-top height Cloud vertical extent	Cloud optical depth	Cloud-ice effective radius	Precipitation intensity at surface (liquid or solid)
Cloud type	Cloud liquid water	Freezing-level height in clouds	Accumulated precipitation (over 24 h or other sub-daily frequency)
Cloud cover	Cloud-droplet effective radius	Melting-layer depth in clouds	Lightning detection

5.3.1 Cloud-top temperature

Definition: Temperature of upper surface of cloud – Physical unit: K – Uncertainty unit: K.

Method 1: IR radiometry – Principle: Derived from IR imagery in a number of channels including "windows" and others (in water-vapour absorption bands) as necessary to evaluate cloud emissivity. Applicable in both LEO and GEO.

Method 2: From IR sounding – Principle: Derived from spectral IR radiance measurements. Measurement of the radiances (brightness temperatures) at different wavelengths enables retrieval of cloud-top temperature within the observed IFOV. Applicable in both LEO and GEO.

5.3.2 Cloud-top height

Definition: Height of the upper surface of the cloud – Physical unit: km – Uncertainty unit: km.

Method 1: IR radiometry – Principle: Derived from spectral radiances (typically from imagers using spectral channels at 11 and 13.4 or 6.7 μm. Methods are referred to as CO_2-slicing or water-vapour intercept method. Cloud-top pressure or height are inferred using a forecast temperature profile. Applicable in both LEO and GEO.

Method 2: From IR sounding – Principle: Derived as a by-product of temperature/humidity sounding retrieval from IR spectroscopy. The different radiative transfer at different wavelengths enables retrieval of cloud-top height within the sounded IFOV. Applicable in both LEO and GEO.

Method 3: Backscatter lidar – Principle: Backscattered radiation in UV, VIS or NIR by lidar. Two wavelengths preferred. Applicable only in LEO.

Method 4: Cloud radar – Principle: Backscattered radiation in MW (~94 GHz) by radar. Applicable only in LEO.

Method 5: A-band spectroscopy – Principle: Observation of columnar O_2 (absorption path length) above the cloud top by spectroscopy of the 760 nm A-band and nearby "window". Applicable in both LEO and GEO.

Method 6: Stereo – Principle: Nearly simultaneous views of clouds from multiple angles allow for the estimation of cloud height above the surface through the use of parallax. In principle applicable to any spectral observation and any combination of LEO and GEO.

5.3.3 **Cloud vertical extent**

Definition: Vertical extent expressed as a temperature, height or pressure of the upper surface of the cloud – Physical unit: km, K or hPa – Uncertainty unit: km, K or hPa. Note: It should be considered that cloud geometric thickness inferred from passive remote sensing from satellites is not very accurate.

Method 1: IR radiometry – Principle: Derived from IR imagery in a number of channels including "windows" and others (in water-vapour absorption bands) as necessary to evaluate cloud emissivity. Measured property can be temperature, height or pressure. Applicable in both LEO and GEO.

Method 2: IR radiometry – Principle: Derived from multiple IR observations in absorption bands of CO_2 or H_2O. Commonly referred to as slicing or intercept techniques. Measured property can be temperature, height or pressure. Applicable in both LEO and GEO.

Method 3: From IR sounding – Principle: Derived as a by-product of temperature/humidity sounding retrieval from IR spectroscopy. The different radiative transfer at different wavelengths enables retrieval of cloud-top height within the sounded IFOV. Applicable in both LEO and GEO.

Method 4: Backscatter lidar – Principle: Backscattered radiation in UV, VIS or NIR by lidar. Two wavelengths preferred. Applicable only in LEO.

Method 5: Cloud radar – Principle: Backscattered radiation in MW (~94 GHz) by radar. Applicable only in LEO.

Method 6: A-band spectroscopy – Principle: Observed defect of columnar O_2 above the cloud top by spectroscopy of the 760 nm A-band and nearby "window". Applicable in both LEO and GEO.

Method 7: Stereo – Principle: Nearly simultaneous views of clouds from multiple angles allow for the estimation of cloud height above the surface through the use of parallax. Applicable to any spectral observation and any combination of LEO and GEO.

5.3.4 **Cloud type**

Definition: Comprehensive properties of the observed cloud. The list of types of interest is predetermined – Uncertainty expressed as number of discriminated types (classes).

Method 1: VIS/IR radiometry – Principle: Multi-spectral analysis of cloud reflectance, top-surface temperature, optical depth, emissivity, cloud brightness temperatures and their temporal/spatial characteristics allows classification of clouds into types defined by their phase, drop size, over different backgrounds, observed in a few discrete channels of relatively large bandwidths (5–10 cm^{-1}). Allows retrieval of ice/water, opacity and vertical structure (single/multi-layer). Applicable in both LEO and GEO.

Method 2: Derived cloud properties from VIS/IR radiometry – Principle: Analysis of the cloud opacity, microphysics, vertical extent and spatial texture allows for estimation of the traditional meteorological cloud types such as stratus, cumulus and cirrus. Applicable in both LEO and GEO.

5.3.5 Cloud cover

Definition: 3D field of fraction of sky where clouds are detected. Required as a 3D field in the troposphere (assumed height: 12 km) and also as a single layer (total column) to provide the total cloud cover – Physical unit: % – Uncertainty unit: %.

Method 1: VIS/IR radiometry – Principle: Derived from cloud imagery in a few discrete channels selected so as to detect all cloud types. The fractional cover refers to the number of cloudy pixels in a given pixel array. Applicable in both LEO and GEO.

Method 2: From IR sounding – Principle: Derived as a by-product of temperature/humidity sounding retrieval from IR spectroscopy. The different radiative transfer at different wavelengths enables retrieval of cloud fraction times cloud emissivity within the sounded IFOV. Applicable in both LEO and GEO.

Method 3: Cloud radar – Principle: Backscattered radiation from cloud droplets observed by high-frequency radar (~94 GHz). Applicable only in LEO.

5.3.6 Cloud-base height

Definition: Height of the bottom surface of the cloud – Physical unit: km – Uncertainty unit: km.

Method 1: Cloud radar – Principle: Derived as lower level of the backscattered radiation from cloud droplets observed by high-frequency radar (~94 GHz). Applicable only in LEO.

5.3.7 Cloud optical depth

Definition: Effective depth of the cloud from the viewpoint of radiation propagation. The definition is $OD = \exp(-K\,\Delta z)$. K is the extinction coefficient (km^{-1}), Δz the optical path (km) between the base and the top of the cloud. It depends on the wavelength but is usually referred to visible radiation. Physical unit: dimensionless – Uncertainty unit: dimensionless.

Method 1: Backscatter lidar – Principle: Backscattered radiation in UV, VIS or NIR by lidar. Two wavelengths preferred. Applicable only in LEO.

Method 2: SW polarimetry – Principle: Scattered solar radiation in several narrowband channels of UV, VIS, NIR and SWIR, some with polarimetric measurements to determine three Stokes parameters. Applicable only in LEO.

Method 3: SW/thermal infrared (SW/TIR) radiometry – Principle: Scattered solar radiation in several narrowband channels of VIS, NIR and SWIR, and emitted radiation in several window channels of TIR. Applicable in both LEO and GEO.

5.3.8 Cloud liquid water

Definition: 3D field of atmospheric water in the liquid phase (precipitating or not). Required in the troposphere (assumed height: 12 km) and for total column – Physical unit: g/kg for layers, g/m^2 for total column – Uncertainty unit: % for layers, g/m^2 for total column.

Method 1: Cloud radar – Principle: Backscattered radiation from cloud droplets observed by high-frequency radar (~94 GHz). Applicable only in LEO.

Method 2: Precipitation radar – Principle: Backscattered radiation from cloud droplets observed by medium-frequency radar (dual-frequency preferred, 14 and 35 GHz). Applicable only in LEO.

Method 3: MW/sub-mm sounding – Principle: MW/sub-mm radiation in window channels (typically, ~10, 19, 37, 90, 150 GHz) with dual polarization, and absorption bands (typically, ~54, 118, 183 GHz). Applicable in LEO and potentially in GEO.

5.3.9 **Cloud-droplet effective radius**

Definition: 3D field of the size distribution of liquid water droplets, assimilated to spheres of the same volume. Required in the troposphere (assumed height: 12 km), and at the cloud-top surface – Physical unit: μm – Uncertainty unit: μm.

Method 1: Cloud radar – Principle: Backscattered radiation from cloud droplets by high-frequency radar (~94 GHz). Applicable only in LEO.

Method 2: Precipitation radar – Principle: Backscattered radiation from cloud droplets by medium-frequency radar (dual-frequency preferred, 14 and 35 GHz). Applicable only in LEO.

Method 3: MW/sub-mm sounding – Principle: MW/sub-mm radiation in window channels (typically, ~10, 19, 37, 90, 150 GHz) with dual polarization, and absorption bands (typically, ~54, 118, 183 GHz). Actually, the cloud-droplet effective radius profile is retrieved with the help of an associated NWP model, possibly cloud-resolving. Applicable in LEO and potentially in GEO.

Method 4: Backscatter lidar – Principle: Backscattered radiation in UV, VIS or NIR by lidar. Essentially limited to cloud top. Applicable only in LEO.

Method 5: SW polarimetry – Principle: Scattered solar radiation in several narrowband channels of UV, VIS, NIR and SWIR, some with polarimetric measurements to determine three Stokes parameters. Essentially limited to cloud top. Applicable only in LEO.

Method 6: VIS/IR radiometry – Principle: Scattered solar radiation in several narrowband channels of VIS, NIR, SWIR and MWIR. Also, differential emission in several channels of thermal infrared (TIR, for cirrus clouds). Essentially limited to cloud top. Applicable in both LEO and GEO.

5.3.10 **Cloud ice**

Definition: 3D field of atmospheric water in the solid phase (precipitating or not). Required in the troposphere (assumed height: 12 km) and for total column – Physical unit: g/kg for layers, g/m^2 for total column – Uncertainty unit: % for layers, g/m^2 for total column.

Method 1: Cloud radar – Principle: Backscattered radiation from ice particles observed by high-frequency radar (~94 GHz). Applicable only in LEO.

Method 2: Precipitation radar – Principle: Backscattered radiation from ice particles by medium-frequency radar (dual-frequency preferred, 14 and 35 GHz). Applicable only in LEO.

Method 3: MW/sub-mm sounding – Principle: MW/sub-mm radiation in window channels (typically, ~37, 90, 150 GHz) with dual polarization, and absorption bands (typically, ~54, 118, 183, and potentially 380, 425 GHz). Actually, the cloud-ice profile is retrieved with the help of an associated NWP model, possibly cloud-resolving. Applicable in LEO and potentially in GEO.

Method 4: Sub-mm imagery – Principle: Emitted and scattered radiation in MW atmospheric windows (243, 664, 874 GHz) in dual polarization supported by channels in H_2O absorption bands (183, 325, 448 GHz). Suitable only for total column. Applicable only in LEO.

Method 5: FIR imagery – Principle: Emitted and scattered radiation in several atmospheric windows of FIR (18.2, 24.4, 52, 87 μm) as compared to TIR (8.7, 11, 12 μm). Suitable only for total column. Applicable only in LEO.

5.3.11 Cloud-ice effective radius

Definition: 3D field of the size distribution of ice particles, assimilated to spheres of the same volume. Required in the troposphere (assumed height: 12 km), and at the cloud-top surface – Physical unit: μm – Uncertainty unit: μm.

Method 1: Cloud radar – Principle: Backscattered radiation from ice particles by high-frequency radar (~94 GHz). Applicable only in LEO.

Method 2: Precipitation radar – Principle: Backscattered radiation from ice particles by medium-frequency radar (dual-frequency preferred, 14 and 35 GHz). Applicable only in LEO.

Method 3: MW/sub-mm sounding – Principle: MW/sub-mm radiation in window channels (typically, ~10, 19, 37, 90, 150 GHz) with dual polarization, and absorption bands (typically, ~54, 118, 183 GHz). Actually, the cloud-ice effective radius profile is retrieved with the help of an associated NWP model, possibly cloud-resolving. Applicable in LEO and potentially in GEO.

Method 4: Backscatter lidar – Principle: Backscattered radiation in UV, VIS or NIR by lidar. Essentially limited to cloud top. Applicable only in LEO.

Method 5: SW polarimetry – Principle: Scattered solar radiation in several narrowband channels of UV, VIS, NIR and SWIR, some with polarimetric measurements to determine three Stokes parameters. Essentially limited to cloud top. Applicable only in LEO.

Method 6: VIS/IR radiometry – Principle: Scattered solar radiation in several narrowband channels of VIS, NIR, SWIR and MWIR. Also, differential emission in several channels of TIR (for cirrus clouds). Essentially limited to cloud top. Applicable in both LEO and GEO.

5.3.12 Freezing-level height in clouds

Definition: Height of the atmospheric layer in cloud where liquid-solid states transform into each other – Physical unit: km – Uncertainty unit: km.

Method 1: Precipitation radar – Principle: Backscattered radiation from cloud drops by medium-frequency radar (dual-frequency preferred, 14 and 35 GHz). Applicable only in LEO.

Method 2: From MW/sub-mm sounding – Principle: Derived from MW and sub-mm wave sounding of temperature. Applicable in LEO and potentially in GEO.

5.3.13 Melting-layer depth in clouds

Definition: Depth of the atmospheric layer in cloud where liquid-solid states transform into each other – Physical unit: km – Uncertainty unit: km.

Method 1: Precipitation radar – Principle: Backscattered radiation from cloud drops by medium-frequency radar (dual-frequency preferred, 14 and 35 GHz). Applicable only in LEO.

Method 2: From MW/sub-mm sounding – Principle: Derived from MW and sub-mm wave sounding of temperature. Applicable in LEO and potentially in GEO.

5.3.14 Precipitation (liquid or solid)

Definition: 3D field of the vertical flux of precipitating water mass. Required in the troposphere (assumed height: 12 km) – Physical unit: $g \cdot s^{-1} \cdot m^{-2}$ (vertical flux of precipitating water mass) – Uncertainty unit: %.

Method 1: Precipitation radar – Principle: Backscattered radiation from cloud drops by medium-frequency radar (dual-frequency preferred, 14 and 35 GHz). Doppler capability also useful. Applicable only in LEO.

Method 2: MW/sub-mm sounding – Principle: MW/sub-mm radiation in window channels (typically, ~10, 19, 37, 90, 150 GHz) with dual polarization, and absorption bands (typically, ~54, 118, 183, 380, 425 GHz). Actually, the precipitation profile is retrieved with the help of an associated NWP model, possibly cloud-resolving. Applicable in LEO and potentially in GEO.

5.3.15 Precipitation intensity at surface (liquid or solid)

Definition: Intensity of precipitation reaching the ground – Physical unit: mm/h (if solid, mm/h of liquid water after melting) – Uncertainty unit: mm/h. Since uncertainty changes with intensity, it is necessary to specify a reference intensity. Assumed intensity: 5 mm/h.

Method 1: Precipitation radar – Principle: Backscattered radiation from cloud drops by medium-frequency radar (dual-frequency preferred, 14 and 35 GHz). Doppler capability also useful. Applicable only in LEO.

Method 2: MW/sub-mm sounding – Principle: MW/sub-mm radiation in window channels (typically, ~10, 19, 37, 90, 150 GHz) with dual polarization, and absorption bands (typically, ~54, 118, 183, 380, 425 GHz). Actually, the precipitation rate at surface is retrieved from the profile reconstructed with the help of an associated NWP model, possibly cloud-resolving. Applicable in LEO and potentially in GEO.

Method 3: VIS/IR radiometry – Principle: Inferred from cloud imagery in a few discrete channels selected so as to detect all cloud types, assisted by conceptual models, generally more responsive to convective rain. Applicable in GEO.

Method 4: Fusion between MW from LEO and IR from GEO – Principle: Combined product of LEO/MW-derived accurate/infrequent measurements with GEO/IR frequent images used either to be "calibrated" by MW measurements or to enable dynamical interpolation between MW-derived precipitation data. Requiring both LEO and GEO.

5.3.16 Accumulated precipitation (over 24 hours or other sub-daily frequency)

Definition: Integration of precipitation intensity reaching the ground in given time intervals. The reference requirement refers to integration over 24 h – Physical unit: mm – Uncertainty unit: mm.

Method 1: From fusion between MW from LEO and IR from GEO – Principle: Derived by time integration of frequent precipitation rate measured by merging MW precipitation rate data from LEO with IR imagery from GEO. Requiring both LEO and GEO.

5.3.17 Lightning detection

Definition: Mapping of lightning events as number of flashes in a given time interval over a given area – Physical unit: counts – Uncertainty expressed as hit rate (HR) and false-alarm rate (FAR).

Method 1: Lightning mapping – Principle: Detection of flashes by a charge-coupled device camera in a very narrow channel in a NIR oxygen absorption band (generally at 777.4 nm) for operability also in daylight. The number of flashes in a given time over a given area, and their intensity, are related to the maturity of the convective process in cloud. Applicable in both LEO and GEO.

5.4 AEROSOL AND RADIATION

This theme comprises variables that affect the Earth radiation budget versus space, cloud–radiation interaction, cloud formation, air quality and several characterizing factors of climate and climate change. The variables observable from space are listed in Table 5.3.

Further variables such as aerosol absorption optical depth, aerosol extinction coefficient, aerosol single scattering albedo and aerosol phase function have not been considered since they are closely linked to the selected ones (optical thickness, concentration, effective radius, and type), which are more understandable to the general user.

Table 5.3. Geophysical variables considered under the theme "Aerosol and radiation"

Aerosol optical depth	Upward spectral radiance at TOA	Earth's surface albedo
Aerosol concentration	Upward LW irradiance at TOA	Earth's surface SW bi-directional reflectance
Aerosol effective radius	Upward SW irradiance at TOA	Upward LW irradiance at Earth's surface
Aerosol type	SW cloud reflectance	Long-wave Earth-surface emissivity
Volcanic ash	Downward LW irradiance at Earth's surface	Photosynthetically active radiation
Downward solar irradiance at TOA	Downward SW irradiance at Earth's surface	Fraction of absorbed photosynthetically active radiation

5.4.1 Aerosol optical depth

Definition: Effective depth of the aerosol column from the viewpoint of radiation propagation. The definition is $OD = \exp(-K\,\Delta z)$. K is the extinction coefficient (km^{-1}), Δz the optical path (km) between the Earth's surface and TOA. It depends on the wavelength – Physical unit: dimensionless – Uncertainty unit: dimensionless.

Method 1: Backscatter lidar – Principle: Backscattered radiation in UV, VIS or NIR by lidar. Applicable only in LEO.

Method 2: SW polarimetry – Principle: Scattered solar radiation in several narrowband channels of UV, VIS, NIR and SWIR, some with polarimetric measurements to determine three Stokes parameters. Also, multi-viewing at different incident angles. Applicable only in LEO.

Method 3: SW spectroscopy (cross-nadir) – Principle: Scattered radiation in UV, VIS, NIR and SWIR observed cross-nadir with high spectral resolution. Applicable in both LEO and GEO.

Method 4: VIS/IR radiometry – Principle: Scattered solar radiation in several channels of VIS, NIR and SWIR. Some information, relevant to absorbing aerosol, also available in thermal IR windows. Applicable in both LEO and GEO.

5.4.2 Aerosol concentration

Definition: 3D field of the mass mixing ratio of condensed particles in the atmosphere (other than water) – Required from surface to TOA (layers: LT, HT, LS, HS&M) + total column – Physical units: g/kg for layers, g/m^2 for total column – Uncertainty unit: % for layers, g/m^2 for total column.

Method 1: Backscatter lidar – Principle: Backscattered radiation in UV, VIS or NIR by lidar. Applicable only in LEO.

Method 2: SW polarimetry – Principle: Scattered solar radiation in several narrowband channels of UV, VIS, NIR and SWIR, some with polarimetric measurements to determine three Stokes parameters. Also, multi-viewing at different incident angles. Applicable only in LEO.

Method 3: SW spectroscopy (cross-nadir) – Principle: Scattered radiation in UV, VIS, NIR and SWIR observed cross-nadir with high spectral resolution. Applicable in both LEO and GEO.

Method 4: SW spectroscopy (limb) – Principle: Scattered radiation in UV, VIS, NIR and SWIR observed in limb mode with high spectral resolution. Also, absorbed radiation from Sun or stars during occultation. Applicable only in LEO.

Method 5: VIS/IR radiometry – Principle: Scattered solar radiation in several channels of VIS, NIR and SWIR. Some information, relevant to absorbing aerosol, also available in thermal IR windows. Suitable only for total column. Applicable in both LEO and GEO.

5.4.3 **Aerosol effective radius**

Definition: 3D field of the mean size of the aerosol particles, assimilated to spheres of the same volume. Required in the troposphere (assumed height: 12 km) and as columnar average – Physical unit: μm – Uncertainty unit: μm.

Method 1: Backscatter lidar – Principle: Backscattered radiation in UV, VIS or NIR by lidar. Applicable only in LEO.

Method 2: SW polarimetry – Principle: Scattered solar radiation in several narrowband channels of UV, VIS, NIR and SWIR, some with polarimetric measurements to determine three Stokes parameters. Also, multi-viewing at different incident angles. A priori information and intensive modelling necessary. Applicable only in LEO.

Method 3: SW spectroscopy (cross-nadir) – Principle: Scattered radiation in UV, VIS, NIR and SWIR observed cross-nadir with high spectral resolution. A priori information and intensive modelling necessary. Applicable in both LEO and GEO.

5.4.4 **Aerosol type**

Definition: 3D field. Comprehensive properties of the aerosol being observed. The list of types of interest is predetermined – Required in the troposphere (assumed height: 12 km) and as columnar average – Uncertainty is typically defined in terms of confidence with which an aerosol can be typed. For example how confidently it can be determined if dust is in a given pixel (0%–100%). Accuracy is reported in terms of probability of correct detection. Note that volcanic ash and even sometimes smoke aerosol (pyrocloud situation) can be found in the stratosphere.

Method 1: Backscatter lidar – Principle: Backscattered radiation in UV, VIS or NIR by lidar. Applicable only in LEO.

Method 2: SW polarimetry – Principle: Scattered solar radiation in several narrowband channels of UV, VIS, NIR and SWIR, some with polarimetric measurements to determine three Stokes parameters. Also, multi-viewing at different incident angles. A priori information and intensive aerosol modelling absolutely necessary. Applicable only in LEO.

Method 3: SW spectroscopy (cross-nadir) – Principle: Scattered radiation in UV, VIS, NIR and SWIR observed cross-nadir with high spectral resolution. A priori information and intensive aerosol modelling absolutely necessary. Applicable in both LEO and GEO.

Method 4: VIS/IR radiometry – Principle: Scattered solar radiation in several channels of VIS, NIR and SWIR. Some information also available in thermal IR windows. A priori information and intensive aerosol modelling necessary. Suitable only for total column. Applicable in both LEO and GEO.

5.4.5 Volcanic ash

Definition: 3D field of concentration of volcanic ash – Required from surface to TOA (layers: LT, HT, LS, HS&M) + total column – Physical units: mg/m^3 or g/kg for layers, g/m^2 for total column – Uncertainty unit: % for layers, g/m^2 for total column.

Method 1: Backscatter lidar – Principle: Backscattered radiation in UV, VIS or NIR by lidar. Applicable only in LEO.

Method 2: SW polarimetry – Principle: Scattered solar radiation in several narrowband channels of UV, VIS, NIR and SWIR, some with polarimetric measurements to determine three Stokes parameters. Also, multi-viewing at different incident angles. Applicable only in LEO.

Method 3: SW spectroscopy (cross-nadir) – Principle: Scattered radiation in UV, VIS, NIR and SWIR observed cross-nadir with high spectral resolution. Applicable in both LEO and GEO.

Method 4: SW spectroscopy (limb) – Principle: Scattered radiation in UV, VIS, NIR and SWIR observed in limb mode with high spectral resolution. Also, absorbed radiation from Sun or stars during occultation. Applicable only in LEO.

Method 5: VIS/IR radiometry – Principle: Scattered solar radiation in several channels of VIS, NIR and SWIR.

Method 6: Passive IR measurements are the backbone of volcanic ash remote sensing. Other methods are considered value-added approaches. Differential absorption in the IR windows is the method used. In addition, hyperspectral IR measurements are used to determine the mineral composition of ash, which is important. Applicable in both LEO and GEO.

5.4.6 Downward solar irradiance at top of atmosphere

Definition: Flux density of the solar radiation at the top of the atmosphere – Physical unit: W/m^2 – Uncertainty unit: W/m^2.

Method 1: Cavity radiometer – Principle: Trapping of total downward solar radiation at satellite altitude into devices such as active cavities. Absolute measurement. Applicable in LEO, GEO, or outer-space orbits, at the L1 Lagrange libration point, for instance.

5.4.7 Upward spectral radiance at top of atmosphere

Definition: Upward radiant power measured at the top of the atmosphere per area unit, per solid angle and per wavelength interval. Spectral range 0.2–200 μm. Resolving power $\lambda/\Delta\lambda$ = 1 000. Uncertainty quoted as signal-to-noise ratio.

Method 1: Wide-range spectroscopy – Principle: Measurement of the radiation in the interval 0.2–200 μm emitted by the Earth–atmosphere system towards space. Several spectrometers are needed to cover short wave and long wave. The objective is to monitor climate change by using the spectrum as an absolute "signature". Applicable only in LEO.

5.4.8 Upward long-wave irradiance at top of atmosphere

Definition: Flux density of terrestrial radiation emitted to space by the Earth's surface, atmosphere and clouds at the top of the atmosphere – Physical unit: W/m^2 – Uncertainty unit: W/m^2.

Method 1: Broadband radiometry – Principle: Measurement of the radiation in the interval 4–200 μm emitted by the Earth–atmosphere system towards space by means of detectors with as flat a response in the interval as possible. Applicable in both LEO and GEO.

5.4.9 Upward short-wave irradiance at top of atmosphere

Definition: Flux density of terrestrial radiation reflected to space by the Earth's surface, atmosphere and clouds at the top of the atmosphere – Physical unit: W/m^2 – Uncertainty unit: W/m^2.

Method 1: Broadband radiometry – Principle: Measurement of the radiation in the interval 0.2–4.0 μm reflected by the Earth–atmosphere system towards space by means of detectors with as flat response in the interval as possible. Information on bi-directional reflectance and modelling are required in order to convert radiance into irradiance. Applicable in both LEO and GEO.

Method 2: SW radiometry – Principle: Measurement of radiation reflected by the Earth–atmosphere system in several narrow VIS and NIR bands. Angular distribution models (bi-directional reflectance) and spectral transformations are required to convert the narrowband radiances into SW irradiance.

5.4.10 Short-wave cloud reflectance

Definition: Reflectance of the solar radiation from clouds – Physical unit: % – Uncertainty unit: %.

Method 1: SW radiometry – Principle: Scattered solar radiation in several channels of VIS, NIR and SWIR. Multi-viewing geometry useful. Applicable in both LEO and GEO.

5.4.11 Downward long-wave irradiance at Earth's surface

Definition: Flux density of LW radiation from Sun, atmosphere and clouds to the Earth's surface – Physical unit: W/m^2 – Uncertainty unit: W/m^2.

Method 1: From IR/MW sounding – Principle: High-level product derived mostly from atmospheric temperature and water-vapour profiles. Contributions also from cloud cover and cloud-base height. Atmospheric modelling necessary. Applicable in both LEO and GEO.

5.4.12 Downward short-wave irradiance at Earth's surface

Definition: Flux density of SW radiation from Sun, atmosphere and clouds to the Earth's surface – Physical unit: W/m^2 – Uncertainty unit: W/m^2. In applications like solar energy the unit used is MJ m^{-2}.

Method 1 : SW radiometry – Principle : High-level product derived from observation of scattered solar radiation in several narrowband (and broadband) channels of VIS, NIR and SWIR to estimate attenuation from clouds and aerosol. Multiple viewing and multi-polarization help. Applicable in both LEO and GEO. It is noteworthy that downward SW irradiance at the surface and the reflected broadband irradiance at the TOA are closely coupled, which helps retrieval.

5.4.13 Earth's surface albedo

Definition: Hemispherically integrated reflectance of the Earth's surface in the range 0.4–0.7 μm (or other specific SW ranges) – Physical unit: % – Uncertainty unit: %.

Method 1: Multi-view SW radiometry – Principle: High-level product after measuring scattered solar radiation in several channels of VIS under several viewing angles and solar angles to estimate anisotropy effects and improve radiative flux computations. Channels for atmospheric corrections also included. Applicable only in LEO and GEO.

Method 2: VIS radiometry – Principle: Measurement of scattered solar radiation in several channels of VIS, including those for atmospheric corrections. Anisotropy effects for hemispheric integration computed by modelling. Applicable in both LEO and GEO.

5.4.14 Earth's surface short-wave bi-directional reflectance

Definition: Reflectance of the Earth's surface as a function of the viewing angle and the illumination conditions in the range 0.4–0.7 μm (or other specific SW ranges) – Physical unit: % – Uncertainty unit: %.

Method 1: SW radiometry – Principle: Scattered solar radiation in several channels of VIS, NIR and SWIR observed under several viewing angles and solar angles to estimate anisotropy effects and improve radiative flux computations. Channels for atmospheric corrections also included. Applicable only in LEO.

5.4.15 Upward long-wave irradiance at Earth's surface

Definition: Flux density of long-wave radiation emerging from the Earth's surface – Physical unit: W/m^2 – Uncertainty unit: W/m^2.

Method 1: Broadband radiometry – Principle: Measurement of the radiation in the interval 4–200 μm emitted by the Earth's surface towards the atmosphere and ultimately to space. Detectors are needed, with as flat response in the interval as possible. Atmospheric corrections, mostly for water vapour and clouds, are necessary. Applicable in both LEO and GEO.

5.4.16 Long-wave Earth-surface emissivity

Definition: Emissivity of the Earth's surface in the thermal IR, function of the wavelength – Physical unit: % – Uncertainty unit: %.

Method 1: IR radiometry – Principle: Emitted radiation in several relatively narrowband IR window channels, to determine equivalent black-body temperatures at several wavelengths. Applicable in both LEO and GEO.

Method 2: IR spectroscopy – Principle: Multiple determination of equivalent black-body temperatures in highest number of narrow windows through the IR spectrum. Applicable in both LEO and GEO.

5.4.17 Photosynthetically active radiation

Definition: Flux density of downward photons of wavelength 0.4–0.7 μm at surface – Physical unit: μ einstein $\cdot$ m^{-2} s^{-1} (1 einstein = $6 \cdot 10^{23}$ photons); most frequently used: W/m^2 – Uncertainty unit: W/m^2.

Method 1: VIS radiometry – Principle: High-level product similar to "downwelling short-wave irradiance at Earth surface" except that it refers to the interval 0.4–0.7 μm used by vegetation for photosynthesis. Applicable in both LEO and GEO.

5.4.18 Fraction of absorbed photosynthetically active radiation

Definition: Fraction of photosynthetically active radiation that is absorbed by vegetation (land or marine) for photosynthesis processes (generally around the "red") – Physical unit: % – Uncertainty unit: %.

Method 1: VIS radiometry – Principle: Computed from the observed photosynthetically active radiation and one measure in the "red" region (~670 nm). Applicable in both LEO and GEO.

5.5 OCEAN AND SEA ICE

This theme comprises variables that characterize the ocean surface, including waves and sea ice. The variables observable from space are listed in Table 5.4.

Many variables have not been considered: underwater profiles of temperature and salinity (impossible to measure from space), currents (derivable from ocean topography as for the geostrophic component, otherwise impossible or too inaccurate), iceberg extension or height (special case of ice cover and thickness), and ice drift (product of multi-temporal analysis).

Table 5.4. Geophysical variables considered under the theme "Ocean and sea ice"

Ocean chlorophyll concentration	Sea-surface temperature	Dominant wave direction	Sea-ice type
Colour dissolved organic matter	Sea-surface salinity	Dominant wave period	Ice-surface temperature
Ocean suspended sediments concentration	Ocean dynamic topography	Wave directional-energy frequency spectrum	Ice motion/drift
Ocean diffuse attenuation coefficient	Coastal sea level (tide)	Sea-ice cover/ concentration	
Oil-spill cover	Significant wave height	Sea-ice thickness	

5.5.1 Ocean chlorophyll concentration

Definition: Indicator of living phytoplankton biomass, extracted from ocean-colour observation. Required in both open ocean and coastal zone – Physical unit: mg/m^3 – Uncertainty unit: mg/m^3 at a specific concentration (1 mg/m^3, for example).

Method 1: VIS radiometry – Principle: Measurement of reflected solar radiation in several channels (most significant: 442.5 nm, 490 nm, 560 nm, 665 nm, 681.25 nm). Spectral resolution of the order of 2%. Applicable in both LEO and GEO.

5.5.2 Colour dissolved organic matter

Definition: Former name: "Yellow substance absorbance". Variable extracted from ocean-colour observation. Indicative of biomass undergoing decomposition processes. Required in both open ocean and coastal zone – Physical unit: m^{-1} – Uncertainty unit: m^{-1} at a specific concentration (such as 1 m^{-1}).

Method 1: VIS radiometry – Principle: Measurement of reflected solar radiation in several channels (most significant: 412.5 nm). Spectral resolution of the order of 2%. Applicable in both LEO and GEO.

5.5.3 Ocean suspended sediments concentration

Definition: Variable extracted from ocean-colour observation. Indicative of river outflow, re-suspension or pollution of other-than-biological origin. Required in both open ocean and coastal zone – Physical unit: g/m^3 – Uncertainty unit: g/m^3 at a specific concentration (such as 2 g/m^3).

Method 1: VIS radiometry – Principle: Measurement of reflected solar radiation in several channels (most significant: 510 nm, 560 nm, 620 nm). Spectral resolution of the order of 2%. Applicable in both LEO and GEO.

5.5.4 Ocean diffuse attenuation coefficient

Definition: Former name: "Water clarity". Indicator of water turbidity and vertical processes in the ocean, extracted from ocean-colour observation. Required in both open ocean and coastal zone – Physical unit: m^{-1} – Uncertainty unit: m^{-1}.

Method 1: VIS radiometry – Principle: Measurement of reflected solar radiation in several channels of the range 400–700 nm. Spectral resolution of the order of 2%. Applicable in both LEO and GEO.

5.5.5 Oil-spill cover

Definition: The fraction of an ocean area polluted by hydrocarbons released from human activities (for example, ships, pipelines), accidentally or deliberately. Oil spills are impacting on ocean-atmosphere exchanges. Required in both open ocean and coastal zone – Physical unit: % – Uncertainty unit: %.

Method 1: VIS/NIR radiometry – Principle: Measurement of reflected solar radiation in several channels of the range 400–1 000 nm. Spectral resolution of the order of 2%. Applicable in both LEO and GEO.

Method 2: SW polarimetry – Principle: Scattered solar radiation in several narrowband channels of VIS, NIR and SWIR, some with dual polarization. Applicable only in LEO.

Method 3: High-resolution optical imagery – Principle: Reflected solar radiation in VIS/NIR/SWIR observed in several discrete channels of relatively narrow bandwidths (1%–5%). Applicable only in LEO.

Method 4: SAR imagery – Principle: Backscattered MW radiation at frequencies of 1.3, 5 or 11 GHz collected by SAR. Polarimetric capability is useful. Applicable only in LEO.

5.5.6 Sea-surface temperature

Definition: Temperature of the seawater at surface. The "depth" temperature typically refers to measurements from drifting (~0.2 m) and moored (~1 m) buoys. The "skin" represents the temperature within the conductive diffusion-dominated sub-layer at ~10–20 μm (the layer to which IR radiation is sensitive). The "sub-skin" represents the temperature at the base of the conductive laminar sub-layer of the ocean surface, typically at ~1 mm (the layer to which MW radiation is sensitive). – Physical unit: K – Uncertainty unit : K.

Method 1: IR radiometry – Principle: Derived from IR imagery, typically using several "window" bands, all sensitive to SST and near-surface atmosphere, but in different ways (so-called differential absorption technique). Applicable in both LEO and GEO.

Method 2: IR spectroscopy – Principle: Derived from a large number of very narrow channels through the IR spectrum, associated with other channels providing information needed for atmospheric corrections. Applicable in both LEO and GEO.

Method 3: MW radiometry – Principle: Emitted and scattered MW radiation in atmospheric windows at low to medium frequencies (for example, 5, 10 GHz). More polarizations are needed, to correct for roughness effects. Applicable only in LEO.

5.5.7 **Sea-surface salinity**

Definition: Salinity of seawater in the surface layer, which is the layer affected by turbulence associated with wind stress, waves and diurnal solar heating cycle. (The layer is a few metres deep but a microwave observation would be representative of the upper ~1 m). In the open ocean the correct term should be "halinity" in order to make reference to the most common anion, chlorine – Physical unit: unitless, expressed on the Practical Salinity Scale (PSS-78), close to 1‰, or 1 g of salt per 1 litre of solution – Uncertainty unit: unitless.

Method 1: MW radiometry – Principle: Emitted and scattered MW radiation at low frequencies (such as 1.4 GHz). More polarizations are needed, to correct for roughness effects. More channels are desirable, to correct for temperature. Applicable only in LEO.

5.5.8 **Ocean dynamic topography**

Definition: Deviation of sea level from the geoid caused by ocean currents (after corrections for tides and atmospheric pressure effects) – Physical unit: cm – Uncertainty unit: cm.

Method 1: Radar altimetry – Principle: Backscattered radiation from sea surface by medium-frequency radar (dual-frequency preferred, 13 and 3 or 5 GHz). Associated with two or three channels of passive MW radiometry (23 and 37 and/or 19 GHz) needed for tropospheric path correction from water vapour and ionosphere-induced rotation. Ocean topography is extracted by filtering the fluctuation of wave heights out of the satellite-to-surface measured range. Applicable only in LEO.

5.5.9 **Coastal sea level (tide)**

Definition: Deviation of sea level from local references in coastal zones, caused by local currents and tides (astronomical and wind-induced) – Physical unit: cm – Uncertainty unit: cm.

Method 1: Radar altimetry – Principle: Backscattered radiation from sea surface by medium-frequency radar (dual-frequency preferred, 13 and 3 or 5 GHz). Associated with two or three channels of passive MW radiometry (23 and 37 and/or 19 GHz) needed for tropospheric path correction from water vapour and ionosphere-induced rotation. Sea level is extracted by filtering the fluctuation of wave heights out of the satellite-to-surface measured range. Applicable only in LEO.

5.5.10 **Significant wave height**

Definition: Average amplitude of the highest 30 of 100 waves – Physical unit: m – Uncertainty unit: m.

Method 1: Radar altimetry – Principle: Backscattered radiation from sea surface by medium-frequency radar (dual-frequency preferred, 13 and 3 or 5 GHz). Wave height is linked to the statistical dispersion of the radar-measured ranges. Applicable only in LEO.

Method 2: From SAR spectra – Principle: From spectral analysis of SAR images at frequencies of 1.3 or 5 GHz by processing spectrum power, wavelength and direction with the help of boundary conditions. Applicable only in LEO.

5.5.11 **Dominant wave direction**

Definition: One feature of the ocean wave spectrum. It is the direction of the most energetic wave in the spectrum – Physical unit: degrees – Uncertainty unit: degrees.

Method 1: From SAR spectra – Principle: From spectral analysis of SAR images at frequencies of 1.3, 5 or 11 GHz. Applicable only in LEO.

5.5.12 **Dominant wave period**

Definition: One feature of the ocean wave spectrum. It is the period of the most energetic wave in the spectrum – Physical unit: s – Uncertainty unit: s.

Method 1: From SAR spectra – Principle: From spectral analysis of SAR images at frequencies of 1.3, 5 or 11 GHz. Applicable only in LEO.

5.5.13 **Wave directional-energy frequency spectrum**

Definition: 2D variable colloquially referred to as "wave spectrum". Describes the wave energy travelling in each direction and frequency band (such as 24 distinct azimuth sectors each 15° wide, and 25 frequency bands) – Physical unit: $m^2 \cdot Hz^{-1} \cdot rad^{-1}$ – Uncertainty unit: $m^2 \cdot Hz^{-1} \cdot rad^{-1}$.

Method 1: From SAR spectra – Principle: From spectral analysis of SAR images at frequencies of 1.3, 5 or 11 GHz. Applicable only in LEO.

5.5.14 **Sea-ice cover/concentration**

Definition: The fraction of an ocean area where ice is detected – Physical unit: % – Uncertainty unit: %.

Method 1: VIS/IR radiometry – Principle: Reflected solar radiation in VIS/NIR/SWIR or emitted radiation in MWIR/IR observed in a few discrete channels of relatively large bandwidths (5%–10%). The fractional cover refers to the number of pixels classified as ice in a given pixel array. Applicable in both LEO and GEO.

Method 2: MW radiometry – Principle: Emitted and scattered MW radiation in atmospheric windows at medium-high frequencies (such as 37, 90 GHz). More polarizations are needed (signal from sea is strongly polarized). The fractional cover refers to the number of pixels classified as ice in a given pixel array. Applicable only in LEO.

Method 3: High-resolution optical imagery – Principle: Reflected solar radiation in VIS/NIR/SWIR observed in several discrete channels. High-resolution is prioritized at the expense of the observing cycle. Applicable only in LEO.

Method 4: SAR imagery – Principle: Backscattered MW radiation at frequencies of 1.3, 5 or 11 GHz collected by SAR. The fractional cover refers to the number of pixels classified as ice in a given array. Applicable only in LEO.

5.5.15 **Sea-ice thickness**

Definition: Thickness of the ice sheet. It is related to sea-ice elevation and ice density – Physical unit: cm – Uncertainty unit: cm.

Method 1: Radar altimetry – Principle: Backscattered radiation from sea surface by medium-frequency radar (dual-frequency preferred, 13 and 3 or 5 GHz). Associated with two-channel passive MW radiometry (23 and 37 GHz) needed for tropospheric path correction from water vapour. Applicable only in LEO.

Method 2: Lidar altimetry – Principle: Backscattered VIS/NIR radiation by lidar. Two wavelengths preferred, such as 532 and 1 064 nm. Applicable only in LEO.

Method 3: SAR interferometry – Principle: Backscattered MW radiation at frequencies of 1.3, 5 or 11 GHz collected by SAR. Height of observed surface determined by interferometry between images from more passes. Applicable only in LEO.

Method 4: VIS/IR radiometry – Principle: Reflected solar radiation in VIS/NIR/SWIR and emitted radiation in the IR spectrum observed in a few discrete channels of relatively large bandwidths provide estimates of surface albedo and skin temperature. These are used to solve a surface energy budget ice model for ice thickness.

Method 5: Passive L-band MW – Principle: Surface L-band (1.4 GHz) emissivity of sea ice, which is a function of partial transmissivity of the emissivity of the underlying seawater, the thickness of the sea ice and the salinity of the sea ice, taking into consideration snow depth on top of the sea ice. Independent ice-surface temperature measurement enhances retrieval. Multiple polarizations preferred. Applicable only in LEO.

5.5.16 **Sea-ice type**

Definition: Comprehensive properties (age, roughness, density, etc.) of the observed sea ice. The list of types of interest is predetermined – Uncertainty expressed as number of discriminated types (classes).

Method 1: Radar scatterometry – Principle: Backscattered radiation by medium-frequency radar scatterometry (around 5 or 11 GHz). Calibrated radar reflectivity depends on roughness and surface conductivity (linked to age). Applicable only in LEO.

Method 2: MW radiometry – Principle: Emitted and scattered MW radiation in atmospheric windows at medium frequencies (such as 19, 37 GHz). Three Stokes parameters (in other words at least four polarizations) desirable. Applicable only in LEO.

Method 3: SAR imagery – Principle: Backscattered MW radiation at frequencies of 1.3, 5 or 11 GHz collected by SAR. Applicable only in LEO.

5.5.17 **Ice-surface temperature**

Definition: The radiative, or "skin" temperature of the sea-ice surface. The surface may be bare ice or snow-covered – Physical unit: K – Uncertainty unit: K.

Method 1: IR radiometry – Principle: Derived from IR imagery in multiple channels including "windows" and others (in water-vapour absorption bands) as necessary to evaluate atmospheric attenuation. Applicable in both LEO and GEO.

Method 2: MW radiometry – Principle: Derived from low-frequency MW channels including "windows" and other sensitive channels as necessary to evaluate atmospheric attenuation. Applicable in both LEO and GEO.

5.5.18 Ice motion/drift

Definition: The movement of the sea-ice cover – Physical unit: m/s and degrees or m/s for U/V components – Uncertainty unit: m/s and degrees.

Method 1: VIS/IR radiometry – Principle: Emitted radiation in IR observed in a few discrete channels of relatively large bandwidths. Ice motion refers to speed and direction of sea-ice drift. Applicable in both LEO and GEO.

Method 2: MW radiometry – Principle: Emitted and scattered MW radiation in atmospheric windows at medium-high frequencies (such as 37, 90 GHz). Ice motion refers to speed and direction of sea-ice drift. Applicable only in LEO.

Method 3: SAR imagery – Principle: Backscattered MW radiation at frequencies of 1.3, 5 or 11 GHz collected by SAR. Ice motion refers to speed and direction of sea-ice drift. Applicable only in LEO.

5.6 LAND SURFACE (INCLUDING SNOW)

This theme comprises variables that characterize the land surface, including vegetation, fire, glaciers and snow. The variables observable from space are listed in Table 5.5.

A few variables have not been considered, such as groundwater (considered covered by soil moisture, snow, glaciers; and land cover); river discharge (products are of too high a level); subsoil temperature profile (impossible from space); snow and lake surface temperature; permafrost (specific cases of surface temperature observation); coastlines (too obvious); biomass (too generic).

Table 5.5. Geophysical variables considered under the theme "Land surface (including snow)"

Land surface temperature	Leaf area index	Snow status (wet/dry)	Land surface topography
Soil moisture at surface	Normalized difference vegetation index	Snow cover	Glacier cover
Soil moisture (in the roots region)	Fire fractional cover	Snow water equivalent	Glacier topography
Fraction of vegetated land	Fire temperature	Soil type	
Vegetation type	Fire radiative power	Land cover	

5.6.1 Land surface temperature

Definition: Temperature of the apparent surface of land (bare soil or vegetation) – Physical unit: K – Uncertainty unit: K.

Method 1: IR radiometry – Principle: Derived from IR imagery in multiple channels including "windows" and others as needed to evaluate emissivity and atmospheric attenuation (from water vapour). Dual-view reduces the uncertainty of atmospheric correction. Applicable in both LEO and GEO.

Method 2: IR spectroscopy – Principle: Derived from a high number of very narrow window channels through the IR spectrum, associated with other channels providing all the information needed for atmospheric corrections. This enables emissivity to be estimated. Applicable in both LEO and GEO.

Method 3: MW radiometry – Principle: Emitted and scattered MW radiation in atmospheric windows at low to medium frequencies (such as 5, 10, 36 GHz). More polarizations are needed to correct for wetness effects. Applicable only in LEO.

5.6.2 Soil moisture at surface

Definition: Fractional content of water in a volume of wet soil. Surface layer (upper few centimetres) – Physical unit: m^3/m^3 – Uncertainty unit: m^3/m^3.

Method 1: MW radiometry – Principle: Emitted MW radiation at low frequencies (1.4 and 2.7 GHz, for example). Multiple polarizations needed, to correct for roughness effects. Multiple channels desirable, to correct for temperature. Higher frequencies (5, 10 GHz) also useful, particularly for bare soil. Applicable only in LEO.

Method 2: Radar scatterometry – Principle: Backscattered MW radiation at relatively low frequencies (such as 5 GHz). The multiple viewing angle capability is exploited to correct for roughness. Applicable only in LEO.

Method 3: SAR imagery – Principle: Backscattered MW radiation at frequencies of 1.3, 5 or 11 GHz collected by SAR. Applicable only in LEO.

Method 4: VIS/IR radiometry – Principle: Several proxies are possible. Examples: damping of reflectivity from VIS/NIR to SWIR; from apparent thermal inertia derived by measuring the delay in land temperature rising in response to incoming solar radiation (valid for bare soil). Applicable in both LEO and GEO.

5.6.3 Soil moisture (in the roots region)

Definition: Subsoil 3D field of the fractional content of water in a volume of wet soil. Required from surface down to ~3 m – Physical unit: m^3/m^3 – Uncertainty unit: m^3/m^3.

Method 1: L-band MW radiometry – Principle: Emitted MW radiation at low frequencies (such as 1.4 GHz). More polarizations are needed, to correct for roughness effects. Applicable only in LEO.

Method 2: L-band SAR imagery – Principle: Backscattered MW radiation at low frequency (typically 1.3 GHz) collected by SAR. P band (~400 MHz) and S band (~2.7 GHz) are also possible. Applicable only in LEO.

5.6.4 Fraction of vegetated land

Definition: The fraction of a land area where vegetation is present – Physical unit: % – Uncertainty unit: %.

Method 1: High-resolution optical imagery – Principle: Reflected solar radiation in VIS/NIR/SWIR observed in several discrete channels of relatively narrow bandwidths (1%–5%). Hyperspectral (several hundred channels) possible. Applicable in LEO and potentially in GEO.

Method 2: SAR imagery – Principle: Backscattered MW radiation at frequencies of 1.3, 5 or 11 GHz collected by SAR. Applicable only in LEO.

5.6.5 Vegetation type

Definition: Observed vegetal species or families. The list of types of interest is predetermined – Uncertainty is expressed as number of identified types (classes).

Method 1: High-resolution optical imagery – Principle: Reflected solar radiation in VIS/NIR/SWIR observed in several discrete channels of relatively narrow bandwidths (1%–5%). Hyperspectral (several hundred channels) possible. Applicable in LEO and potentially in GEO.

Method 2: SAR imagery – Principle: Backscattered MW radiation at frequencies of 1.3, 5 or 11 GHz collected by SAR. Applicable only in LEO.

5.6.6 Leaf area index

Definition: One half of the total projected green leaf fractional area in the plant canopy within a given area. Representative of total biomass and health of vegetation – Physical unit: % – Uncertainty unit: %.

Method 1: SW radiometry – Principle: Scattered solar radiation through VIS/NIR and deeply into SWIR (up to 2.4 μm, for example). Several channels needed, relatively narrow (2%–3%). Applicable in both LEO and GEO.

Method 2: Radar scatterometry – Principle: Backscattered radiation by medium-frequency radar scatterometry (about 5 or 11 GHz). Calibrated radar reflectivity depends on surface conductivity (linked to biomass). Applicable only in LEO.

Method 3: High-resolution optical imagery – Principle: Reflected solar radiation in VIS/NIR/SWIR observed in several discrete channels of relatively narrow bandwidths (1%–5%). Hyperspectral (several hundred channels) possible. Applicable in LEO and potentially in GEO.

5.6.7 Normalized difference vegetation index

Definition: Difference between maximum (in NIR) and minimum (around the "red") vegetation reflectance, normalized to the summation. Representative of total biomass, supportive for computing leaf area index if not directly measured – Physical unit: % – Uncertainty unit: %.

Method 1: VIS/NIR radiometry – Principle: Scattered solar radiation in VIS ("red", minimum reflectance from vegetation) and NIR (typically, 865 nm, high reflectance). Applicable in both LEO and GEO.

Method 2: High-resolution optical imagery – Principle: Scattered solar radiation in VIS ("red", minimum reflectance from vegetation) and NIR (typically, 865 nm, high reflectance). Applicable in LEO and potentially in GEO.

5.6.8 Fire fractional cover

Definition: The fraction of a land area where fire is present – Physical unit: % – Uncertainty unit: %.

Method 1: VIS/NIR radiometry – Principle: Reflected solar radiation in VIS/NIR/SWIR or emitted radiation in MWIR/IR observed in a few discrete channels of relatively large bandwidths (5%–10%). The fractional cover refers to the number of pixels classified as fire in a given pixel array. Applicable in both LEO and GEO.

Method 2: High-resolution optical imagery – Principle: Reflected solar radiation in VIS/NIR/SWIR observed in several discrete channels. Useful post factum for damage inventory. High resolution is prioritized at the expense of the observing cycle. Applicable only in LEO.

Method 3: SAR imagery – Principle: Backscattered MW radiation at frequencies of 1.3, 5 or 11 GHz collected by SAR. The fractional cover refers to the number of pixels classified as fire in a given array. Useful post factum for damage inventory. Applicable only in LEO.

5.6.9 **Fire temperature**

Definition: Temperature of the fire occurring within an area – Physical unit: K – Uncertainty unit: K.

Method 1: IR radiometry – Principle: Derived from IR imagery in a number of window channels. MWIR (3.7 μm) most sensitive. Applicable in both LEO and GEO.

5.6.10 **Fire radiative power**

Definition: Power radiated by the fire occurring within an area – Physical unit: $kW \cdot m^{-2}$ – Uncertainty unit: $kW \cdot m^{-2}$.

Method 1: IR radiometry – Principle: Derived from IR imagery in a number of window channels. MWIR (3.7 μm) most sensitive. Applicable in both LEO and GEO.

5.6.11 **Snow status (wet/dry)**

Definition: Binary product (dry or melting/thawing) expressing the presence of liquid water in a snow layer – Uncertainty expressed as HR and FAR when classifying the status as either wet or dry.

Method 1: MW radiometry – Principle: Emitted and scattered MW radiation in atmospheric windows at medium-high frequencies (such as 37, 90 GHz). More polarizations are needed. Since wet snow can be confused with underlying soil, preventive snow detection (mask) is necessary. Applicable only in LEO.

Method 2: SAR imagery – Principle: Backscattered MW radiation collected by SAR at relatively high frequencies, such as ~10 GHz (X band), possibly ~19 GHz (K band), since dry snow tends to be transparent to SAR. More useful for change detection during thawing and freezing cycles. Applicable only in LEO.

5.6.12 **Snow cover**

Definition: The fraction of a given area which is covered by snow – Physical unit: % – Uncertainty unit: %.

Method 1: VIS/IR radiometry – Principle: Reflected solar radiation in VIS/NIR/SWIR or emitted radiation in MWIR/IR observed in a few discrete channels of relatively large bandwidths (5%–10%). The fractional cover refers to the number of pixels classified as snow in a given pixel array. Alternatively, retrieval can be carried out at pixel level by exploiting the "defect" of brightness due to mixed snow/no-snow in the pixel ("effective snow cover"). Applicable in both LEO and GEO.

Method 2: MW radiometry – Principle: Emitted and scattered MW radiation in atmospheric windows at medium-high frequencies (such as 37, 90 GHz). More polarizations are needed. The fractional cover refers to the number of pixels classified as snow in a given pixel array. Snow surface status (dry or wet) is also determined. Applicable only in LEO.

Method 3: High-resolution optical imagery – Principle: Reflected solar radiation in VIS/NIR/SWIR observed in several discrete channels. High-resolution is prioritized at the expense of the observing cycle. Applicable in LEO and potentially in GEO.

5.6.13 **Snow water equivalent**

Definition: Vertical depth of the water that would be obtained by melting a snow layer. The snow depth may be inferred by exploiting auxiliary information on the density of the snow layer – Physical unit: mm – Uncertainty unit: mm.

Method 1: MW radiometry – Principle: Emitted and scattered MW radiation in atmospheric windows at medium-high frequencies (such as 37, 90 GHz), preferred because at low frequency dry snow is transparent. More polarizations are needed. Applicable only in LEO.

Method 2: Radar scatterometry – Principle: Backscattered MW radiation at low-medium frequencies (5, 13 GHz). Higher frequency preferred over dry snow. The multiple viewing angle capability is exploited to correct for roughness. Applicable only in LEO.

Method 3: SAR imagery – Principle: Backscattered MW radiation collected by SAR at relatively high frequencies (dry snow is transparent to SAR). An optimal frequency would be ~19 GHz (K_u band). Lower frequencies can be used for monitoring changes by interferometry. Applicable only in LEO.

5.6.14 **Soil type**

Definition: Observed soil composition or structure (acid, alkaline, rough, and the like). The list of types of interest is predetermined – Uncertainty is expressed as number of discriminated types (classes).

Method 1: High-resolution optical imagery – Principle: Reflected solar radiation in VIS/NIR/SWIR observed in several discrete channels of relatively narrow bandwidths (1%–5%). Hyperspectral (several hundred channels) possible. Applicable in LEO and potentially in GEO.

Method 2: SAR imagery – Principle: Backscattered MW radiation at frequencies of 1.3, 5 or 11 GHz collected by SAR. Applicable only in LEO.

5.6.15 **Land cover**

Definition: Observed land utilization (urban, cultivated, desertic, etc.). The list of types of interest is predetermined – Uncertainty expressed as the number of identified types (classes).

Method 1: High-resolution optical imagery – Principle: Reflected solar radiation in VIS/NIR/SWIR observed in several discrete channels of relatively narrow bandwidths (1%–5%). Hyperspectral (several hundred channels) possible. Applicable in LEO and potentially in GEO.

Method 2: SAR imagery – Principle: Backscattered MW radiation at frequencies of 1.3, 5 or 11 GHz collected by SAR. Applicable only in LEO.

5.6.16 **Land surface topography**

Definition: Map of land surface heights – Physical unit: m – Uncertainty unit: m.

Method 1: High-resolution VIS stereoscopy – Principle: Reflected solar radiation in VIS observed in one or more channels of relatively narrow bandwidths (1%–5%) from at least two viewing directions, generally from successive orbits, so as to implement stereoscopy. Applicable only in LEO.

Method 2: SAR interferometry – Principle: Backscattered MW radiation at frequencies of 1.3, 5 or 11 GHz collected by SAR. Interferometry from successive orbital passes. Applicable only in LEO.

Method 3: Radar altimetry – Principle: Backscattered radiation from land surface by medium-frequency radar (dual-frequency preferred, 13 and 3 or 5 GHz). Associated with two or three channels of passive MW radiometry (23 and 37 and/or 19 GHz) needed for tropospheric path correction from water vapour and ionosphere-induced rotation. Along-track SAR processing is needed for acceptable resolution. Only nadir view. Applicable only in LEO.

Method 4: Lidar altimetry – Principle: Backscattered VIS/NIR radiation by lidar. Two wavelengths preferred, such as 532 and 1 064 nm. Only nadir view. Applicable only in LEO.

5.6.17 **Glacier cover**

Definition: The fraction of a land area covered by permanent ice – Physical unit: % – Uncertainty unit: %.

Method 1: High-resolution VIS stereoscopy – Principle: Reflected solar radiation in VIS/NIR/SWIR observed in several discrete channels of relatively narrow bandwidths (1%–5%). Applicable in LEO and potentially in GEO.

Method 2: SAR imagery – Principle: Backscattered MW radiation at frequencies of 1.3, 5 or 11 GHz collected by SAR. Interferometry used to detect changes. Applicable only in LEO.

5.6.18 **Glacier topography**

Definition: Map of the height of the glacier surface – Physical unit: cm – Uncertainty unit: cm.

Method 1: SAR interferometry – Principle: Backscattered MW radiation at frequencies of 1.3, 5 or 11 GHz collected by SAR. Interferometry from successive orbital passes. Applicable only in LEO.

5.7 **SOLID EARTH**

This theme comprises variables that characterize the solid Earth (space geodesy and Earth interior). The variables observable from space are listed in Table 5.6.

Table 5.6. Geophysical variables considered under the theme "Solid Earth"

Geoid	Crustal plates positioning	Crustal motion (horizontal and vertical)	Gravity field	Gravity gradients

5.7.1 **Geoid**

Definition: Equipotential surface which would coincide exactly with the mean ocean surface of the Earth, if the oceans were in equilibrium, at rest, and extended through the continents (such as with very narrow channels) – Physical unit: cm – Uncertainty unit: cm.

Method 1: Radar altimetry – Principle: Backscattered radiation from sea surface by medium-frequency radar (dual-frequency preferred, 13 and 3 or 5 GHz). Associated with two or three channels of passive MW radiometry (23 and 37 and/or 19 GHz) needed for tropospheric path correction from water vapour and ionosphere-induced rotation. Highly stable orbits needed (relatively high altitude, 50°–70° inclination and accurate repeat cycle). Multi-orbital analysis enables transient perturbations to be filtered out of waves, ocean currents and tides. Applicable only in LEO.

Method 2: Gravity-field observation – Principle: Observation of the gravity field at satellite altitude by accelerometers, gradiometers, satellite–satellite tracking (coupled satellites or with GPS satellites). Low orbits are used, changing during mission time. Applicable only in LEO.

5.7.2 Crustal plates positioning

Definition: Basis for monitoring the evolution of the lithosphere dynamics – Physical unit: cm – Uncertainty unit: cm.

Method 1: Laser ranging – Principle: Accurate measurement of the satellite–ground distance by pointing the satellite using a surface-based laser that collects the light reflected by cube-corner mirrors covering the surface of the satellite. A worldwide network can provide both precision orbitography and the position of the crustal plates supporting the laser ranging stations. Applicable only in LEO.

Method 2: GPS receiver – Principle: Statistical analysis of the position of a surface-based GPS receiver localized by the constellations of navigation satellites (GPS, GLONASS, Compass, Galileo). Applicable only in LEO.

5.7.3 Crustal motion (horizontal and vertical)

Definition: Changes over time of the position and height of the Earth's plates. Indicative of the lithosphere dynamics, thus useful for earthquake prediction – Physical unit: mm/y – Uncertainty unit: mm/y.

Method 1: Laser ranging – Principle: Analysis of changes in crustal plate positioning, accurately measured by satellite-ground distance through a surface-based laser that collects the light reflected by cube-corner mirrors covering the surface of the satellite. A worldwide network of laser-ranging stations enables this analysis to be performed. Applicable only in LEO.

Method 2: GPS receiver – Principle: Analysis of changes in crustal plate positioning, accurately measured by surface-based GPS receivers localized by the constellations of navigation satellites (GPS, GLONASS, Compass, Galileo). Applicable only in LEO.

5.7.4 Gravity field

Definition: 3D field, actually measured in situ at orbital height. Indicative of the statics and dynamics of the lithosphere and the mantle – Physical unit: mGal (1 Gal = 0.01 m/s^2, so 1 mGal $\approx 10^{-6}\ g_0$. "Gal" stands for Galileo) – Uncertainty unit: mGal.

Method 1: Gradiometry – Principle: Appropriate network of accelerometers sensitive to anomalies in the gravity field crossed by the satellite during its motion in orbit. Applicable only in LEO.

Method 2: Satellite-to-satellite tracking – Principle: Continuous monitoring of the distance between satellites in coordinated orbits, for example by means of K-band radar or lidar. Applicable only in LEO.

5.7.5 Gravity gradients

Definition: 3D field, actually measured in situ at orbital height. Indicative of fine details of the statics and dynamics of the lithosphere and the mantle – Physical unit: E, Eötvös (1 E = 1 mGal/10 km) – Uncertainty unit: E.

Method 1: Gradiometry – Principle: Appropriate network of accelerometers sensitive to anomalies of the gravity field crossed by the satellite during its motion in orbit. Applicable only in LEO.

Method 2: Satellite-to-satellite tracking – Principle: Continuous monitoring of the distance between satellites in coordinated orbits by means of K-band radar or lidar, for example. Applicable only in LEO.

5.8 ATMOSPHERIC CHEMISTRY

This theme deals with species that impact the ozone cycle, and/or provoke the greenhouse effect and/or affect air quality. The species observable from space and which are so far the subject of explicit requirements are listed in Table 5.7.

Table 5.7. Geophysical variables considered under the theme "Atmospheric chemistry"

O_3	C_2H_2	CFC–11	CH_2O	ClO	CO	COS	HCl	HNO_3	N_2O_5	NO_2	Peroxyacetyl nitrate	SF_6
BrO	C_2H_6	CFC–12	CH_4	$ClONO_2$	CO_2	H_2O	HDO	N_2O	NO	OH	Polar stratospheric cloud occurrence	SO_2

Various space missions address the measurement of atmospheric composition and some are described in the present volume, Chapter 3 (Remote-Sensing Instruments). Under CEOS, the Atmospheric Composition Virtual Constellation (AC-VC) has the goal to collect and deliver data to improve monitoring, assessment, and prediction of changes in the ozone layer, air quality, and climate forcing associated with changes in the environment. This is done through the coordination of existing and future international space assets. Specifically addressed are satellite constellations to measure CO_2 and air quality from GEO.

The CEOS AC-VC webpage will be useful for readers who would like to know more about measuring atmospheric composition from space: http://ceos.org/ourwork/virtual-constellations/acc/.

Note that this chapter appendix includes a description of all variables and their requirements, as well as a link to the OSCAR website, describing how these variables are measured.

5.9 SPACE WEATHER

This theme comprises variables that characterize space weather. The variables relevant to this theme are classified below according to three categories:

(a) Solar processes monitoring (Table 5.8);

(b) Sun–Earth interplanetary space, dominated by the solar wind (Table 5.9);

(c) Earth proximity: the magnetosphere and ionosphere (Table 5.10).

Table 5.8. Satellite observations relevant to solar processes monitoring

Variable	*Details*	*Physical unit*
Solar gamma rays, X-rays, EUV, UV, VIS	Integrated flux density Flux spectrum Flux image	$W \cdot m^{-2}$ $W \cdot m^{-2} \cdot nm^{-1}$ $W \cdot m^{-2} \cdot arcsec^{-2}$
Solar Ca II-K image	K-line of Ca-II (393.4 nm)	$W \cdot m^{-2} \cdot arcsec^{-2}$
Solar H-alpha image	Hydrogen-alpha transition (656.3 nm)	$W \cdot m^{-2} \cdot arcsec^{-2}$
Solar Lyman-alpha image	Hydrogen Lyman-alpha transition (121.6 nm)	$W \cdot m^{-2} \cdot arcsec^{-2}$
Solar Lyman-alpha flux	Hydrogen Lyman-alpha transition (121.6 nm)	$W \cdot m^{-2} \cdot nm^{-1}$
Solar magnetic field	Magnetic field at the solar surface (photosphere)	nT
Solar radio flux spectrum	Radio flux integrated over the solar disk	$W \cdot m^{-2} \cdot Hz^{-1}$
Solar radio flux image	Radio flux received from the solar disk	$W \cdot m^{-2} \cdot Hz^{-1} \cdot arcsec^{-2}$
Solar velocity fields	3D map of plasma velocity in the photosphere	$m \cdot s^{-1} \cdot arcsec^{-2}$
Solar electric field	Map of the electric field in the photosphere	$mV \cdot m^{-1} \cdot arcsec^{-2}$
Solar corona image	Image of the corona surrounding the Sun	$W \cdot m^{-2} \cdot arcsec^{-2}$

Table 5.9. Satellite observations relevant to Sun–Earth interplanetary space and solar wind

Variable	*Details*	*Physical unit*
Electrons, protons, neutrons, alpha-particles	Integrated flux density Differential directional flux Integral directional flux	$particles \cdot m^{-2} \cdot s^{-1}$ $particles \cdot m^{-2} \cdot s^{-1} \cdot sr^{-1} \cdot eV^{-1}$ $particles \cdot m^{-2} \cdot s^{-1} \cdot sr^{-1}$
Heavy ions [2(He) < Z ≤ 26(Fe)]	Angular flux energy and mass spectrum Integral directional flux	$particles \cdot m^{-2} \cdot s^{-1} \cdot sr^{-1}$ $(MeV/nucleon)^{-1}$ $particles \cdot m^{-2} \cdot s^{-1} \cdot sr^{-1}$
Cosmic rays	Neutron flux	$neutron \cdot m^{-2} \cdot s^{-1}$
Gamma rays, X-rays, EUV, UV, VIS, NIR, SWIR	Flux Flux spectrum Sky image	$W \cdot m^{-2}$ $W \cdot m^{-2} \cdot nm^{-1}$ $W \cdot m^{-2} \cdot arcsec^{-2}$
Radio waves	Integrated flux density	$W \cdot m^{-2} \cdot Hz^{-1}$
Heliospheric image	Image of the solar wind environment	$W \cdot m^{-2} \cdot arcsec^{-2}$
Interplanetary magnetic field	Magnetic field in the solar wind	nT
Solar wind density	Density of the solar wind plasma	$particles \cdot cm^{-3}$
Solar wind temperature	Temperature of solar wind plasma	K
Solar wind velocity	Velocity of the solar wind plasma	$km \cdot s^{-1}$

Table 5.10. Satellite observations specific to the magnetosphere and ionosphere

Variable	*Details*	*Physical unit*
Ionospheric plasma velocity	Velocity of bulk plasma or electrons, a function of altitude	km · s^{-1}
Ionospheric scintillation	Random fluctuations of radio waves and refractive index	dimensionless
Ionospheric total electron content	Number of electrons between two points	Total electron content units (TECU)
Electron density	3D distribution of the electron density in the ionosphere	electrons · m^{-3}
Magnetic field	Magnetic field in the Earth environment (magnetosphere)	nT
Electric field	Magnitude and direction of the Earth's electric field	mV · m
Electrostatic charge	Accumulated electric charge on a satellite platform	pA · cm^{-2}
Radiation dose rate	3D field of the dose rate of energetic particles	mSv · h^{-1}

In the following sections, some details are given for a few variables that are relevant to the ionosphere and magnetosphere.

5.9.1 Ionospheric total electron content

Definition: Number of electrons along a path between two points. Observed under different viewing angles so as to generate vertical profiles by tomography. Required in the ionosphere and plasmasphere – Physical unit: electrons/m^2; practical unit: TECU = 10^{16} electrons/m^2 – Uncertainty unit: %.

Method 1: GNSS radio-occultation – Principle: Differential refraction between two frequencies (~1.2 and 1.6 GHz) transmitted by a navigation satellite and received by a LEO satellite during the occultation phase. Path-integrated content observed at changing tangent heights so as to provide vertical profile. Applicable only in LEO.

Method 2: Radar altimetry – Principle: Differential phase delay between signals from dual-frequency radar altimeter (~13 GHz and ~3 or 5 GHz). Phase rotation measurement, primarily needed to correct the altimeter ranging measurement, is also used to infer the column-integrated total electron content. Applicable only in LEO.

Method 3: GPS–LEO signal phase delay – Principle: Differential phase delay between signals from two-frequency GPS transmitters (~1.2 and 1.6 GHz) and a receiver in LEO using GPS for navigation. In principle, any satellite equipped with a GPS navigation system is suitable. The information refers to the topside ionosphere and plasmasphere, namely the layer between the satellite altitude and the GPS altitude (~20 000 km). Applicable only in LEO.

5.9.2 Electron density

Definition: 3D distribution of the electron density. Required in the ionosphere and plasmasphere – Physical unit: electrons/m^3 – Uncertainty unit: %.

Method 1: GNSS radio-occultation – Principle: Differential refraction between two frequencies (~1.2 and 1.6 GHz) transmitted by a navigation satellite and received by a LEO satellite during the occultation phase. Derived by tomography of the total electron content. Applicable only in LEO.

5.9.3 **Magnetic field**

Definition: Magnitude and direction of the Earth's magnetic field. Indicative of the degree of geomagnetic disturbance within the magnetosphere, and also in the Earth's interior. Required in the magnetosphere – Physical unit: nT (1 tesla = 10^4 gauss) – Uncertainty: nT.

Method 1: Magnetometry – Principle: more magnetometers for in situ measurement along the orbit as the satellite moves. Applicable in LEO, in GEO and in highly elliptical orbits.

5.9.4 **Electric field**

Definition: Magnitude and direction of the Earth's electric field. Required in the ionosphere – Physical unit: $mV \cdot m^{-1}$ – Uncertainty: $mV \cdot m^{-1}$.

Method 1: Ion drift – Principle: Measurement of magnitude and direction of the incoming ion flux. The electric field is derived from the relationship between electric field, measured ion drift velocity and measured magnetic field strength. In situ measurement along the orbit as the satellite moves. Applicable in LEO and in highly elliptical orbits.

ANNEX. USER REQUIREMENTS FOR SPACE-BASED OBSERVATIONS

The OSCAR/Requirements database is the official repository of requirements for observation of physical variables in support of WMO programmes and co-sponsored programmes. These requirements are maintained by the focal points designated for each application area. The database is the foundation of the Rolling Review of Requirements (RRR) process overseen by the Joint Expert Team on Earth Observing System Design and Evolution (JET-EOSDE) of the WMO Commission for Observation, Infrastructure and Information Systems (INFCOM).

The requirements are regularly reviewed by groups of experts nominated by these organizations and programmes. For WMO, this process is conducted by IPET-OSDE and its designated focal points for each of the Application areas.

Themes offer an additional, cross-cutting view on variables and requirements.

This estimate is made for each applicable remote-sensing principle for geophysical variables of the eight following themes:

(1) Basic atmospheric 3D and 2D variables;

(2) Cloud and precipitation variables;

(3) Aerosols and radiation;

(4) Ocean and sea ice;

(5) Land surface (including snow);

(6) Solid Earth;

(7) Atmospheric chemistry;

(8) Space weather.

Requirements are expressed for geophysical variables in terms of six criteria: uncertainty, horizontal resolution, vertical resolution, observing cycle, timeliness and stability (where appropriate). For each of these criteria the table indicates three values determined by experts:

- The “threshold” is the minimum requirement to be met to ensure that data are useful;
- The “goal” is an ideal requirement above which further improvements are not necessary;
- The “breakthrough” is an intermediate level between “threshold” and “goal” which, if achieved, would result in a significant improvement for the targeted application. The breakthrough level may be considered as an optimum, from a cost–benefit point of view, when planning or designing observing systems.

The “uncertainty” characterizes the estimated range of observation errors on the given variable, with a 68% confidence interval (1σ).

1. BASIC ATMOSPHERIC 3D AND 2D VARIABLES

ID	*Variable (link to OSCAR/ Requirements)*	*Definition*
13	Atmospheric temperature	3D field of the atmospheric temperature.
161	Specific humidity	3D field of the specific humidity in the atmosphere. The specific humidity is the ratio between the mass of water vapour and the mass of moist air.
179	Wind (horizontal)	3D field of the horizontal vector component (2D) of the 3D wind vector. The accuracy is meant as vector error, that is, the module of the vector difference between the observed vector and the true vector.
183	Wind vector over the surface (horizontal)	Horizontal vector component (2D) of the 3D wind vector, conventionally measured at 10 m height. The accuracy is meant as vector error, that is, the module of the vector difference between the observed vector and the true vector.
80	Height of the top of the planetary boundary layer (PBL)	Height of the surface separating the PBL from the free atmosphere.
81	Height of the tropopause	Height of the surface separating the troposphere from the stratosphere.
164	Temperature of the tropopause	Atmospheric temperature at the height of the surface separating the troposphere from the stratosphere.

2. CLOUD AND PRECIPITATION VARIABLES

ID	*Variable (link to OSCAR/ Requirements)*	*Definition*
36	Cloud-top temperature	Temperature of the upper surface of the cloud.
35	Cloud-top height	Height of the upper surface of the cloud.
37	Cloud type	Result of cloud type classification – Accuracy expressed as inverse of number of classes, so that smaller figures correspond to better performance.
27	Cloud cover	3D field of fraction of sky filled by clouds.
26	Cloud-base height	Height of the bottom surface of the cloud.
34	Cloud optical depth	Effective depth of a cloud from the viewpoint of radiation propagation. $OD = \exp(-K\,\Delta z)$ where K is the extinction coefficient (km^{-1}) and Δz the vertical path (km) between the base and the top of the cloud.
32	Cloud liquid water	3D field of atmospheric water in the liquid phase (precipitating or not).
33	Cloud liquid water (total column)	2D field of atmospheric water in the liquid phase (precipitating or not), integrated over the total column.
28	Cloud-droplet effective radius	Size distribution of liquid water drops, assimilated to spheres of the same volume. Considered as both a 3D field throughout the troposphere and a 2D field at the top of cloud surface.
29	Cloud ice	3D field of atmospheric water in the solid phase (precipitating or not).
31	Cloud-ice effective radius	Size distribution of ice particles, assimilated to spheres of the same volume. Considered as both a 3D field throughout the troposphere and a 2D field at the top of cloud surface.
67	Freezing-level height in clouds	Height of the atmospheric layer in cloud where liquid-solid states transform into each other.

ID	*Variable (link to OSCAR/ Requirements)*	*Definition*
101	Melting-layer depth in clouds	Depth of the atmospheric layer in cloud where liquid-solid states transform into each other.
127	Precipitation (liquid or solid)	3D field of the vertical flux of precipitating water mass (precipitation intensity).
128	Precipitation intensity at surface (liquid or solid)	Intensity of precipitation reaching the ground – Physical unit: (mm/h) (if solid, mm/h of liquid water after melting) – Accuracy unit: (mm/h). Since accuracy changes with intensity, it is necessary to specify a reference intensity. Assumed rate: 5 mm/h.
1	Accumulated precipitation (over 24 h)	Integration of precipitation rate reaching the ground over several time intervals. The reference requirement refers to integration over 24 h.
302	Lightning detection (Total lightning density)	Total number of detected flashes in the corresponding time interval and the space unit. The space unit (grid box) should be equal to the horizontal resolution and the accumulation time to the observing cycle.
303	Lightning detection (Cloud to ground lightning density)	Number of detected cloud-to-ground flashes in the corresponding time interval and the space unit. The space unit (grid box) should be equal to the horizontal resolution and the accumulation time to the observing cycle.

3. AEROSOL AND RADIATION

ID	*Variable (link to OSCAR/ Requirements)*	*Definition*
6	Aerosol optical depth (AOD)	The AOD is the effective depth of the aerosol column from the viewpoint of radiation propagation: Vertical column integral of spectral aerosol extinction coefficient $AOD = \exp(-K\,\Delta z)$ where K is the extinction coefficient (km^{-1}) and Δz the vertical path (km).
208	Aerosol dust concentration	3D field of mean aerosol particle size, defined as the ratio of the third and second moments of the number size distribution of aerosol particles. Requested in the troposphere (assumed height: 12 km) and as columnar average.
3	Aerosol effective radius	Selection, out of a predefined set of aerosol classes, of the one that best fits an input data set (observed or modeled). The predefined set of aerosol classes includes specification of the particle composition, mixing state, complex refractive index, and shape as a function of particle size. The definition of aerosol type includes specification of all the classes as well as the algorithm used to choose the best fit to the input data.
9	Aerosol type	Selection, out of a predefined set of aerosol classes, of the one that best fits an input data set (observed or modeled). The predefined set of aerosol classes includes specification of the particle composition, mixing state, complex refractive index, and shape as a function of particle size. The definition of aerosol type includes specification of all the classes as well as the algorithm used to choose the best fit to the input data.
173	Aerosol volcanic ash	3D field of mass mixing ratio of volcanic ash.
174	Aerosol volcanic ash total column	2D Field of mass of volcanic ash, integrated over the total column.
51	Downward short-wave (SW) irradiance at TOA	Flux density of the solar radiation at the top of the atmosphere.

ID	*Variable (link to OSCAR/ Requirements)*	*Definition*
168	Upward spectral radiance at TOA	Upward radiant power measured at the top of the atmosphere per area unit, per solid angle and per wavelength interval. Spectral range 0.2–200 μm. Resolving power $\lambda/\Delta\lambda$ = 1000. Accuracy quoted as SNR (signal-to-noise ratio) (actually, SNR^{-1} is used so that smaller figure means better performance, as usual).
169	Upward long-wave (LW) irradiance at TOA	Flux density of terrestrial radiation emitted by the Earth surface and the gases, aerosols and clouds of the atmosphere at the top of the atmosphere.
167	Upward short-wave (SW) irradiance at TOA	Flux density of solar radiation, reflected by the Earth surface and atmosphere, emitted to space at the top of the atmosphere.
141	Short-wave cloud reflectance	Reflectance of the solar radiation from clouds.
52	Downward long-wave (LW) irradiance at Earth surface	Flux density of radiation emitted by the gases, aerosols and clouds of the atmosphere to the Earth surface.
50	Downward short-wave (SW) irradiance at Earth surface	Flux density of the solar radiation at the Earth surface.
54	Earth surface albedo	Hemispherically integrated reflectance of the Earth surface in the range 0.4–0.7.
55	Earth surface short-wave (SW) bi-directional reflectance	Reflectance of the Earth surface as a function of the viewing angle and the illumination angle in the range 0.4–0.7. The distribution of this variable is represented by the Bidirectional Reflectance Distribution Function (BRDF).
170	Upward long-wave (LW) irradiance at Earth surface	Flux density of terrestrial radiation emitted by the Earth surface.
100	Long-wave Earth surface emissivity	Emissivity of the Earth surface in the thermal IR, function of the wavelength.
126	Photosynthetically active radiation (PAR)	Flux of downwelling photons of wavelength 0.4–0.7.
65	Fraction of absorbed photosynthetically active radiation (FAPAR)	Fraction of PAR absorbed by vegetation (land or marine) for photosynthesis processes (generally around the red).

4. OCEAN AND SEA ICE

ID	*Variable (link to OSCAR/ Requirements)*	*Definition*
110	Ocean chlorophyll concentration	Indicator of living phytoplankton biomass, extracted from ocean colour observation. Uncertainty is expressed in mg/m^3 for a given concentration of 1 mg/m^3.
42	Colour dissolved organic matter (CDOM)	Optically measurable component of the dissolved organic matter in water.
117	Ocean suspended sediments concentration	Variable extracted from ocean colour observation. Indicative of river outflow, re-suspension or pollution of other-than-biological origin. Uncertainty expressed in g/m^3 at a specific concentration (for example, 2 g/m^3).

ID	*Variable (link to OSCAR/ Requirements)*	*Definition*
111	Ocean diffuse attenuation coefficient	Indicator of water turbidity and vertical processes in the ocean, extracted from ocean colour observation.
121	Oil spill cover	Fraction of an ocean area polluted by hydrocarbons released from ships or offshore platforms, accidentally or deliberately.
134	Sea surface temperature	Temperature of the seawater at surface. The "bulk" temperature refers to the depth of typically 2 m, the "skin" temperature refers to within the upper 1 mm.
133	Sea surface salinity	Salinity of seawater in the surface layer (upper ~ 1 m if observed in MW). In the open ocean the correct term should be "halinity" with reference of the diversity of salts involved.
112	Ocean dynamic topography	Deviation of sea level from the geoid caused by ocean currents (after corrections for tides and atmospheric pressure effects) – Physical unit: cm – Accuracy unit: cm.
40	Coastal sea level (tide)	Deviation of sea level from local references in coastal zones, caused by local currents and tides (astronomical and wind-induced).
142	Significant wave height	Average amplitude of the highest 30 of 100 waves.
48	Dominant wave direction	One feature of the ocean wave spectrum. It is the direction of the most energetic wave in the spectrum – Physical unit: degrees – Accuracy unit: degrees.
49	Dominant wave period	The period of the most energetic wave in the ocean wave spectrum.
176	Wave directional energy frequency spectrum	2D variable colloquially referred to as wave spectrum. Describes the wave energy travelling in each direction and frequency band (for example, 24 distinct azimuth sectors each 15° wide, and 25 frequency bands).
135	Sea-ice cover	Fraction of an ocean area where ice is present.
138	Sea-ice thickness	Thickness of the ice sheet. It is related to sea-ice elevation and ice density.
139	Sea-ice type	Variable convolving several factors (age, roughness, density, etc.) – Accuracy expressed as number of classes. Actually, classes^{-1} is used, so that smaller figure corresponds to better performance, as usual.

5. LAND SURFACE (INCLUDING SNOW)

ID	*Variable (link to OSCAR/ Requirements)*	*Definition*
96	Land surface temperature	Temperature of the apparent surface of land (bare soil or vegetation) – Physical unit: K – Accuracy unit: K.
149	Soil moisture at surface	Fractional content of water in a volume of wet soil. Surface layer (upper few centimetres).
148	Soil moisture (in the roots region)	Sub-soil 3D field of the fractional content of water in a volume of wet soil. Requested from surface down to ~3 m.
66	Fraction of vegetated land	Fraction of a land area where vegetation is present.
172	Vegetation type	Result of the classification of different types of vegetation within a vegetated area – Accuracy expressed as inverse of the number of classes, so that smaller figures correspond to better performance.

ID	*Variable (link to OSCAR/ Requirements)*	*Definition*
98	Leaf area index (LAI)	LAI is the total one-sided area of photosynthetic tissue per unit ground surface area.
107	Normalized difference vegetation index (NDVI)	Difference between maximum (in NIR) and minimum (around the red) vegetation reflectance, normalized to the summation. Representative of total biomass, supportive for computing LAI if not directly measured.
60	Fire fractional cover	Fraction of a land area where fire is occurring.
62	Fire temperature	Temperature of the fire occurring within an area.
61	Fire radiative power	Power radiated by the fire occurring within an area.
144	Snow status (wet/dry)	Binary product (dry or melting/thawing) expressing the presence of liquid water in a snow layer – Accuracy expressed as hit rate (HR) and false alarm rate (FAR).
143	Snow cover	Fraction of a given area which is covered by snow.
145	Snow water equivalent	Vertical depth of the water that would be obtained by melting a snow layer. Linked to snow depth through the density of the snow layer.
150	Soil type	Result of the classification of different types of soil within an area – Accuracy expressed as inverse of the number of classes, so that smaller figures correspond to better performance.
95	Land cover	Processed from land surface imagery by assigning identified cluster(s) within a given area to specific classes of objects – Accuracy expressed as number of classes. Actually, classes^{-1} is used, so that smaller figure corresponds to better performance, as usual.
97	Land surface topography	Map of land surface heights – Physical unit: m – Accuracy unit: m.
69	Glacier cover	Fraction of a land area covered by permanent ice.
71	Glacier topography	Map of the height of the glacier surface.

6. SOLID EARTH

ID	*Variable (link to OSCAR/ Requirements)*	*Definition*
68	Geoid	Equipotential surface which would coincide exactly with the mean ocean surface of the Earth, if the oceans were in equilibrium, at rest, and extended through the continents (such as with very narrow channels) – Physical unit: cm – Accuracy unit: cm.
46	Crustal plates positioning	Basis for monitoring the evolution of the lithosphere dynamics – Physical unit: cm – Accuracy unit: cm.
45	Crustal motion (horizontal and vertical)	Changes in time of the position and height of the Earth's plates. Indicative of the lithosphere dynamics, thus useful for earthquake prediction – Physical unit: mm/y – Accuracy unit: mm/y.
72	Gravity field	Indicative of the statics and dynamics of the lithosphere and the mantle – Physical unit: mGal where: 1 Gal = 0.01 m·s^{-2}.
73	Gravity gradients	Gradient of the Earth's gravity field measured at the satellite orbital height – Physical unit: E , Eötvös (1 E = 1 mGal/10 km) – Accuracy unit: E.

7. ATMOSPHERIC CHEMISTRY

ID	*Variable (link to OSCAR/ Requirements)*	*Definition*
108	O_3 amount of substance fraction	3D field of mole fraction of O_3 (ozone).
109	O_3 total column	2D field of ozone, integrated over the total column.
16	BrO	3D field of mole fraction of BrO = bromine monoxide.
17	C_2H_2	3D field of dry air mole fraction of C_2H_2 = acetylene.
18	C_2H_6	3D field of dry air mole fraction of C_2H_6 = ethane.
19	CFC-11	3D field of dry air mole fraction of CFC-11 = trichlorofluoromethane = Freon-11 – Physical unit: mol/mol.
20	CFC-12	3D field of dry air mole fraction of CFC-12 = dichlorodifluoromethane = Freon-12.
21	HCHO (CH_2O) amount of substance fraction	3D field of dry air mole fraction of CH_2O (HCHO = formaldehyde).
22	HCHO (CH_2O) total column	2D field of concentration of CH_2O = HCHO = formaldehyde, integrated over the total atmospheric column.
23	CH_4 amount of substance fraction	3D field of dry air mole fraction of CH_4 (methane). Note: the uncertainty is meant here as compatibility.
315	CH_4 total column	2D field of column averaged of amount of CH_4 (methane) (expressed in moles) divided by the total amount of all constituents in dry air (also expressed in moles).
318	(13)CH_4 delta	3D field of delta C-13 in CH_4 (methane) (isotopic signature).
319	(14)CH_4 delta	3D field of delta C-14 in CH_4 (methane) (isotopic signature).
320	CH_3D delta	3D field of delta deuterium (H-2) in CH_4 (methane) (isotopic signature).
340	CH_4 tropospheric column	2D field of tropospheric column average of amount of CH_4 (expressed in moles) divided by the total amount of all constituents in dry air (also expressed in moles).
346	CH_4 amount of substance fraction (background (BG))	3D field of amount of background (BG) CH_4 (carbon dioxide) (expressed in moles) divided by the total amount of all constituents in dry air (also expressed in moles).
347	CH_4 amount of substance fraction (source region (SR))	3D field of amount of source region (SR) CH_4 (carbon dioxide) (expressed in moles) divided by the total amount of all constituents in dry air (also expressed in moles).
24	Chlorine monoxide (ClO)	3D field of mole fraction of ClO = chlorine monoxide = hypochlorite.
25	Chlorine nitrate ($ClONO_2$)	3D field of mole fraction of $ClONO_2$ = chlorine nitrate.
38	CO amount of substance fraction	3D field of dry air mole fraction of CO (carbon monoxide). Note: the uncertainty is meant here as compatibility.
329	CO total column	2D field of total number of CO modelcues (carbon monixide) per area in the atmosphere from surface to the top of the atmosphere.
343	CO amount of substance fraction	2D field of tropospheric column averaged of amount of CO (expressed in moles) divided by the total amount of all constituents in dry air (also expressed in moles).
123	Partial pressure of CO_2 (pCO_2)	Partial pressure of carbon dioxide at the surface of the sea.
185	CO_2 flux	Flux of carbon dioxide from the surface to the atmosphere.

ID	*Variable (link to OSCAR/ Requirements)*	*Definition*
314	CO_2 total column	2D field of column averaged of amount of CO_2 (expressed in moles) divided by the total amount of all constituents in dry air (also expressed in moles).
316	C-14 in CO_2 ($C(14)CO_2$ delta)	3D field of delta C-14 in CO_2 (carbon dioxide) (isotopic signature).
332	C-13 in CO_2 ($C(13)CO_2$ delta)	3D field of delta C-13 in CO_2 (carbon dioxide) (isotopic signature).
317	O-18 in CO_2 ($O(18)CO_2$ delta)	3D field of delta O-18 in CO_2 (carbon dioxide) (isotopic signature).
326	O-17 in CO_2 ($O(17)CO_2$ delta)	3D field of delta O-17 in CO_2 (carbon dioxide) (isotopic signature).
337	CO_2 tropospheric column	2D field of tropospheric column averaged of amount of CO_2 (expressed in moles) divided by the total amount of all constituents in dry air (also expressed in moles).
39	CO_2 amount of substance fraction	3D field of dry air mole fraction of CO_2 (carbon dioxide). Note: the uncertainty here is meant as compatibility.
338	CO_2 amount of substance fraction (source region (SR))	3D field of column averaged of amount of source region (SR) CO_2 (carbon dioxide) (expressed in moles) divided by the total amount of all constituents in dry air (also expressed in moles).
339	CO_2 amount of substance fraction (background (BG))	3D field of column averaged of amount of background (BG) CO_2 (carbon dioxide) (expressed in moles) divided by the total amount of all constituents in dry air (also expressed in moles).
43	Carbonyl sulfide (COS)	3D field of mole fraction of COS = carbonyl sulfide.
76	Water vapour	3D field of mole fraction of H_2O = water vapour (intended as a chemical species relevant for atmospheric chemistry).
77	Hydrogen chloride (HCl)	3D field of mole fraction of HCl = hydrogen chloride.
78	HDO	3D field of mole fraction of HDO = water vapour (with one hydrogen nucleus replaced by its deuterium isotope).
84	Nitric acid (HNO_3)	3D field of mole fraction of HNO_3 (nitric acid).
102	Nitrous oxide (N_2O)	3D field of dry air mole fraction of N_2O = nitrous oxide.
324	Delta N-15 in N_2O (N(15)NO delta)	3D field of delta N-15 in N_2O (nitrous oxide) (isotopic signature).
325	Delta O-18 in N_2O ($N_2O(18)$ delta)	3D field of delta O-18 in N_2O (nitrous oxide) (isotopic signature).
333	N(15)NO-alpha delta	3D field of delta N-15 in alpha-N_2O (nitrous oxide where the outer nitrogen atom is N-15) (isotopic signature).
334	N(15)NO-beta delta	3D field of delta N-15 in beta-N_2O (nitrous oxide where the middle nitrogen atom is N-15) (isotopic signature).
351	N_2O_5 amount of substance fraction	3D field of amount of N_2O_5 (expressed in moles) divided by the total amount of all constituents in dry air (also expressed in moles).
104	NO amount of substance fraction	3D field of mole fraction of NO (nitric oxide).
106	NO_2 total column	2D Field of NO_2 (nitrogen dioxide), integrated over the total column.
342	NO_2 tropospheric column	2D field of tropospheric column averaged of amount of NO_2 (expressed in moles) divided by the total amount of all constituents in dry air (also expressed in moles).

ID	*Variable (link to OSCAR/ Requirements)*	*Definition*
105	NO_2 amount of substance fraction	3D field of mole fraction of NO_2 (nitrogen dioxide).
348	NO_2 amount of substance fraction (background (BG))	3D field of amount of background (BG) NO_2 (expressed in moles) divided by the total amount of all constituents in dry air (also expressed in moles).
349	NO_2 amount of substance fraction (source region (SR))	3D field of amount of source region (SR) NO_2 (expressed in moles) divided by the total amount of all constituents in dry air (also expressed in moles).
120	OH amount of substance fraction	3D field of amount of OH (hydroxil radical) fraction.
140	Sulfur hexafluoride (SF_6)	3D field of dry air mole fraction of SF_6 = sulfur hexafluoride. Note: Uncertainty here is meant as compatibility.
147	SO_2 total column	2D feld of SO_2 (sulfur dioxide), integrated over the total column.
146	SO_2 amount of substance fraction	3D field of mole fraction of SO_2 (sulfur dioxide).

8. SPACE WEATHER

ID	*Variable (link to OSCAR/ Requirements)*	*Definition*
594	Ionospheric vertical total electron content (VTEC)	Number of electrons between two points.
591	Ionospheric plasma velocity	Velocity of bulk plasma or electrons (depending on measurement technique) as a function of altitude in the ionosphere.
593	Ionospheric scintillation	Random fluctuations of radio waves resulting from small-scale variations of the ionospheric electron density in space and time.
592	Ionospheric radio absorption	Attenuation of a radio waves passing through the lower ionosphere.
N/A	Electron density	3D field of the electron density in the ionosphere.
N/A	Electron flux density	Flux density of low-, medium- and high-energy electrons from the magnetosphere, the radiation belts or the interplanetary medium.
739	Electron differential directional flux	Flux density energy spectrum of low-, medium- and high-energy electrons from the magnetosphere, the radiation belts or the interplanetary medium, per unit solid angle.
740	Proton differential directional flux	Flux density energy spectrum of low-, medium- and high-energy protons from the magnetosphere, the radiation belts or the interplanetary medium, per unit solid angle.
598	Solar magnetic field	Vector magnetic field (1D or 3D) at the solar surface (photosphere/ chromosphere).
603	Solar EUV flux	Integrated extreme ultraviolet (EUV) flux over the solar disk.
600	Solar X-ray flux	Integrated X-ray flux over the solar disk.
609	Geomagnetic field	Magnitude and direction of the 3D magnetic field on the surface of Earth and within the magnetosphere (that is, in LEO and GEO).

ID	*Variable (link to OSCAR/ Requirements)*	*Definition*
613	Interplanetary magnetic field	Vector magnetic field (3D) in the solar wind. The reference frame is cartesian or cylindrical with many different axis orientations. Important in space weather to monitor magnetic disturbances of the near Earth environment.
590	Electric field	Magnitude and direction of the Earth's electric field.
N/A	foEs	The highest ordinary-wave frequency reflected back from a sporadic E layer and observed by an ionosonde.
581	foF2	Critical frequency of the F2 layer of the ionosphere. This critical frequency (f, in MHz) is associated with the electron density (Ne, in cm^{-3}): $f = 9 \cdot 10^{-3} \cdot sqrt(Ne)$.
582	h'F	Virtual height of the bottom of the ionospheric F-layer.
583	hmF2	Altitude of the peak density in the ionospheric F2 layer.
589	Spread F	Vertical thickness of highly structured ion density in the F-region of the ionosphere.
611	Heliospheric image	Image of the interplanetary space between the Sun and Earth.
588	Solar Ca II-K image	Image of the Sun in the K-line of Ca-II (393.4 nm).
599	Solar EUV image	Images of the Sun in the extreme ultraviolet (EUV) wavelengths in order to identify features such as filaments, active regions and coronal holes.
601	Solar H-alpha image	Image of the Sun in the hydrogen-alpha transition wavelength (656.3 nm).
602	Solar white light image	Image of the Sun in white light.
605	Solar X-ray image	Image of the Sun in X-ray wavelengths.
609	Solar coronagraphic image	Image of the solar corona surrounding the Sun.
615	Ionospheric vertical total electron content (VTEC)	Number of electrons between two points.

CHAPTER 6. CALIBRATION AND VALIDATION

6.1 INSTRUMENT CALIBRATION

6.1.1 Introduction and overview

Calibration is the process of quantitatively defining the satellite instrument response to known controlled signal inputs (for example, Ohring, 2007). The calibration information is contained in a calibration formula or in calibration coefficients that are then used to convert the instrument output (for instance, measured in "counts") into physical units (for example, radiance values W m^{-2} sr^{-1}). Instrument calibration is critical for quantitative data processing, especially for deriving products. Combining data from different instruments also necessitates adequate calibration in order to make the data comparable. For climate applications, the requirement for accurate calibration is particularly stringent since detection of small trends over long periods requires the ability to compare different instruments flown on different satellites at different times. Building homogeneous climate data records is contingent on stable calibration and uncertainty characterization.

Five characterization domains should be generally considered: radiometric calibration and spectral, spatial, temporal, and polarization characterization. A complete calibration record should include estimates of uncertainties in calibration parameters. Satellite instrument calibration should take into account the phases of an instrument's lifetime. In practice, this means that relevant changes (for example temporal changes in sensor characteristics) need to be considered (Ohring, 2007). Recent overview papers on satellite calibration explain the key aspects of satellite calibration and intercalibration. Zhou et al. (2015) address in some detail calibration of solar channels of satellite instruments. Chander et al. (2013) explain the need for satellite intercalibration and take the reader through all relevant aspects and caveats of satellite calibration. The paper also gives a comprehensive list of references on satellite intercalibration and vicarious calibration methods, described below. More details are provided by Doelling et al. (2004), Goldberg et al. (2011) and Meirink et al. (2013).

A long-standing method of calibration uses well-characterized, stable Earth targets; the moon is a fallback when a satellite instrument cannot be directly traceable to an agreed reference standard, for example due to the absence of a reliable on-board calibration device. This is the case for most shortwave observations from operational meteorological satellites (for example Govaerts et al., 2004). Such methods are generally referred to as 'vicarious calibration', meaning such methods are used in lieu of direct calibration with a well-known source of radiation.

The concept of satellite intercalibration has quite a long history in the satellite community. In principle, calibration is a comparison with another instrument that is higher in hierarchy than the instrument under calibration, and which is closer to SI or closer in the traceability chain to the SI standard. When comparing instruments that have an equal position in this hierarchy we use the term comparison, or intercomparison for mutual assessment between a set of instruments. Such (inter-) comparisons determine differences between instruments, not errors of a given instrument as is the case for a calibration. In metrology mutual differences and errors have different meanings (see JCGM 200, 2012).

Since space-based observing systems face particular challenges in calibration, intercalibration (defined and explained in this chapter) is often used. The intercalibration of instruments against a common reference instrument allows for consistency among space-based measurements at a given point in time. A calibration to an absolute standard would be necessary to allow assessment of errors and unambiguous detection of any long-term drift over time, which is essential for climate monitoring (Wielicki et al., 2013). However, calibration to an absolute standard and a direct equivalent in SI units is often not possible once the instrument is in space, and an alternative method is necessary.

As an early example, the International Satellite Cloud Climatology Project (ISCCP) used the AVHRR instrument on NOAA satellites as a pseudo-reference standard since the thermal IR window channels of AVHRR had an on-board black-body calibration. The estimated overall uncertainty in the AVHRR radiance calibrations was 5%–10% for the visible and about 2%–3% for infrared or 1.5–2.5 K at 300 K in brightness temperature (Rossow et al. 1996), and other instruments on other satellites were compared to AVHRR. Since such a system is neither a true calibration nor a classical intercomparison, the term intercalibration was coined.

Another example is the first effort to systematically intercompare the thermal IR channels of geostationary meteorological satellites (Menzel et al., 1993), which intercompared European Meteosat satellites with US GOES satellites. International participation in this process expanded within the CGMS and eventually led to the Global Space-based Inter-calibration System (GSICS) (Goldberg et al., 2011).

Finally, by comparing model-simulated and observed satellite radiances in data assimilation schemes, major NWP centres can also help determine relative biases between instruments. However, it is not possible to determine absolute biases with radiances computed from NWP model fields because models have their own biases.

Use of all these tools is explained on the Integrated Calibration and Validation System website addressing long-term monitoring from satellites (https://www.star.nesdis.noaa.gov/icvs-team/about.php).

Data records from past instruments can be "recalibrated" retrospectively, if additional information on the state of these instruments becomes available and new ways of intercalibration are developed. The work by John et al. (2019) demonstrates a recalibration of geostationary imagers using calibrated radiance observations from HIRS (High-resolution Infrared Radiation Sounder) and the hyperspectral sounders IASI (Infrared Atmospheric Sounding Interferometer) and AIRS (Atmospheric Infrared Sounder). A comparison of the recalibrations with operational calibrations revealed a significant reduction of biases. Such work is important because it makes historic satellite radiance observations useful for climate applications.

Of note here are also the Global Climate Observing System (GCOS) Climate Monitoring principles, which have been developed with a focus on providing adequate data for climate monitoring. Those principles provide a succinct list of requirements to be fulfilled by satellite (and ground-based measurements): https://gcos.wmo.int/en/essential-climate-variables/about/gcos-monitoring-principles.

Useful further information related to calibration is provided by the CEOS Calibration and Validation (Cal/Val) Working Group: http://calvalportal.ceos.org.

6.1.2 Factors affecting calibration

The response of an instrument to signal input, for example, the relationship between the radiance the instrument is exposed to and the numerical value assigned to the measurement (in physical units, for example, W m^{-2} sr^{-1} or W m^{-2} μm^{-1} sr^{-1}) depends at any point in time on several elements, such as:

(a) The viewing geometry, shielding effects, stray light, and antenna pattern;

(b) Detector sensitivity and ageing;

(c) Filter optics, as well as the possible contamination and its change over time, and stability of the filter material;

(d) The environment (temperature, radiation, vibration) for all parts of the instrument, including the front-end optics, mirrors in the optical path, detector and back-end electronics (focal plane electronics, preamplifier, and so forth);

(e) The signal-processing system (gain, analogue-to-digital converter, and so forth).

These elements also impact the spectral response function and the point spread function that are characteristic of the instrument. They must be determined before launch and should be monitored, if possible, in flight. Instrument software models simulating the instrument performance and functionality are useful for understanding the instrument status and trends as well as for predicting and correcting biases. However, it is generally not possible to analytically describe the exact variation of the instrument response resulting from the many factors that can affect the calibration. Therefore, reference measurements (for example with an on-board black body) are mandatory in performing an accurate calibration.

6.1.3 Pre-launch calibration

The pre-launch calibration of an instrument is performed in the laboratory by using accurately known radiation sources under controlled conditions. Simulating expected instrument states and factors influencing a calibration is necessary before launch; it is the only way to accurately characterize and model the instrument before it is exposed to the harsh orbital environment. Housekeeping data systems, which provide information about the satellite and its status including the instruments , need to be robust enough to withstand the physical stress incurred during launch and the in-orbit phase. Housekeeping data, in combination with post-launch calibration information, will allow operators to infer the calibration status of the instrument and help to resolve eventual on-orbit anomalies. It is beyond the scope of the present WMO Guide to dive into the details of pre-launch characterization and calibration activities. However, interested readers are referred to the paper by Datla et al. on this subject (2011) for a comprehensive description of the pre-launch characterization and calibration of passive optical remote sensing instruments.

6.1.4 On-board calibration

On-board calibration of an instrument in orbit is commonly performed with reference targets (such as black bodies in the infrared, and solar diffusers, lunar views and lamp line sources in the short wave) for passive instruments, or by internal calibration systems (such as gain monitors) for active instruments.

Some heritage instruments have been in operation over decades without adequate means of on-board calibration, such as the solar channels of the AVHRR. Other means of calibration (such as vicarious calibration or intercalibration with other instruments) are required for such instruments.

The accuracy of in-flight instrument calibration depends on the stability of the on-board calibration systems throughout the instrument's lifetime. Therefore, calibration must be regularly checked by intercalibration against more accurate references. In the case of IR imaging channels this can be done with hyperspectral sounding instruments like AIRS, IASI and CrIS (Cross-Track Infrared Sounder) (for example Goldberg et al. 2011; Hewison et al. 2013). For satellite instruments measuring reflected solar radiation an intercomparison of various instruments over longer time series assesses a relative performance; bias corrections can enable the study of trends (Zhan and Davies, 2016).

In the case of infrared instruments and if the radiometer detectors are assumed to have a linear response, the output voltage is given as:

$$V = \alpha R + V_0$$

where R is the input radiance, α is the radiometer responsivity and V_0 is the system offset. Calibration consists of determining α and V_0, which is accomplished by exposing the radiometer

to at least two reference targets with significantly different brightness temperatures. In practice the linear relationship may not hold true, and a non-linearity correction (such as a quadratic term) needs to be considered in the operational calibration.

For infrared and microwave instruments, one reference target is usually deep space, at a temperature of 2.7 K. However, direct viewing of deep space is not always possible for instruments on a satellite platform. For instance, instruments constantly pointing to the Earth's surface need to be equipped with a sub-reflector to supply the deep space view at intervals. A second target is usually a well-characterized source with temperature in the medium to upper dynamic range, often an on-board black body, which is ideally traceable to the SI, that is, to a radiance scale provided by a national metrology institute.

For ultraviolet, visible and near-infrared instruments, on-board calibration is more challenging since it is affected by many factors. At the low-signal side, deep space is a useful reference, provided that disrupting effects (for example, reflections from other parts of the satellite) are avoided. At the high-signal end, an absolute source is generally replaced by the sun viewed through solar diffusers that provide a relatively stable reference. The moon may also be used as a reference target, with the advantage that it can be viewed without an attenuator; however, it must be used in conjunction with an accurate model of the moon's bi-directional reflectance properties (Kieffer and Stone 2007). Neither the solar diffuser nor the moon provides an absolute calibration at present. Another system often used is an on-board bench of lamp line sources of well-controlled intensity. Spectrally dependent polarization effects induced by the reflecting surfaces of the instrument optics also need to be taken into account.

6.1.5 Vicarious calibration

A problem with on-board calibration is that often the instrument structure does not allow illumination of the full primary optics with reference sources. For example, a spin-stabilized radiometer in geostationary Earth orbit uses an internal black body requiring a model of the contributions of the telescope and foreoptics to the background radiation. For older generations of instruments (such as Meteosat First Generation), the reference black-body source was used more for stability monitoring than for absolute calibration. As a work-around, vicarious calibrations using a fast radiative transfer model with ancillary input data, that is atmospheric profiles from NWP and radiosondes, have been employed (for example, van de Berg et al., 1995) for the thermal IR channels. The broader issues with those early meteorological satellites are briefly discussed by Schmetz and Menzel (2015).

For the calibration of solar channels, dedicated aircraft campaigns were flown with well-calibrated radiometers and solar calibrations for the first generation Meteosat satellites. Calibrations were derived by comparing the satellite-measured counts with the aircraft-measured radiances (Kriebel and Amann, 1993). If only radiative transfer calculations were used (Köpke, 1982), then the Earth targets needed to be well known at the time of the satellite overpass in order to infer reflected solar radiance towards space.

Vicarious calibration can involve different kinds of targets, for instance, snow fields, sunglint, homogeneous desert areas, and deep convective cloud tops for the upper end of the visible dynamic range; cloud-free ocean surface as a dark target in the visible spectrum; and corner reflectors for synthetic aperture radars (requiring the minimization of errors due to construction and deployment of the reflectors so that the radar cross-section is known accurately). The tropical rainforest has a remarkable stability and homogeneity for microwave radiometers and radar scatterometers although it does exhibit some spatial and temporal variability.

Calibration field sites like the Atmospheric Radiation Measurement (ARM) Climate Research Facility – a US Department of Energy (DOE) user facility (https://www.arm.gov/) equipped with in situ observations – are used for the calibration of high spatial resolution space-based instruments. During initial payload commissioning or at regular intervals, aircraft overflights of a target area synchronous with the satellite overpass offer additional vicarious calibration data.

6.1.6 Intercalibration by simultaneous observations

The intercalibration of satellite instruments (Chander et al., 2013) relates collocated and simultaneous measurements of one instrument to those of another. This is done for the purpose of:

(a) Providing vicarious calibration to instruments that have no or an inferior internal calibration device;

(b) Merging the data from several instruments to generate consistent time-series.

(c) Reducing bias errors by comparing with very well-calibrated instruments, an example is the intercomparison of IR imaging instruments with hyperspectral sounding instruments.

The importance of satellite intercalibration has been well recognized. For instance, as part of the ISCCP undertaken by the World Climate Research Programme (WCRP), simultaneous observations from geostationary and polar orbiting imagers have been performed on a monthly basis for more than 30 years as a means to normalize geostationary satellite imagery (Rossow et al. 1996). More recently, GSICS (https://gsics.wmo.int/en) (Goldberg et al., 2011) has developed an operational methodology for such intercalibrations, specifically for simultaneous collocated observations. A good description and analysis is provided by Hewison (2013) and Hewison et al. (2013). The methodology considers the trade-off between accurate spatial–temporal co-registration of the instruments and the frequency of such events, and takes into account the corrections to be applied for:

(a) Different viewing geometries (with regard to both the instrument scan angle and the sun);

(b) Different atmospheric states in the line of sight, including aerosols and clouds;

(c) Different spectral response functions.

It should be noted that nearly simultaneous observations between two Sun-synchronous satellites can only occur at the intersections of their orbital planes, which are always located at a given local solar time and at a given – generally high – latitude. For a 98° inclination, the crossing latitude is above 70° when the equatorial crossing times (ECTs) of the two orbits differ by less than 8 h, and only drops significantly when the ECT difference increases towards 12 h. An example of a simultaneous nadir observation (SNO) operationally performed by GSICS is shown at https://gsics.wmo.int/en/objectives.

6.1.7 Bias adjustment of long-term data records

Long-term data records stretching over decades of observations from different satellite instruments are needed for monitoring of climate variability and climate trends. Successful examples are the temperature trend records from the Microwave Sounding Unit (MSU) onboard the NOAA polar-orbiting satellites. This instrument measures the atmospheric temperature from the surface to the lower stratosphere under all weather conditions, excluding precipitation. Although MSU was designed primarily for monitoring weather processes, its observations have been extensively used for detecting climate trends. Per se, the calibration for an individual instrument has too large a bias for climate monitoring. To reduce this uncertainty, an intercalibration method based on the simultaneous nadir overpass (SNO) matchups (Cao et al., 2004) for the MSU instruments on the NOAA-10, -11, -12 and -14 satellites was developed. Due to orbital geometry, the SNO matchups are confined to the polar regions, where the brightness temperature range is smaller than the global range. Nevertheless, the resulting calibration coefficients are applied globally to the entire life cycle of an MSU satellite (for example Zou et al., 2009 and references therein).

John et al. (2019) performed a recalibration of imagers on operational geostationary satellites using calibrated radiance observations from polar orbiting satellites with HIRS, and from the

hyperspectral sounders IASI and AIRS. A comparison of the recalibrations with operational calibrations of the geostationary imagers revealed significant biases in operational calibrations, which can be corrected to make the data useful for monitoring of climate variability.

6.1.8 Using calibration information

The type of calibration information available depends on the processing level and on the instrument considered. Each instrument has its own operating mode and calibration cycle, which includes regular measurements of calibration targets each time a certain number of observations are performed. For instance, Table 6.1. indicates the calibration cycles of the Advanced Microwave Sounding Unit – A (AMSU-A), the Microwave Humidity Sounder (MHS) and the High-resolution Infrared Sounder 4 (HIRS/4).

Table 6.1. Examples of observation/calibration cycles

	AMSU-A	*MHS*	*HIRS/4*
Number of Earth views (observation)	1 line of 30 pixels	1 line of 90 pixels	38 lines of 56 pixels
Number of warm target views (calibration)	2 (~300 K)	4 (~273 K)	48 (~290 K)
Number of cold target views (calibration)	2 (deep space ~2.73 K)	4 (deep space ~2.73 K)	56 (deep space ~2.73 K)
Overall duration of the cycle	8 s	8/3 s	256 s

An important step in the pre-processing from Level 0 to Level 1b data is to extract the calibration information. Table 6.1 provides an example for AMSU where warm/cold view counts are used to compute calibration coefficients in accordance with the calibration model (such as a linear or quadratic calibration function or a lookup table) commonly provided by the satellite instrument operator. An early example describing the AMSU-A calibration was been provided by Mo (1995).

For applications requiring high accuracy and consistency among different instrument data records, a correction can be applied on top of the operational calibration to take into account the latest results of the intercalibration activities. Such corrections are provided by GSICS (see Goldberg et al., 2011). The corrected calibration coefficients may be included in the Level 1.b/Level 1.5 data formats as additional calibration information.

6.1.9 Traceability of space-based measurements

While intercalibration can ensure consistency between satellite instruments, it does not necessarily provide traceability to SI standards unless a reference instrument in orbit is SI-traceable. There are major challenges to achieving SI traceability in orbit as most sensors degrade physically during and after launch. Achieving SI traceability poses instrument design challenges and remains a research topic for all but a few measurement types.

The proposed Climate Absolute Radiance and Refractivity Observatory (CLARREO) mission (Wielicki et al., 2013) consists of a highly accurate infrared interferometer with a high-emissivity reference black body using multiple phase-change cells for SI-traceable thermometer calibration, an ultraviolet, visible and near-infrared spectrometer calibrated by Sun and moon views, a cryogenically cooled active cavity radiometer, and radio occultation measurements. This suite of instruments would be intended to provide fully traceable measurements of the entire Earth-emitted and -reflected solar spectrum. Implementing and maintaining such a mission would provide anchor points in support of the calibration and the traceability to SI standards of the many operational radiometers.

For measurement traceability, one could also take advantage of instruments that do not depend on radiometric calibration, such as radio occultation and sun or star occultation sensors.

However, the use of measurements from such instruments requires radiative transfer calculations to compute radiances for comparison with the satellite observations. The resulting issue is that those calculations may have a bias.

6.2 VALIDATION

Validation is the process of assessing, by independent means, the accuracy of the products derived from space-based instrument measurements. The validation of Level 1 data requires a deep understanding of the instruments and, therefore, should be done by the instrument operator with support from the instrument engineers. Product (Level 2) validation should be performed by product developers, downstream of instrument calibration. Both processes need to be documented in instrument-specific and product-specific validation plans, respectively (for example Spezzi et al., 2018).

As the validation of geophysical products is complex, highly diversified and specific to the many geophysical products, it should suffice here to recall the salient points:

— Geophysical products are generated from satellite data (often radiance measurements) by applying an algorithm that is most often based on physics. Alternatively, empirical or statistical approaches can be used. Comparing retrieved products with in situ observations or model outputs is an important part of the process to assess and document the reliability of given retrieval algorithms and define their domain of applicability.

— For many products, validation is a complex problem since the comparison between products derived from space-based measurements and independent reference products, often from in situ measurements, is subject to errors from several sources: (i) an inherent error in satellite-derived products, (ii) the bias error in the reference data, and (iii) the error introduced by the comparison methodology, often due to non-coincident collection in time and space – so-called representativeness error. It is also notable that different measurement techniques measure different things, for instance, a space-based observation often refers to a relatively large area (the instantaneous field of view) and atmospheric volume and is a nearly instantaneous measurement (within milliseconds), whereas ground (in situ) measurements are generally point measurements integrated over time. Surface-based remote sensing usually provides information representative of the atmospheric column. It is important that such product validations adhere to one defined method of averaging over time and space in order to maintain consistency.

A validation assessment model can be used to improve comparisons by understanding and accounting for these differences and to better appreciate the advantages and disadvantages of different validation approaches. Validation campaigns run by satellite operators are usually accompanied by such assessment models.

6.2.1 Validation strategies

The validation of satellite-derived products should follow defined best-practice and variable-dependent protocols, such as those developed by the CEOS Working Group on Calibration and Validation (http://ceos.org/ourwork/workinggroups/). The validation of satellite-derived parameters and products can be carried out using the following well-characterized sources:

(a) Upper-air in situ measurements (for example radiosondes);

(b) Surface-based remote-sensing measurements;

(c) Comparison with model output and/or use in data assimilation;

(d) Desert targets;

(e) Other satellite-derived or blended products of a similar type.

To use such validation sources, it is essential that:

(a) Measurement uncertainties be well known;

(b) Temporal and spatial sampling of the different products are taken into account and, a priori allow for an intercomparison.

For example, to support validated generation of combined sea-surface temperature satellite products, the Group for High Resolution Sea Surface Temperature (GHRSST) has developed a comprehensive validation strategy which includes careful descriptions of the data, the measurements and the comparison process. For further information see: https://www.ghrsst.org/ghrsst-data-services/services/.

6.2.2 Validation of Level 1 data

Level 1 product performance validation addresses various issues. Generally, the methodologies include cross-calibration with other instruments (possibly even on the same platform), intercomparisons with other comparable observations during simultaneous nadir overpasses (Goldberg et al., 2011), comparisons with ground-based observations and lunar calibration. The Level 1B product performance will be validated with respect to geometric, spectral and radiometric requirements for all geographic regions including their seasonal variability. In particular, the following specific activities are included: (i) calibration verification, (ii) validation of radiometry, (iii) geometric verification, (iv) image quality verification (Phillips et al., 2018). Such tests are commonly performed during the commissioning phase, that is, during a limited period of time. However, it is also necessary to conduct these activities during routine operations in order to maintain long-term stability of the calibrated radiances.

6.2.3 Validation of geophysical products (Level 2)

The validation of Level 2 products requires independent products from other satellites or from ground-based measurements (Spezzi et al., 2018). An important consideration is the comparability of the temporal and spatial scales of the products. Here the representativeness error becomes important (Kitchen, 1989). Validation is also possible by intercomparison with another validated product from a different satellite mission. Comparisons with ground-based observations are also useful. A further method is validation with the help of NWP models (see section 6.2.4). The goal of validation is to assess product quality in terms of precision, accuracy (bias), stability, and whether continuity/consistency of temporal product records is assured. Whether a validation has been successful is to some extent dependent on user requirements for the product, with some applications requiring more stringent validation than others. A good description of geophysical validation is provided by Loew et al. (2017); this paper reviews state-of-the-art methods of satellite validation and documents their similarities and differences.

During the lifetime of a satellite mission products usually undergo changes and improvements are usually made to the algorithms used for the product retrieval. In principle such changes require a new validation, however much of this can be covered via a validation with an NWP system.

6.2.4 Validation by way of NWP

Experience shows that putting radiance products (Level 1) or geophysical products into an NWP data assimilation system is an excellent way to validate satellite data. This is especially true when a satellite instrument is based on a recurrent design and predecessors have already been used

in NWP. In that case, experience already exists to judge the performance of the measurements to be validated. Another advantage of validation via NWP systems is that comparisons for different geographic regions and seasons are at hand.

More effort is required if new satellite measurements are used in an NWP assimilation system. For instance, a new forward operator needs to be coded in order to simulate the satellite measurements on the basis of NWP model output fields.

An enormous advantage of monitoring satellite products within NWP systems is also the continuity of such monitoring throughout the lifetime of a satellite mission. Monitoring by different NWP centres provides further benefit because it may cast light on problems inherent to a specific NWP system. This is because NWP fields do not represent the truth as such; in particular in sparsely observed regions the NWP background errors may be significant. Time and dedicated research are usually required to reap the maximum benefit from new satellite observations for NWP and climate monitoring.

Examples of such monitoring for different products can be found on websites of EUMETSAT Satellite Application Facilities (SAFs), for instance: https://www.nwpsaf.eu/site/; https://www.romsaf.org.

REFERENCES AND FURTHER READING

Achieving Satellite Instrument Calibration for Climate Change (ASIC³); Report of a Workshop Organized by the National Oceanic and Atmospheric Administration, National Institute of Standards and Technology, National Aeronautics and Space Administration, National Polar-orbiting Operational Environmental Satellite System-integrated Program Office, and Space Dynamics Laboratory of Utah State University; Ohring, G., Ed.; National Oceanic and Atmospheric Administration: Washington, DC, 2007.

Cao, C.; Weinreb, M.; Xu, H. Predicting Simultaneous Nadir Overpasses among Polar-Orbiting Meteorological Satellites for the Intersatellite Calibration of Radiometers. *Journal of Atmospheric and Oceanic Technology* **2004**, *21* (4), 537–542. https://doi.org/10.1175/1520-0426(2004)021<0537:PSNOAP>2.0.CO;2.

Chander, G.; Hewison, T.; Fox, N. et al. Overview of Intercalibration of Satellite Instruments. *IEEE Transactions on Geoscience and Remote Sensing* **2013**, *51* (3), 1056–1080. https://doi.org/10.1109/TGRS.2012.2228654.

Datla, R. U.; Rice, J. P.; Lykke, K. R. et al. Best Practice Guidelines for Pre-Launch Characterization and Calibration of Instruments for Passive Optical Remote Sensing. *Journal of Research of the National Institute of Standards and Technology* **2011**, *116* (2), 621–646. https://doi.org/10.6028/jres.116.009.

Doelling, D.; Nguyen, L.; Minnis, P. On the Use of Deep Convective Clouds to Calibrate AVHRR Data. In *Optical Science and Technology*, Proceedings of the 49th Annual Meeting of SPIE, the International Society for Optics and Photonics, Denver, USA, 2–6 August 2004; SPIE: Bellingham, USA, 2004; Vol. 5542: Earth Observing Systems IX. https://doi.org/10.1117/12.560047.

Goldberg, M.; Ohring, G.; Butler, J. et al. The Global Space-based Inter-calibration System. *Bulletin of the American Meteorological Society* **2011**, *92* (4), 467–475. https://doi.org/10.1175/2010BAMS2967.1.

Govaerts, Y.; Clerici, M.; Clerbaux, N. Operational Calibration of the Meteosat Radiometer VIS Band. *IEEE Transactions on Geoscience and Remote Sensing* **2004**, *42* 1900–1914. https://doi.org/10.1109/TGRS.2004.831882.

Hewison, T. An Evaluation of the Uncertainty of the GSICS SEVIRI-IASI Intercalibration Products. *IEEE Transactions on Geoscience and Remote Sensing* **2013**, *51* (3), 1171–1181. https://doi.org/10.1109/TGRS.2012.2236330.

Hewison, T.; Wu, X.; Yu, F. et al. GSICS Inter-Calibration of Infrared Channels of Geostationary Imagers Using Metop/IASI. *IEEE Transactions on Geoscience and Remote Sensing* **2013**, *51* (3), 1160–1170. https://doi.org/10.1109/TGRS.2013.2238544.

John, V. O.; Tabata, T.; Rüthrich, F. et al. On the Methods for Recalibrating Geostationary Longwave Channels Using Polar Orbiting Infrared Sounders. *Remote Sensing* **2019**, *11*, 1171. https://doi.org/10.3390/rs11101171.

Joint Committee for Guides in Metrology (JCGM). *International Vocabulary of Metrology – Basic and General Concepts and Associated Terms (VIM)*; JCGM 200:2012; JCGM: Sèvres, France, 2012.

Kieffer, H. H.; Stone, T. C. The Spectral Irradiance of the Moon. *The Astronomical Journal* **2005**, *129* 2887–2901. https://doi.org/10.1086/430185.

Kitchen, M. Representativeness Errors for Radiosonde Observations. *Quarterly Journal of the Royal Meteorological Society* **1989**, *115* (487), 673–700. https://doi.org/10.1002/qj.49711548713.

Köpke, P. Vicarious Satellite Calibration in the Solar Spectral Range by Means of Calculated Radiances and its Application to Meteosat. *Applied Optics* **1982**, *21*, 2845–2854. https://doi.org/10.1364/AO.21.002845.

Kriebel, K.-T.; Amann, V. Vicarious Calibration of the Meteosat Visible Channel. *Journal of Atmospheric and Oceanic Technology* **1993**, *10*, 225–232. https://doi.org/10.1175/1520-0426(1993)010<0225:VCOTMV>2.0.CO;2.

Loew, A.; Bell, W.; Brocca, L. et al. Validation Practices for Satellite-based Earth Observation Data across Communities. *Reviews of Geophysics* **2017**, *55*, 779–817. https://doi.org/10.1002/2017RG000562.

Meirink, J. F.; Roebeling, R. A.; Stammes, P. Inter-calibration of Polar Imager Solar Channels Using SEVIRI. *Atmospheric Measurement Techniques* **2013**, *6*, 2495–2508. https://doi.org/10.5194/amt-6-2495-2013.

Menzel, P.; Schmetz, J.; Nieman, S. et al. *Intercomparison of the Operational Calibration of GOES-7 and Meteosat-3/4*; NOAA Technical Report NESDIS 73; National Oceanic and Atmospheric Administration: Washington, DC, USA, 1993.

Mo, T. *Calibration of the Advanced Microwave Sounding Unit-A for NOAA-K*; NOAA Technical Report NESDIS 85, National Oceanic and Atmospheric Administration: Washington, DC, USA, 1995.

Ohring, G.; Wielicki, B.; Spencer, R. et al. Satellite instrument calibration for measuring global climate change: Report of a workshop. *Bulletin of the American Meteorological Society* **2005**, *86*, 1303–1314. https://doi.org/10.1175/BAMS-86-9-1303.

Phillips, P.; Bonsignori, R.; Just, D. et al. Calibration and Validation of Level 1B Radiances of the EUMETSAT Polar System – Second Generation (EPS-SG) Visible/Infrared Imager METimage. In Proceedings of SPIE Remote Sensing, Berlin, Germany, 10–13 September 2018; SPIE: Bellingham, USA, 2018; Vol. 10785: Sensors, Systems, and Next-Generation Satellites XXII. https://doi.org/10.1117/12.2325545.

Rossow, W. B.; Brest, C. L.; Roiter, M. *International Satellite Cloud Climatology Project (ISCCP) Update of Radiance Calibrations* (WMO/TD-No. 736). World Climate Research Programme.

Schmetz, J.; Menzel, W. P. A Look at the Evolution of Meteorological Satellites: Advancing Capabilities and Meeting User Requirements. *Weather, Climate, and Society* **2015**, *7*, 309–320. https://doi.org/10.1175/WCAS-D-15-0017.1.

Spezzi, L.; Borde, R.; Phillips, P. L. et al. Validation Activities for the Level 2 Geophysical Products of the EUMETSAT Polar System – Second Generation (EPS-SG) Visible/Infrared Imager (METimage). In Proceedings of SPIE Remote Sensing, Berlin, Germany, 10–13 September 2018; SPIE: Bellingham, USA, 2018; Vol. 10786: Remote Sensing of Clouds and the Atmosphere XXIII. https://doi.org/10.1117/12.2325586.

van de Berg, L.; Schmetz, J.; Whitlock, J. On the Calibration of the Meteosat Water Vapor Channel. *Journal of Geophysical Research: Atmospheres* **1995**, *100* (D10), 21069–21076. https://doi.org/10.1029/95JD01880.

Wielicki, B.; Young, D. F.; Mlynczak, M. G. et al. Achieving Climate Change Absolute Accuracy in Orbit. *Bulletin of the American Meteorological Society* **2013**, *94* (10), 1519–1539. https://doi.org/10.1175/BAMS-D-12-00149.1.

Zhan, Y.; Davies, R. Intercalibration of CERES, MODIS, and MISR Reflected Solar Radiation and its Application to Albedo Trends. *Journal of Geophysical Research: Atmospheres* **2016**, *121*, 6273–6283. https://doi.org/10.1002/2016JD025073.

Zhou, G.; Li, C.; Yue, T. et al. An Overview of In-orbit Radiometric Calibration of Typical Satellite Sensors. In *The International Archives of the Photogrammetry, Remote Sensing and Spatial Information Sciences*; Copernicus GmbH, 2015; Volume XL-7/W4, 235–240. https://doi.org/10.5194/isprsarchives-XL-7-W4-235-2015.

Zou, C.-Z.; Gao, M.; Goldberg, M. D. Error Structure and Atmospheric Temperature Trends in Observations from the Microwave Sounding Unit. *Journal of Climate* **2009**, *22*, 1661–1681. https://doi.org/10.1175/2008JCLI2233.1.

CHAPTER 7. CROSS-CUTTING ISSUES

7.1 FREQUENCY PROTECTION ISSUES

7.1.1 Overall frequency management

A critical issue for sustaining space-based Earth observations is whether the radio-frequency spectrum in the microwave range (1 to 300 GHz and above) remains available. This is important for:

(a) Passive observations of the Earth surface in atmospheric windows and atmospheric gases in absorption bands;

(b) Active observations with radar (altimeters, scatterometers, synthetic aperture radars);

(c) Communications necessary for data downloading and satellite control.

The use of the radio-frequency spectrum is coordinated at the global level by the International Telecommunication Union (ITU). Radio Regulations are adopted by ITU Members at the World Radiocommunication Conferences (WRC) every four years. ITU regulates the allocation of radio-frequency bands to the different applications known as services, such as fixed and mobile telecommunications, broadband mobile applications, radio navigation, ground-based radars, short-range devices and electronic news gathering. Earth observation applications are identified by ITU as two particular services: the Earth exploration-satellite service (EESS) and Meteorological satellite (Metsat) service. While some bands are allocated to a service on an exclusive basis, most bands are allocated to several services with certain conditions (such as the limitation of the number, the emitting power and the geographical distribution of sources) that aim at avoiding harmful interference.

With the rapid expansion of the telecommunication sector and its increasing spectrum needs, the protection of frequencies required for EESS and Metsat has become very critical. Concerns include:

(a) Interference from uncontrolled emissions within exclusive EESS or Metsat bands, or to out-of-band emissions from nearby frequency bands;

(b) Sharing bands under conditions that are not stringent enough to guarantee reliable protection;

(c) The desire of other services to expand to bands currently allocated to EESS or Metsat;

(d) The need of EESS or Metsat to use new bands arising due to the evolving remote-sensing technology (for example, microwave above 300 GHz), growing data rates or expanding telecommunication bandwidths.

In addressing these issues, it should be noted that frequencies used for passive Metsat measurements are governed by the physics of the required observations. That means, selected frequencies for Metsat must correspond to either absorption bands of the atmospheric components to be observed or, in the case of surface observations, to atmospheric window channels with minimal atmospheric absorption. It is also important to note that natural emissions are extremely weak compared to most artificial sources, and hence they are easily corrupted. Therefore, passive radiometric bands must be considered as a natural and non-renewable resource to be preserved.

7.1.2 Passive microwave radiometry

The spectral microwave range used for Earth observation stretches from ~1.4 GHz (for example, for ocean salinity) to ~2 500 GHz and beyond. The most critical issues are for frequencies below 300 GHz. The use of frequencies above ~300 GHz is still emerging; moreover, since the water vapour continuum impacts viewing the lower troposphere, most of the instruments operating at those frequencies are designed for atmospheric chemistry and exploit limb viewing, which makes them less prone to interferences from ground sources. The ITU has identified a limited number of bands allocated to EESS, of which active uses are either prohibited or limited. As the radio-frequency spectrum is utilized by more users and users have a need for higher data rates, there is increasing pressure on higher frequencies, leading the ITU to share EESS bands with active services. Only a few narrowbands are assigned to EESS on an exclusive basis ensuring reliable legal protection. This has the following effects:

(a) The position of the allocated microwave channels often does not coincide with the sensitivity peak for the needed geophysical variable, and may not be free of contamination;

(b) The protected bandwidth may be so narrow that the signal-to-noise ratio is poor; this may force consideration of an unprotected band where a wider bandwidth is available, accepting the risk of contamination.

Unfortunately, the pressure from other users of the spectrum, including commercial and mobile services, is continuously increasing; specialized groups from WMO, the Coordination Group for Meteorological Satellites (CGMS), and space agencies must continuously monitor the situation at each update of the ITU Regulations. One very important such group is the Space Frequency Coordination Group (SFCG), which provides a forum for coordination between space operators for effective use and management of those radio frequency bands that are allocated by the ITU to the space research, space operations, Earth exploration satellite and meteorological satellite services.

7.1.3 Active microwave sensing

The problem of frequency protection also holds for active sensing (altimeters, scatterometers or synthetic aperture radars). For some applications of radar backscattering, like precipitation measurement, the sensing frequency has to be chosen in relation with the target properties. In other cases, like altimetry or synthetic aperture radar imagery, it is not very selective and there is some flexibility to find a frequency allocation in any of the L, S, C, X, K_u, K, K_a, V or W bands (see Chapter 2 of the present volume, Table 2.8 for definitions).

7.1.4 Satellite operation and communication frequencies

Frequency allocation for satellite–ground communications is another critical issue. As this involves active usage, the ITU Regulations are very restrictive in terms of allowed frequency, bandwidth and emitted power. The consequences are:

(a) Higher cost for a ground receiving station that works with low signals;

(b) Higher cost because the insufficient bandwidth available in one band for the data rate to be handled forces relocation to higher-frequency bands that require more challenging technology and antenna pointing;

(c) Ultimately, more difficulty to secure a frequency, particularly for real-time transmission; fewer frequencies are available, and sometimes this provokes interferences between satellites of the same family that are in orbit simultaneously.

In any event, frequency protection is difficult to guarantee, and users are experiencing problems, especially in industrialized areas. It requires dedicated resources at satellite agencies and WMO to maintain the protection. The table in this section provides the frequency bands allocated to

Available frequency band allocations for Metsat data transmissions

Space-to-Earth direction	*Earth-to-space direction*
137–138 MHz (Metsat primary)	401–403 MHz (EESS and Metsat primary)
400.15–401 MHz (Metsat primary)	2 025–2 110 MHz (EESS primary) (Note 1) (and space-to-space direction)
460–470 MHz (EESS and Metsat secondary)	8 175–8 215 MHz (Metsat primary)
1 670–1 710 MHz (Metsat primary)	28.5–30.0 GHz (EESS secondary) (Note 1)
2 200–2 290 MHz (EESS primary) (Note 1) (and space-to-space direction)	40.0–40.5 GHz (EESS primary) (Note 1)
7 450–7 550 MHz (Metsat primary, limited to geostationary satellites only)	
7 750–7 900 MHz (Metsat primary, limited to non-geostationary satellites only)	
8 025–8 400 MHz (EESS primary) (Note 1)	
18.0–18.3 GHz (Metsat primary for space-to-Earth direction in Region 2, limited to geostationary satellites only)	
18.1–18.4 GHz (Metsat primary for space-to-Earth direction in Regions 1 and 3, limited to geostationary satellites only)	
25.5–27.0 GHz (EESS primary) (Note 1) (and space-to-space direction in 25.25–27.5 GHz)	
37.5 40.0 GHz (EESS secondary) (Note 1)	
65.0–66.0 GHz (EESS primary) (Note 1)	

Note 1. Since the Metsat is a sub-class of the Earth exploration-satellite service (EESS), those allocations (for example: 8 025–8 400 MHz and 25 500–27 000 MHz) can also be used for the operation of Metsat satellites and their applications.

data transmission to and from meteorological satellites (from WMO/ITU, 2008). It also takes into account the band 7 850–7 900 MHz, which was added at previous WRCs. A list of all frequencies used for transmitting data to and from Earth observation satellites or for microwave active or passive remote sensing can be found at: https://space.oscar.wmo.int/satellitefrequencies.

7.2 INTERNATIONAL COORDINATION

7.2.1 The Coordination Group for Meteorological Satellites

Focusing on long-term sustained missions, the Coordination Group for Meteorological Satellites (CGMS), in accordance with an agreed baseline, coordinates satellite constellations in geostationary and low Earth orbit in support of WMO and co-sponsored programmes. Established in 1972 with a focus on weather monitoring by geostationary satellites for weather forecasting, CGMS initially defined common standards for low-resolution image dissemination

in weather facsimile (WEFAX) format and for the International Data Collection System to support mobile stations viewed by the different satellites. CGMS initially also focused on geostationary satellites and fostered the establishment of a ring of geostationary satellites around the Earth.

The scope of CGMS was extended in 1992 to include polar-orbiting meteorological satellites and research satellite missions contributing to the global space-based observing system. CGMS is now increasingly addressing Earth system observations for climate, oceanography and environmental monitoring. The agreed CGMS baseline describes the mission classes and orbits to be maintained with long-term continuity; it serves as a reference for the intended contributions of the participating members to the WMO Integrated Global Observing System (WIGOS) in response to the WMO Vision for WIGOS in 2040.

CGMS defines technical standards or best practices to ensure interoperability across the global system. It has developed contingency plans which provide a framework for action in case of satellite outage or other unexpected difficulties in fully implementing the agreed baseline.

In addition, the Committee on Earth Observation Satellites (CEOS/CGMS Joint Working Group on Climate (WGClimate) coordinates and encourages collaborative activities between the world's major space agencies in the area of climate monitoring with the overarching goal of improving the systematic availability of climate data records through the coordinated implementation and further development of a global architecture for climate monitoring from space. WGClimate was established in 2010 to coordinate the CEOS contribution to climate change monitoring.

CGMS operates through working groups dedicated to: (i) satellite systems and telecommunications, (ii) satellite products, (iii) continuity and contingency planning, and (iv) global data dissemination. Those working groups are always convened at the annual CGMS meetings. Together with WMO, CGMS launched major collaboration initiatives including the Global Space-based Inter-calibration System (GSICS), the Sustained and Coordinated Processing of Environmental Satellite Data for Climate Monitoring (SCOPE-CM) and SCOPE-Nowcasting projects, and the Virtual Laboratory for Education and Training in Satellite Meteorology (VLab). CGMS has also initiated several International Science Working Groups, which in turn regularly report at annual CGMS meetings., CGMS currently sponsors and helps to organize dedicated meetings of the following five International Science Working Groups:

(a) The International TIROS Operational Vertical Sounder (TOVS) Working Group (ITWG);

(b) The International Winds Working Group (IWWG);

(c) The International Precipitation Working Group (IPWG);

(d) The International Radio Occultation Working Group (IROWG);

(e) The International Cloud Working Group (ICWG).

More details on CGMS are available from: https://www.cgms-info.org/.

7.2.2 The Committee on Earth Observation Satellites

The Committee on Earth Observation Satellites (CEOS) was established in September 1984 in response to a recommendation from a Panel of Experts on Remote Sensing from Space that was set up under the aegis of the G7 Economic Summit of Industrial Nations Working Group on Growth, Technology and Employment. This panel recognized the multidisciplinary nature of space-based Earth observations and the value of coordinating international Earth observation efforts to benefit society. Accordingly, the original function of CEOS was to coordinate and harmonize Earth observations to make it easier for the user community to access and utilize data. CEOS initially focused on interoperability, common data formats, the intercalibration of instruments, and common validation and intercomparison of products.

Since the inception of CEOS, the circumstances surrounding the collection and use of space-based Earth observations have changed. The number of Earth-observing satellites has vastly increased. Onboard instruments became more advanced and are capable of collecting new types of data in ever-growing volumes. The user community has expanded and become more diverse, as different data types become available and new applications for Earth observations are developed. Users have become more organized, forming several international bodies that coordinate and levy Earth observation requirements. In response to this changing environment, CEOS has also evolved, becoming more complex, and expanding the number and scope of its activities. In addition to its original charge, CEOS now focuses on validated requirements levied by external organizations, works closely with other satellite coordinating bodies (such as the CGMS), and continues its role as the primary forum for international coordination of space-based Earth observations.

Over the past three decades, CEOS has significantly contributed to the advancement of space-based Earth observation community efforts. CEOS plenary sessions provide a regular opportunity for CEOS agencies to communicate, collaborate and exchange information on Earth observation efforts. Such international coordination has spurred useful partnerships such as the Integrated Global Observing Strategy (IGOS), and CEOS played an influential role in the establishment and ongoing development of the Group on Earth Observations (GEO) and the Global Earth Observation System of Systems (GEOSS). Indeed, CEOS coordinates the GEOSS space segment. CEOS agencies are working together to launch multi-agency collaborative missions, and such cooperative efforts have become the primary approach to Earth observation mission development. CEOS also provides an established means of communicating with external organizations, enabling CEOS to understand and then act upon these organizations' Earth observation needs and requirements.

CEOS ensures international coordination of the capabilities and assets of individual CEOS agencies. The guiding principle behind all such coordination activities is the demonstration of the feasibility and added value of sustained space-based Earth observations, particularly in the context of responding to stakeholder requirements. More specifically, the scope of the coordination encompasses both current and future satellite observation systems, with the aim of ensuring their complementarity and completeness with respect to the stakeholder requirements.

Internal coordination is implemented through a variety of CEOS mechanisms. At the working level, this coordination is generally achieved using a combination of working groups (for the coordination of infrastructure and cross-cutting issues) and virtual constellations (for the coordination of thematic/topical-based areas). In addition, and depending on the context, these permanent, working-level CEOS mechanisms may be augmented by ad hoc arrangements for specific, shorter-term activities.

The five working groups are (http://ceos.org/ourwork/workinggroups/):

(a) WGCapD: The Working Group on Capacity Building & Data Democracy;

(b) WGClimate: The CEOS/CGMS Working Group on Climate;

(c) WGCV: The Working Group on Calibration & Validation;

(d) WGDisasters: The Working Group on Disasters;

(e) WGISS: The Working Group on Information Systems & Services.

There are currently seven virtual constellations (http://ceos.org/ourwork/virtual-constellations/):

(a) Atmospheric composition;

(b) Land surface imaging;

(c) Ocean surface topography;

(d) Precipitation;

(e) Ocean colour radiometry;

(f) Ocean surface vector wind;

(g) Sea-surface temperature.

When working groups and virtual constellations are not sufficient, CEOS can create an ad hoc team (see https://ceos.org/ourwork/ad-hoc-teams/).

7.3 SATELLITE MISSION PLANNING

7.3.1 Satellite programme life cycle

Following well-established programme/project management methodologies, the activities conducted during the life cycle of a satellite programme/project are grouped into phases.

Each phase advances the programme/project from one milestone to another and is usually concluded by a formal review.

The exact terminology used by the developing organization may differ, but typically a satellite programme/project life cycle consists of the following phases:[1]

- Phase 0: Definition of user requirements, involving the user community, and of mission requirements, that is, identification of the possible techniques to fulfil the user requirements.
- Phase A: Feasibility assessment at system level (including a preliminary definition of the ground segment) and of critical instruments (possibly including instrument simulations), and rough order-of-magnitude cost estimation.
- Phase B: Preliminary design, preparatory activities (including airborne campaigns) and detailed cost estimation.
- Phase C: Detailed design and development and testing of all systems (including the ground segment) and subsystems.
- Phase D: Integration of all subsystems, testing of the whole satellite, launch campaign and in-orbit commissioning.
- Phase E: Exploitation phase.
- Phase F: Post-operational phase encompassing final payload mission data consolidation after de-orbiting for transition into long-term archives.

For larger satellite programmes/projects Phase 0 to Phase D can last up to 15 years (for instance for a larger GEO mission: 3–4 years for Phase 0, ~2 years for Phase A, ~2 years for Phase B, ~5 years for Phase C, and ~1–2 years for Phase D). For smaller satellite programmes/projects, the duration of Phase 0 to Phase D can be as short as 1–2 years.

The exploitation phase (Phase E) can last from a few months for a low Earth orbiting satellite to many years for a GEO satellite programme. For example, for an operational programme including a series of three or four satellites, with some overlap for contingency purposes, the

[1] See ECSS-M-ST-10C Rev.1 (*Space Project Management: Project Planning and Implementation*), page 19, "Project Phasing".

exploitation phase may be planned for 15 or more years (the typical lifetime of a low Earth orbit satellite is five years, and it is seven years for a GEO satellite). Phase F is mostly concluded 3–5 years after de-orbiting.

In general, the duration of a satellite generation is a trade-off between the need for a long series to offset the development cost and the user learning curve, and the need to develop a new generation of satellite instruments to benefit from state-of-the-art technology.

The organization of a space programme involves many stakeholders: the applications and user community, scientific institutes, space agencies focused on research and development, industry, and governments with their industrial policy and budget constraints.

In the case of satellite programmes with worldwide scope, there must be as much coordination as possible with international partners, which may further complicate the decision-making process.

7.3.2 Continuity and contingency planning

The continuity of space-based observations has been a critical requirement for the meteorological satellite constellation in geostationary orbit ever since nowcasting and severe weather forecasting, including tropical cyclone warning, began relying on satellite monitoring. The operational continuity of GEO imagery entails round-the-clock operation, high availability, near-real-time data dissemination, and long-term continuity guaranteed by robust programmes that include provisions for in-orbit backups.

When the polar-orbiting constellation was established, and numerical weather prediction models were increasingly relying on satellite radiance data (infrared, and microwave) and radio-occultation data, as well as other key satellite observations such as ocean surface winds and upper air winds (for example, atmospheric motion vectors), a similar requirement for operational continuity was applied to the morning and afternoon satellites that became the core meteorological constellation in polar orbit.

While satellite operators are committed to maintaining the operational geostationary and polar Sun-synchronous constellations, CGMS developed a Global Contingency Plan (see section 7.2.1 and box below) providing a technical and legal framework for contingency measures to be taken on a "help your neighbour" basis in case of deficiency of one of the elements of the operational configuration.

CGMS continuity and contingency planning

The CGMS baseline expresses the long-term commitments of satellite operators in response to the WIGOS Vision, in terms of measurements, orbits and services. The baseline defines (i) a geostationary constellation comprising at least six satellites nominally located at well-separated longitudes (approximately 135°W, 75°W, 0°, 76°E, 105°E, 140°E) and performing a set of agreed missions, (ii) a core meteorological constellation in polar Sun-synchronous orbit performing imagery and sounding from three orbital planes (early morning, mid-morning and afternoon orbits), and (iii) different constellations dedicated to additional missions in either Sun-synchronous or inclined low Earth orbits. The CGMS Working Group on Operational Continuity and Contingency Planning keeps under review the implementation of the baseline, the availability of in-orbit backups and the risks of interruption of key missions.

The Coordination Group for Meteorological Satellites has adopted a Global Contingency Plan which includes guidelines to ensure continuity, for example, in terms of in-orbit backup and re-launch policy, sets criteria for entering into contingency mode and identifies actions to be taken in such contingency situations. In particular, the Global Contingency Plan defines a generic procedure for relocating a spare geostationary satellite to take over from a failing satellite, which is referred to as the "help your neighbour" strategy. This global plan is supplemented by bilateral contingency agreements between geostationary satellite operators. On several occasions over the past three decades, such contingency relocations have been essential to preserve the continuity of vital operational missions.

For geostationary satellites, contingency support can be provided if the number of satellites is sufficiently high and their nominal positions are appropriately spaced along the Equator (see, for instance, Volume IV, Chapter 4, Figure 4.1) to fully cover the lower latitudes. Moving a satellite from one longitude to another requires little fuel if implemented at a slow pace. As laid out in the contingency plans, several satellites are maintained in backup positions and it is possible to relocate a satellite to fill a gap through a manoeuvre lasting a few days or weeks depending on the urgency and the fuel available on board. Several examples have taken place: Meteosat-3 satellite was moved to cover the West Atlantic Ocean when the Geostationary Operational Environmental Satellite (GOES) system suffered a launch problem in the early 1990s (de Waard et al., 1992); a spare GOES satellite filled the gap in the Western Pacific Ocean during the transition from the Geostationary Meteorological Satellite (GMS) to the Multifunctional Transport Satellite (MTSAT) in the early 2000s; in the last two decades the Indian Ocean position has been covered on occasions by spare Meteosat satellites; and since 2018, Fengyun satellite (FY) also provided the Indian Ocean coverage providing observations to global users.

For Sun-synchronous satellites, contingency is more complicated. Changing the orbital plane of a satellite requires a very large amount of fuel and is not envisaged apart from the natural drift of the orbital plane due to precession or orbit-keeping manoeuvres to correct this drift. The contingency plan therefore focuses on the availability of backup satellites in each orbital plane along with regular spacing of the equatorial crossing times of these planes, as well as usage of standalone research and development missions that can help bridge gaps and provide additional redundancy.

The scope of the operational space-based observing system as expressed in the WIGOS Vision now encompasses support to climate monitoring, reflecting both the requirement to monitor the climate on a continuing basis and the maturity of space-based systems, which are becoming sufficiently accurate for climate monitoring. Continuity is as crucial for climate monitoring as for operational weather forecasting; however, the requirements are different because climate monitoring involves different timescales. First, near-real-time availability and short-term gaps in a daily cycle are not driving requirements. Second, major importance is attached to long-term continuity and stability of measurements throughout decades. The Global Climate Observing System (GCOS) Climate Monitoring Principles require systematic overlap between all consecutive satellites to allow for intercalibration and traceability. Stability and traceability could also be achieved by maintaining one highly secured reference mission, with in-orbit backup, that serves as a calibration reference standard for all the others (as discussed in Volume IV, Chapter 6, 6.1.9). Such a provision should be a major element in the definition of the Architecture for Climate Monitoring from Space.

7.3.3 Long-term evolution

The evolving user requirements for satellite data and the dramatic progress of space and remote-sensing technology call for continuous improvements to satellite systems and instrumentation.

At the same time, the strong pressure on resources stresses the need to seek an optimization of the global effort to assure the availability of a comprehensive observing system and avoid unnecessary redundancy beyond the required margins for robustness. Operational satellite programmmes procure several satellites of the same type in order to profit from economies of scale, thus making expensive programmes more affordable. The downside of that necessary approach is that technological capabilities become `frozen` throughout the lifetime of a satellite programme. Optimization is also needed in the development, validation and sustained processing of derived products, and requires data sharing, interoperability and quality assurance. Global coordination under the auspices of WMO aims at ensuring such optimization under the overall context of the WIGOS, building on the Rolling Review of Requirements (https://public.wmo.int/en/resources/bulletin/global-observing-system, https://community.wmo.int/rolling-review-requirements-process), the high-level guidance provided by the Vision for the GOS, the Statement of Guidance in each application area, and the Implementation Plan for the Evolution of Global Observing Systems which consolidates the recommendations addressed to agents implementing observing systems. A notable initiative is also the Architecture for

Climate Monitoring from Space, promoted by WMO, CEOS and CGMS, which aims to provide an end-to-end response from the space-based observing system to the climate monitoring requirements – see also: http://ceos.org/ourwork/workinggroups/climate/.

REFERENCES AND FURTHER READING

Achieving Satellite Instrument Calibration for Climate Change (ASIC3); Report of a Workshop Organized by the National Oceanic and Atmospheric Administration, National Institute of Standards and Technology, National Aeronautics and Space Administration, National Polar-orbiting Operational Environmental Satellite System-integrated Program Office, and Space Dynamics Laboratory of Utah State University; Ohring, G., Ed.; National Oceanic and Atmospheric Administration: Washington, DC, 2007.

Bizzarri, B. Satellite Data for Numerical Weather Prediction. *Rivista di Meteorologia Aeronautica* **1982**, *42* (4), 369–382.

Bizzarri, B. Basic Principles of Remote Sensing. In *Proceedings of the Course on Satellite Meteorology and its Extension to Agriculture*; EUMETSAT, EUM P03; Erice, Ed.; 1986; pp. 1–10.

Bizzarri, B.; Tomassini, C. Retrieval of Information from High-resolution Images. In *Proceedings of the Symposium on Meteorological Observations from Space*; Committee on Space Research: Philadelphia, USA, 1976; pp. 140–144.

Chander, G.; Hewison, T. J.; Fox, N. et al. Overview of Intercalibration of Satellite Instruments. *IEEE Transactions on Geoscience and Remote Sensing* **2013**, *51* (3), 1056–1080.

Committee on Earth Observation Satellites. *Mission, Instruments and Measurements database online*. http://database.eohandbook.com.

Datla, R. V.; Rice, J. P.; Lykke, K. R. et al. *Best Practice Guidelines for Pre-launch Characterization and Calibration of Instruments for Passive Optical Remote Sensing*; NIST IR 7637; National Institute of Standards and Technology: Gaithersburg, USA, 2009.

de Waard, J.; Menzel, W. P.; Schmetz, J. Atlantic data coverage by METEOSAT-3. *Bulletin of the American Meteorological Society* **1992**, *73*, 977–983. https://doi.org/10.1175/1520-0477(1992)073<0977:ADCB>2.0.CO;2.

Earth Science Reference Handbook; Parkinson, C. L.; Ward, A.; King, M. D., Eds.; NASA Goddard Space Flight Center: Greenbelt, USA, 2006.

European Cooperation for Space Standardization (ECSS). *System Engineering General Requirements*; ECSS-E-ST-10C Rev.1. ECSS, 2017. https://ecss.nl/standard/ecss-e-st-10c-rev-1-system-engineering-general-requirements-15-february-2017/.

European Space Agency, Sharing Earth Observation Resources. Satellite Missions Database. https://earth.esa.int/eogateway/mission.

Fox, N. *QA4EO – A Quality Assurance Framework for Earth Observation: A Guide to "Reference Standards" in Support of Quality Assurance Requirements of GEO;* Greening, M. C., Ed.; QA4EO-QAEO-GEN-DQK-003; Group on Earth Observations: Geneva, 2010. http://www.qa4eo.org/docs/QA4EO-QAEO-GEN-DQK-003_v4.0.pdf.

Joint Committee for Guides in Metrology (JCGM). *International Vocabulary of Metrology – Basic and General Concepts and Associated Terms (VIM)*; JCGM 200:2012; JCGM: Sèvres, France, 2012.

Klein, M.; Gasiewski, A. J. Nadir Sensitivity of Passive Millimeter and Submillimeter Wave Channels to Clear Air Temperature and Water Vapor Variations. *Journal of Geophysical Research: Atmospheres* **2000**, *105* (D13), 17481–17511.

Kramer, H. J. *Observation of the Earth and its Environment – Survey of Missions and Sensors*; Springer: Berlin, 2002.

Menzel, W. P. *Applications with Meteorological Satellites* (SAT-No. 28; WMO/TD-No. 1078). World Meteorological Organization: Geneva, 2001.

National Aeronautics and Space Administration (NASA). *NASA System Engineering Handbook*; NASA SP-2016-6105 Rev2, 2016. https://www.nasa.gov/connect/ebooks/nasa-systems-engineering-handbook.

Tobin, D. C.; Revercomb, H. E.; Knuteson, R. O. et al. Radiometric and Spectral Validation of Atmospheric Infrared Sounder Observations with the Aircraft-based Scanning High-Resolution Interferometer Sounder. *Journal of Geophysical Research: Atmospheres* **2006**, *111* (D09S02). https://doi.org/10.1029/2005JD006094.

Tobin, D. C.; Revercomb, H. E.; Moeller, C. C. et al. Use of Atmospheric Infrared Sounder High-spectral Resolution Spectra to Assess the Calibration of Moderate Resolution Imaging Spectroradiometer on EOS Aqua. *Journal of Geophysical Research: Atmospheres* **2006**, *111* (D09S05).

World Meteorological Organization. *Observing Systems Capability Analysis and Review (OSCAR) database and tool*. 2014. http://www.wmo-sat.info/oscar/.

World Meteorological Organization (WMO). *World Meteorological Congress: Abridged Final Report of the Eighteenth Session* (WMO-No. 1236), Annex to Resolution 37 (Cg-18), WMO Integrated Global Observing System (WIGOS). Geneva, 2019.

World Meteorological Organization (WMO). *World Meteorological Congress: Abridged Final Report of the Eighteenth Session* (WMO-No. 1236), Resolution 51 (Cg-18) Implementation of the Architecture for Climate Monitoring from Space. Geneva, 2019.

World Meteorological Organization (WMO), International Telecommunication Union (ITU). *Handbook on Use of Radio Spectrum for Meteorology: Weather, Water and Climate Monitoring and Prediction*. WMO/ITU: Geneva, 2008.

For more information, please contact:

World Meteorological Organization

7 bis, avenue de la Paix – P.O. Box 2300 – CH 1211 Geneva 2 – Switzerland

Strategic Communications Office

Tel.: +41 (0) 22 730 83 14 – Fax: +41 (0) 22 730 80 27

Email: cpa@wmo.int

public.wmo.int

JN 211524